Koji Ikura
Masaya Nagao
Akira Ichikawa
Kiichiro Teruya
Sanetaka Shirahata
Editors

VOLUME 15

Animal Cell Technology: Basic & Applied Aspects

Proceedings of the 19th Annual Meeting of the Japanese Association for Animal Cell Technology (JAACT), Kyoto, Japan, September 25–28, 2006

Springer

Animal Cell Technology:
Basic & Applied Aspects

Volume 15

For other titles published in this series, go to
www.springer.com/series/7552

JAACT 2006 Organizing Committee

Meeting Chairman
Koji Ikura (Kyoto Institute of Technology, Japan)

Meeting Vice Chairman
Masaya Nagao (Kyoto University, Japan)

Meeting Secretaries
Akira Ichikawa (Kyoto Institute of Technology, Japan)
Yoshinori Katakura (Kyushu University, Japan)
Seiji Masuda (Kyoto University, Japan)
Keiko Momma (Kyoto University, Japan)
Kiichiro Teruya (Kyushu University, Japan)

Organizing Boards

H. Anazawa (Japan)	S. Asahi (Japan)	K. Dairiki (Japan)
D. Ejima (Japan)	A. Enomoto (Japan)	Y. Fuke (Japan)
Y. Fukui (Japan)	S. Hachimura (Japan)	S. Hashizume (Japan)
C. Hirashima (Japan)	M. Hosobuchi (Japan)	H. Hoshi (Japan)
S. Iijima (Japan)	M. Kamei (Japan)	Y. Kamei (Japan)
M. Kamihira (Japan)	S. Kida (Japan)	M. Maeda-Yamamoto (Japan)
T. Matsuda (Japan)	Y. Miura (Japan)	H. Nakano (Japan)
G. Schmid (Switzerland)	T. Shigehisa (Japan)	M. Shimizu (Japan)
S. Shirahata (Japan)	H. Shinmoto (Japan)	M. Takagi (Japan)
M. Tanokura (Japan)	M. Totsuka (Japan)	H. Tsumura (Japan)
K. Yagasaki (Japan)	M. Yokota (Japan)	

Advisory Boards

D. W. Barnes (USA)	S. Kaminogawa (Japan)	Y. Kitagawa (Japan)
K. Nagai (Japan)	R. Sasaki (Japan)	G. H. Sato (USA)
T. Suzuki (Japan)	J. Wérenne (Belgium)	

Koji Ikura
Masaya Nagao • Akira Ichikawa
Kiichiro Teruya • Sanetaka Shirahata
Editors

Animal Cell Technology: Basic & Applied Aspects

Proceedings of the 19th Annual Meeting of the Japanese Association for Animal Cell Technology (JAACT), Kyoto, Japan, September 25–28, 2006

Springer

Editors
Masaya Nagao
Kyoto University
Kyoto, Japan

Kiichiro Teruya
Kyushu University
Kyoto, Japan

Koji Ikura
Kyoto Institute of Technology
Kyoto, Japan

Akira Ichikawa
Kyoto Institute of Technology
Kyoto, Japan

Sanetaka Shirahata
Kyushu University
Fukuoka, Japan

ISBN: 978-1-4020-9645-7 e-ISBN: 978-1-4020-9646-4
DOI 10.1007/978-1-4020-9646-4
Springer Dordrecht Heidelberg London New York

Library of Congress Control Number: 2009929388

Preface

The 19th Annual and International Meeting of the Japanese Association for Animal Cell Technology (JAACT 2006 Kyoto) was held at the PALULU Plaza Kyoto in Kyoto, Japan from September 25 to 28, 2006. The meeting chairman was Prof. Koji Ikura, Kyoto Institute of Technology. The satellite symposium was also held at Fukuoka on September 22, 2006. The motto of the meeting was "Animal Cell Technology for New Biosciences and Bioindustries". The meeting focused on recent advancement of animal cell technologies from basic and applied aspects. We invited academic and industrial scientists from all over the world to make the JAACT 2006 truly successful and scientifically fruitful. More than 300 participants from 16 countries joined the meeting and gave presentations as follows:

Plenary Lectures

Dr. John Sinden. A front line of stem cell technology.
Dr. Sten Orrenius. Mitochondrial regulation of cell death as a potential target for drug discovery.

Murakami Memorial Lecture

Dr. Gordon Sato. Tissue culture – the unrealized potential.

ESACT Lecture

Dr. John Werenne. Validable single use bioreactor for cell expansion on microcarriers and potentialities of a newly designed digital holographic microscope to follow bioprocesses depending on animal cell culture.
Dr. Mohamed Al-Rubeai. Cell line engineering for controlled proliferation and apoptosis.
Dr. Georg Schmid. Monitoring and control of animal cell culture processes by online capcitance measurement.

Symposia

1. Evaluation of polyphenols as functional constituents in food by animal cells.
2. In vivo analysis of brain function by mouse molecular genetics and imaging.
3. Cellular and molecular mechanism to prevent the brain aging: the role of adult neurogenesis.
4. Ex vivo expansion of stem cells for regenerative medicine.
5. Autophagy as a novel regulatory system for various cell functions.
6. New strategy for rapid development of productive cell lines.
7. Frontline of biologics production.
8. Animal cells for safety evaluation of chemical substances.

Thirty-seven oral presentations and 63 poster presentations were brought together on the following themes:

1. Cell culture engineering
2. Production of biologicals
3. Functional cell lines
4. Glycoengineering
5. Immunologicals, monoclonal antibodies, and vaccines
6. Transplantation, artificial organs, and organ substitutes
7. Gene therapy
8. Transgenic animals
9. Safety and regulation
10. Cell regulatory factors and signal transduction
11. Functional substances in food and natural sources
12. Animal cells for in vitro assay
13. Other topics concerning animal cell technology

The Satellite Symposium "New Technologies for Creation of the Century of Life on the Blue Planet Earth"
Dr. Gordon H. Sato. Low technologies to change dessert to mangrove forest.
Dr. Masayoshi Takahashi. Microbubbles and nanobubbles potentially useful for sterilization, environmental remediation, agriculture and fisheries.
Dr. Sen Orrenius. Mitochondria, free radicals, ageing and cell death.
Dr. Sei Sasaki. Aquaporin water channel and diseases.
Dr. Sanetaka Shirahata. Action mechanisms of reduced water for prevention of oxidative stress-related diseases.

Dr. Zbigniew Gadek. "Nordenau phenomenon" – Application of naturally reduced water to therapy. Follow up study upon 411 diabetes patients.
We believe that all participants enjoyed the innumerable Japanese traditional treasures of Kyoto as well as scientific fruits. The editors express their sincere gratitude to all the participants, organizers of the symposia, members of the organizing

committee for their dedication in assuring the success of the meeting. We also deeply thank to the Japan Society for the Promotion of Sciences for their financial supports.

The editors hope this proceedings book of JAACT2006 Kyoto will greatly contribute to the development of animal cell technology or innovation of life science.

The editors

Contents

Non-fucosylated Therapeutic Antibodies: The Next Generation of Therapeutic Antibodies

Mitsuo Satoh, Shigeru Iida, Naoko Yamane-Ohnuki, Katsuhiro Mori, Yutaka Kanda, Reiko Kuni-Kamochi, Ryosuke Nakano, Harue Imai-Nishiya, Akira Okazaki, Toyohide Shinkawa, Akihito Natsume, Rinpei Niwa, and Kenya Shitara

Abstract Therapeutic antibody IgG1 has two *N*-linked oligosaccharide chains bound to the Fc region. The oligosaccharides are of the complex biantennary type, composed of a trimannosyl core structure with the presence or absence of core fucose, bisecting *N*-acetylglucosamine (GlcNAc), galactose, and terminal sialic acid, which gives rise to structural heterogeneity. Both human serum IgG and therapeutic antibodies are well known to be heavily fucosulated. Recently, antibody-dependent cellular cytotoxicity (ADCC), a lytic attack on antibody-targeted cells, has been found to be one of the critical effector functions responsible for the clinical efficacy of therapeutic antibodies such as anti-CD20 IgG1 rituximab (Rituxan^{R}) and anti-Her2/neu IgG1 trastuzumab (Herceptin^{R}). ADCC is triggered upon the binding of lymphocyte receptors (FcγRs) to the antibody Fc region. The activity is dependent on the amount of fucose attached to the innermost GlcNAc of *N*-linked Fc oligosaccharide via an α-1,6-linkage, and is dramatically enhanced by a reduction in fucose. Non-fucosylated therapeutic antibodies show more potent efficacy than their fucosylated counterparts both in vitro and in vivo [7–14], and are not likely to be immunogenic because their carbohydrate structures are a normal component of natural human serum IgG. Thus, the application of non-fucosylated antibodies is expected to be a powerful and elegant approach to the design of the next generation therapeutic antibodies with improved efficacy. In this review, we discuss the importance of the oligosaccharides attached to the Fc region of therapeutic antibodies, especially regarding the inhibitory effect of fucosylated therapeutic antibodies on the efficacy of non-fucosylated counterparts in one medical agent. The impact of completely non-fucosylated therapeutic antibodies on therapeutic fields will be also discussed.

Keywords Therapeutic antibody • *N*-linked Fc oligosaccharide • core-fucosylation • α-1,6-fucosyltransferase (FUT8) knockout • Chinese hamster ovary (CHO) • ADCC • FcγRIIIa binding • human plasma IgG

M. Satoh S. Iida, N.Yamane-Ohnuki, K. Mori, Y. Kanda, R. Kuni-Kamochi, R. Nakano, H.I-Nishiya, A. Okazaki, T. Shinkawa, A. Natsume, and K. Shitara
Tokyo Research laboratories, Kyowa Hakko Kogyo Co., Ltd., 3-6-6 Asahi-machi, Machida-shi, Tokyo, 194-8533, Japan

K. Ikura et al. (eds.), *Animal Cell Technology: Basic & Applied Aspects*,
Animal Cell Technology: Basic & Applied Aspects 15,
DOI 10.1007/978-1-4020-9646-4_1,

1 Introduction

Most of the current therapeutic antibodies that have been licensed and developed as medical agents are human IgG1 isotype including mouse/human chimeric, humanized and human IgG1. Human IgG1 is a glycoprotein bearing two *N*-linked biantennary complex-type oligosaccharides bound to the antibody constant region (Fc), in which the majority of the oligosaccharides are core-fucosylated [1–4], and it exercises effector functions of antibody-dependent cellular cytotoxicity (ADCC) and complement-dependent cytotoxicity (CDC) through the interaction of the Fc with either leukocytes receptors (FcγRs) or complement. Some therapeutic antibodies can mediate direct apoptosis to the target cells as well. The efficacy of therapeutic antibodies results from specificity for the target antigen and the antibody effector functions, which are activated by the formation of immune complexes (Fig. 1). Recently, therapeutic antibodies have been shown to improve overall survival as well as time to disease progression in a variety of human malignancies such as breast, colon and haematological cancers [5–8], and genetic analysis of FcγR polymorphisms of cancer patients has clearly demonstrated that ADCC is one of the major anti-neoplasm mechanism responsible for clinical efficacy [9–13].

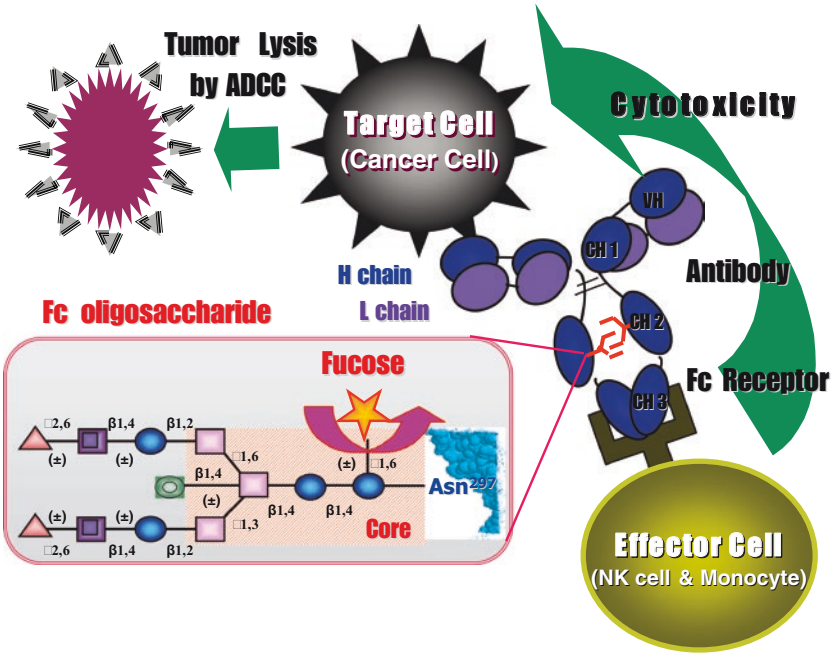

Fig. 1 Schematic drawing of immune complex-induced effector function of ADCC. Antibody-coated tumor cells are killed by effector cells through the binding of the antibodies to Fc receptors on the effector cells. Complex-type *N*-linked Fc oligosaccharides (consists of GlcNAc (●), mannose (□), bisecting GlcNAc (◎), fucose (★), galactose (▣), sialic acid (▲)) attached to the CH_2 domains of the Fc affect the cellular cytotoxicity of ADCC

Table 1 Recombinat therapeutic antibodies on the market USA

Trade	Company	Type	Antigen	Indication	Approval Date
Reopro^{R}	Centocor/Lilly	Chimera	gpIIb/IIIa	Thrombosis	12/24/1994
Rituxan^{R}	IDEC/Genentech/ Roche	Chimera	CD20	NHL	11/26/1997
Zenepax^{R}	Roche	Humanized	IL-2R	Transplantation	12/10/1997
Simulect^{R}	Novartis	Humanized	IL-2R	Transplantation	05/12/1998
Synagis^{R}	MedImmune/Abott	Humanized	RSV	RSV infection	06/19/1998
Remicade^{R}	Centocor/J&J	Chimera	TNF-α	RA, Chron's	08/24/1998
Herceptin^{R}	Genentech/Roche	Humanized	Her2	Breast cancer	09/25/1998
Mylotarg^{R}	Cellutech/AHP	Drug-conjugate	CD33	AML	05/17/2007
Campath^{R}	ILEX/Schering	Humanized	CD52	B-CLL	05/05/2001
Zevalin^{R}	IDEC/Schering	^{90}Y-conjugate	CD20	NHL	02/19/2002
Humira^{R}	Abott/CAT	Fully human	TNF-α	RA	12/31/2002
Xolair^{R}	Genentech/ Novartis/Tanox	Humanized	IgE	Allergic asthma	06/20/2003
Bexxar^{R}	Corixa/SKB	^{131}I-conjugate	CD20	NHL	06/27/2003
Raptiva^{R}	Genentech/Xoma	Humanized	LFA-1	Psoriasis	10/27/2003
Erbitux^{R}	ImClone/BMS/ Merck	Chimeric	EGFR	Colon cancer	02/12/2004
Avastin^{R}	Genentech	Humanized	VEDF	Colon cancer	02/26/2004
Tysabri^{R,a}	Biogen-IDEC/Elan	Humanized	Integrin4β1	MS	12/23/2004

RSV: respiratory syncytial virus, NHL: non-Hodgin lymphoma, AML: acute myeloid leukemia, B-CLL: B-cell lymphocytic leukemia, RA: rheumatoid arthiritis, MS: multiple sclerosis.
[a] Voluntary suspension of Tysabri^{R} marketing has been announced on February 2005, and reintroduced on July 2006.

The common features of antibody therapeutics, representing as high specificity to the target, long stability in blood, and high physiological functions induced effective clinical efficacy, are just about to be the features necessary for molecular-target based medicines. Thus, therapeutic antibodies now comprise the majority of recombinant proteins currently used in the clinic. A number of trials using therapeutic antibodies are ongoing, including more than 200 pre-clinical and 150 clinical studies [14], and 17 types of recombinant monoclonal therapeutic antibodies have been approved in the United States, and these agents represent a major new class of drugs (Table 1). It is generally expected that the indications for the use of therapeutic antibodies will be dramatically expanded in near future. Worldwide sales of total therapeutic antibodies have already exceeded 10 billion dollars in 2004 [15].

2 Current Feature of Therapeutic Antibodies

Although antibody therapeutics are currently recognized as new medicines that confer great benefits to patients suffering from various obstinate diseases, we also realize that these agents yield a serious issue of medical economy, so called "economical toxicity". A common feature of therapeutic antibodies used for cancer treatment is

that their anti-tumor efficacy requires high serum concentrations and continued therapy for several months. The treatment cycles thereby consume several grams of therapeutic antibody, resulting in a significant amount of drug needed and very high costs [16–18]. In fact, administration of a high dose (2–8 mg/kg) of either anti-CD20 IgG1 rituximab (Rituxan^{R}) or anti-Her2/neu IgG1 trastuzumab (Herceptin^{R}) is required to keep the effective serum concentration of over 10 μg/mL, which is more than 100-fold high administrated dose of cytokine therapy such as erythropoietin (EPO) and granulocyte colony-stimulating factor (G-CSF) regimens. The drug cost of one cycle medical treatment with such therapeutic antibodies amounts to being over 20,000 dollars. This is one of the reasons why annual sales of rituximab and trastuzumab have exceed and almost reached 2 billion dollars, respectively, although the population of either non-Hodgkin's lymphoma or breast cancer patients is limited; both patients are not major in whole cancer patients. As mentioned above, the indication of therapeutic antibodies will be more expanded in near future, and the economical situation of antibody therapy will soon no longer be viable, i.e., will be at risk of collapse. Moreover, there still remains the need to improve the efficacy of therapeutic antibodies such that they can be used to achieve not only remission, but also complete recovery from disease; many of the currently approved therapeutic antibodies remain unable to induce more than remission. Currently, numerous efforts to improve the efficacy of therapeutic antibodies are underway. These include the introduction of amino acid mutations in the Fc region [19, 20] and the co-administration of CpG as an adjuvant [21, 22], or that of cytokines such as IL-2 [23] and GM-CSF [24]. Among these efforts, the modification of *N*-linked Fc oligosaccharides, especially core-fucose removal, has been of note as a key of next generation therapeutic antibodies with improved efficacy [25–38].

3 Human Serum IgG Inhibits Therapeutic Antibody-Induced ADCC

We should note that there is a huge discrepancy between the potency of therapeutic antibodies in vitro and in vivo, in terms of dosing therapeutic antibodies, especially anticancer antibodies. Cancer patients treated with therapeutic antibodies typically need to receive weekly doses of several hundred milligrams over several months for keeping the effective serum concentration of more than 10 μg/ml [16–18]. On the contrary, the maximal in vitro cellular cytotoxicity by ADCC of these therapeutic antibodies can be achieved at antibody concentrations of less than 10 ng/mL, which is several orders of magnitude below the targeted serum concentrations [39, 40]. This discrepancy, the low in vivo efficacy of therapeutic antibodies in contrast to the high in vitro ADCC, has been recently disclosed to be mainly due to competition between serum IgG and therapeutic antibodies for binding to FcγRIIIa on natural killer (NK) cells; endogenous human serum IgG inhibits ADCC induced by therapeutic antibodies [41, 42]. Human serum IgG dose not affect antigen binding by therapeutic antibodies however significantly impairs interaction of the antibodies with FcγRIIIa, and

induce the inhibition of the ADCC of therapeutic antibodies. This phenomenon leads to the elucidation of necessity of the use of high doses in the clinical treatment, and also elucidates the molecular mechanism for the enhanced efficacy of non-fucosylated therapeutic antibodies in humans. Non-fucosylated therapeutic antibodies have much higher binding affinity for FcγRIIIa than fucosylated human serum IgG, which is a preferable character to conquer the interference by human plasma IgG [37, 38]. Therefore, non-fucosylated therapeutic antibodies can evade the inhibitory effect of human plasma IgG on ADCC through their high FcγRIIIa bonding.

4 Fucosylated Therapeutic Antibodies Spoil the Non-Fucosylated Antibody-Induced ADCC

More importantly, the enhanced ADCC of non-fucosylated therapeutic antibodies against a specific antigen has been shown to be inhibited in a dose-dependent manner by fucosylated antibodies against the same antigen in the case of both rituximab and trastuzumab in vitro and ex vivo [37, 38]. Non-fucosylated therapeutic antibodies existing in the antibody mixtures, composed of non-fucosylated and fucosylated forms, do not exhibit activity equivalent to that of equal amounts of non-fucosylated therapeutic antibodies alone. This phenomenon reflects the fact that the maximum efficacy of both in vitro and ex vivo ADCCs of fucosylated therapeutic antibodies never reaches the level as high as that by non-fucosylated therapeutic antibodies, even when employed high doses of the fucosylated antibodies. One of the major mechanisms for the inhibitory effect of fucosylated therapeutic antibodies on the ADCC activity of non-fucosylated counterparts is considered to be through the competition of the two antibodies for the antigens on target cells. Therapeutic antibodies have the same antigen binding ability irrespective of core-fucosylation, and the density of the non-fucosylated antibodies binding on the target cells is thus reduced by fucosylated antibody occupation, which yields a similar effect to shed the target antigens from capture by the therapeutic agent possessing high ADCC activity, i.e., non-fucosylated therapeutic antibodies, even in human plasma. To overcome the interference of human plasma IgG, the target tumor cells need to be coated with therapeutic antibodies possessing higher binding affinity to FcγRIIIa than human plasma IgG. Hence, therapeutic antibodies consisting of only the non-fucosylated human IgG1 form (i.e., not including any of its fucosylated counterparts) is thought to be ideal.

5 Manufacturing of Non-Fucosylated Therapeutic Antibodies

All therapeutic antibodies currently licensed on the market are produced in rodent mammalian cell lines such as Chinese hamster ovary (CHO), mouse myeloma NS0 and SP2/0 and mouse hybridoma, and almost all of molecules produced by these

cell lines have core-fucosylation in the Fc oligosaccharides [43, 44] which means that ADCC of the products is unfortunately far from optimal. These cell lines retain the intrinsic α-1,6-fucosyltransferase (*FUT8*) enzyme activity responsible for the core-fucosylation of the Fc oligosaccharides. *FUT8* catalyzes the transfer of fucose from GDP-fucose to the innermost GlcNAc in an α-1,6 linkage [45], and complete and irreversible inactivation of *FUT8* function in antibody producing cells is essential to manufacture non-fucosylated therapeutic antibodies. A production process in which the core-fucosylation levels of the products vary depending on culture condition should introduce severe clinical issues, and is therefore unacceptable from a practical industrial standpoint. Robust stable production of completely non-fucosylated therapeutic antibodies in a fixed quality has been achieved by the generation of a unique host cell line, in which the endogenous *FUT8* gene is knocked out [27, 30]. *FUT8*-knockout CHO/DG44 cells exhibit a morphology, growth kinetics, and productivity similar to those of the parent cells, and enable to stably produce non-fucosylated therapeutic antibodies with fixed quality and consistent ADCC activity of the ingredients in fed-batch serum-free cultures using bioreactors commonly employed in pharmaceutical industry. Thus, the application of non-fucosylated antibodies is expected to be a promising approach as a nest-generation of therapeutic antibodies with improved efficacy even when administrated in low doses in humans in vivo [38]. Clinical trials using non-fucosylated antibody therapeutics are currently underway.

References

1. T. W. Rademacher, R. B. Parekh, and R. A. Dwek, Glycobiology, *Annu. Rev. Biochem.* 57, 785–838 (1988).
2. T. Mizuochi, T. Taniguchi, A. Shimizu, and A. Kobata, Structural and numerical variations of the carbohydrate moiety of immunoglobulin G, *J. Immunol.* 129, 2016–2020 (1982).
3. H. Harada, M. Kamei, Y. Tokumoto, S. Yui, F. Koyama, N. Kochibe, T. Endo, and A. Kobata, Systematic fractionation of oligosaccharides of human immunoglobulin G by serial affinity chromatography on immobilized lectin columns, *Anal. Biochem.* 164, 374–381 (1987).
4. R. Jefferis, Glycosylation of human IgG antibodies: Relevance to therapeutic applications, *BioPharm.* 14, 19–26 (2002).
5. J. S. de Bono and E. K. Rowinsky, The ErbB receptor family: A therapeutic target for cancer, *Trends Mol. Med.* 8(Suppl 4), S19–S26 (2002).
6. A. Forero and A. F. Lobuglio, History of antibody therapy for non-Hodgkin's lymphoma, *Semin. Oncol.* 30, 1–5 (2003).
7. A. J. Grillo-Lopez, Rituximab (Rituxan/Mab Thera): The first decade (1993–2003), *Expert Rev. Anticancer Ther.* 3, 767–769 (2003).
8. C. L. Vogel and S. X. Franco, Clinical experience with trastuzumab (Herceptin), *Breast J.* 9, 452–462 (2003).
9. G. Cartron, L. Dacheux, G. Salles, P. Solal-Celigny, P. Bardos, P. Colombat, and H. Watier, Therapeutic activity of humanized anti-CD20 monoclonal antibody and polymorphism in IgG Fc receptor Fc gamma RIIIa gene, *Blood* 99, 754–758 (2002).
10. S. Dall'Ozzo, S. Tartas, G. Paintaud, G. Cartron, P. Colombat, P. Bardos, H. Watier, and G. Thibault, Rituximab-dependent cytotoxicity by natural killer cells: Influence of FCGR3A polymorphism on the concentration-effect relationship, *Cancer Res.* 64, 4664–4669 (2004).

11. J. H. Anolik, D. Campbell, R. E. Felgar, F. Young, I. Sanz, J. Rosenblatt, and R. J. Looney, The relationship of FcγRIIIa genotype to degree of B cell depletion by rituximab in the treatment of systemic lupus erythematosus, *Arthritis Rheum.* 48, 455–459 (2003).
12. W. K. Weng, and R. Levy, Two immunoglobulin G fragment C receptor polymorphisms independently predict response to rituximab in patients with follicular lymphoma, *J. Clin. Oncol.* 21, 3940–3947 (2003).
13. R. Gennari, S. Menard, F. Fagnoni, L. Ponchio, M. Scelsi, E. Tagliabue, F. Castiglioni, L. Villani, C. Magalotti, N. Gibelli, B. Oliviero, B. Ballardini, G. D. Prada, A. Zambelli, and A. Costa, Pilot study of the mechanism of action of preoperative trastuzumab in patients with primary operable breast tumors overexpressing HER2, *Clin. Cancer Res.* 10, 5650–5655 (2004).
14. J. M. Reishert, C. J. Rosensweig, L. B. Faden, and M. C. Dewitz, Monoclonal antibody successes in the clinic, *Nat. Biotechnol.* 23, 1073–1078 (2005).
15. M. Baker, Upping the ante on antibodies, *Nat. Biotechnol.* 23, 1065–1072 (2005).
16. J. Baselga and J. Albanell, Mechanism of action of anti-HER2 monoclonal antibodies, *Ann. Oncol.* 12(Suppl 1), S35–S41 (2001).
17. N. L. Berinstein, A. J. Grillo-Lopez, C. A. White, I. Bence-Bruckler, D. Maloney, M. Czuczman, D. Green, J. Rosenberg, P. McLaughlin, and D. Shen, Association of serum rituximab (IDEC-C2B8) concentration and anti-tumor response in the treatment of recurrent low-grade or follicular non-Hodgkin's lymphoma, *Ann. Oncol.* 9, 995–1001 (1998).
18. M. M. Goldenberg, Trastuzumab, a recombinant DNA-derived humanized monoclonal antibody, a novel agent for the treatment of metastatic breast cancer, *Clin. Ther.* 21, 309–318 (1999).
19. R. L. Shields, A. K. Namenuk, K. Hong, Y. G. Meng, J. Rae, J. Briggs, D. Xie, J. Lai, A. Stadlen, B. Li, J. A. Fox, and L. G. Presta, Resolution mapping of the binding site on human IgG1 for FcγRI, FcγRII, FcγRIII, and FcRn and design of IgG1 variants with improved binding to the FcγR, *J. Biol. Chem.* 276, 6591–6604 (2001).
20. G. A. Lazar, W. Dang, S. Karki, O. Vafa, J. S. Peng, L. Hyun, C. Chan, H. S. Chung, A. Eivazi, S. C. Yoder, J. Vielmetter, D. F. Carmichael, R. J. Hayes, and B. I. Dahiyat, Engineered antibody Fc variants with enhanced effector function, *Proc. Natl. Acad. Sci. USA* 103, 4005–4010 (2006).
21. H. H. van Ojika, L. Bevaart, C. E. Dahle, A. Bakker, M. J. Jansen, M. J. van Vugt, J. G. van de Winkel, and G. J. Weiner, CpG-A and B oligodeoxynucleotides enhance the efficacy of antibody therapy by activating different effector cell population, *Cancer Res.* 63, 5595–5600 (2003).
22. B. Jahrsdorfer, and G. J. Weiner, Immunostimulatory CpG oligodeoxynucleotides and antibody therapy of cancer, *Semin. Oncol.* 30, 476–482 (2003).
23. J. W. Friedberg, D. Neuberg, J. G. Gribben, D. C. Fisher, C. Canning, M. Koval, C. M. Poor, L. M. Green, J. Daley, R. Soiffer, J. Ritz, and A. S. Freedman, Combination immunotherapy with rituximab and interleukin 2 in patients with relapsed or refractory follicular non-Hodgkin's lymphoma, *Br. J. Haematol.* 117, 828–834 (2002).
24. B. Stockmeyer, D. Elsasser, M. Dechant, R. Repp, M. Gramatzki, M. J. Glennie, J. G. van de Winkel, and T. Valerius, Mechanisms of G-CSF- or GM-CSF- stimulated tumor cell killing by Fc receptor-directed bispecific antibodies, *J. Immunol. Methods* 248, 103–111 (2001).
25. R. L. Shields, J. Lai, R. Keck, L. Y. O'Connell, K. Hong, Y. G. Meng, S. H. Weikert, and L. Prest, Lack of fucose on human IgG1 N-linked oligosaccharide improves binding to human FcγRIII and antibody-dependent cellular toxicity, *J. Biol. Chem.* 277, 26733–26740 (2002).
26. T. Shinkawa, K. Nakamura, N. Yamane, E. Shoji-Hosaka, Y. Kanda, M. Sakurada, K. Uchida, H. Anazawa, M. Satoh, M. Yamasaki, N. Hanai, and K. Shitara, The absence of fucose but not the presence of galactose or bisecting *N*-acetylglucosamine of human IgG1 complex-type oligosaccharides shows the critical role of enhancing antibody-dependent cellular cytotoxicity, *J. Biol. Chem.* 278, 3466–3473 (2003).
27. N. Yamane-Ohnuki, S. Kinoshita, M. Inoue-Urakubo, M. Kusunoki, S. Iida, R. Nakano, M. Wakitani, R. Niwa, M. Sakurada, K. Uchida, K. Shitara, and M. Satoh, Establishment of

FUT8 knockout Chinese hamster ovary cells: An ideal host cell line for producing completely defucosylated antibodies with enhanced antibody-dependent cellular cytotoxicity, *Biotechnol. Bioeng.* 87, 614–622 (2004).
28. K. Mori, R. Kuni-Kamochi, N. Yamane-Ohnuki, M. Wakitani, K. Yamano, H. Imai, Y. Kanda, R. Niwa, S. Iida, K. Uchida, K. Shitara, and M. Satoh, Engineering Chinese hamster ovary cells to maximize effector function of produced antibodies using FUT8 siRNA, *Biotechnol. Bioeng.* 88, 901–908 (2004).
29. A. Okazaki, E. Shoji-Hosaka, K. Nakamura, M. Wakitani, K. Uchida, S. Kakita, K. Tsumoto, I. Kumagai, and Shitara, K, Fucose depletion from human IgG1 oligosaccharide enhances binding enthalpy and association rate between IgG1 and FcγRIIIa, *J. Mol. Biol.* 336, 1239–1249 (2004).
30. Y. Kanda, N. Yamane-Ohnuki, N. Sakai, K. Yamano, R. Nakano, M. Inoue, H. Misaka, S. Iida, M. Wakitani, Y. Konno, K. Yano, K. Shitara, S. Hosoi, and M. Satoh, Comparison of cell lines for stable production of fucose-negative antibodies with enhanced ADCC, *Biotechnol. Bioeng.* 94, 680–688 (2006).
31. R. Niwa, E. Shoji-Hosaka, M. Sakurada, T. Shinkawa, K. Uchida, K. Matsushima, R. Ueda, N. Hanai, and K. Shitara, Defucosylated anti-CC chemokine receptor 4 IgG1 with enhanced antibody-dependent cellular cytotoxicity shows potent therapeutic activity to T cell leukemia and lymphoma, *Cancer Res.* 64, 2127–2133 (2004).
32. R. Niwa, S. Hatanaka, E. Shoji-Hosaka, M. Sakurada, Y. Kobayashi, A. Uehara, H. Yokoi, K. Nakamura, and K. Shitara, Enhancement of the antibody-dependent cellular cytotoxicity of low-fucose IgG1 is independent of FcγRIIIa functional polymorphism, *Clin. Cancer Res.* 10, 6248–6255 (2004).
33. R. Niwa, M. Sakurada, Y. Kobayashi, A. Uehara, K. Matsushima, R. Ueda, K. Nakamura, and K. Shitara, Enhanced natural killer cell binding and activation by low-fucose IgG1 antibody results in potent antibody-dependent cellular cytotoxicity induction at lower antigen density, *Clin. Cancer Res.* 11, 2327–2336 (2005).
34. R. Niwa, A. Natsume, A. Uehara, M. Wakitani, S. Iida, K. Uchida, M. Satoh, and K. Shitara, IgG subclass-independent improvement of antibody-dependent cellular cytotoxicity by fucose removal from Asn297-linked oligosaccharides, *J. Immunol. Methods* 306, 151–160 (2005).
35. A. Natsume, M. Wakitani, N. Yamane-Ohnuki, E. Shoji-Hosaka, R. Niwa, K. Uchida, M. Satoh, and K. Shitara, Fucose removal from complex-type oligosaccharide enhances the antibody-dependent cellular cytotoxicity of single-gene-encoded antibody comprising a single-chain antibody linked the antibody constant region, *J. Immunol. Methods* 306, 93–103 (2005).
36. R. Jefferis, Glycosylation of recombinant antibody therapeutics, *Biotechnol. Prog.* 21, 11–16 (2005).
37. S. Iida, H. Misaka, M. Inoue, M. Shibata, R. Nakano, N. Yamane-Ohnuki, M. Wakitani, K. Yano, K. Shitara, and M. Satoh, Non fucosylated therapeutic IgG1 antibody can evade the inhibitory effect of serum immunoglobulin G on antibody-dependent cellular cytotoxicity through its high binding to FcγIIIa, *Clin. Cancer Res.* 12, 2879–2887 (2006).
38. M. Satoh, S. Iida, and K. Shitara, Non-fucosylated therapeutic antibodies as next-generation therapeutic antibodies, *Expert Opin. Biol. Ther.* in press.
39. M. X. Sliwkowski, J. A. Lofgren, G. D. Lewis, T. E. Hotaling, B. M. Fendly, and J. A. Fox, Nonclinical studies addressing the mechanism of action of trastuzumab (Herceptin), *Semin. Oncol.* 26, 60–70 (1999).
40. G. D. Lewis, L. Figari, B. Fendly, W. L. Wong, P. Carter, C. Gorman, and H. M. Shepard, Differential responses of human tumor cell lines to anti-p185HER2 monoclonal antibodies, *Cancer Immunol. Immunother.* 37, 255–263 (1993).
41. Y. Vugmeyster, and K. Howell, Rituximab-mediated depletion of cynomolgus monkey B cells in vitro in different matrices: Possible inhibitory effect of IgG, *Int. Immunopharmacol.* 4, 1117–1124 (2004).
42. S. Preithner, S. Elm, S. Lippold, M. Locher, A. Wolf, A. J. da Silva, P. A. Baeuerle, and N. S. Prang, High concentrations of therapeutic IgG1 antibodies are needed to compensate for

inhibition of antibody-dependent cellular cytotoxicity by excess endogenous immnunoglobulin G, *Mol. Immunol.* 43, 1183–1193 (2006).
43. S. Kamoda, C. Nomura, M. Kinoshita, S. Nishiura, R. Ishikawa, K. Kakehi, N. Kawasaki, and T. Hayakawa, Profiling analysis of oligosaccharides in antibody pharmaceuticals by capillary electrophoresis, *J. Chromatogr. A* 1050, 211–216 (2004).
44. M. A. Schenerman, J. N. Hope, C. Kletke, J. K. Singh, R. Kimura, E. I. Tsao, and G. Folena-Wasserman, Comparability testing of a humanized monoclonal antibody (SynagisR) to support cell line stability, process validation, and scale-up for manufacturing, *Biologicals* 27, 203–215 (1999).
45. N. Uozumi, S. Yanagidani, E. Miyoshi, Y. Ihara, T. Sakuma, C. X. Gao, T. Teshima, S. Fujii, T. Shiba, and N. Taniguchi, Purification and cDNA cloning of porcine brain GDP-l-Fuc: N-acetyl-beta-d-glucosaminide alpha1,6-fucosyltransferase, *J. Biol. Chem.* 271, 27810–27817 (1996).

Selective Expansion of Genetically Modified T Cells Using a Chimeric IL-2 Receptor for Cancer Therapy

Takahiro Sogo, Masahiro Kawahara, Hiroshi Ueda, and Teruyuki Nagamune

Abstract T cells have been used for cancer immunotherapy because they play a central role in the cellular immunity. One approach to cure cancers is that tumor-specific T cells are activated in vitro and subsequently injected into patients. However, desired therapeutic effect has not been attained due to difficulty to maintain activated T cells for a prolonged period after injection. To solve this problem, we thought to use an interleukin (IL)-2-dependent growth signal in T cells for maintenance of activated T cells. If non-toxic molecules can substitute for the function of IL-2, genetically modified T cells can be expanded selectively without IL-2 and no side effect would occur. In this study, we replaced IL-2 binding domains of IL-2 receptor (IL-2R) β and γ chains by antibody variable regions recognizing a cognate antigen. Because these chimeric IL-2Rs could replace an IL-2-mediated signal by an antigen-mediated one, only the T cells with these chimeric receptors would grow in the presence of the cognate antigen but without IL-2.

Keywords T cell • IL-2 • IL-2 receptor • antibody variable region • chimeric receptor

1 Introduction

T cells are the major components of the immune defense system. $CD4^+$ helper T cells stimulate both the humoral and the cellular immunity through secreting various cytokines, whereas $CD8^+$ cytotoxic T lymphocytes (CTLs) directly attack as effector cells to virus-infected cells and the tumor cells. Therefore, a number of studies using T cells have been performed for cancer immunotherapy.

Adoptive transfer therapy is one approach for cancer immunotherapy using autologous T cells. In this therapy, tumor-specific T cells derived from patients are isolated, expanded in vitro and reinfused with a growth factor such as IL-2 for

T. Sogo, M. Kawahara, H. Ueda, and T. Nagamune
Department of Chemistry and Biotechnology, Graduate School of Engineering, The University of Tokyo, 7-3-1, Hongo, Bunkyo-ku, Tokyo, Japan

K. Ikura et al. (eds.), *Animal Cell Technology: Basic & Applied Aspects*,
Animal Cell Technology: Basic & Applied Aspects 15,
DOI 10.1007/978-1-4020-9646-4_2,

further expansion in vivo. However, desired therapeutic effect has not been attained due to difficulty to maintain activated T cells for a prolonged period after injection. It is essential for the effective immunotherapy to maintain as high proportion of tumor-specific T cells to circulating T cells as possible.

To overcome this problem, we focused on IL-2 as a factor that enables T cells to grow for the maintenance of tumor-specific T cells in vivo. IL-2 is a cytokine that was initially described as a T cell growth factor and was an early candidate for the immunotherapy of cancer. However, administration of high dose of IL-2 causes undesirable side effect such as inflammation because IL-2 also activates several other immune cells including NK cells, B cells, neutrophils, and macrophages.

Although IL-2 binds to a heterotrimeric receptor complex consisting of IL-2Rα, IL-2Rβ and IL-2Rγ chains, consequently induced heterodimer of IL-2Rβ and γ chains can transduce the proliferative signal to T cells. To specifically expand tumor-specific T cells, we use IL-2Rβ and γ chains to construct antibody/IL-2R chimeras that can mimic an IL-2-mediated growth signal with a nontoxic antigen-mediated one (Fig. 1a). We transfected these chimeric IL-2R genes into an IL-2-dependent murine T cell line CTLL-2 followed by culture in the medium including

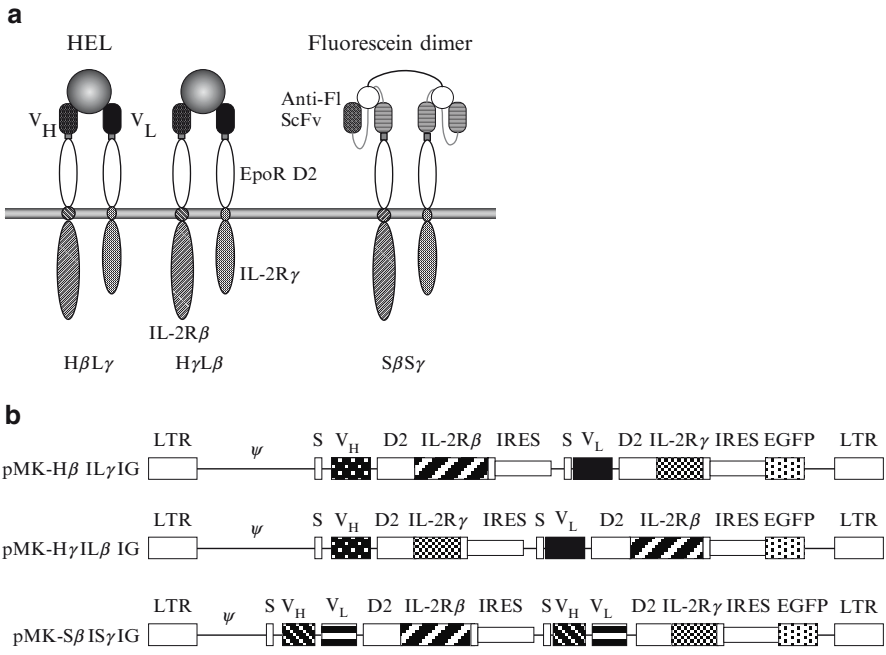

Fig. 1 The construct of chimeric receptors. **(a)** The schematic illustration of chimeric IL-2Rs. **(b)** The construction of chimeric IL-2R vectors. A retroviral vector with long terminal repeats (LTRs) and a packaging signal (Ψ) was used. An immunoglobulin heavy chain secretion signal sequence (S) is placed upstream of the chimeric receptor genes for surface expression of them. Each C-terminus of IL-2Rβ and IL-2Rγ was tethered with Flag tag and c-Myc tag, respectively, to detect chimeric IL-2Rs

an antigen as a ligand for chimeric IL-2Rs, resulting in selective expansion of genetically modified T cells.

2 Materials and Methods

2.1 Vector Construction

The expression vector pMXs-neo, encoding a neomycin-resistant gene, was kindly provided by Dr. T. Kitamura (University of Tokyo). In expression vector pMK-HβILγ-IG, Hβ or Lγ encodes VH or VL of anti-hen egg lysozyme (HEL) antibody HyHEL-10, human EpoR extracellular D2 domain, transmembrane and cytoplasmic domains of human IL-2Rβ or IL-2Rγ, respectively. In pMK-HγILβ-IG, VH or VL was linked with γ or β chain, respectively, considering conformational difference. pMK-SβISγ-IG encodes ScFv of anti-fluorescein (FL) antibody clone 31IJ3 instead of VH or VL in pMK-HβILγ-IG (Fig. 1b). Chimeric β chain, γ chain and enhanced green fluorescent protein (EGFP) are linked with internal ribosomal entry sites (IRESs) for coexpression.

2.2 Cell Culture

A murine T cell line CTLL-2 was cultured in RPMI 1640 medium (Nissui Pharmaceutical) supplemented with 10% FBS, 2 ng/ml murine IL-2 (GT), 1 mM sodium pyruvate, 50 μM α-thioglycerol and 20 nM bathocuproine disulfonate [1].

2.3 Vector Transfection and Selection of the Transfectants

CTLL-2 cells were transfected with chimeric IL-2R genes (pMK-HβILγ-IG, and pMK-HγILβ-IG) by electroporation, and transfected cells were designated as CT/HβLγ and CT/HγLβ, respectively. CTLL-2 cells were co-transfected with pMK-SβISγ-IG and pMXs-neo genes, and transfected cells were designated as CT/SβSγ. Cells (3×10^6 in 500 μl of RPMI medium) were transferred to a 0.4-cm gap cuvette. Twenty micrograms of chimeric IL-2R genes and 1 μg of pMXs-neo were used. Electroporations were performed at 300 V and 1,000 μF. The cells were inoculated into a 100 mm diameter dish in a complete medium and cultured in a 5% CO_2 incubator at 37°C.

Subsequently, CT/HβLγ and CT/HγLβ were selected in the media containing 2 μg/ml HEL (Seikagaku Corporation) or 2 ng/ml IL-2. CT/SβSγ was initially

selected in the medium containing 2 ng/ml IL-2 and 800 μg/ml G418 (Calbiochem), followed by selection in the medium with 5 μg/ml fluorescein-conjugated BSA (BSA-FL) (Sigma).

2.4 Cell Proliferation Assay

Cells were washed with PBS once and 10^4 cells were seeded into 24-well plates with indicated concentrations of each ligand. The viable cell numbers were counted by a hemocytometer and trypan blue exclusion assay.

2.5 Western Blotting

Western blot analysis was performed as described previously [2]. In brief, the cells were lysed with 100 μl of lysis buffer and incubated on ice for 10 min. The supernatant was mixed with Laemmli's sample buffer and boiled. The lysate was resolved by SDS-PAGE and transferred to a nitrocellulose membrane (Millipore). The blot was probed with appropriate dilutions of primary and secondary antibodies.

3 Results and Discussion

3.1 Selective Expansion of Genetically Modified Cells

CT/HβLγ and CT/HγLβ were washed with PBS, and selected in the media with HEL or IL-2. Because CT/SβSγ failed to expand selectively by direct antigen selection, they initially selected in the medium with IL-2 and G418 and subsequently with BSA-FL. Flow cytometric analysis revealed that EGFP-positive cell ratios of IL-2-selected cells were similar to those before selection while those of HEL- and BSA-FL-selected cells were almost 100% (data not shown).

To investigate whether cell proliferation in the selection medium with HEL or BSA-FL was induced by the expressed chimeric IL-2Rs, the amounts of expressed chimeric receptors was detected by Western blotting (Fig. 2). As a result, all selected cells expressed chimeric IL-2Rs whose expression levels were almost comparable.

These results show that only the cells transfected with the chimeric IL-2R genes can proliferate in response to the cognate ligand, leading to successful mimicry of an IL-2 signal in CTLL-2 cells.

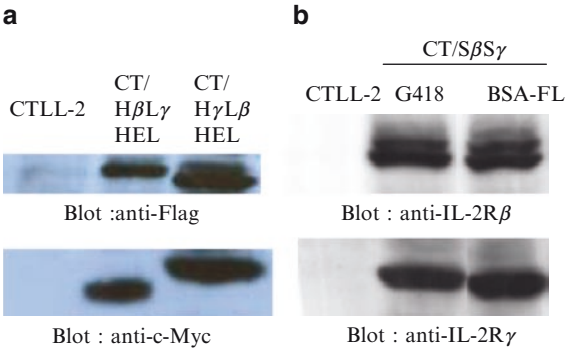

Fig. 2 Western blot analysis to confirm the chimeric IL-2R expression in selected transfectants. **(a)** The chimeric IL-2Rβ and IL-2Rγ expressions in CT/HβLγ and CT/HγLβ were detected with anti-Flag and anti-c-Myc antibodies, respectively. **(b)** The chimeric IL-2Rβ and IL-2Rγ expressions in CT/SβSγ were detected with anti-IL-2Rβ and anti-IL-2Rγ antibodies, respectively

3.2 Chimeric IL-2R Transduces a Proliferative Signal in Response to HEL or Fluorescein-Conjugated BSA (BSA-FL)

To determine whether growth of the selected cells is dependent on the cognate antigen or not, we performed a cell proliferation assay. Both CT/HβLγ and CT/HγLβ showed a HEL dose-dependent proliferation (Fig. 3a and 3b). The lower limits for HEL-dependent cell growth were 0.5 μg/ml and 0.1 μg/ml for CT/HβLγ and CT/HγLβ, respectively. CT/HγLβ grew more rapidly than CT/HβLγ at lower HEL concentrations. Such different ligand dependency might be due to conformational difference between these two chimeric IL-2Rs. CT/SβSγ also showed BSA-FL dose-dependent cell growth (Fig. 3c).

While CT/SβSγ was selected with BSA-FL, we attempt to use dimerized fluorescein (FL-dimer) as a small hapten ligand that might not induce immune response in vivo. To make FL-dimer, 5′-FL-labeled oligo-DNA with a palindromic sequence was self-annealed. Based on the X-ray crystallographic analysis of the peptide agonist-EpoR complex, oligo-DNA linker lengths were ranged from 8mer to 14mer. Interestingly, FL-dimer with a linker length of 11mer, 12mer or 13mer induced much higher cell growth than others (Fig. 4a). Thus, we used FL-dimer with 13mer linker as a representative to investigate dose dependency. The optimal 13mer concentration for the growth of CT/SβSγ was around 0.5 μM (Fig. 4b). The inhibitory effect of cell growth at higher concentration of FL-dimer might be due to the preferred formation of 1:1 FL-dimer/receptor complex suppressing receptor dimerization.

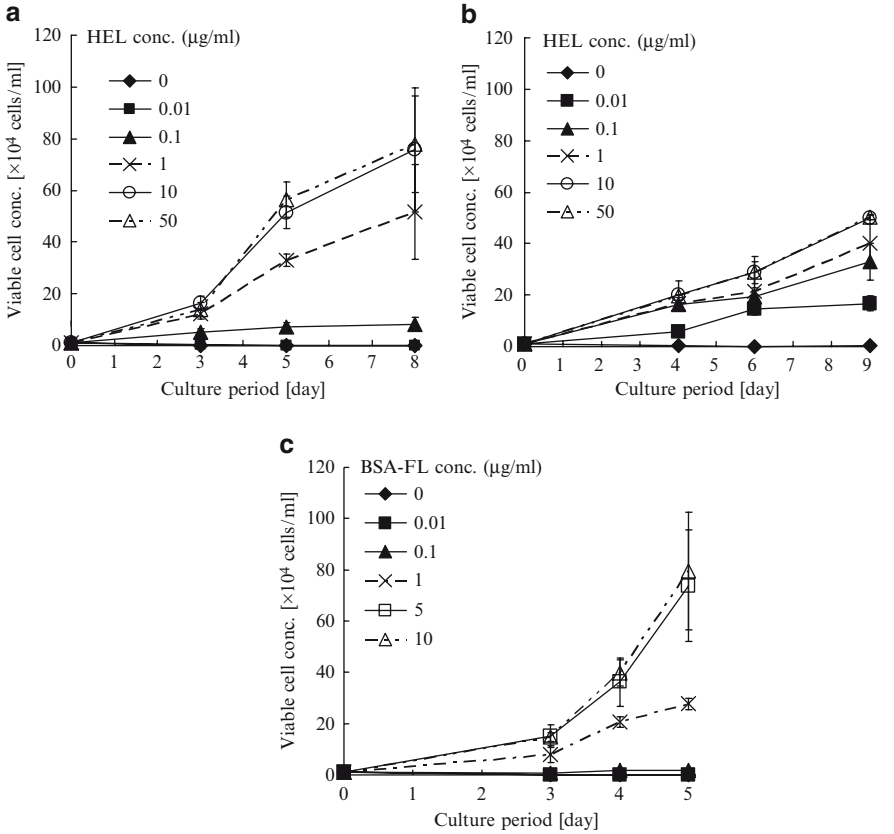

Fig. 3 Cell growth curves of transfected CTLL-2 cells. HEL selected CT/HβLγ **(a)**, CT/HγLβ **(b)** were cultured with various concentrations of HEL, whereas BSA-FL-selected CT/SβSγ (**c**) were cultured with BSA-FL. Viable cell concentration in triplicates was plotted with average and 1 S.D.

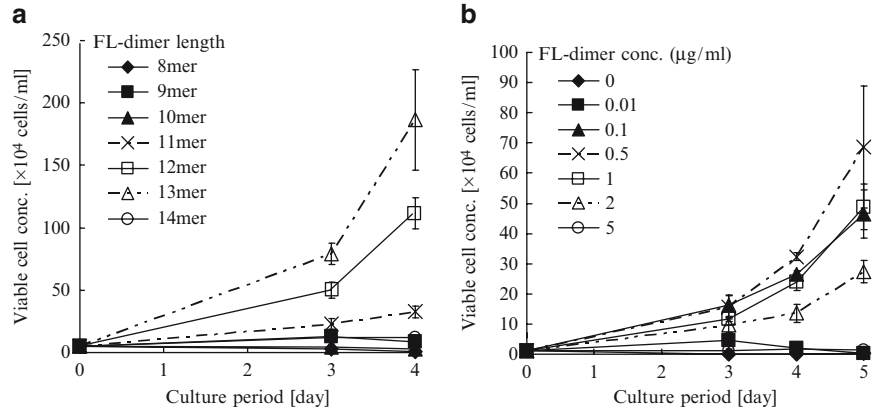

Fig. 4 FL-dimer dependency of CT/SβSγ cells. CT/SβSγ cells were cultured with 0.5 μM FL-dimer of various linker lengths **(a)** and various concentrations of FL-dimer with 13mer linker **(b)**

3.3 Signal Transduction of the Chimeric IL-2Rs

Heterodimerization of IL-2Rβ/IL-2Rγ subunits triggers downstream signaling events that involve the tyrosine phosphorylation of various cellular proteins. The IL-2 signaling activates three major pathways (Jak/STAT, Ras/MAPK, PI3K/Akt pathways) through cellular protein tyrosine kinases. Jak-mediated phosphorylation of signal transducers and activators of transcription (STATs) leads to their dimerization, resulting in translocation to the nucleus where they regulate gene transcriptions. IL-2 signaling also induces activation of phosphatidylinositol 3 kinase (PI3K) and its downstream effector Akt, and the tyrosine phosphorylation of IL-2Rβ results in the recruitment of Shc and Grb2, followed by activation of the Ras/MAPK pathway. The main functional outcomes of these signaling cascades are cell proliferation and cytoskeletal regulation.

To examine whether the chimeric IL-2Rs mimic IL-2 signaling or not, phosphorylations of STAT5, STAT3, and ERK1/2 were detected by Western blotting (Fig. 5). After cell depletion for 12 h, cells were stimulated for 15 min in the media with 2 ng/ml IL-2, 1 μg/ml HEL, or 5 μg/ml BSA-FL, or left unstimulated.

STAT3 and STAT5 were phosphorylated when CT/HβLγ and CT/HγLβ were stimulated with HEL and when CT/SβSγ were stimulated with BSA-FL at the similar levels to those stimulated with IL-2 (Fig. 5b and c). Although the ERK1/2 phosphorylation was also detected in all transfectants which were stimulated with their cognate ligands, the phosphorylation levels were less than those stimulated with IL-2 (Fig. 5a). This fact should be further confirmed but there was no

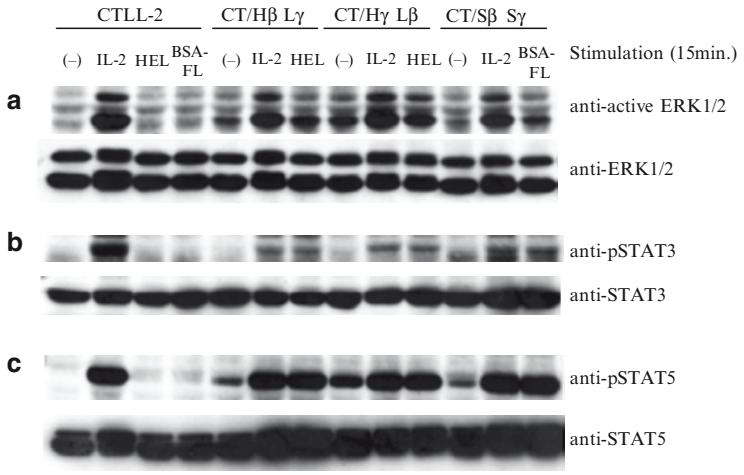

Fig. 5 Signal transcuction to ERK1/2, STAT3, and STAT5. **(a)** CTLL-2 and its transfectants were stimulated with IL-2 or cognate antigen, or left unstimulated, followed by Western blot analysis with anti-active ERK1/2 antibody and reprobed with anti-ERK1/2 antibody. Tyrosine phosphorylation of **(b)** STAT3 and **(c)** STAT5 was detected with anti-phospho-STAT3 and anti-phospho-STAT5 antibody, respectively

significant difference among signals from IL-2R and chimeric IL-2Rs on cell proliferation. CT/HγLβ cells showed phosphorylation of ERK and STAT5 even without stimulation. This effect may contribute to the higher sensitivity to HEL (0.01 μg/ml) in HγLβ chimera. These results indicated that the chimeric IL-2Rs can control CTLL-2 cell proliferation through transducing an IL-2-like growth signal in response to the specific antigen.

References

1. Brielmeier M. et al., Improving stable transfection efficiency: antioxidants dramatically improve the outgrowth of clones under dominant marker selection. Nucleic Acids Res., **26**, 2082–2085 (1998).
2. Kawahara M. et al., Selection of genetically modified cell population using hapten-specific antibody/receptor chimera. Biochem. Biophys. Res. Commun., 315, 132–138 (2004).

Effects of Serum and Growth Factors on HEK 293 Proliferation and Adenovirus Productivity

Angela Buckler and Mohamed Al-Rubeai

Abstract The effect of serum on cell growth and virus production in both basal and serum free media was examined in Human Embryonic Kidney (HEK) 293. A 40-fold decrease in virus titre was observed in Dulbecco's Modified Eagles Medium (DMEM) cultures supplemented with 10% FBS when compared to 1% FBS. However, a 90-fold increase in virus titre was observed in DMEM supplemented with 1% FBS as compared with EX-CELL™ 293 serum free culture. A similar effect was also seen for the efficiency of gene transfer as indicated by the expression level of GFP. The results demonstrated that although serum at higher concentrations has a negative and dose-dependent effect on titre its supplementation in small quantity is essential for virus productivity. The effect of Insulin-like growth factors on proliferation of HEK 293 cells as well as on infection and specific productivity was also studied in serum free media. It was found that LONG™ R^3 IGF-1, an analogue of IGF-1 promotes cell proliferation and viability more effectively than Insulin and IGF-1. Similarly, cultures supplemented with LONG™ R^3 IGF-1 showed relatively higher virus productivity in comparison to other supplemented cultures but virus productivity was found to be significantly ($p < 0.05$) higher when there were no growth factors at all.

Keywords Serum • HEK 293 • adenovirus • growth factors

1 Introduction

The HEK 293 cell line came about from Kidney cells derived from an aborted human foetus and produced by transfection of sheared Adenovirus human type 5 DNA so they contain the E1 gene needed for viral replication [1]. These cells are

A. Buckler
Department of Chemical Engineering, University of Birmingham, Birmingham, B15 2TT, UK

M. Al-Rubeai
School of Chemical and Bioprocess Engineering, University College Dublin, Belfield, Dublin 4, Ireland

K. Ikura et al. (eds.), *Animal Cell Technology: Basic & Applied Aspects*,
Animal Cell Technology: Basic & Applied Aspects 15,
DOI 10.1007/978-1-4020-9646-4_3,

widely used in cell biology research and particularly in the propogation of adenovirus vectors. Adenoviruses are used in gene therapy so high production levels of these vectors are important.

HEK 293 cells can be grown as an attached culture in basal medium, typically DMEM, supplemented with serum. They can also be adapted to serum free media, which is more desirable than serum containing media for the production of biotherapeutics due to the risks and regulations associated with serum.

Serum free media is normally supplemented with a variety of components, including hormones and growth and attachment factors. For example Insulin is known to be essential for cell proliferation in serum free culture [2]. Along with insulin there are a variety of Insulin like growth factors available, which also stimulate cell proliferation. IGF-1 and Insulin belong to the same family of structurally related acid peptides and so have similar tertiary structures [3]. LONG™ R^3 IGF-1 was created for use in cell culture by substituting the third amino acid of IGF-1 with an arginine and adding a 13 amino acid N-terminal extension [2, 4]. LONG™ R^3 IGF-1 is used to provide an inexpensive yet high quality potent IGF-I analog for use as a growth factor supplement for serum-free or reduced-serum culture media.

Most cell types secrete IGF binding proteins in various forms [2, 3], which inhibit the activity of IGF-1 by requisitioning the peptide and preventing interactions between IGF-1 and IGF-1 receptor [3]. LONG™ R^3 IGF-1 avoids this problem due to the amino acid substitution which allows for LONG™ R^3 IGF-1 having a 100-fold reduced affinity for IGF binding proteins, making it a more potent growth factor which elicits similar responses to IGF-1 and insulin but at much lower concentrations [2, 4].

In this study we investigated the effect of serum in both basal and serum free cultures on cell proliferation and adenovirus productivity. Since serum free media is more desirable than serum containing media and that growth factors are essential components of both media we compared the effect of LONG™ R^3 IGF-1, insulin and IGF-1 on proliferation of HEK 293 cells as well as on infection and specific productivity of Adenovirus.

2 Results and Discussion

2.1 Effect of Serum Concentration on Cell Number and Viability in Basal and Serum Free Media

Table 1 shows the maximum cell growth of HEK 293 cells in EX-CELL™ 293 and DMEM + different concentrations of serum on day 6 of a batch culture run over a period of 10 days. These data clearly show that when serum is not added to basal medium no cell growth is accomplished and that serum produces maximum cell growth when added at concentrations between 5% and 10%. It also shows that cells grow well in serum free media and when serum is added at low concentrations, i.e. 1% and 5% in contrast to 10% where reduced cell numbers is obtained.

Table 1 Values represent the average of three batches and show the maximum cell growth and viability taken on day 6 of a batch culture

Culture	Average Cell Growth ($\times 10^6$ mL^{-1})	Average Viability (%)
EX-CELL™ 293	1.4	83
EX-CELL™ 293 + 1% FBS	2.0	82
EX-CELL™ 293 + 5% FBS	1.8	83
EX-CELL™ 293 + 10% FBS	1.2	84
DMEM	0.03	8
DMEM + 1% FBS	1.1	14.4
DMEM + 5% FBS	1.45	85.5
DMEM + 10% FBS	1.9	88.7

The viability of the cultures in EX-CELL™ 293 is consistently high whereas in cultures grown in basal medium and with 1% FBS the viability is poor.

2.2 Effect of Serum Concentrations on Virus Productivity

Table 2 shows the amount of virus produced in HEK 293 cells in EX-CELL™ 293 and DMEM + different concentrations of serum after a 96 h period. The virus titre was measured by flow cytometry according to the protocol reported by Gueret et al. [5].

2.3 The Effect of Insulin and Insulin-Like Growth Factors on Propagation

Table 3 shows the cell growth and viability of HEK 293 cells in EX-CELL™ 293 with insulin like growth factors over a period of 10 days. Previous experimental work determined the optimum concentrations of these growth factors (data not shown). These data clearly show that LONG™ R^3 IGF-1 was able to increase cell proliferation significantly more than other growth factors when used individually or in combination. The viability of the LONG™ R^3 IGF-1 dropped more dramatically at the end of the culture, which was probably due to limiting nutrients in the culture.

2.4 The Effect of Insulin and Insulin-Like Growth Factors on Virus Productivity

Table 4 shows the virus titre obtained in HEK 293 cells that were previously grown and infected in media containing a variety of growth factors. When no growth

Table 2 Virus productivity (gfu mL^{-1}) at 96 h post infection

Culture	Virus Titre (gfu mL^{-1})
EX-CELL™ 293	2.58×10^7
EX-CELL™ 293 + 1% FBS	4.06×10^7
EX-CELL™ 293 + 5% FBS	2.11×10^7
EX-CELL™ 293 + 10% FBS	1.74×10^7
DMEM	9.34×10^8
DMEM + 1% FBS	2.57×10^9
DMEM + 5% FBS	7.41×10^8
DMEM + 10% FBS	2.29×10^8

Table 3 Values represent the average of three batches and show the maximum cell growth and viability taken on day 6 of a batch culture

Culture	Average Cell Growth ($\times 10^5$ mL^{-1})	Average Viability (%)
LONG™ R^3 IGF-1 + INSULIN	15.53	72.3
IGF-1 + INSULIN	14.96	62.67
INSULIN	6.96	70.66
IGF-1	14.73	68.66
W/O growth factor	3.26	55
EX-CELL™ 293	18.66	76.6
LONG™ R^3 IGF-1	30.7	78.7

Table 4 Virus productivity (gfu mL^{-1}) at 96 h post infection

Culture	Virus Titre (gfu mL^{-1})
LONG™ R^3 IGF-1 + insulin	1.74×10^7
IGF-1 + insulin	1.39×10^7
Insulin	1.30×10^7
IGF-1	1.10×10^7
W/O growth factors	2.82×10^7
EX-CELL™ 293	2.37×10^7
LONG™ R^3 IGF-1	2.571×10^7

factors were present the virus titre was higher than cultures containing growth factors. LONG™ R^3 IGF-1 produces the next highest number of virus particles. We reasoned that due to the presence of IGF-1 and Insulin in the media the cells were secreting IGF binding proteins, which were then binding to the IGF-1 and Insulin molecules and causing non-specific binding of the virus so that it could not infect the cells. The reason for the higher virus titres produced in cultures with no growth factors is that no IGF binding protein is produced. Similarly in culture supplemented with LONG™ R^3 IGF-1 a lower binding affinity for IGF BP's resulted in a fewer complexes for the virus to bind to and consequently inactivated leading to a higher virus titre.

3 Conclusions

In serum free medium we have shown that LONG™ R^3 IGF-1 promotes cell proliferation more effectively than IGF-1 and/or insulin in serum free condition. The results obtained show that when there are no growth factors present in serum free media the cells die at a consistent rate in a shorter period of time. The results also confirm that growth factors are important in preventing cell death and that LONG™ R^3 IGF-1 is the most effective growth factor in maintaining viability when compared to Insulin and IGF-1.

It has been also shown that serum has a negative dose dependent effect on virus production, although it is essentially to be added in small dose (i.e. 1%) to achieve high productivity. In general, basal media containing serum produces higher virus titres than complete serum free media, although it is not clear why this is the case. A possibility could be that the growth factors are acting as weak inhibitors of virus activity through a mechanism involves secreted IGF binding proteins.

References

1. Graham, F. L. et al. (1977) Characteristics of a Human Cell Line Transformed by DNA from Human Adenovirus Type 5. *Journal of General Virology* **36** (1): 59–72.
2. Yandell, C. et al. (2004) An Anolgue of IGF-1. A Potent Substitute for Insulin in Serum-Free Manufacture of Biologics by CHO Cells. *Bioprocess International* 56–64.
3. Sunstrom, N. A., Baig, M., Cheng, L., Sugyiono, D. P., and Gray, P. (1998) Recombinant Insulin-Like Growth Factor-I (IGF-1) Production in *Super*-CHO Results in the Expression of IGF-1 receptor and IGF Binding Protein 3. *Cytotechnolgy* **28**: 91–99.
4. Francis, G. L., Ross, M., Ballard, F. J., Milner, S. J., Senn, C., McNeil, K. A., Wallace, J. C., King, R. and Wells, J. R. (1992) Novel Recombinant Fusion Protein Analogues of Insulin-Like Growth Factor (IGF)-I Indicate the Relative Importance of IGF-Binding Protein and Receptor Binding for Enhanced Biological Potency. *Journal of Molecular Endocrinology* **8** (3): 213–223.
5. Gueret, V., Negrete-Virgen, J. A., Lyddiatt, A. and Al-Rubeai, M. (2002) Rapid Titration of Adenoviral Infectivity by Flow Cytometry in Batch Culture of Infected HEK 293 Cells. *Cytotechnology* **38**: 87–97.

Simple and Efficient Establishment of Recombinant Protein Hyper-Producing Cells by Using RAS-Amplified CHO Cell Line

Tsukasa Fujiki, Toshiki Matsuo, Makiko Yamashita, Yoshinori Katakura, Shin-Ei Matsumoto, Kiichiro Teruya, and Sanetaka Shirahata

Abstract Chinese hamster ovary (CHO) cells is a widely used host cell line and can mass-produce recombinant proteins by using various amplifiable selectable marker gene and selection drugs. However, the establishment of highly productive cell line is a laborious and time-consuming work. In the present study, we developed a novel efficient method. We transfected CHO cells with plasmid expressing a gene of interest along with that expressing cell surface marker protein, and we selected recombinant CHO cells by their expression of cell surface marker protein and seed them into 96-well plates by single cell sorting. This method enabled a rapid and efficient establishment of recombinant CHO cells without drug selection. Furthermore, by using ras-amplified CHO cell line (CHO-hp1) as host cells, recombinant protein hyper-producing CHO cells can be easily obtained within a relatively short period. Actually, larger number of recombinant clones were obtained by using CHO-hp1 cells as host cells (188 clones/1,000 seeded wells), while clones cannot be obtained by using conventional CHO cells as host cells (0 clones/1,000 seeded wells). Furthermore, these recombinant cells obtained from CHO-hp1 cells demonstrated higher productivity (45 μg/10^6 cells/day). These results demonstrate that this method enables a rapid and efficient establishment of recombinant protein hyper-producing cell lines, and can be applicable to production of various recombinant proteins.

Keywords Antibody • recombinant protein production • CHO

1 Introduction

Mammalian cells are useful host cells for producing complex and/or glycosilated form of recombinant proteins for clinical applications. Chinese Hamster ovary (CHO) dihydrofolate reductase ($DHFR^-$) cells [1] is a most popularly used host cell

T. Fujiki, Y. Katakura, Shin-Ei Matsumoto, K. Teruya, and S. Shirahata
Faculty of Agriculture, Kyushu University, 6-10-1 Hakozaki, Higashi-ku, Fukuoka, 812-8581, Japan

T. Matsuo, M. Yamashita, Y. Katakura, and S. Shirahata
Graduate School of Systems Life Sciences, Kyushu University, 6-10-1 Hakozaki, Higashi-ku, Fukuoka, 812-8581, Japan

K. Ikura et al. (eds.), *Animal Cell Technology: Basic & Applied Aspects*,
Animal Cell Technology: Basic & Applied Aspects 15,
DOI: 10.1007/978-1-4020-9646-4_4, © Springer Science + Business Media B.V. 2009

line and can mass-produce recombinant proteins by using amplifiable selectable marker gene of DHFR and selection drug of methotrexate (MTX) [2–4]. However, even by using this method, it is laborious and time-consuming task to establish highly productive cell lines. These backgrounds promoted us to develop an oncogene-activated production (OAP) system which enables rapid establishment of recombinant protein hyper-producing cell lines. The OAP system is constructed by introducing a reporter plasmid carrying a gene of interest and effector plasmids carrying oncogenes into host cells. Previously, we have optimized the combination between oncogenes and promoters used in the OAP system. Among the combinations tested, the most suitable combination for efficient protein production was found to be the c-Ha-ras oncogene and the cytomegalovirus immediate early (CMV) promoter [5]. In this combination, c-Ha-ras oncoprotein is thought to affect and enhance the transcriptional ability of the CMV promoter which drives the transcription of the gene of interest. Furthermore, to rapidly and easily establish recombinant proteins hyper-producing cell lines, we primed CHO cells with c-Ha-ras oncogene and further amplifying the copy number with MTX, and named CHO-hp1 cells. In this study, we tried to develop a method to establish recombinant hyper-producing cells by using CHO-hp1 cells.

2 Materials and Methods

2.1 Cells and Cell Culture

CHO cells lacking the dhfr gene were cultured in Dulbecco's modified Eagle's medium (DMEM) (Nissui Oharmaceutical, Tokyo, Japan) supplemented with 0.1 mM hypoxanthine (Invitrogen, CA) and 0.016 mM thymidine (Invitrogen, CA) with 5% FBS. The CHO cells transfected with pCMVD-c-Ha-ras was cultured in DMEM with 5% dialyzed FBS and 50 nM methotrexate (MTX) (Sigma, St. Louis, MO, USA). Cells were cultured in 5% CO_2/95% air atmosphere at 37°C.

2.2 Establishment of Recombinant CHO Cells

CHO cells were cotransfected with pCMV-AE6F4, pSV2-bsr and pMACS4.1-CD4 (Miltenyi Biotec, Germany) by LipofectAmine™ Reagent (Invitrogen, USA). Then cells were harvested after 48 h post transfection and selected by Magnetic Cell Sorting (MACS). The next day, 5 μg/ml of blasticidin S (Funakoshi, Tokyo, Japan) was added to the medium. Single clones were isolated using limiting dilution cloning or FACSAria cell-sorting system (BD bioscience, CA, USA). Production of AE6F4 was evaluated by ELISA. We previously established a ras amplified CHO cell line named CHO-hp1, which was derived from CHO cells transfected with pCMV-c-Ha-ras [6]. In this study, pCMV-AE6F4 was also introduced into the CHO-hp1 as above.

2.3 Determination of the Concentration of Secreted AE6F4 Antibody

Cell-culture supernatants were assayed by sandwich ELISA using goat anti-human λ polyclonal antibody (TAGO, Burlingame, CA, USA) as capturing antibody and peroxidase-labeled goat anti-human λ polyclonal antibody (TAGO) as detecting antibody.

3 Results and Discussion

3.1 Evaluation for Availability of the CHO-hp1 Cell at the Single Cell Cloning

We introduced pCMV-AE6F4 which express AE6F4 antibody protein under the control of CMV promoter, along with the selection marker gene pSV2-bsr into the CHO cells lacking the dhfr gene. After transfection, transfected CHO cells were immediately isolated using limiting dilutional cloning and selected with blasticidine S and performed the dhfr gene amplification by MTX addition. We cannot obtain the recombinant clones (0 clones/1,000 seeded wells) by limiting dilution cloning (Fig. 1). Then, we demonstrated CHO cell lines transfected with ras-oncogene

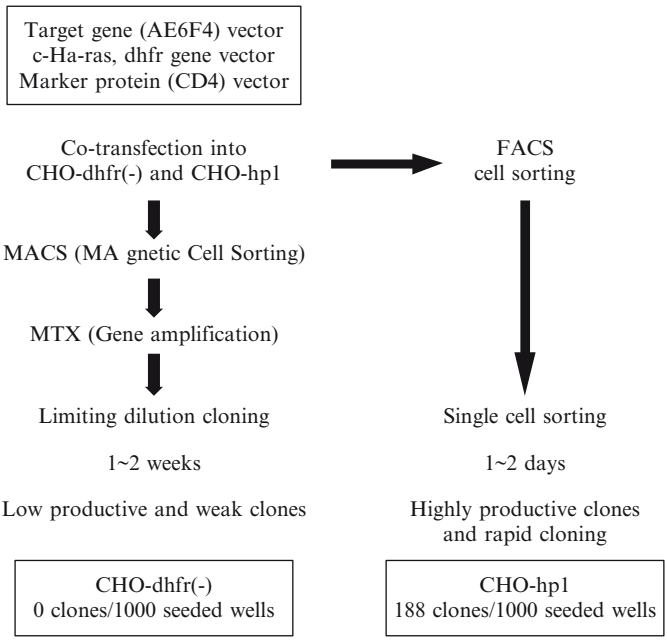

Fig. 1 The method of the establishment of highly productive cell line

and the dhfr gene, named CHO-hp1 cells. The number of clones established from CHO-hp1 cells was found to increase. The cloning efficiency was further enhanced by single cell sorting (188 clones/1,000 seeded wells) (Fig. 1).

3.2 *Evaluation of Marker Protein for the Isolation of Single Cell Cloning*

The usage of CHO-hp1 cells instead of CHO cells lacking the dhfr gene enhanced the efficiency of cloning on both limiting dilution and single cell sorting. We anticipated that the high expression of marker protein might indicate high expression of recombinant protein because of using same CMV promoter regulating target genes. Then we introduced marker protein to select higher productive clones from bulk culture. pMACS4.1 vector was transfected into CHO cells to select by anti-CD4-FITC antibody with FACS. The higher intensity of anti-CD4 FITC fluorescence showed about 12.6% in total transfected CHO cells (Data not shown). We isolated single cell clone utilizing CD4 marker protein from higher fluorescent intensity by FACS. Here the selection by marker protein and utilization of CHO-hp1 shortens the period for selection from a few weeks to a few days (Fig. 1). We anticipate that this shortening of the selection period might improve the efficiency for obtaining hyper-producing cells from bulk culture.

3.3 *Evaluation for Productivity of AE6F4 in Hyper-Producing Cell Line*

We have established single cell clones of AE6F4 producing cell using CHO-hp1 cell and selection marker protein. In order to evaluate the productivity, we measured

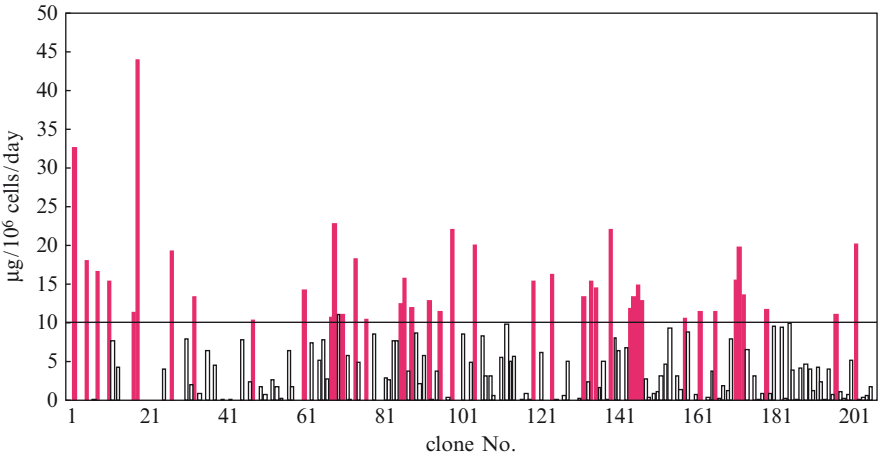

Fig. 2 Efficient establishment of human antibody hyper-producing cells

the amount of recombinant protein AE6F4 antibody by sandwich ELISA. To evaluate the productivity of AE6F4 expression, we calculated by antibody production and cell number per each wells and established 188 clones per 1,000 wells (Fig. 1). The highest productivity of AE6F4 antibody in recombinant cell lines of 188 clones demonstrated 45 μg/10^6 cells/day.

We have established a useful host cell line termed CHO-hp1 cell, which enable us to rapidly establish recombinant protein hyper-producing cell lines. These results demonstrate that this method enables a rapid and efficient establishment of recombinant protein hyper-producing cell lines, and can be applicable to production of various recombinant proteins.

References

1. Urlaub G and Chasin LA (1980) Isolation of Chinese hamster cell mutants deficient in dihydrofolate reductase activity. *Proc Natl Acad Sci USA* 77: 4216–4220.
2. Kemball-Cook G, Garner I, Imanaka Y, Nishimura T, O'Brien DP, Tuddenham EGD and McVey JH (1994) High-level production of human blood coagulation factors VII and XI using a new mammalian expression vector. *Gene* 139: 275–279.
3. Kim NS, Kim SJ and Lee GM (1998) Clonal variability within dihydrofolate reductase-mediated gene amplified Chinese hamster ovary cells: Stability in the absence of selective pressure. *Biotechnol Bioeng* 60: 679–688.
4. Lucas BK, Giere LM, DeMarco RA, Shen A, Chisholm V and Crowley CW (1996) High-level production of recombinant proteins in CHO cells using a dicistronic DHFR intron expression vector. Nucleic Acids Res 24: 1774–1779.
5. Yano T, Teruya K, Shirahata S, Watanabe J, Osada K, Tachibana H, Ohashi H, Kim E-H and Murakami H (1994) Ras oncogene enhances the production of a recombinant protein regulated by the cytomegarovirus promoter in BHK-21 cells. *Cytotechnology* 12: 1–12.
6. Katakura Y, Seto P, Miura T, Ohashi H, Teruya K and Shirahata S (1999) Productivity enhancement of recombinant protein in CHO cells via specific promoter activation by oncogenes. *Cytotechnology* 31: 103–109.

Effects of Sericin on Promoting Proliferation and Inhibiting Apoptosis of Mammalian Cells

Kana Yanagihara, Masao Miki, Akiko Ogawa, Masahiro Sasaki, Hideyuki Yamada, and Satoshi Terada

Abstract We have previously reported that sericin improves proliferation of all cells tested, as well suppressing cell death induced by heat stress, implying that sericin inhibits apoptosis. In sericin treatment, caspase7/3 activity, executioners for inducing apoptosis, was decreased, while caspase9 activity was not. In order to analyze the mode of action of sericin in detail, the gene expression pattern was studied by transcriptome analysis using cDNA microarrays. The expression of several genes was significantly upregulated, and others were downregulated by sericin treatment. Among the detected genes, some growth- and apoptosis-related genes may be involved in the proliferative and survival effects of sericin.

Keywords Sericence • apoptosis • caspase • transcriptome analysis

1 Introduction

Mammalian cell culture is widely used for production of various bio-active proteins and gene therapy vectors. However, current mammalian cell culture systems face various challenges, including the requirement of serum-free culture. Although serum and its derivatives are effective for mammalian cells, they also have several disadvantages, such as high cost and concerns about the risk of bovine spongiform encephalopathy. Therefore, an economical and safe mitogenic supplement is desired, in order to improve mammalian cell culture.

We focused on sericin, one of the main components of virgin silk, as such a mitogenic supplement. We have previously reported that it improves proliferation and survival of all cells tested [1, 2]. We have also shown that sericin improves cultures for the production of adenovirus-based gene-therapy vectors [3]. In this study, we investigated cell proliferation under conditions of growth factor starva-

K. Yanagihara, M. Miki, and S. Terada
Department of Applied Chemistry and Biotechnology, University of Fukui 3-9-1, Bunkyo, Fukui, 910-8507, Japan

A. Ogawa, M. Sasaki, and H. Yamada
SEIREN Co. Ltd., 48-113-2, Yonozu, Mikuni-Cho, Sakai, Fukui, 913-0038, Japan

K. Ikura et al. (eds.), *Animal Cell Technology: Basic & Applied Aspects*,
Animal Cell Technology: Basic & Applied Aspects 15,
DOI 10.1007/978-1-4020-9646-4_5,

tion, preventing heat stress-induced cell death, intercellular caspase activity, and gene expression in the presence of sericin, in order to elucidate the mechanism of action of sericin in cell proliferation and survival.

2 Materials and Methods

2.1 Preparation of Sericin

Sericin hydrolysate with an average molecular weight of 30 kDa was prepared by boiling cocoon shells under alkaline conditions [4], and then drying to a powder. Sericin was dissolved in medium at 0.1% concentration.

2.2 Cell Line and Culture Conditions

A mouse hybridoma 2E3-O cell line was grown in serum-free medium ASF103 (Ajinomoto, Japan) at 37°C in a humidified atmosphere of 5% CO_2 in air [5].

2.3 Cell Proliferation Assay

To assay the effect of sericin on proliferation under conditions of growth factor starvation, 2E3-O cells were seeded at a density of 13×10^5 cells in 6 ml ASF104 medium (Ajinomoto) with reduced growth supplements. After 12 h, the culture was added with 2 ml supplement-free ASF104 medium containing 0.1% sericin. Viable cell density was measured by counting using the trypan blue dye exclusion method, under phase-contract microscopy at several time points for 37 h.

2.4 Cell Death Induced by Heat Stress

To estimate the anti-apoptotic effect of sericin on heated cells, 2E3-O cells were seeded at a density of 2.5×10^4 cells into a 1.5 ml tube in 100 μl ASF104 medium containing 0.1% sericin. The sample tubes were heated at 46–48°C for 5–30 min in a water bath. After 30 min incubation at 37°C, cell survival was determined by counting using the trypan blue dye.

2.5 Caspase Activity

To examine caspase activity, 2E3-O cells were seeded at a density of 7.0×10^3 cells in 80 μl ASF104 medium with reduced growth supplements and cultured in 96-well

plates (Sumitomo Bekelito, Japan). After 12 h, the culture was added to 20 μl supplement-free ASF104 medium containing 0.1% sericin. At 12 h after sericin treatment, caspase activity was measured with Caspase-Glo™ Assay kit (Promega, USA). Briefly, Caspase-Glo™ reagent, proluminescent substrate containing the DEVD sequence, was added to 96-well sample plates. The sample plates were incubated for 1 h, and then a substrate for luciferase was released through cleavage of the proluminescent substrate by the caspases in the samples, resulting in a luciferase reaction. The luminescence was measured by luminometer.

2.6 Transcriptome Analysis

The gene expression pattern was measured by cDNA microarray analysis. 2E3-O cells were seeded at a density of 1.3×10^6 cells in 6 ml ASF104 medium with reduced growth supplements. After 12 h, the culture was added to 2 ml supplement-free ASF104 medium containing 0.1% sericin. At 12 h after sericin treatment, total RNA was extracted from the cells individually using the acid guanidinium/phenol extraction method, and mRNA was extracted from total RNA by Oligotex™ –dT30 mRNA Purification kit (Takara Bio, Japan). mRNA (2.5 μg) from cells cultured in the absence of sericin was labeled during reverse transcription with Cy3-dUTP, while 2.5 μg mRNA from cells treated with sericin was labeled with Cy5-dUTP to make cDNA probes. cDNA probes from both preparations were mixed and hybridized to a cDNA microarray, IntelliGene™ II Mouse CHIP with 4,277 cDNA fragments of mouse genes (Takara Bio). After filtration, separate images from each fluorescent signal were scanned by an Affymetrix 428 Array Scanner. The scanning images were analyzed using BioDiscovery ImaGene, and the gene expression regulated by sericin treatment was determined.

3 Results and Discussion

3.1 The Effect of Sericin on Cell Proliferation and Survival

3.1.1 The Effect of Sericin on Proliferation During Growth Factor Starvation

We have previously reported that sericin has mitogenic activity in all mammalian cells tested [1, 2]. To estimate the effect of sericin on cell proliferation, hybridoma 2E3-O cells were cultured without any growth factors but sericin. Figure 1 shows that the viable cell density was increased in the presence of sericin, whereas in the absence of sericin, the viable cell density was not increased for 24 h, and then decreased.

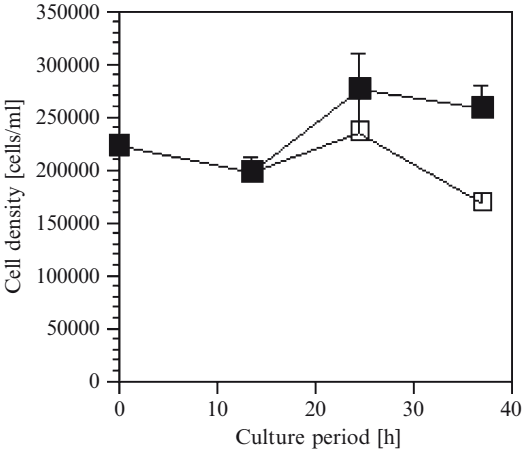

Fig. 1 Effect of sericin on proliferation of 2E3-O cells under conditions of growth factor starvation. 2E3-O cells were seeded in ASF104 medium with reduced growth supplements. After 12 h, culture was supplemented with 0.1% sericin (closed squares) or not (open squares). Viable cell density was determined at several time points for 37 h

Table 1 Effect of sericin on heat stress-induced cell death

Cell Survival (%)	5 min	10 min	20 min	30 min
46°C		89.3		
		(75.8*)		
47°C	91.0	85.8		41.8
	(85.3*)	(59.4*)		(38.9*)
48°C		68.7	45.9	20.7
		(58.7*)	(47.9*)	(21.1*)

Asterisk indicates cell survival in the absence of sericin.

3.1.2 Effect of Sericin on Heat Stress-Induced Cell Death

Cell survival in the presence of sericin was determined after heat stress (Table 1). Sericin successfully improved cell survival under heat stress.

3.2 Mechanism of Action of Sericin

3.2.1 Effect of Sericin on Caspase Activity

Sericin suppressed cell death, therefore, we examined whether sericin inhibited caspase activity. Figure 2 shows that activity of caspase3/7, an executioner for inducing apoptosis, was decreased by sericin treatment. In contrast, caspase9 activity

was not decreased by sericin (data not shown). These results suggest that sericin suppressed apoptosis via suppression of caspase3/7.

3.2.2 Detection of Genes Involved in the Mode of Action of Sericin

To analyze the mode of action of sericin in detail, we examined the gene expression pattern from 2E3-O cells by utilizing cDNA microarrays. The expression of several genes was significantly regulated by sericin treatment. Table 2 shows that growth- and apoptosis-related genes were regulated by sericin, suggesting that these genes may be involved in the mechanism of sericin on cell proliferation and survival.

Acknowledgements We thank Ms. Y. Tanaka and Ms. M. Sassa for their helpful advice.

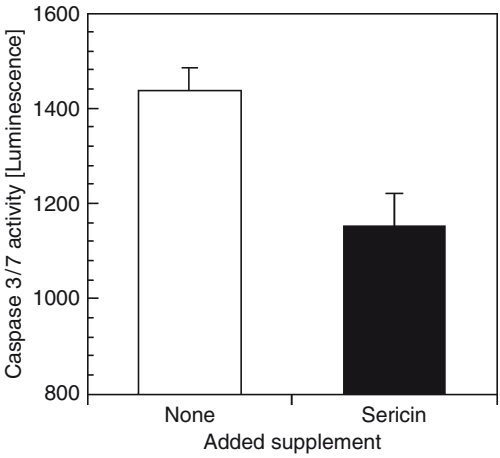

Fig. 2 Inhibition of caspase3/7 activity by sericin. 2E3-O cells were seeded in ASF104 medium with reduced growth supplements, and cultured in 96-well plates. After 12 h, the culture was supplemented with 0.1% sericin (closed bar) or not (open bar). Caspase3/7 activity was measured 12 h after sericin treatment

Table 2 Up- or down-regulated genes in sericin treatment

Function	Gene
Proliferation and growth suppression	cyclinD2
	DDA3
	HCK
Cell survival and apoptosis	fatso
	InSrr
	ASK1
	caspase7

References

1. S. Terada, T. Nishimura, M. Sasaki, H. Yamada, M. Miki (2002) Cytotechnology, 40, 3–12.
2. S. Terada, M. Sasaki, K. Yanagihara, H. Yamada (2005) J. Biosci. Bioeng., 100, 667–671.
3. K. Yanagihara, S. Terada, M. Miki, M. Sasaki, H. Yamada (2006) Biotechnol. Appl. Biochem., 45, 59–64.
4. N. Kato, S. Sato, A. Yamanaka, H. Yamada, N. Fuwa, M. Nomura (1998) Biosci. Biotechnol. Biochem., 62, 145–147.
5. F. Makishima, S. Terada, T. Mikami and E. Suzuki (1992) Cytotechnology, 10, 15–23.

Molecular Biological Analysis of Mitogenic and Anti-Apoptotic Mechanisms of Sericin

Takuya Saito, Akiko Ogawa, Masahiro Sasaki, Hideyuki Yamada, and Satoshi Terada

Abstract We have previously reported that the silk protein sericin has mitogenic activity in all cells tested, as well as preventing cell death from several stimuli such as hyperthermia. The mechanism of how sericin induces cell proliferation and suppresses cell death has not been established. In order to identify which proteins are induced by sericin, and which signaling pathway is involved, we performed proteome analysis using two-dimensional electrophoresis, and several spots were detected. This result indicates that sericin treatment affects the cells and alters their protein expression. Further study will identify these spots, resulting in definition of the signaling pathways involved in protein induction by sericin.

Keywords Sericin • proteome analysis • two-dimensional electrophoresis (2-DE)

1 Introduction

Currently, fetal bovine serum (FBS) is used extensively in cell culture, but it has various problems, such as the risk of contamination with viruses and prions. Therefore, a novel factor for cell culture is needed.

We have previously reported the effectiveness of silk protein sericin, which is removed by alkali treatment during the purification of raw silk, as a growth factor for cell culture. Sericin easily dissolves in water, and its bioactivity is not impaired by autoclave sterilization. Thus, we expect that sericin may be a novel factor for cell culture. Mitogenic effects of sericin have been observed on various mammalian cell lines, including murine hybridoma 2E3-O, human hepatoblastoma HepG2, human kidney 293, HeLa and fibroblasts [1]. It also improves cell survival against hyperthermia,

T. Saito and S. Terada
Department of Applied Chemistry and Biotechnology, University of Fukui, 3-9-1 Bunkyo, Fukui, 910-8507, Japan

A. Ogawa, M. Sasaki, and H. Yamada
SEIREN Co. Ltd. 48-113-2 Yonozu, Mikuni-Cho, Sakai, Fukui, 913-0038, Japan

K. Ikura et al. (eds.), *Animal Cell Technology: Basic & Applied Aspects*,
Animal Cell Technology: Basic & Applied Aspects 15,
DOI 10.1007/978-1-4020-9646-4_6,

surfactants, including SDS and organic solvents, such as DMSO and ethanol. Therefore, sericin is a strong candidate as a serum substitute. However, the mechanism of how sericin affects cultured cells has not been elucidated. In this study, we investigated the mitogenic and anti-apoptotic activities of sericin. To reveal the mechanism, proteome analysis using two-dimensional electrophoresis (2-DE) was performed, where proteins were separated by isoelectric point in the first dimension using immobilized pH gradient gels, and subsequently by their molecular masses in the second dimension. Using this approach, proteins can be comprehensively studied.

2 Materials and Methods

2.1 Cell Line and Culture Conditions

A hybridoma cell line 2E3-O was derived from mouse myeloma P3X63 AG8U.1, by electric fusion with mouse spleen cells [2]. The cells were cultured in serum-free ASF103 or serum- and BSA-free ASF104 (Ajinomoto, Japan) at 37°C in humidified air containing 5% CO_2. The number of cells and viability were measured with trypan blue dye.

2.2 DE Analysis

2.2.1 First Dimension Isoelectric Focusing (IEF)

For IEF, Immobiline Dry-Strips (Amersham Bioscience, USA), pH 3–10, were swelled in a solution containing 8 M urea, 2 M thiourea, 20% TritonX-100, 1 mM DTT, 0.1 M acetic acid, IPG buffer (Amasham Bioscience) and 0.1% bromphenol blue, and were incubated overnight at room temperature. After mounting the strips in the electrofocusing chamber unit (Anatech, Japan), the proteins were separated according to their isoelectric points. The details of the steps are shown in Table 1.

2.2.2 Second Dimension SDS-PAGE

After the first dimension IEF, the individual strips were consecutively incubated in equilibration solution A for 30 min and solution B for 15 min; 50 mM Tris–HCl,

Table 1 Steps of IEF

Step	Voltage (V)	Time (h)	Step	Voltage (V)	Time (h)
1	500	2	5	2,000	1
2	700	1	6	2,500	1
3	1,000	1	7	3,000	1
4	1,500	1	8	3,500	18

pH 6.8, 6 M urea, 30% glycerol, and 4% SDS, with addition of 10 mg/ml DTT (solution A) or 90 mg/ml iodoacetamide instead of DTT (solution B). After equilibration, proteins were separated in the second dimension on 12.5% SDS-polyacrylamide gels with the Cool Phorestar (Anatech). The immobiline Dry-Strips were sealed on the top of the gels using a sealing 1% agarose solution. The proteins were separated by 20–40 mA/slab, according to their molecular weight, until the BPB dye approached the bottom of the gel [3, 4].

Immediately after electrophoresis, the gels were fixed overnight in 50% methanol and 10% acetic acid. The gels were then stained using Ez Stain Silver (ATTO, Japan).

3 Results and Discussion

3.1 Examination for Determining Optimal Concentration of Sericin

To determine optimal concentration of sericin, hybridoma cells were cultured in the presence of sericin at various concentrations. As shown in Fig. 1, the cell proliferation rates in the presence of sericin were higher than those in its absence. At less than 0.1%, the proliferation was increased in a dose-dependent manner, but the mitogenic effect was slightly decreased at 0.15%. The result indicates that the optimal concentration of sericin in cell culture is 0.1%.

3.2 Proteome Analysis Using 2-DE

To investigate the protein profiles of 2E3-O cells treated with sericin, 2-DE was performed. The results are shown in Fig. 2. Several distinct spots were identified

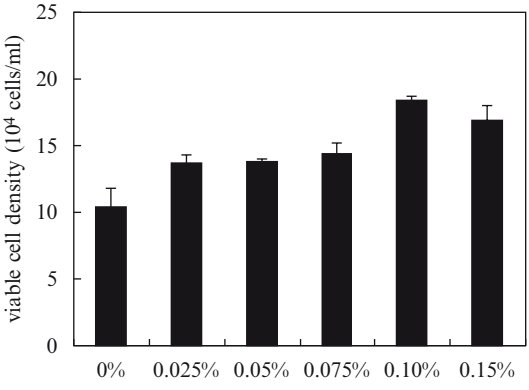

Fig. 1 Mitogenic effect of sericin at various concentrations. Sericin was added to serum-free medium (0–0.15%). 2E3-O cells were cultured for 3 days and the number of viable cells was measured with trypan blue dye

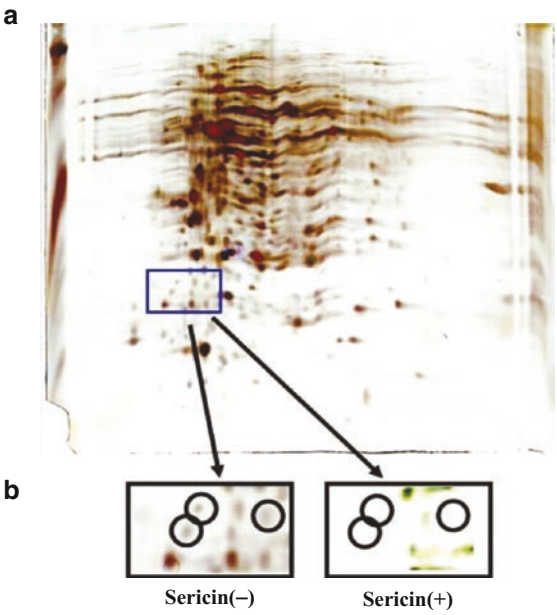

Fig. 2 (**a**) 2-D protein profile of the 2E3-O cell line. The vertical axis indicates the molecular weight, while the horizontal axis indicates the isoelectric point. (**b**) Differential spots between the samples from cells treated with sericin and those without

between the sample from cells treated with sericin and those without. As shown in Fig. 2b, three spots vanished during treatment with sericin. This result indicates that sericin affects protein expression pattern.

References

1. Terada S, Nishimura T, Sasaki M, Yamada H and Miki M (2002) Sericin, a protein derived from silkworms, accelerates the proliferation of several mammalian cell lines including a hybridoma. *Cytotechnology*, 40, 3–12.
2. Makishima F, Terada S, Mikami T and Suzuki E (1992) Interleukin-6 is antiproliferative to a mouse hybridoma cell line and promotive for its antibody productively. *Cytotechnology*, 10, 15–23.
3. Möller A, Soldan M, Völker U and Maser E (2001) Two-dimensional gel electrophoresis: a powerful method to elucidate cellular responses to toxic compounds. *Toxicology*, 160, 129–138.
4. Toda T, Kaji K. and Kimura N (1998), TMIG-2DPAGE: A new concept of two-dimensional gel protein database for research on aging. *Electrophoresis*, 19, 344–348.

Novel Serum-Free Cryopreservation of Mammalian Cells Using Sericin

Tomohiro Toyosawa, Yoko Oumi, Akiko Ogawa, Masahiro Sasaki, Hideyuki Yamada, and Satoshi Terada

Abstract Cryopreservation is a pivotal process for obtaining a continuous source of functional cell lines. Currently, fetal bovine serum (FBS) supplemented with 10% dimethyl sulfoxide (DMSO) is extensively used as a cryopreservative solution. However, FBS carries the risk of infection by abnormal prion proteins and viruses. Therefore, development of serum-free cryopreservative solutions is desirable. We have previously developed a novel serum-free cryopreservative solution using sericin. Sericin cryopreservative solution consists of phosphate-buffered saline, 1% sericin, 0.5% maltose, 0.3% proline, 0.3% glutamine and 10% DMSO. In this study, we evaluated sericin cryopreservative solution using the rat insulinoma cell line RIN5F and the mouse hybridoma cell line 2E3-O. After thawing, proliferation and production of biological substances by cells cryopreserved in sericin solution were similar to those of cells cryopreserved in FBS solution. These results indicate that sericin solution is suitable as a serum-free cryopreservative.

Keywords Cryopreservation • hybridoma • insulinoma • sericin • serum-free

1 Introduction

Mammalian cell culture is applicable to many fields. Various biological substances are produced as medicines by cultured mammalian cells, because of their high bioactivity due to glycosylation. In cell culture, the risk of contamination by bacteria, fungi, mycoplasmas and viruses is always a concern. In addition, cell function is impaired gradually during the culture period.

During cryopreservation, cells arrest their metabolic pathways, therefore making it possible to maintain their functions. Accordingly, cryopreservation is very

T. Toyosawa, Y. Oumi, and S. Terada
Depertment of Applied Chemistry and Biotechnology, University of Fukui,
3-9-1, Bunkyo, Fukui, 910-8507, Japan

A. Ogawa, M. Sasaki, and H. Yamada
SEIREN Co. Ltd., 48-113-2, Yonozu, Mikuni-Cho, Sakai, Fukui, 913–0038

K. Ikura et al. (eds.), *Animal Cell Technology: Basic & Applied Aspects*,
Animal Cell Technology: Basic & Applied Aspects 15,
DOI 10.1007/978-1-4020-9646-4_7,

important for stable cell culture. However, freeze–thawing gives rise to cell damage and often leads to a high level of cell death. As a result, cryoprotectants are added to the cryopreservative solution. Currently, fetal bovine serum (FBS) is extensively used as such a cryoprotectant, although FBS carries the risk of infection with abnormal prion proteins and viruses, and therefore should be avoided.

In our previous study, novel serum-free cryopreservative solutions were developed by using sericin as a cytoprotective supplement [1]. Sericin is a protein derived from cocoon silk, and contains an abundance of serine residues. Sericin promotes the proliferation of various cell lines [2], enhances antibody production by hybridoma cells, and protects cells from toxicity of such things as surfactants and DMSO (S. Terada, unpublished work). Therefore, it is expected that sericin can be used as an alternative to FBS in cryopreservative solutions, in order to develop serum-free cryopreservative solutions.

The purpose of this study was to evaluate sericin solutions. Rat insulinoma cell line RIN5F and mouse hybridoma cell line 2E3-O [3] were used in this study.

2 Materials and Methods

2.1 Cell Lines and Culture Conditions

The rat insulinoma cell line RIN5F was cultured in RPMI 1640 medium (Nissui, Tokyo, Japan) supplemented with 10% FBS. The murine hybridoma cell line 2E3-O was cultured in ASF103 serum-free medium (Ajinomoto, Tokyo, Japan).

2.2 Determination of Cell Number and Viability

The numbers of viable and dead cells were determined by the trypan blue exclusion staining method, using a Neubauer improved haemocytometer (Erma, Tokyo, Japan). Trypan blue was purchased from Dojindo (Kumamoto, Japan).

2.3 Cryopreservative Solutions

Sericin cryopreservative solution consisted of phosphate-buffered saline (PBS) containing 1% (w/v) sericin, 0.5% (w/v) maltose, 0.3% (w/v) proline, 0.3% (w/v) glutamine and 10% (v/v) DMSO. The conventional FBS solution, containing 90% (v/v) FBS and 10% (v/v) DMSO, was used as a control.

2.4 Cryopreservation

Cells in the logarithmic growth phase were collected and rinsed with PBS, then resuspended at about 5×10^4 cells/ml in cryopreservative solution. Cell-suspensions (0.5 ml) were dispensed into cryovials, and these were ice-chilled for 5 min, and then stored at −80°C for 1 week.

2.5 Thawing

Frozen tubes were incubated at 37°C for 5 min, then thawed cell-suspensions were collected and added to 5 ml fresh medium. Cells were centrifuged and resuspended in 5 ml fresh medium, and 2 ml cell suspensions were seeded onto 35 mm dishes.

2.6 Evaluation of Cellular Functions

The concentration of products secreted by freeze–thawed cells were measured at day 3 after thawing. Insulin concentration in the RIN5F culture supernatant was measured by Rat insulin ELISA kit (Shibayagi, Gunnma, Japan). Antibody concentration in the 2E3-O culture supernatant was measured by ELISA, using rabbit anti-mouse IgG primarily antibody and HRP conjugated anti-mouse IgG secondary antibody (Cappel, USA).

3 Results

3.1 Effect of Sericin Solution on Cryopreservation of Insulinoma Cells

Rat insulinoma RIN5F cells were used as a model of cell therapy for diabetes. RIN5F cells were frozen in the cryopreservative solutions at 50.1×10^4 cells/ml for 1 week at −80°C. After thawing, the numbers of viable and dead cells were counted, and the growth curves are shown in Fig. 1a. Cells cryopreserved by sericin solution proliferated for 25 h after thawing, as did those preserved in FBS solution, but after 25 h, proliferation of the former was significantly superior to the latter. On the other hand, insulin production at day 3 after thawing was superior in cells preserved in FBS solution, but the difference was small (Fig. 1b).

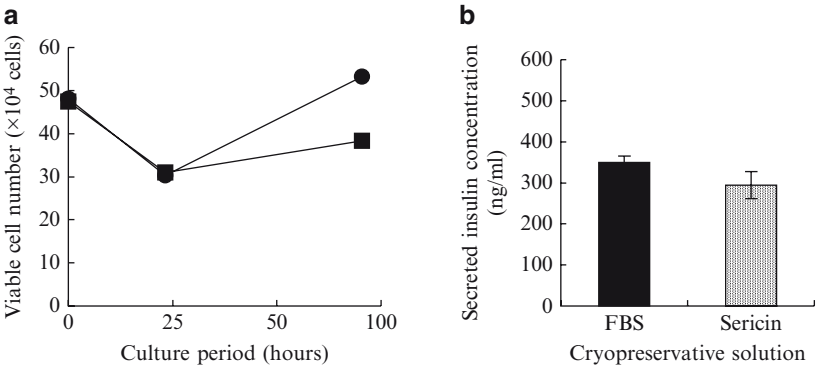

Fig. 1 Cell proliferation and insulin secretion after thawing. RIN5F cells were cryopreserved at a density of 50.1×10^4 cells/ml and after thawing, they were cultured in RPMI 1640 medium supplemented with FBS. (**a**) The number of viable cells was counted using the trypan blue exclusion method. Cryopreservation was performed in the presence of sericin (closed circles) and FBS (closed squares). (**b**) Secreted insulin concentration was measured with the Rat insulin ELISA kit (Shibayagi, Gunma, Japan) at day 3 after thawing

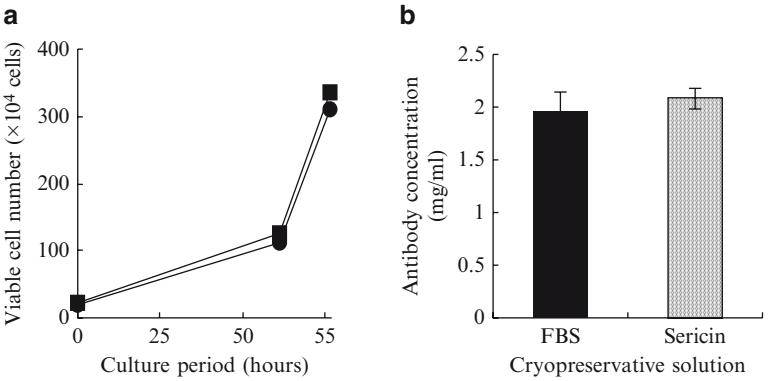

Fig. 2 Cell proliferation and antibody production after thawing. Hybridoma 2E3-O cells were cryopreserved at a density of 56.0×10^4 cells/ml and after thawing, cells were cultured at 37°C in ASF103 medium. (**a**) The number of viable cells was counted using the trypan blue exclusion method. Cryopreservation was performed in the presence of sericin (closed circles) and FBS (closed squares). (**b**) Antibody concentration was measured by ELISA at day 3 after thawing

3.2 Effect of Sericin Solution on Cryopreservation of Hybridoma Cells

Hybridoma cell line 2E3-O was used as a model for commercial antibody production. 2E3-O cells were frozen in the cryopreservative solution at 56.0×10^4 cells/ml for 1 week at −80°C. After thawing, the numbers of viable and dead cells were counted, and the growth curves are shown in Fig. 2a. Cells cryopreserved in sericin

and FBS solution proliferated similarly after thawing. Antibody production was also similar in both cultures (Fig. 2b).

4 Conclusion

Both insulinoma and hybridoma cells cryopreserved in sericin solution immediately proliferated and recovered their function, insulin release and antibody production. The effect of sericin solution was similar to that of FBS solution. Sericin solution can be considered an infection-free and safe alternative to conventional FBS solution.

References

1. Sasaki M., Kato Y., Yamada H. and Terada S.: Development of a novel serum-free freezing medium for mammalian cells using the silk protein sericin, *Biotechnol. Appl. Biochem.*, 42, 183–188 (2005).
2. Terada S., Nishimura T., Sasaki M., Yamada H. and Miki M.: Sericin, a protein derived from silkworms, accelerates the proliferation of several mammalian cell lines including a hybridoma, *Cytotechnology*, 40, 3–12 (2002).
3. Makishima F., Terada S., Mikami T. and Suzuki E.: Interleukin-6 is antiproliferative to a mouse hybridoma cell line and promotive for its antibody productivity, *Cytotechnology*, 10, 15–23 (1992).

The Effect of Interleukin-6 and Leukemia Inhibitory Factor on Hybridoma Cells

Masato Tanaka, Tatsuya Yamashita, and Satoshi Terada

Abstract In mammalian cell culture, adaptation to serum-free medium is very important. We found that such adaptation influenced the sensitivity of hybridoma cells to cytokines. Both interleukin-6 (IL-6) and leukemia inhibitory factor (LIF) are known as mitogens for hybridomas. Before adaptation, in the presence of IL-6, the proliferation of parental 2E3 hybridoma cells was increased, as well as in the presence of LIF. After adaptation to serum-free medium, the response of the hybridoma cells to the cytokines was transformed. In the presence of IL-6 and LIF, the proliferation of 2E3-O cells, sub-line adapted to serum-free medium, was suppressed. Despite this, DNA fragments were not observed in 2E3-O cells treated with IL-6 and LIF, suggesting that neither cytokine induces apoptosis.

Keywords Cytokines • hybridoma • interleukin-6 • leukemia inhibitory factor • serum-free culture

1 Introduction

Production of biological substances by cultured mammalian cells has increased in importance in recent years. In particular, antibody production has increased by 20-fold over the last 20 years [1]. Such antibodies are useful for the treatment of many diseases, e.g., Remicade, an anti-tumor necrosis factor antibody, is used to treat rheumatism. The market in therapeutic antibodies was worth about 55 billion yen in 2005 in Japan. However, mammalian cell culture needs large amounts of money. In particular, the cost of medium is very expensive, so serum-free media are widely required in order to cut the cost of mammalian cell culture, and to improve productivity.

Previously, we have reported that interleukin (IL)-6 accelerates the proliferation of the murine hybridoma cell line 2E3, while it suppresses that of the sub-line

M. Tanaka, T. Yamashita, and S. Terada
Department of Applied Chemistry and Biotechnology, University of Fukui,
3-9-1, Bunkyo, Fukui, 910-8507, Japan

K. Ikura et al. (eds.), *Animal Cell Technology: Basic & Applied Aspects*,
Animal Cell Technology: Basic & Applied Aspects 15,
DOI 10.1007/978-1-4020-9646-4_8,

2E3-O, generated by adaptation to serum-free medium [2]. The present study aimed to gain a better understanding of how IL-6 controls the proliferation of hybridoma cells. Knowing how the IL-6 signal is transmitted in the cell will be of great benefit in the development of cell culture techniques. Leukemia inhibitory factor (LIF), an IL-6-related cytokine, was also tested for comparison.

2 Materials and Methods

2.1 Cell Lines and Culture Conditions

The hybridoma cell line 2E3 was cultured in RPMI 1640 medium (Nissui, Tokyo, Japan) supplemented with 10% (v/v) FBS, 10 mM HEPES, 0.2% $NaHCO_3$, 2 mM glutamine, and 0.06 mg/ml kanamycin. 2E3-O cells were cultured in serum-free medium ASF103 (Ajinomoto, Tokyo, Japan). The culture was carried out at 37°C in 5% CO_2 in air.

2.2 Cell Proliferation Assay

2E3 and 2E3-O cells were cultured in serum-free medium ASF104 (Ajinomoto) in the presence of IL-6 or LIF. Recombinant human IL-6 was purchased from Wako Junyaku (Osaka, Japan). Recombinant mouse LIF was purchased from Sigma (MO, USA). 2E3 and 2E3-O cells were cultured in 24 well plates, and the viable and dead cell numbers were determined by counting in a hemocytometer under a phase contrast microscope, using the trypan blue exclusion method.

2.3 DNA Ladder Assay

The cells were rinsed with phosphate-buffered saline (PBS), and centrifuged at 3,000 r.p.m. for 10 min. The pellets were lysed in a buffer containing 20 mM EDTA, 100 mM Tris, and 10% Triton X 100, and incubated in the presence of 0.1 µg/ml ribonuclease A at 37°C for 1 h. After treatment with proteinase K at 50°C for 30 min, DNA was concentrated by precipitation in isopropanol containing 0.13 M NaCl, and redissolved in 10 mM Tris buffer. The DNA preparations were added to 5 µl loading buffer (10 mM EDTA, 0.25% bromophenol blue, and 50% glycerol) and were electrophoresed on 2.0% agarose gel in TBE buffer (pH 8.0, 2 mM EDTA, 89 mM Tris and 89 mM boric acid).

3 Results

Figure 1a shows the effect of IL-6 on 2E3 cells. Although 2E3 cells had not been adapted to serum-free medium, they were maintained viably in serum-free ASF104 medium. At IL-6 concentrations of 0.1–10 ng/ml, proliferation was enhanced. Figure 1b shows the effect of LIF. At LIF concentrations of 0.1–1 ng/ml, proliferation was also increased, but at a concentration of 10 ng/ml, proliferation was inhibited.

After adaptation to serum-free medium, the response to the cytokines was altered. Figure 2a shows that IL-6 suppressed the proliferation of 2E3-O cells adapted to serum-free medium. Figure 2b shows that LIF also inhibited the proliferation of 2E3-O cells.

In the presence of IL-6 and LIF, the cells retained high viability despite their proliferation being strongly inhibited (Fig. 3a and b), suggesting that the cytokines moderately suppressed proliferation without induction of apoptosis.

We tested whether cytokine treatment induced DNA fragmentation.

Figure 3c indicates that the inhibitory effect of TGF-β on the proliferation of 2E3-O cells was similar to that of the same amount of IL-6. Figure 3d shows the results of gel electrophoresis of DNA from cells treated with various cytokines. In the lane of the cells treated with TGF-β, a DNA ladder was observed. On the other hand, no DNA ladder was detected in the cells treated with IL-6 and LIF. This result indicates that IL-6 and LIF did not induce apoptosis, despite strong suppression of cell proliferation.

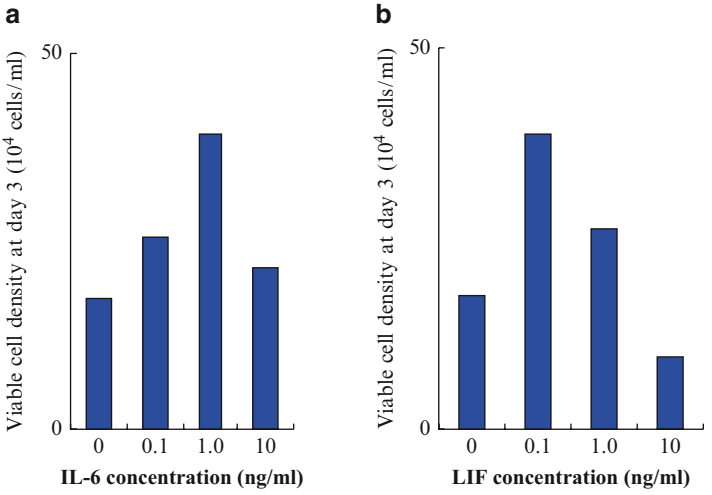

Fig. 1 Effect of cytokines on 2E3 cell proliferation. The cells were cultured with IL-6 0.1–10 ng/ml (**a**) and LIF 0.1–10 ng/ml (**b**). 2E3 cells were cultured in serum-free ASF104 medium

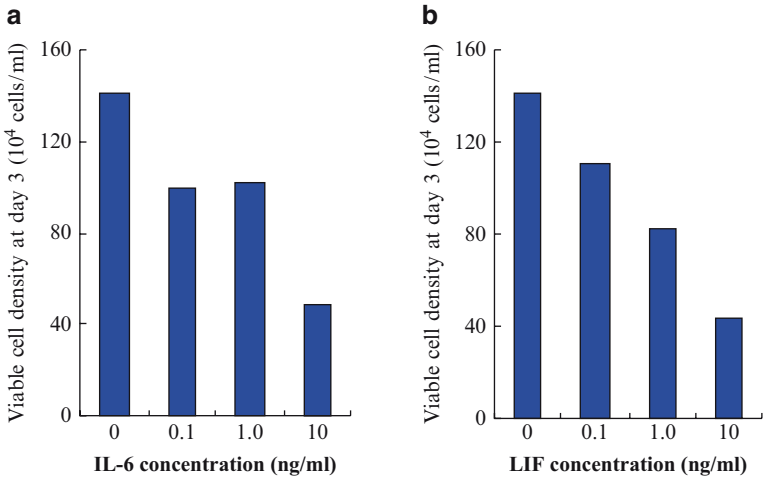

Fig. 2 Effect of cytokines on proliferation of 2E3-O cells adapted to serum-free medium. The cells were cultured with IL-6 0.1–10 ng/ml (**a**) and LIF 0.1–10 ng/ml (**b**). 2E3-O cells were cultured in serum-free ASF104 medium

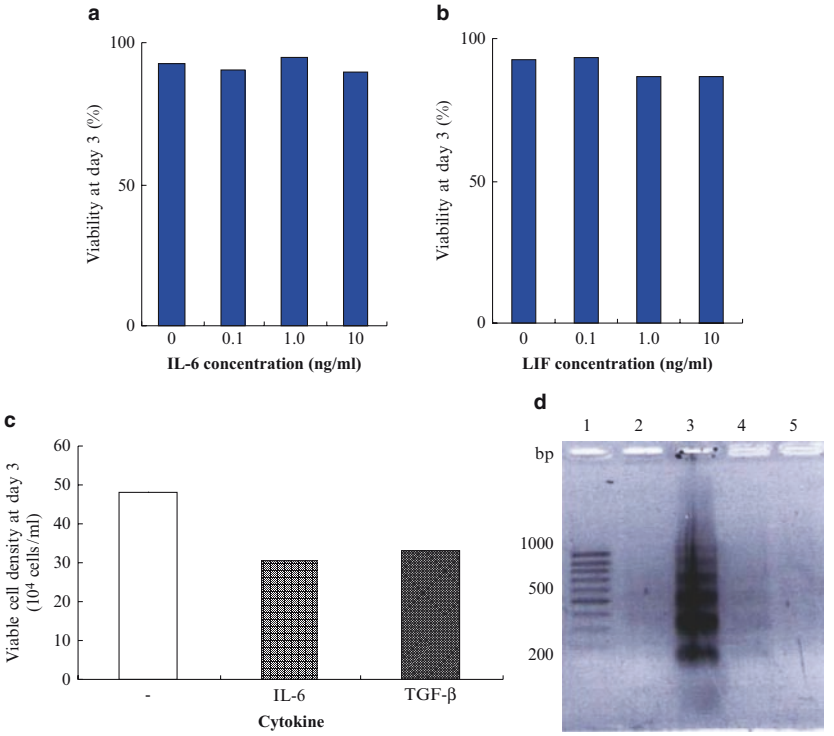

Fig. 3 Effect of cytokines on viability of 2E3-O cells adapted to serum-free medium: (**a**) IL-6, (**b**) LIF, (**c**) inhibition of the growth of 2E3-O cells in the presence of cytokines at 5 ng/ml, (**d**) gel electrophoresis for detection of DNA fragmentation. 2E3-O cells were cultured in the presence of 5 ng/ml cytokines. Lane 1, DNA size markers; lane 2, cytokine-free; lane 3, transforming growth factor (TGF)-β; lane 4, IL-6; lane 5, LIF

References

1. F. M. Wurm (2004) *Nature Biotechnology*, 22, 1393–1398.
2. S. Terada et al. (1996) *Cytokine*, 8, 889–894.

In-Situ Observation of a Cell Growth Using Surface Infrared Spectroscopy

Ko-ichiro Miyamoto, Takami Muto, Parida Yamada, Michio Niwano, and Hiroko Isoda

Abstract In this study, we report on a novel method for in-situ observation of cell growth using surface infrared spectroscopy. Human breast cell line MCF-7 cells were cultured on small Si prisms and monitored using infrared absorption spectroscopy in the geometry of multiple internal reflections (MIR-IRAS). Infrared spectra of cultured MCF-7 cells on Si prisms were collected for 300 min. The growth of MCF-7 cells was monitored by observing changes in the well-known "amide II" protein absorption band at 1,545 cm^{-1}.

Keywords Infrared absorption spectroscopy • cell growth • in-situ observation

1 Introduction

Bioassay is the search for new chemicals in living matter and an effective method to discover a new drug. Many kinds of new biological active substances have been found from biological resources. It is necessary to improve speedy screening techniques because most of bioprospecting is a race against the clock. The bioassay using cultured cell has been developed to screen kinds of the biological active substances and its influences [1, 2].

Recently we proposed to in-situ monitoring of biomolecular interactions using infrared absorption spectroscopy (IRAS) [3, 4]. High surface sensitivity was achieved using the multiple internal reflections IRAS (MIR-IRAS) geometry using a small Si prism, with MIR-IRAS particularly well-suited for observing interactions or conformational changes of the biomolecules in aqueous environment. Thus MIR-IRAS can be a powerful tool for the primary screening of bioassay. Infrared absorp-

Ko-ichiro Miyamoto, T. Muto, and M. Niwano
Research Institute of Electrical Communication, Tohoku University,
2-1-1 Katahira, Aoba-ku, Sendai, Miyagi, 980-8577, Japan

P. Yamada and H. Isoda
Alliance for Research on North Africa, Graduate School of Life and Environmental Sciences,
University of Tsukuba, 1-1-1Tennodai, Tsukuba, Ibaraki, 305-8572, Japan

K. Ikura et al. (eds.), *Animal Cell Technology: Basic & Applied Aspects*,
Animal Cell Technology: Basic & Applied Aspects 15,
DOI 10.1007/978-1-4020-9646-4_9,

tion spectrum provides various information of conformation or structure of biomolecules and it may attend to needs of multifactorial explore of screening.

On the other hand, there is a large body of literatures about IRAS measurement of biomolecules; DNA, protein, tissue sample, bacteria sample and cultured cells [5, 6]. T. Hutson et al. have reported on a technique for monitoring cell growth of Chinese hamster ovary cells using ATR FT-IR measurement [7], however, general ATR method needs expensive ATR crystal made of germanium or zinc selenide and a size of the crystal is much larger than our MIR-IRAS prism. Then MIR-IRAS prism made of Si has advantages in its cost and size. And a surface stability of Si prism covered with chemical oxide layer should be another advantage.

In this study, we report on a method for in-situ observation of cell growth using MIR-IRAS. We maintained the environment of a sample chamber as same as a general cell culture and succeeded in in-situ observation of the cell growth on the Si prism. The result of the MIR-IRAS measurement shows spectral enhancements at amide-I and amide-II absorption bands due to the cell growth.

2 Experiment

Figure 1 illustrates the equipment made of Teflon® we used in this study for MIR-IRAS measurements. This equipment was also used in our past studies [3, 4]. The volume of the sample solution was 100–200 µl. A Si prism was $0.5 \times 10 \times 30$ mm^3 with 45° bevels on each of the short edges, and contacts with the sample solution. An infrared light beam from an interferometer (BOMEM MB-100) was focused at normal incidence onto one of the two bevels of the Si prism, and penetrated through the Si prism, internally reflecting about 60 times. The light that propagated the Si prism through the other bevel was focused onto a liquid-nitrogen cooled Mercury-Cadmium-Telluride (MCT) detector. The internally reflections excite an evanescent field on the Si prism surface, and the chemical species of the biomolecules inside of the evanescent field influence to the propagated light.

To observe the living cultured cell, first we mounted a homemade temperature controller (a heater, a small fan and a thermo controller) to the infrared spectrometer described above. Second, a mixed gas containing 5% of CO_2 gas was introduced

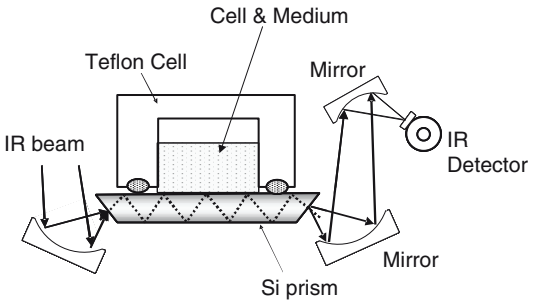

Fig. 1 MIR-IRAS measurement

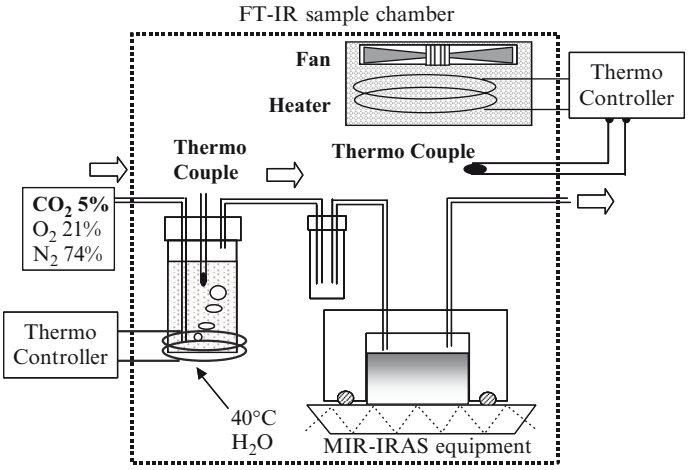

Fig. 2 MIR-IRAS system for living cell

into MIR-IRAS equipment via a bubbler bottle. To humidify the mixed gas, the bubbler bottle was maintained at about 40°C using a thermal controller and an attached heater. The temperature of the sample chamber of the spectrometer was maintained at 37°C and the sample cell can be cultured under enough humidity and CO_2 5% as same as a typical cell culture environment. A schematic view of the environment control system is shown in Fig. 2.

The Human Breast Tumor Cells (MCF-7) were purchased from the Riken cell bank. The cells were cultured in RPMI 1640 medium (Gibco), supplemented with 10% heat inactivated FBS (Sigma), penicillin (50 I.U./ml) and streptomycin (50 μg/ml). The cells were maintained at 37°C in a humidified 5% CO_2 atmosphere in an incubator.

3 Result and Discussion

MCF-7 cells (2×10^5 cells/ml, 200 μl) were introduced into the MIR-IRAS equipment in Fig. 1, and incubated for 24 h in the incubator. Figure 3a shows the MCF-7 cells on the Si prism after the incubation. The MCF-7 cells adhered on the Si prism surface, and cell confluence was about 70%.

Then the MIR-IRAS equipment was set in the sample chamber of the spectrometer and infrared spectra of the cultured MCF-7 cells on the Si prism were collected at an interval of 30 min for 300 min. (A reference spectrum was collected at 60 min.) The collected spectra of MCF-7 on Si are shown in Fig. 4a. In Fig. 4a, mainly two absorption peaks were enhanced as incubation time was increased. The absorption band at about 1,640 cm^{-1} is well-known as "amide-I" protein absorption band mainly attributed to C = O stretching mode, and the another

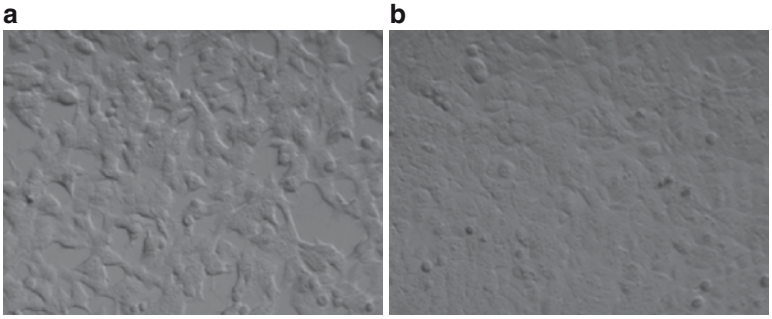

Fig. 3 The micrographs of the MCF-7 cell on the Si prism (**a**) before MIR-IRAS measurement and (**b**) after 300 min

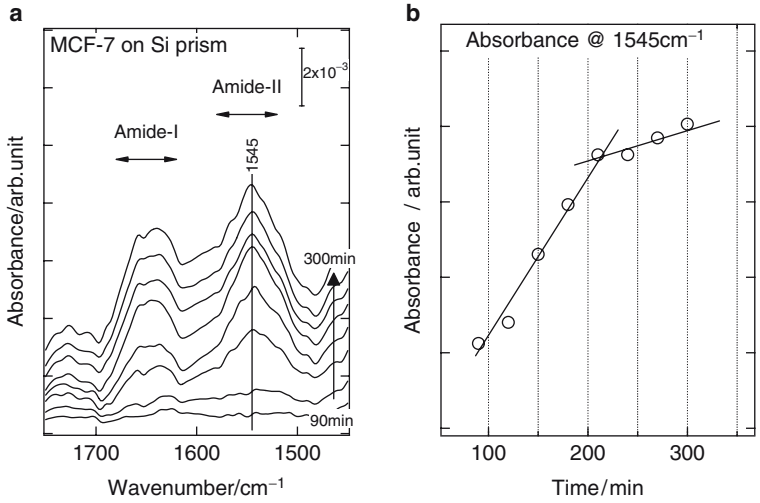

Fig. 4 (**a**) IRAS spectra of MCF-7 and (**b**) the peak intensity at 1,545 cm^{-1} (the lines are drawn as a guide)

absorption band at 1,545 cm^{-1} is also well-known as "amide-II" protein absorption band mainly attributed to N-H bending mode and C-N stretching mode [8].

Figure 5a is a cross-sectional scanning electron microscopy (SEM) image of the MCF-7 cells on a Si substrate. We estimated the thickness of the MCF-7 cells is about 1–2 μm, and the thickness of the excited evanescent field on the Si prism can be estimated about 500 nm from the surface as shown in Fig. 5b. The thickness of the evanescent field covers 25–50% of that of the MCF-7 cells, thus the obtained absorption spectra should contain many absorption bands of lipid membranes, membrane proteins, parts of nuclear and also organelle proteins of the MCF-7 cells. Miyazawa et al. have assigned absorption bands of typical secondary structures of protein; α-helix, β-sheet and random coil [9]. If these absorption bands in Fig. 4a were mainly attributed to the kinds of protein, the absorption band at 1,545 cm^{-1}

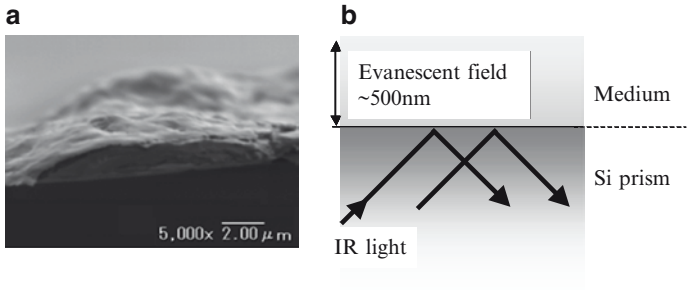

Fig. 5 (**a**) The cross sectional SEM image of MCF-7 cells on the Si prism and (**b**) the exited evanescent field on the Si prism

can be assigned to the α-helix structure. However, it is considerable that the amide-II absorption band contains other absorption bands attributed to the β-sheet and random coil structure at 1,530 and 1,535 cm^{-1} respectively. According to their study, although the α-helix structure also has another strong absorption band at 1,650 cm^{-1} in amide-I band, it is difficult to identify the peak from Fig. 4a. This is because of an overlapping of H_2O strong absorption band at about 1,640 cm^{-1} to amide-I band. And it is also difficult to identify the bands attributed to the β-sheet and the random coil structured proteins for the same reason.

And besides, it is considerable that the absorption bands of other cell components such as the nucleic acid [3, 4] or the lipids [8] complicate the obtained spectra. For example; the absorption bands attributed to the asymmetric stretching mode of COO^- group overlaps to the amide-II region, the bending vibrational mode of the N-H group also overlaps to the amide-I and amide-II region, and the base residues of the nucleic acid also have kinds of absorption bands in the amide-I region.

As discussed above, the assignment of these absorption bands in the amide-I and amide-II are difficult. However, any significant spectral changes were not observed in a control experiment without the MCF-7 cells (data not shown). It suggests that the spectral changes in Fig. 4a are due to the MCF-7 activities.

The intensity of the strongest absorption peak at 1,545 cm^{-1} is plotted as a function of the time in Fig. 4b. The intensity increased and saturated after 180 min. According to the microscopic observation, prior to MIR-IRAS measurement, cell confluence changes from 70% (Fig. 3a) to 100% as shown in Fig. 3b suggesting that the environment of the spectrometer was maintained appropriately for cell growth and with in-situ monitoring MIR-IRAS. Then the changes of the intensity are due to the growth of MCF-7 cells. The cell adhesion should affect on the infrared absorption spectrum.

4 Conclusion

We developed the monitoring system of living cultured cell using infrared spectroscopy and demonstrated that MIR-IRAS is capable of in-situ observation of living culture cell in this study, specially the cell growth without any reagents. The sample

chamber of the spectrometer was maintained for the cell culture, and the confluence of MCF-7 can be monitored by the absorption intensity at 1,545 cm^{-1} of Amide-II protein band. To screen various biological active substances, one of the important information is cell viability or toxicity, which affect to the cell growth. Thus this novel method can be applied for the screening of many biological active substances. We have tried to observe the other cell activities using MIR-IRAS, these results will be discussed elsewhere.

References

1. H. Isoda, T. P. N. Talorete, M. Kimura, T. Maekawa, Y. Inamori, N. Nakajima and H. Seki, Phytoestrogens genistein and daidzin enhance the acetylcholinesterase activity of the rat pheochromocytoma cell line PC12 by binding to the estrogen receptor, *Cytotechnology*, **40**, 117–123 (2002).
2. J. Han, H. Isoda and T. Maekawa, Analysis of the mechanism of the tight-junctional permeability increase by capsaicin treatment on the intestinal Caco-2 cells, *Cytotechnology*, **40**, 93–98 (2002).
3. K. Miyamoto, K. Ishibashi, K. Hiroi, Y. Kimura, H. Ishii, and M. Niwano, Label-free detection and classification of DNA by surface vibration spectroscopy in conjugation with electrophoresis, *Appl. Phys. Let.*, **86**, 053902 (2005).
4. K. Miyamoto, K. Ishibashi, R. Yamaguchi, Y. Kimura, H. Ishii and M. Niwano, In-situ observation of DNA hybridization and denaturation by surface infrared spectroscopy, *J. Appl. Phys.*, **99**, 094702 (2006).
5. H. H. Mantsch, D. Chapman (Eds.), *Infrared Spectroscopy of Biomolecules* (Eiley-Liss, Inc., New York, 1996).
6. H.-U. Gremlich, and B. Yan (Eds.), *Infrared and Raman Spectroscopy of Biological Materials* (Marcel Dekker, Inc., New York, 2001).
7. T. B. Hutson, M. L. Mitchell, J. T. Keller, D. J. Long and M. J. W. Chang, Mammalian cell growth studied in situ by Fourier transform infrared spectroscopy, *Anal. Biochem.*, **174**, 415–422 (1988).
8. G. Socrates, *Infrared and Raman Characteristic Group Frequencies* (John Wiley & Sons Ltd, 2001), pp. 333–338.
9. T. Miyazawa and E. R. Blout, The infrared spectra of polypeptides in various conformations: amide I and II bands, *J. Am. Chem. Soc.*, **83** 712–719 (1961).

Scale-Down Perfusion Process for Recombinant Protein Expression

Delia Fernandez, Javier Femenia, Diana Cheung, Isabelle Nadeau, Lia Tescione, Bryan Monroe, Jim Michaels, and Stephen Gorfien

Abstract The complexity and expense associated with large-scale perfusion culture systems make them impractical for medium optimization studies involving DOE approaches. We have employed scale-down processes involving shake flask cultures seeded at high density, or at several different densities with daily replacement of the culture media (maintaining a constant cell density). These model systems were used to test effects of media components on growth of recombinant CHO cells expressing a therapeutic protein with the ultimate goal being to apply the media modifications to a large-scale perfusion system. Basal media employed were protein-free, chemically defined formulations that were supplemented with various combinations of additives to test effects on cell growth and recombinant protein expression. Additives tested included amino acids, vitamins, lipids, growth factors, nucleic acid precursors, iron chelating substances, and trace elements. In addition, the effects of osmolality and ammonium concentration were examined. Results suggest that perfusion systems are difficult to model in shake flasks. Several media components showed positive effects in standard batch shake flask culture, but had no effect in simulated perfusion shake flask cultures. Several media components showed positive effects when tested in simulated perfusion shake flask cultures, but had no effect in the larger perfusion system. One possible explanation for the discrepancy in results between the standard batch shake flask cultures, simulated perfusion shake flask cultures and large-scale perfusion system is the accumulation of metabolites and resulting pH shift downward in the shake flask cultures. Batch shake flask cultures have no pH regulation; simulated perfusion shake flask cultures have only limited pH control (when the medium is replaced once each day) while large-scale perfusion cultures have real-time pH control.

Keywords Perfusion • bioreactor • scale-down model • DOE • media optimization • lipids

D. Fernandez, L. Tescione, B. Monroe, and S. Gorfien
Invitrogen Corporation, 3175 Staley Road, Grand Island, New York, 14072, USA

J. Femenia, D. Cheung, I. Nadeau, and J. Michaels
BioMarin Pharmaceutical Inc., 105 Digital Drive, Novato, California, 94949, USA

K. Ikura et al. (eds.), *Animal Cell Technology: Basic & Applied Aspects*,
Animal Cell Technology: Basic & Applied Aspects 15,
DOI 10.1007/978-1-4020-9646-4_10, © Springer Science+Business Media B.V. 2009

1 Introduction

DOE studies in large-scale perfusion cell culture systems for medium or process optimization are too complex to be cost-effective. Methods to predict steady state responses to environmental parameters using a non-steady state transient response have been previously described [1]. In this work, two scale-down processes in shake flasks were developed to test effects of media components on growth of recombinant CHO cells expressing a therapeutic protein, with the ultimate goal being to apply the media modifications to a commercial manufacturing-scale perfusion system. To this end, two models were developed. The push up model focuses on its application to determine optimum cell specific perfusion rate (CSPR), meanwhile the simulation of perfusion model focuses on its application in media optimization and DOE studies.

2 Material and Methods

A CHO-K1 derived recombinant cell line secreting therapeutic lysosomal protein was grown in 125 mL shake flasks with 30 mL working volume agitated at 125 rpm (Innova 2100 orbital shaker, New Brunswick Scientific Co., Inc., Edison, NJ) and maintained at 37°C in a humidified incubator with 8% CO_2 in air. A customized mixture of GIBCO® CD17 prototype (0040136DK) and CD CHO (10743–029) supplemented with 6 mM glutamine (25030–081) and Anticlumping Agent (0010057AE) (Invitrogen Corp., Carlsbad, CA) was used.

Two scale down models were developed: (1) Simulation of perfusion: to achieve a pseudo- steady state, an aliquot of the cells was removed from the flasks, centrifuged and the pellet was resuspended in fresh medium or in a fraction of fresh medium. (2) Push up experiments: all the cells were collected, centrifuged and resuspended in fresh media.

A DOE study full factorial design 2^3 using the simulation of perfusion scale-down process was performed. The factorial experiment was designed and analyzed using Design Expert v7.0 (Stat-Ease Inc., Minneapolis, MN).

The bioreactor perfusion experiment was performed using a 7L Applikon bioreactor (Applikon Biotechnology Inc., Foster City, CA) with 4L working volume agitated at 100 rpm with a pitched-blade impeller, and maintained at pH 7.0, DO 40% and 37°C. A CS20 settler was used for cell retention (Biotechnology Solutions, CA). The same basal medium composition as above was used, omitting glutamine. Dilute Antifoam C (SAFC, St. Louis, MO) was added (15–30 ppm) to prevent foaming due to sparging.

Cell count and viability was analyzed using a Cedex automatic cell counter (Innovatis Inc., Malvern, PA). Glucose, lactate and glutamine were determined using a YSI 2700 analyzer (Yellow Spring Instruments, Yellow Springs, OH). The product titers were determined by enzymatic activity using a substrate analog.

3 Results

3.1 *Perfusion Bioreactor Compared to Push Up and Simulation of Perfusion Scale-Down Models*

The operating CSPRs in the bioreactor were set at 0.18 +/− 0.02 nL/cell/day from day 7 to day 11, 0.11 +/− 0.02 nL/cell/day from day 12 to day 15 and 0.07 +/− 0.1 nL/cell/day from day 17 to day 19 (Fig. 1). The target cell density was set at 25×10^6 vc/mL, maintaining viabilities higher than 95% (data not shown) during the entire study. To maintain the target cell density at 25×10^6 vc/mL the culture was bled continuously at 2%, 10% and 8% of the working volume at the target CSPRs 0.2, 0.12 and 0.07 nL/cell/day, respectively. The highest specific production was obtained at CSPRs between 0.12 and 0.20 nL/cell/day. Lower CSPRs at the target cell density 25×10^6 vc/mL resulted in a decrease in specific production.

In order to model the bioreactor perfusion rates, these were normalized based on volumetric throughput and cell density (Eq. 1) and the same CSPR maintained in bioreactors were evaluated in simulation of perfusion in flasks.

$$\text{CSPR} = \frac{\text{D}}{\text{VCD}} \tag{1}$$

where
CSPR: cell specific perfusion rate (nL/cell/day)
D: perfusion rate (day^{-1})
VCD: viable cell density (vc/mL)

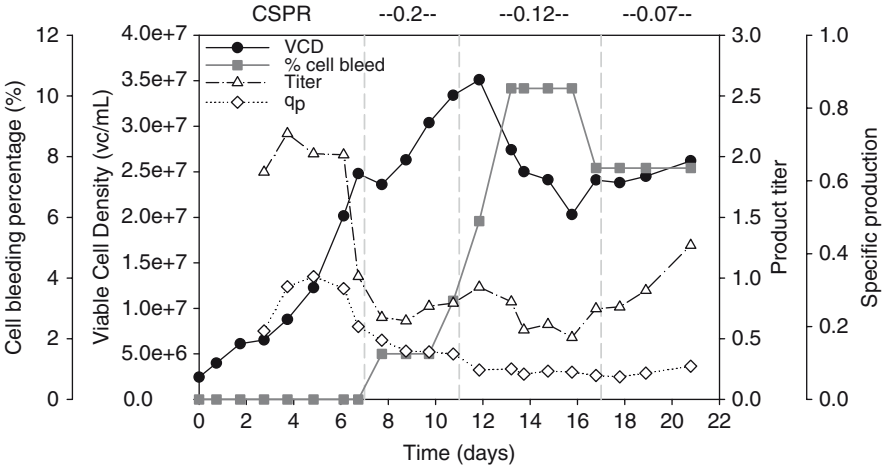

Fig. 1 Bioreactor perfusion mode growth and production

By performing a daily media exchange and bleeding the culture to a target cell density of 5×10^5 vc/mL, the culture was maintained for 4 days at constant growth and metabolic rates without compromising culture viability (>90%) (Fig. 2a).

Increased CSPR in bioreactors resulted in increased specific production rate (q_p) at the given target cell density (Fig. 2b). In the example shown, the highest q_p was found at CSPRs in the range of 0.15 nL/cell/day. By performing a daily media exchange in shake flasks, the peak cell density was increased from 4×10^6 vc/mL in batch mode to 28×10^6 vc/mL in push up mode (Fig. 2a). Viability was higher than 90% up to day 5 and it decreased to 80% in the following days. The specific production calculated from the product titer (data not shown) from the push experiment showed a step increase from CSPR 0.06 to 0.10 nL/cell/day and appears to be maximum in the range of CSPR 0.17 nL/cell/day (Fig. 2b).

With the goal of optimizing media in shake flasks to be applied in a perfusion bioreactor, the spent media from batch, simulation of perfusion and a perfusion bioreactor were analyzed (Table 1). Asparagine and glutamine were depleted in

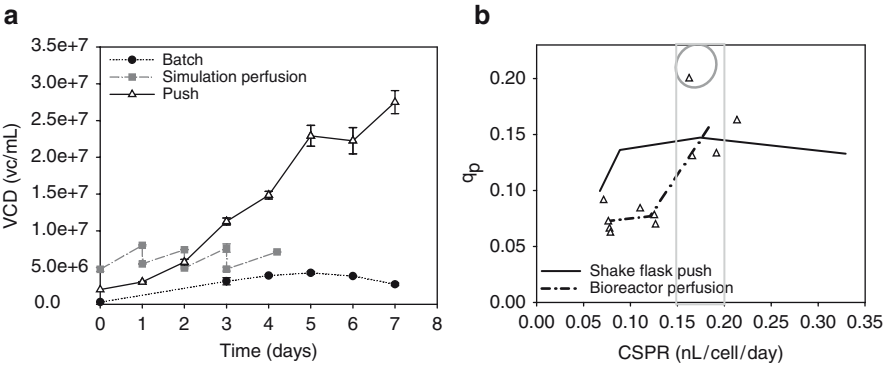

Fig. 2 **(a)** Growth in shake flasks in batch, simulation of perfusion and push modes, n = 3. **(b)** Specific production over different CSPRs. The circle indicates outliers that were not included in the calculations. Lines indicate the trend calculated. Dots indicate values

Table 1 Amino acids concentration in relative concentration to the control remaining in the culture at the end of the cycle or culture

		Shake Flasks		Bioreactor		
Mode	Batch	Simulation of Perfusion		Perfusion		
		CSPR (nL/cell/day)				
	–	0.2	0.12	0.2	0.12	0.07
Asparagine	0%	24%	22%	43%	38%	19%
Aspartate	23%	32%	65%	54%	47%	18%
Cysteine[a]	0%	0%	0%	15%	0%	0%
Glutamate	51%	48%	83%	53%	45%	7%
Glutamine	0%	9%	10%	ND[b]	ND	ND

[a]The amount of L-cysteine cannot be accurately quantified in the presence of L cystine. L-cysteine and cystine results in one single peak.
[b]Not determined. Perfusion bioreactor did not contain glutamine.

shake flasks in batch mode but not in simulation of perfusion or in the perfusion bioreactor. Cysteine was depleted in batch and simulation of perfusion in shake flasks. In the perfusion bioreactor, cysteine was depleted only at CSPR lower than 0.2 nL/cell/day.

3.2 Lipids Study: Batch Mode and Simulation of Perfusion

In batch mode, the lipids evaluated in this study showed an inhibitory effect on cell growth. The inhibitory effect was reflected in the lower peak cell density and lower average doubling time (Fig. 3a). Culture longevity was not affected. Lipid *A* resulted in comparable or lower product titers and specific production. Lipid *B* resulted in 1.3-fold higher product titer and 4.1-fold higher specific production. Lipid *C* resulted in comparable product titers but 1.6-fold higher specific production.

In simulation of perfusion (Fig. 3b), the addition of lipids *A*, *C* or the combination of *A/B/C* resulted in comparable growth and production to the basal medium. The addition of lipid *B* resulted in decreased growth and increased specific production that were statistically significant with p-values lower than 0.05. However, the differences observed in simulation of perfusion were not higher than 1.2-fold at any time and so were much lower than the increase observed in batch mode.

The amount of lipid *C* supplied per cell in simulation of perfusion was lower than in batch mode (Fig. 4a). Specific production showed a linear relation ($R^2 = 0.88$) with the amount of lipid *C* available per cell (Fig. 4b).

4 Discussion and Conclusions

Comparable cell densities to target bleeding density in bioreactors (25×10^6 vc/mL) at viabilities higher than 90% were achieved by applying the push up model. Further experiments are needed to demonstrate applicability of the push up model to predict optimum CSPR in perfusion bioreactors.

Cell densities of 5×10^6 vc/mL were maintained successfully for 4 days at viabilities higher than 90% by applying the simulation of perfusion model. Growth, production and metabolism were consistent between cycles allowing averaging of the results and reducing the number of replicates needed, being then applicable for DOE studies during media development.

Simulation of perfusion is a better model than batch mode to predict metabolic limitations in perfusion bioreactor. The metabolic profile at a specific CSPR in simulation of perfusion is similar to the metabolic profile in bioreactors at lower CSPR. For example, CSPR 0.2 nL/cell/day in flasks correlates closely with CSPR 0.12 nL/cell/day in the bioreactor. The higher amino acid concentration remaining in the perfusion bioreactor at a specific CSPR when compared to simulation of perfusion in shake flasks could be explained by the discontinuity of the simulation of perfusion process. The theoretical residence time for a given nutrient is higher in

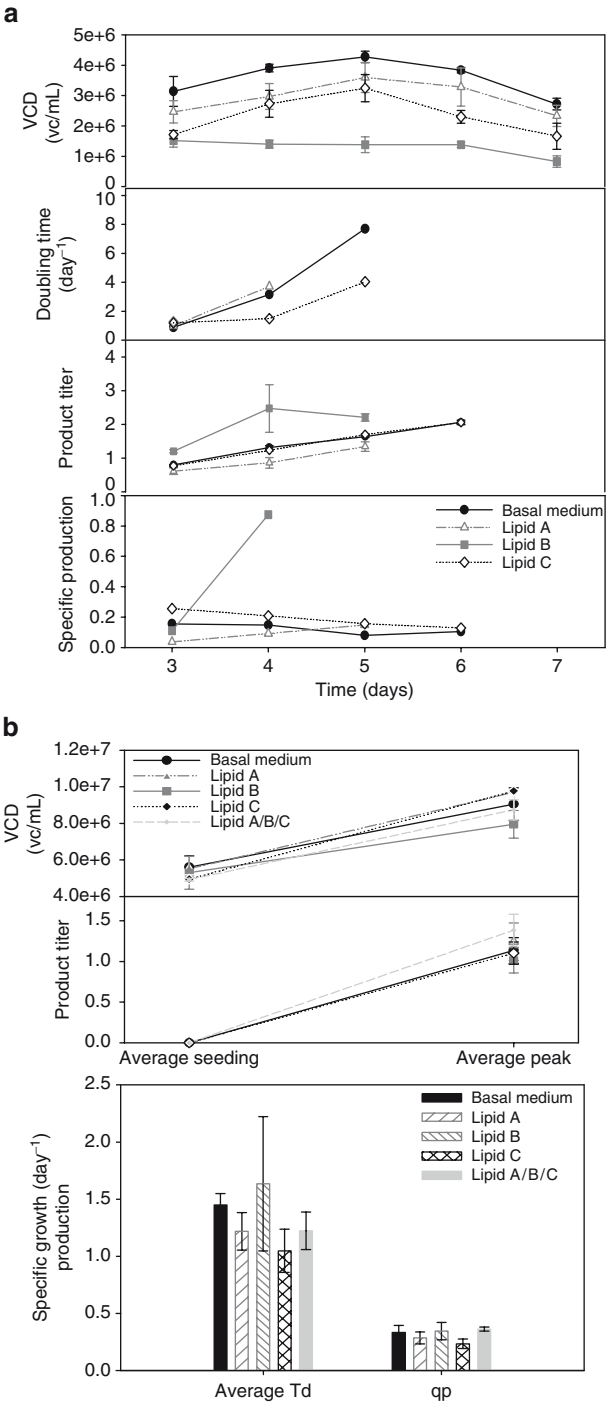

Fig. 3 Growth and production in (**a**) batch mode (n = 3) and in (**b**) simulation of perfusion in shake flasks (n = 3)

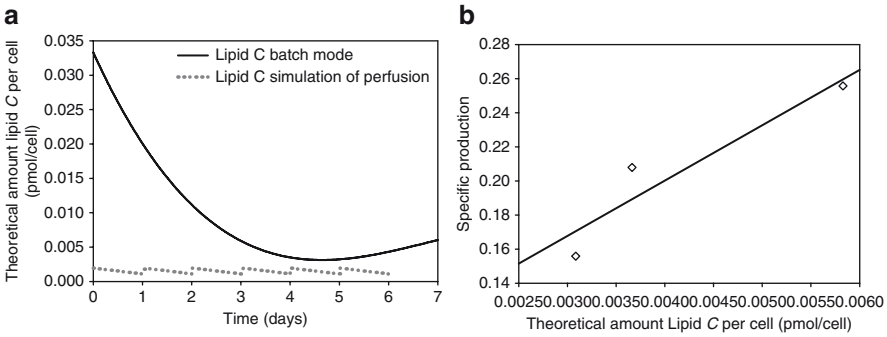

Fig. 4 (**a**) Theoretical amount of lipid C per cell over the time of culture. (**b**) Specific production over theoretical amount of lipid C per cell. Dots indicate values. Line indicate linear regression

simulation of perfusion than in bioreactors at the same CSPR [2]. As a result, lower nutrient concentration remains in the culture prior to next media exchanged in simulation of perfusion than in bioreactors.

The effect of lipids in batch culture were not confirmed in simulation of perfusion mode. The amount of lipids available per cell in simulation of perfusion mode was at all times lower than in batch mode when the same concentration was added to the medium. Higher amount of lipid per cell in batch mode resulted in higher q_p. It is hypothesized that the minimum or negligible response in simulation of perfusion when the same lipid concentrations as in batch mode were added was due to the lower amount of lipid available per cell, which might not reach the amount needed to generate a significant response.

Further studies are needed to better understand the relationship in CSPRs between the scale-down models described in this work and perfusion bioreactors and the relationship between component concentrations and cell density.

References

1. Angepat S., Gorenflo V.M. and Piret J.M. 2005, Accelerating Perfusion Process Optimization by Scanning Non-Steady-State Responses. *Biotechnol Bioeng* **92** (4): 472–478.
2. Fogler H.S. and Brown L.F. 1992, Distributions of Residence Times for Chemical Reactors, Chapter 13 (pp. 708–750) in *Elements of Chemical Reaction Engineering*, 2nd Ed, Prentice Hall, NJ.

Computer-Based Matrix to Evaluate Optimal Medium Delivery Format for Biopharmaceutical Production

David W. Jayme and Stephen Gorfien

Abstract High efficiency biopharmaceutical production from eukaryotic cell culture requires significant volumes of complex nutrient media to sustain elevated biomass and biological productivity in batch, fed-batch and perfusion bioreactors. The elevated cost and complexity of animal cell nutrient media may adversely impact the projected cost-of-goods sold for large-scale bioproduction. Eukaryotic nutrient formulations historically have been commercialized in two formats: milled powdered medium or fully-diluted liquid medium. Several years ago, we applied the technology of fluid bed granulation to complex nutrient media to develop a third alternative, a granulated dry-form medium. We showed that granulated media exhibited several technical and operational advantages over the two traditional formats. Nutrient media in granulated format have already been successfully utilized for large-scale biological production. Recently, we devised a computer-based spreadsheet to facilitate comparative economic evaluation of the relative benefits and limitations of these three media formats. The multiple inputs included costs associated with purchase, qualification and storage of incoming raw materials and costs for production media kitchen conversion and quality assessment. Our analysis evaluated capital depreciation of new or renovated facilities and potential impacts of medium format on operational and culture performance factors. This paper identifies key economic drivers that prefer a particular medium format over its alternatives and provides comparative examples to illustrate bioproduction planning applications.

Keywords Nutrient medium • serum-free • format • bioproduction • cost modeling

D.W. Jayme
Brigham Young University-Hawaii, 55-220 Kulanui Street #1967, Laie, Hawaii 96762, USA

S. Gorfien
Invitrogen Corporation, 3175 Staley Road, Grand Island, New York, 14072, USA

K. Ikura et al. (eds.), *Animal Cell Technology: Basic & Applied Aspects*,
Animal Cell Technology: Basic & Applied Aspects 15,
DOI 10.1007/978-1-4020-9646-4_11,

1 Introduction

Large scale manufacture of biopharmaceuticals has necessitated significant changes in the composition, quality and format of nutrient medium. Technical and regulatory concerns have accelerated the trend towards adoption of serum-free and protein-free nutrient formulations, with increasing emphasis on eliminating animal constituents that might introduce adventitious viral or prion contaminants [1]. Consumer utility and manufacturer profitability mandate continuous improvement in cost of goods sold (COGS) through reduction in production costs and enhanced efficiency [2]. Competitive market pressures to accelerate the biopharmaceutical product developmental timeline are facilitated by scalable pilot and production processes.

Historically, nutrient media to support biopharmaceutical production were offered in two formats: bulk liquid and powdered media. Each traditional medium format offers significant benefits but exhibits practical limitations [3]: For example, bulk liquid medium is conveniently pre-solubilized, sterile and ready-to-use, but batch production scale is typically limited to ~10,000 L. Labile medium components may exhibit limited stability in liquid format and convenience comes at a premium, both in purchase price and quarantined, refrigerated storage requirements. Powdered medium (DPM) may be manufactured in significantly larger batch sizes and overcomes many stability concerns of bulk liquid. However, formulation complexity and solubilization kinetics may result in substantial production variability and/or scrap costs. Absent blending, the size attrition processes routinely used for powdered medium production fail to yield uniformity of trace components and heat generated during the milling process may reduce bioactivity of thermolabile nutrient constituents.

We applied fluid bed granulation techniques to complex nutrient medium to develop a granulated (AGT™) alternative to overcome many limitations of traditional medium formats [3–6]. Technical and practical benefits of AGT technology [3–6] included manufacture of a broad range of complex serum-free formulations as a single-component, complete medium, exhibiting superior levels of biochemical homogeneity and substantial production suite handling advantages. cGMP manufacturability was validated to a scale appropriate for biopharmaceutical production requirements. Within the pilot or production bioproduction suite, the inherent properties of granulated (AGT) medium offered the cost and stability benefits of milled powder medium, providing many of the convenience factors of bulk liquid, while offering biological performance that appeared equivalent or, in some cases, superior to the traditional medium formats.

This study was initiated to determine the primary financial drivers that suggested or contraindicated use of each of these three alternative formats as a source for high performance nutrient medium. Specifically, given Invitrogen's unique investment and proprietary position regarding the AGT format, we desired to understand the economic factors, in addition to the technical factors previously explored, that would favor or disfavor the AGT format as an alternative to traditional formats.

2 Economic Modeling

Our primary objective was to develop a financial tool that models nutrient media format options to assist both industrial clients and account managers. The spreadsheet model will provide an objective mechanism to visualize key factors that influence the optimal medium format, accounting for different nutrient formulations, cultivation systems and production scales.

The defined scope of this modeling exercise was to develop a spreadsheet to evaluate factors that contribute to the relative cost and eukaryotic culture productivity for a targeted biological, comparing three nutrient medium format options, specifically:

1. Liquid medium commercially produced at the 10,000 L batch scale and provided to the client in bulk disposable plastic packaging
2. Liquid medium produced at the client's manufacturing facility from commercially-supplied bulk powdered medium
3. Liquid medium produced at the client's manufacturing facility from commercially-supplied bulk granulated medium (AGT™)

The prospective factors that might contribute to overall nutrient medium cost and that were input into the comparative matrix included:

- Purchase price of bulk nutrient product in each of the three targeted formats
- Storage requirements, including raw, intermediate and finished nutrient medium
- Media kitchen production costs, including both batch-related and capital equipment expenses relating to conversion of raw nutrient medium to finished product
- Quality testing & documentation costs for nutrient medium manufacture (including both incoming raw material and final product costs)
- Target biological productivity projections (including potential incremental specific and total yield of target biological product often observed in serum-free nutrient media derived from AGT raw materials
- Various miscellaneous variable costs, such as packaging and delivery systems, freight, scrap, consistency, nutrient deterioration, etc.

The preferred method for input of matrix data was to obtain, wherever possible, actual manufacturing cost figures directly from the client. Where such values were unavailable, either because the actual cost was unknown to the client or the client declined to provide actual cost information, default values based upon our practical experience were inserted into the comparative cost matrix. Typically, an iterative refinement of initial assumptions and data inputs was required to achieve cost comparison inputs that seemed reasonable.

Unfortunately, specific data for individual clients were proprietary and unavailable for publication. To illustrate the potential features of this comparative cost matrix for publication, we used the following default assumptions:

- Production scale at 1.5 million liters per year.
- Comparable product quality with all three formats.

- Complete nutrient medium may be manufactured in all three formats, but the bulk liquid and powdered medium format options would require two supplemental additives to produce the complete formulation, while the AGT format would already contain those biochemical constituents.
- Standard industry costs for materials purchase, freight, controlled warehouse storage, technical labor, quality testing, facility renovation and equipment depreciation, etc.
- Commonly-reported format-specific impacts on media conversion process, quality testing, and production efficiency.

3 Results

After input of sample data, based upon the default assumptions noted above, the spreadsheet matrix generated the following summary results for total cost of procurement, raw material qualification, controlled storage, media production (conversion) to final form, and quality release of final medium product, respectively.

As noted in Table 1, for an established bioproduction scale of 1.5 million liters, the procurement and storage costs of bulk liquid medium become prohibitively expensive and outweigh the conversion and quality release cost benefits. When purely analyzing the cost of nutrient medium manufacture at this production scale (for the medium in this hypothetical example), the cost to produce the annual medium requirement from AGT-derived raw materials exceeded the direct expenses associated with manufacturing an equivalent volume of nutrient medium from powder-derived raw materials by 10–15%.

Incorporating additional tangible cost benefits associated with utilization of AGT-derived raw materials to the media manufacturing process, such as improved efficiency of media manufacturing equipment and space, and the frequently-observed 10–15% enhancement in product yield, we generated a more comprehensive summary matrix, as noted in Table 2.

Table 1 Sample cost comparison – summary of basic medium production

Cost Parameter	Powdered Format	Bulk Liquid Format	AGT Granular Format
Procurement	$1,005,488	$7,055,488	$1,830,000
Raw material qualification	$1,380	$21,225	$506
Storage (RM & WIP)[a]	$115,667	$486,370	$42,773
Media conversion	$3,566,738	$43,472	$3,447,958
Media quality control	$119,340	$22,590	$118,404
Sub-total costs[b]	$4,808,612	$7,629,145	$5,439,642

[a] Value includes total storage costs for raw materials (basal medium plus supplements), in-process materials and complete final production medium.

[b] Sub-total of annualized nutrient medium costs, based upon assumptions described above.

Table 2 Sample cost comparison – summary of comprehensive analysis

Cost Parameter	Powdered Format	Bulk Liquid Format	AGT Granular Format
Sub-total costs[a]	$4,808,612	$7,629,145	$5,439,642
Amortized depreciation[b]	$318,917 (2,752,500)	$35,833 ($537,500)	$297,417 ($2,430,000)
Performance-adjusted cost[c]	$4,808,612	$ 7,629,145	$4,533,035
Total cost of operation	$5,127,529	$7,664,978	$4,830,451
Cost per liter	$3.42	$5.11	$3.22

[a]Value is carried over from Table 1.
[b]Value refers to the annualized expense for depreciation on the calculated capital base.
[c]Value includes enchanced specific biological productivity as described above.

Adjustments in the cost analysis reflected in differential amortized depreciation of capital media manufacturing equipment and facility costs and enhanced specific productivity in serum-free media derived from AGT raw materials resulted in the total cost and cost per liter data provided in Table 2. As illustrated, this comprehensive analysis reinforces that, for the manufacturing scale and other elements noted in the default assumptions for this sample, production of nutrient medium from AGT raw materials resulted in a total annual cost savings of nearly $300,000, or 6%. This nutrient medium-associated cost savings translated to approximately $0.20 per liter.

4 Discussion and Conclusions

The data presented above illustrate a hypothetical situation based upon the default assumptions described and do not necessarily reflect actual client production cost analysis. Different circumstances, such as the required annual production volume, availability of a fully-depreciated, cGMP quality media production suite and water system, and various other parameters might affect cost analysis significantly, to the point where utilization of bulk liquid medium or of powdered medium might offer cost advantages over AGT-derived medium.

We electronically ramped various factors to determine which elements contributed most significantly to overall cost. Based upon this modeling analysis (data not shown), we determined the most cost influential factors for each medium format and used this analysis to suggest the principal cost drivers that might predict the least expensive nutrient medium format for each client circumstance.

4.1 Comparison of Liquid vs. Dry Media Formats

We determined that the principal cost drivers that distinguished between bulk liquid and either of the dry medium formats (powdered or granulated medium) included

the status of the media manufacturing suite, purchase price, cost of controlled storage and quality control evaluation.

Two major contributory factors to media kitchen cost included the availability and capacity of the water system and the validated capacity of the media formulation tank, which tended to drive many batch-related costs. Costs and potential delays associated with cGMP validation of newly-commissioned capabilities and the financial depreciation stage were also influential.

Negotiated purchase price for all medium constituents, basal nutrient medium and supplemental additives, significantly impacted overall cost. These factors were affected both by the vendor batch size production capability and the medium production batch scale at the client facility. More subtle factors were the stage of the product approval cycle and the willingness of the client to consider introducing medium manufacturing changes that might favorably impact overall COGS.

Storage costs were clearly higher for bulk liquid medium, owing to incremental square footage of refrigerated storage to minimize deterioration of thermo-labile medium constituents. Achieving the optimal balance between minimizing storage costs by increased inventory turns of incoming raw and in-process materials and of finished product vs. reduced quality testing costs through batch size maximization might require careful consideration of the direct cost impact and of potential fluctuations in bioreactor performance or product quality resulting from variable raw material quality.

Costs associated with quality control evaluation of raw, in-process and final materials may be sub-divided into batch-driven and lot-driven expenses. For batch-driven costs, overall cost may be minimized by the economies of bioreactor production scale. By contrast, lot-driven costs were typically primarily impacted by production scale economies of the raw material supplier. Additional cost factors were associated with the number and complexity of additives necessary to supplement the basal medium to achieve the complete nutrient formulation.

4.2 Comparison of Powdered vs. AGT Media Formats

Discrimination a priori whether a particular formulation might offer cost or performance advantages, as either a powdered or an AGT granulated medium, may be more challenging to predict than a simple comparison of liquid vs. dry formats. Factors that appear to contribute include the nutrient formulation composition, the costs associated with conversion of dry-format to final liquid medium, and any performance advantages associated with a particular format. Among bioproduction situations examined to date, client responses to the following questions frequently distinguished both cost and performance preferences among the two dry format options:

Questions relevant to nutrient formulation composition include: Is the formulation serum-free? Does the formulation contain thermo-labile and/or trace biochemical components? May the formulation be manufactured in this format as a complete medium or will it require further supplementation?

Questions pertaining to the conversion cost within the client media manufacturing suite include: What is the required skill level and salary base for media kitchen technicians? What is the desired formulation tank turnover rate? What is the incidence and cost of scrap due to misformulated nutrient medium?

Finally, two key questions regarding performance advantage include: Does liquid medium derived from a particular dry-format yield elevated cellular proliferative rate or biomass density? Are there format-specific enhancements in specific or volumetric biological productivity at pilot or production scale?

4.3 Conclusion

Comprehensive cost modeling can assess breakpoints to justify transition from bulk liquid medium to more economical production-scale format alternatives. For pilot scale production and certain other applications, bulk liquid may remain an economical option. In many situations, complete granulated (AGT) medium format may offer a convenient and cost-effective alternative to milled powdered nutrient medium. The superior nutrient stabilization and uniformity of delivery of for thermo-labile and trace elements observed in AGT formulated media yields a potential for enhanced biological performance that should be factored into the economic model.

References

1. Jayme DW and Gruber DF (2006) Development of Serum-Free Media: Optimization of Nutrient Composition and Delivery Format. In: *Cell Biology: A Laboratory Handbook* (3rd ed.), JE Celis, ed., Elsevier Science, chapter 5, pp. 33–41.
2. Jayme D, Kubiak J, Fike R, Rashbaum S, and Smith S (1998) Cost-Saving Design and Operational Options for Large-Scale Production of Nutrient Medium and Buffers. In: *Animal Cell Technology: Basic & Applied Aspects*, volume 9, pp. 223–227, Kluwer (Dordrecht).
3. Fike R, Dadey B, Hassett R, Radominski R, Jayme D, and Cady D, Advanced Granulation Technology (AGTTM): An Alternate Format for Serum-Free, Chemically-Defined and Protein-Free Cell Culture Media, *Cytotechnology* (2001) 36: 33–39.
4. Radominski R, Hassett R, Dadey B, Fike R, Cady D, and Jayme D, Production-Scale Qualification of a Novel Cell Culture Medium Format, *BioPharm* (2001) 14 (7): 34–39.
5. Jayme D, Fike R, Radominski R, Dadey B, Hassett R, and Cady D (2002) A Novel Application of Granulation Technology to Improve Physical Properties and Biological Performance of Powdered Serum-Free Culture Media. In: *Animal Cell Technology: Basic & Applied Aspects*, S. Shirahata, K. Teruya and Y. Katajura, eds., volume 11, pp. 155–159, Kluwer (Dordrecht).
6. Walowitz JL, Fike RM and Jayme DW, Efficient Lipid Delivery to Hybridoma Culture by use of Cyclodextrin in a Novel Granulated Dry-Form Medium Technology, *Biotechnol. Prog.* (2003) 19: 64–68.

A Serum Substitute for Fed-Batch Culture of Hybridoma Cells

Keisuke Shibuya, Ryoichi Haga, and Masaru Namba

Abstract A serum substitute consisting of 12 components has been developed to produce fed-batch cultures of hybridoma cells in serum-free medium. We did a fed-batch culture of hybridoma cells using this substitute and confirmed that the cells could be successfully cultivated this way. The specific production rates of lactate and ammonia, which are harmful byproducts from cells, were significantly reduced compared with a conventional serum-containing batch culture. This reduction led to a higher cell concentration and a longer production lifetime. As a result, the final concentration of monoclonal antibody was 400 mg/l, or five times greater than that in the conventional serum-containing batch culture. The developed substitute will enable fed-batch cultivation in a serum-free condition.

Keywords Serum-free culture • fed-batch culture • hybridoma cells

1 Introduction

Fed-batch cultivation of mammalian cells has been routinely used for industrial production of biologicals [1–3]. In vitro culturing of hybridoma cells has been extensively studied for a high production rate of monoclonal antibody for several decades, and many efficient nutrient feeding strategies [4–6] have been developed. The most important strategy for doing fed-batch culture is to reduce the formation of byproducts, such as lactate and ammonia, and keep the nutrient concentration balanced and stable. Low accumulation of metabolites is critical to produce a high viable cell density and a long production lifetime, which can lead to high production of biologicals. Cell growth over time, i.e. the integral of viable cells (IVC) is often used as an indicator for a cultivation producing monoclonal antibody. Lactate and ammonia are derived mainly from the cellular metabolism of glucose and

K. Shibuya, R. Haga, and M. Namba
Hitachi, Ltd. Power & Industrial Systems R&D Laboratory, 7-2-1, Omika-cho, Hitachi-shi, Ibaraki 319-1221, Japan

K. Ikura et al. (eds.), *Animal Cell Technology: Basic & Applied Aspects*,
Animal Cell Technology: Basic & Applied Aspects 15,
DOI 10.1007/978-1-4020-9646-4_12, © Springer Science+Business Media B.V. 2009

glutamine respectively. Their production can be partly decreased by reducing the glucose and glutamine concentrations in the medium. In recent studies, effective cultures of hybridoma and CHO cells have been developed through comprehensive research on nutrient metabolism [4–6]. The models in these studies incorporated not only major pathways of glucose and glutamine metabolism but also pathways of other amino acids into the stoichiometric model. As a result, high efficient production of monoclonal antibody was achieved.

However, most of these studies have been done using serum-supplemented culture systems. Using serum is undesirable for the following reasons. There have been a lot of problems related to virus infections transmitted by animal serum for production of biologicals. Infectious risks can threaten safety of the products. Regarding nutrient feedings for fed-batch cultivation, unknown factors contained in serum might affect the cellular metabolism. This can complicate optimizing nutrient feeding. Furthermore, using serum has much reliance on experimental data because cell proliferation depends strongly on serum lots. Then, developing a serum-free culture system has been strongly desired.

In order to mitigate these problems, in this study, we have developed a substitute for serum for fed-batch cultures of hybridoma cells and confirmed the cells could be successfully cultivated using this substitute.

2 Strategies for Serum-Free Fed-Batch Culture

Mammalian cells require a complex nutrient environment for growth and survival in vitro. The typical cell culture medium is composed of carbon sources such as glucose, amino acids, vitamins, inorganic salts, buffers and various other components including serum. Some of these components, such as inorganic salts, are generally abundant, while others are often present in small amounts for cell growth. Most of the components will be consumed in large amounts; but even if consumption is low, there are some components such as trace metals which are needed for biological functions. Media for batch cultivation must contain abundant nutrients that will not be exhausted, while media for fed-batch cultivation contain low concentrations of glucose and amino acids which are optimized according to a variety of stochiometric models.

Recently, some serum-free media for batch cultivation have been developed and commercially marketed. We confirmed proliferation of CRL-1606, STK-1 and CHO cells in batch cultivation using one of the commercially available serum-free media (data are not shown). This medium has all the components for cell growth and survival. Unlike the composition of the medium containing serum, we selected the 12 components shown in Table 1 as a substitute for serum. We omitted some components (e.g. glucose, amino acids) that are included in stochiometric models from the serum-free medium and modified the concentration of the remainder. We assumed that using 12 components instead of serum makes the medium more adaptable for fed-batch cultivation of CRL-1606, STK-1 and CHO cells.

Table 1 Components of a substitute for serum

Component	Concentration (mg/l)	Component	Concentration (mg/l)
Insulin	100	Hypoxanthine	13.5
Transferin	100	Linolecic acid	0.21
Aminobenzoic acid	2.5	Lipoic acid	0.515
Pyridoxinehydrochloride	22	Putrescine	0.4
Sodium selenite	0.065	Thymidine	1.81
Phenylpyruvic acid sodium salt	825	Glutathione	2.5

3 Materials and Methods

3.1 Cell Line and Culture Medium

The host cell line in this experiment was a mouse-mouse hybridoma, CRL-1606, producing anti-human fibronectin monoclonal antibody. We purchased the cell line from American Type Culture Collection (ATCC; Manassas, USA).

In the serum supplied batch culture we used Iscove's Modified Dulbecco's Medium (IMDM; Sigma-Aldrich, St. Louis, USA) and 5% of fetal bovine serum (BioSource International, Inc., Camarillo, USA). In the serum-free batch culture we used IBL Media III medium (Immuno-Biological Laboratories, Takasaki, Japan).

In the serum-free fed-batch cultivation we prepared the culture media according to the method of Xie and Wang [7]. The culture media consisted of an initial medium and a feeding medium. The initial medium was based on IMDM, which is often used in combination with serum for the conventional cultivation of hybridoma. The concentration of inorganic salts and vitamins in the initial medium was similar to that in IMDM. However, to reduce harmful ammonia formation, the level of amino acids was kept lower than in IMDM. In this fed-batch culture we prepared the initial medium just using the 12 components shown in Table 1 instead of serum. The feeding medium contained multiple nutrients with a stoichiometrically balanced composition. These nutrients were controlled simultaneously through feeding by controlling one of them. The feeding medium had the same composition as the medium of Xie and Wang did.

3.2 Culture Conditions

The experiment was performed in a 1-l bioreactor (Able Co., Tokyo, Japan) with a volume of 800 ml of culture medium and an initial cell density of 1×10^8 cells/l. Dissolved oxygen and pH were monitored and controlled at 60% of saturated air and 7.2, respectively, by adjusting the inlet gas composition. The inlet gas, composed of oxygen, carbon dioxide, and nitrogen, was passed through a porous sparger immersed in the culture medium. We aseptically took 5 ml of samples twice

or three times a day to measure the density and viability of the cells as well as the concentrations of glutamine, glucose, ammonia and lactate. After centrifugation at 800 g for 10 min, supernatant was then stored at −20°C for later analysis of monoclonal antibody concentration. In the fed-batch culture, feeding medium was added to maintain a relatively constant nutritional environment. We adopted glutamine as an indicator for feeding control. The glutamine concentration ranged from 0.3 to 1.8 mM for the cultivations.

3.3 Analytical Methods

The concentration of viable cells and viability were automatically determined using the Vi-CELL™ automated cell viability analyzer (Beckman Coulter, Fullerton, USA). The concentration of the main components of the culture medium such as glucose, glutamine, glutamate, ammonia and lactate was determined using a Nova Bioprofile 100 Plus Analyzer (Nova Biomedical Corp., Waltham, USA). The enzyme-linked immunosorption assay (ELISA) was employed to determine the titer of the monoclonal antifibronectin antibody. Cells were centrifuged for 10 min at 800 g with a centrifuge (Kokusan, Tokyo, Japan) prior to the antibody assay. Kappa mouse IgG1 (Sigma) was used as a standard. First, 100 µL antigen solution (antibody to mouse IgG1; Sigma, USA) were placed in a 96-well microtiter plate and incubated for 1 h. After rinsing with 3 × 100 µL washing buffer (1:10 diluted Block Ace solution plus 0.05% Tween20; Snow Brand Milk Products Co., Ltd., Tokyo, Japan), the wells were blocked with 1:4 diluted Block Ace solution at 37°C for 1 h. Samples were added to the wells, and antibody was enabled to bind them by incubating the wells at 37°C for 1 h. The wells were then washed three times with washing buffer. Bound antibodies were detected with alkaline phosphatase conjugate antibody (Vector Laboratories, Inc., Burlingame, USA). Incubation and washing steps were as described above. Signals were developed with p-nitrophenyl phosphate (PNPP) substrate (Vector Laboratories, Inc.), and the absorbance at 405 nm was measured.

4 Results and Discussion

A selected fed-batch example of CRL-1606 cell line is given here to demonstrate the fed-batch capacity and potential by using our developed substitute for serum.

As shown in Fig. 1, CRL-1606 cells began to increase after a lag phase and the increase of viable cells stopped on the 21st day. The maximum viable cell density reached 3×10^9 cells/l for the serum-free fed-batch cultivation. The values of proliferation and viable cell density were both the highest among the values obtained by the other cultivations (batch cultivation with serum or without serum). That meant that we achieved enhancement of ICV. That is, we could effectively cultivate CRL-1606 cells using our substitute for serum.

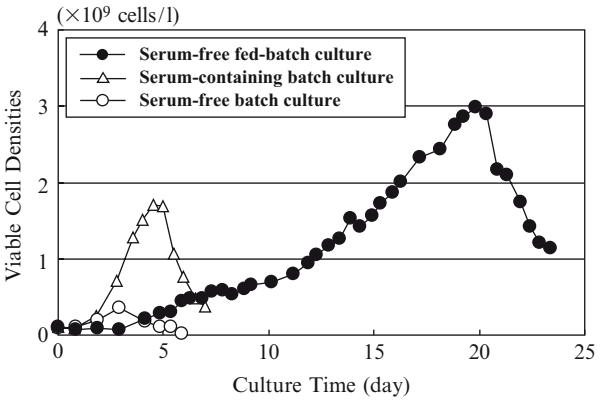

Fig. 1 Growth profiles of CRL-1606 cells in fed-batch and batch cultures

Table 2 Comparison of culture performance

	Fed-Batch without Serum	Batch without Serum	Batch with Serum
Culture span (day)	21	5	5
Maximum viable cell density (10^9 cells/l)	3.0	0.36	1.7
Monoclonal antibody concentration (mg/l)	400	9	80
Average specific antibody production rate (10^{-9}mg cell^{-1} h^{-1})	0.45	0.45	0.39
Average specific formation rate of ammonia (10^{-9} mM cell^{-1} h^{-1})	0.054	0.30	0.06
Average specific formation rate of lactate (10^{-9} mM cell^{-1} h^{-1})	0.25	2.0	0.44

The concentration of antibody increased concomitant with the integrated value of viable density over time (data not shown), and then, as seen from Table 2, the final concentration of monoclonal antibody of the serum-free fed-batch culture was 400 mg/l, or five times greater than that in the serum supplied batch culture, which is the conventional method. Average specific antibody production rate of serum-free batch and fed-batch cultures remained the same. Therefore we could reason that the enhancement of antibody production by the fed-batch cultivation was due to the improvement of ICV. The rate of average specific formation of ammonia and lactate was significantly reduced by keeping glucose, glutamine and other amino acids at a low level through feeding control of concentrate. This reduction of byproducts improved ICV in the fed-batch cultivation. Thus, the substitute we developed was effective for maintaining the features of fed-batch cultivation.

This substitute would have a potential for application to other cell lines, based on our finding that we could culture CHO and STK-1 cells successfully in the batch cultivation using the substitute.

5 Conclusion

We have developed a substitute for serum for fed-batch cultivation. When using the developed substitute, we confirmed effective reduction of amounts of ammonia and lactate produced and enhancement of monoclonal antibody production in the serum-free fed-batch culture of CRL-1606 cells. We expect that this substitute will be suitable for fed-batch culture application to other cell lines (e.g. CHO and STK-1 cells) judging from the proliferation of CHO and STK-1 cells in the batch cultivation using the substitute. Thus, serum-free fed-batch culture can be done easily by using our developed substitute.

References

1. Khoudi H, Laberge S, Ferullo JM, Bazin R, Darveau A, Castonguary Y, Allard G, Lemieux R and Vezina LP, Production of a diagnostic monoclonal antibody in perennial Alfalfa plants. Biotechnol Bioeng **64**, 135–143 (1999).
2. Liddell E and Weeks I, Anitibody Technology. Bios Scientific, UK, pp. **65**–130 (1995).
3. Spier RE, Animal cell biotechnology in the 1990s, from models to morals, in Animal Cell Biotechnology, Eds. Spier RE and Griffiths JB. Cambridge, Academic Press, UK, pp. 1–43 (1994).
4. Bibila TA and Robinson DK, In pursuit of the optimal fed-batch process for monoclonal antibody production. Biotechnol Prog **11**, 1–13 (1995).
5. Distefano DJ, Mark GE and Robinson DK, Feeding of nutrients delays apoptotic death in fed-batch cultures of recombinant NS0 myeloma cells. Biotechnol Lett **18**, 1067–1072 (1996).
6. Birch JR and Racher AJ, Antibody production. Adv Drug Deliv Rev **58**(5–6), 671–85 (2006).
7. Xie L and Wang DI, Applications of improved stoichiometric model in medium design and fed-batch cultivation of animal cells in bioreactor. Cytotechnology **15**(1-3), 17–29 (1994).

Effects of Sugar Chain Precursors on Recombinant Protein Production in BHK Cells

Megumi Hayashi, Kaori Doi, Ichiro Ebata, Shinya Yamaguchi, Yasuhiro Ohta, and Satoshi Terada

Abstract Glycosylation of bioactive proteins is a pivotal posttranslational modification for their biological activities, and therefore constant production of glycoproteins with high levels of glycosylation is required for industrial production. Among the residues in sugar chains, sialic acids are important for the in vivo stability of glycoproteins and high levels of sialylation are desirable. However, sialic acids are scarcely able to be incorporated from the medium. *N*-acetyl-D-mannosamine (ManNAc), an intracellular precursor for sialic acid synthesis, has been tested as a culture substrate for improving sialylation. In the present study, the influences of ManNAc on cell proliferation and product yield were investigated. ManNAc was added to cultures of BHK-EPO cells producing a recombinant EPO protein as a model for glycoprotein production. Although the cell proliferation was seriously inhibited in the presence of 200 mM ManNAc, the recombinant protein production was improved. Analysis by two-dimensional electrophoresis revealed that the EPO glycosylation level was improved in the presence of ManNAc. These results imply that BHK cells would be suitable for producing glycoproteins with high levels of sialylation in the presence of concentrated ManNAc.

Keywords Glycosylation • ManNAc • sialic acid • BHK • EPO

1 Introduction

Glycoproteins represent an important category of therapeutic pharmaceuticals for human health care, and their physicochemical and biological properties are affected by glycosylation. However, since the proteins produced by prokaryotes such as

M. Hayashi, K. Doi, and S. Terada
Department of Applied Chemistry and Biotechnology, University of Fukui,
3-9-1 Bunkyou, Fukui, 910-8507, Japan

I. Ebata, S. Yamaguchi, and Y. Ohta
Marukin Bio Inc., 27 Monnomae, Todo, Uji, Kyoto, 611-0013, Japan

K. Ikura et al. (eds.), *Animal Cell Technology: Basic & Applied Aspects*,
Animal Cell Technology: Basic & Applied Aspects 15,
DOI 10.1007/978-1-4020-9646-4_13,

E. coli are not glycosylated, most bioactive proteins are produced in eukaryotes, such as yeasts, molds and mammalian cells. Among these, mammalian cells are extensively used for glycoprotein production, due to their relatively proper glycosylation processes. However, the glycosylation patterns are strongly dependent on the producers. In other words, recombinant proteins produced in different host cells contain different patterns of oligosaccharides, and this will affect their biological functions [1]. Moreover, the glycosylation patterns are also influenced by the culture conditions and parameters such as the dissolved oxygen and ammonia concentrations [2–5], indicating the difficulties associated with the production of glycoproteins containing constantly high levels of glycosylation. Hence, development of technology for producing proper glycoproteins is urgently required.

Recently, a variety of metabolic substrate-based approaches toward glycosylation have been developed through cell culture engineering. In particular, the targets of these approaches are the biosynthetic pathways of sugar residues such as sialic acids. Sialic acids, the terminal sugars in N-linked complex glycan structures, have pivotal effects on the lifetimes and biological activities of the linked glycoproteins. Increases in the intracellular pool of sialic acids would contribute to the sialylation level, but these acids almost are not incorporated into cells when they are directly supplemented into the medium at high concentrations. Gu et al. [6] reported that supplementation of cultured cells with *N*-acetyl-D-mannosamine (ManNAc), a precursor for sialic acid biosynthesis, successfully elevated the sialylation level. In the present study, BHK cells were cultured in the presence of ManNAc and its effects on their cell proliferation, survival, recombinant protein production and glycosylation levels were assessed.

2 Materials and Methods

2.1 Cell Line and Culture Conditions

BHK cells (CRL-13001), producing a recombinant human erythropoietin (rhEPO), were obtained from the American Type Culture Collection (ATCC, USA) and are referred to as BHK-EPO cells in this article. BHK-EPO cells were cultured in DMEM (Nissui, Japan) supplemented with 10% FBS, 10 mM HEPES, 0.2% $NaHCO_3$, 0.06 mg/ml kanamycin, 2 mM glutamine and 0.4 mg/ml G418. For several analyses, the cells were cultured in a serum-free and low-protein medium (ASF104; Ajinomoto, Japan). All cultures were performed at 37°C in air containing 5% CO_2.

2.2 Proliferation Assay

The effects of ManNAc on cell proliferation were determined by the following method. BHK-EPO cells suspended in DMEM were seeded onto 24-well plates (Sumitomo Bakelite, Japan) and incubated at 37°C for 1 day. The medium was then exchanged for fresh ASF104 medium supplemented with a range of ManNAc concentrations. Viable cell densities were determined by hemocytometer counting.

2.3 Determination of EPO Concentrations

The EPO concentrations in culture supernatants were determined by ELISA. Briefly, 96-well plates (Falcon, USA) were coated with a rabbit anti-EPO antibody (4 μg/ml; Sigma, USA) in 0.1 M sodium bicarbonate buffer (pH 8.3) at 4°C overnight. The plates were blocked with 3% BSA/PBS for 2 h and then incubated with serial dilutions of an EPO standard or culture supernatant samples for 4 h at room temperature. After washing, the bound EPO was incubated with a mouse anti-EPO antibody (IgG; 1 μg/ml; a kind gift from Prof. Sasaki) at 4°C overnight and then with HRP-conjugated anti-mouse IgG (1.1 μg/ml; Cappel, USA) for 2 h in 1% BSA/PBS/0.05% Tween-20. For detection of the antigen-antibody reactions, OPD (Wako, Japan) and H_2O_2, substrates of HRP, were added and incubated at 4°C overnight. The optical absorbances at 490 and 630 nm were measured using a microplate reader (Sankojunyaku, Japan). Each incubation step was followed by four washes with PBS/0.05% Tween-20.

2.4 Two-Dimensional Electrophoresis

Culture supernatants were collected and concentrated by centrifugation using an ultrafiltration membrane (Amicon Ultra-15 Centrifugal Filter Device; Millipore, USA). The EPO samples for analysis were prepared by adding an equal volume of sample buffer. The mixtures were incubated on ice for 20 min, and then separated according to their isoelectric points using Immobiline DryStrip (GE Healthcare, USA). After the first dimension, the strip was mounted on a 12% SDS-gel, and the EPO was separated by SDS-PAGE. EPO was visualized by immunoblot analysis as follows. The proteins in the gel were electrophoretically transferred onto a PVDF membrane (GE Healthcare), and the membrane was blocked with 5% skim milk at 4°C overnight. Next, the membrane was incubated with the rabbit anti-EPO antibody (0.5 μg/ml) at room temperature for 1.5 h and then with an HRP-conjugated anti-rabbit antibody (Chemicon, USA). Finally, the membrane was treated with ECL western blotting detection reagents (GE Healthcare) to detect EPO protein.

3 Results and Discussion

3.1 Effects of ManNAc on BHK Cell Proliferation

To assess the effects of ManNAc supplementation, BHK-EPO cells were cultured in the presence of 0, 2, 20 or 200 mM ManNAc. ManNAc concentrations of less 20 mM did not affect the cell proliferation, whereas 200 mM ManNAc seriously inhibited it (Fig. 1). However, the cell viabilities remained largely unaffected by the presence of ManNAc at any of the concentrations examined. These data were obtained for cultures

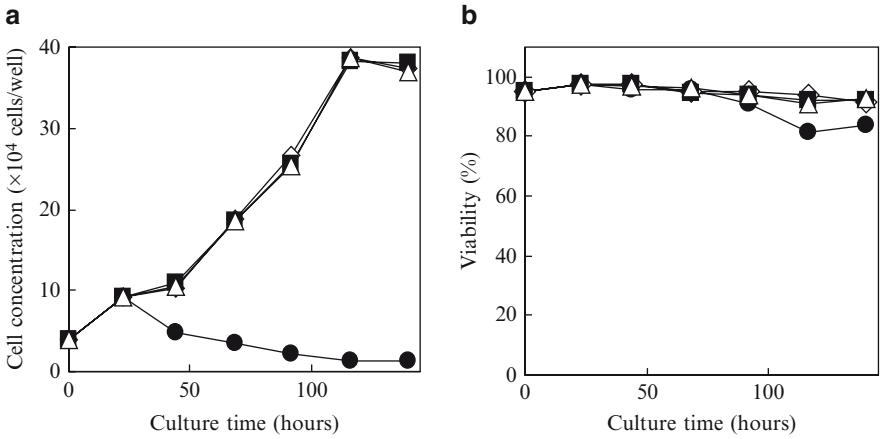

Fig. 1 Effects of ManNAc on BHK-EPO cell proliferation and viability. BHK cells were seeded at a density of 4×10^4 cells/well and incubated at 37°C in DMEM supplemented with FBS for 1 day. Next, the medium was exchanged for ASF104 medium containing a range of ManNAc concentrations: 0 mM (*open diamonds*), 2 mM (*closed squares*), 20 mM (*open triangles*) or 200 mM (*closed circles*)

of BHK cells transfected with an EPO expression vector, although similar results were obtained for cultures of wild-type BHK cells (data not shown).

3.2 EPO Productivity

The EPO concentrations in the culture supernatants were determined by ELISA. The EPO concentration in the culture supplemented with 200 mM ManNAc was significantly higher than those in other cultures (Fig. 2), despite the fact that 200 mM ManNAc strongly inhibited the cell proliferation (Fig. 1). This result suggests that the suppression of cell proliferation actually contributes to the EPO production due to the use of surplus resources for protein production. This result also implies that the BHK cell line may be suitable for producing glycoproteins with high levels of sialylation in the presence of concentrated ManNAc.

3.3 Two-Dimensional Electrophoresis of EPO Samples

The heterogeneity of the glycosylated EPO proteins obtained from the culture supernatants was analyzed by protein separation via two-dimensional electrophoresis followed by immunoblotting for band detection (Fig. 3). EPO samples were prepared from BHK cell cultures containing 0, 20, 40 or 80 mM ManNAc, and distinct pI values were observed for the EPO isoforms. In the absence of ManNAc, no EPO isoforms were observed in the higher MW and higher pI areas, whereas

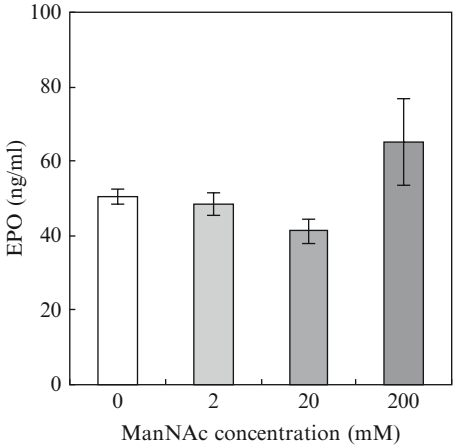

Fig. 2 EPO production by BHK cells in the presence of ManNAc. The culture supernatants were collected after 140 h of culture and the EPO concentrations were determined by ELISA

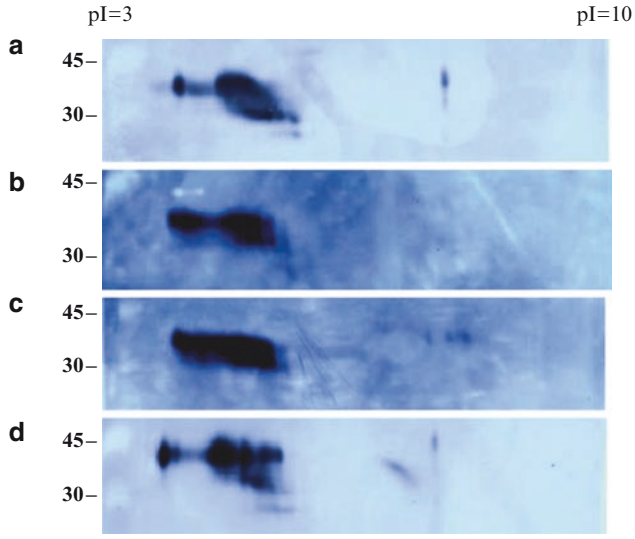

Fig. 3 Two-dimensional electrophoresis of EPO samples. Supernatants from BHK cell cultures containing 0 mM (**a**), 20 mM (**b**), 40 mM (**c**) and 80 mM (**d**) ManNAc were analyzed by 2-D electrophoresis, involving separation by pI (ampholyte pH 3–10) in the first dimension and SDS-PAGE in the second dimension, and detected by immunoblotting

isoforms were observed in these locations in the presence of EPO. In particular, EPO isoforms with higher MW and higher pI were easily identified in the culture treated with 80 mM ManNAc, compared with the cultures at lower concentrations of ManNAc. This indicates that the glycosylation levels were successfully elevated following the addition of ManNAc, and that these increases were dependent on the ManNAc concentration.

Acknowledgement The mouse anti-EPO antibody was a kind gift from Prof. Sasaki.

References

1. T. S. Raju, J. B. Briggs, S. M. Borge, A. J. S. Jones (2000) Species-specific variation in glycosylation of IgG: evidence for the species-specific sialylation and branch-specific galactosylation and importance for engineering recombinant glycoprotein therapeutics, *Glycobiology* 10, 477–486
2. M. Gawlitzek, U. Valley, M. Nimtz, R. Wagner, H. S. Conradt (1995) Characterization of changes in the glycosylation pattern of recombinant proteins from BHK-21 cells due to different culture conditions, *Journal of Biotechnology* 42, 117–131
3. M. Yang, M. Butler (2000) Effect of ammonia on CHO cell growth, erythropoietin production, and glycosylation, *Biotechnology and Bioengineering* 68, 370–380
4. F. L. Floch, B. Tessier, S. Chenuet, J. Guillaume, P. Cans, A. Marc, J. Goergen (2004) HPCE monitoring of the N-glycosylation pattern and sialylation of murine erythropoietin production by CHO Cells in batch processes, *Biotechnology Progress* 20, 864–871
5. J. A. Serrato, L. A. Palomares, A. Meneses-Acosta, O. T. Ramirez (2004) Heterogeneous conditions in dissolved oxygen affect N-glycosylation but not productivity of a monoclonal antibody in hybridoma cultures, *Biotechnology and Bioengineering* 88, 176–188
6. X. Gu, D. Wang (1998) Improvement of interferon-γ sialylation in Chinese hamster ovary cell culture by feeding of N-acetylmannosamine, *Biotechnology and Bioengineering* 58, 642–648

Promoting Non-Hematopoietic Cell Proliferation by Chimeric Receptors

Kento Tanaka, Masahiro Kawahara, Hiroshi Ueda, and Teruyuki Nagamune

Abstract In our previous study, a selection method, antigen mediated genetically modified cell amplification (AMEGA) [1], was developed, where chimeric receptor was employed as a growth switch of hematopoietic cells. In this study, we attempted to apply the AMEGA system to non-hematopoietic cells. For this application, new chimeric receptors consisting of antibody ScFv and receptor tyrosine kinase were constructed. We confirmed that these chimeric receptors could promote proliferation of not only hematopoietic but also non-hematopoietic cells, and this promotion was ligand-dependent.

Keywords Chimeric receptor • AMEGA • growth promotion

1 Introduction

Recently biomedicines including cytokines and monoclonal antibody have been attracting attention especially in clinical applications, since they have a big potential to cure many diseases. However, they are unaffordable because we need a big amount of medium including expensive serum or growth factors in production process. To overcome this problem, such approaches as enhancement of protein activity [2], prolonging half-life of therapeutic protein in our body, regulation of cell growth [3], medium characterization, and utilization of animals [4] or plants are now studied. In our previous study, a novel method to promote cell growth was developed, where chimeric receptors consisting of an antibody fragment and a cytokine receptor transduce a growth signal in response to a cheap antigen instead of an expensive cytokine. However, so far we tried to apply chimeric receptors only for growth promotion of hematopoietic cells. In this study, we aimed to promote

K. Tanaka, M. Kawahara, H. Ueda, and T. Nagamune
Department of Chemistry and Biotechnology, School of Engineering,
The University of Tokyo, 7-3-1, Hongo, Bunkyo-ku, Tokyo, Japan

K. Ikura et al. (eds.), *Animal Cell Technology: Basic & Applied Aspects*,
Animal Cell Technology: Basic & Applied Aspects 15,
DOI 10.1007/978-1-4020-9646-4_14,

growth of non-hematopoietic cells, which are also used for industrial protein production. For this purpose, we developed new chimeric receptors comprising an antibody fragment and a receptor tyrosine kinase that is known to be active in non-hematopoietic cells, and examined whether they could promote cell growth in response to a cognate antigen.

2 Materials and Methods

2.1 Vector Construction

Plasmid pMK-SEbeta-IGFP was constructed in our laboratory. Human EGFR gene was digested from pco12 EGFR (RIKEN). Human fms gene was amplified from Multiple ChoiceTM (OriGene Technologies). From pMK-SEbeta-IGFP and human EGFR gene or fms gene, we constructed two vectors of EGFR or fms chimeric receptor (Fig. 1). These consisted of an anti-fluorescein (FL) ScFv fused to the extracellular D2 domain of erythropoietin receptor and transmembrane/intracellular domains of EGFR or fms receptor. They were named pMK-S-EGFR-IGFP or pMK-S-fms-IGFP, respectively. Both vectors are bicistronic, and express chimeric receptor and EGFP as a marker/model protein.

2.2 Cell Culture

A murine IL-3 dependent pro-B cell line, Ba/F3, was cultured in RPMI 1640 medium (Nissui Pharmaceutical Co., Ltd.) supplemented with 10% FBS and 2 ng/ml IL-3 (Genzyme-Techne). A mouse fibroblast NIH/3T3 was cultured in Dulbecco's modi-

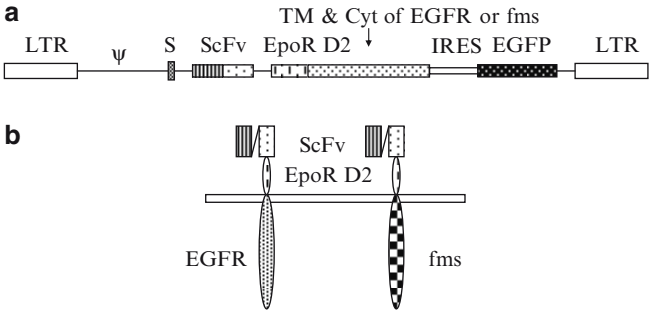

Fig. 1 (**a**) The construction of pMK-S-EGFR-IGFP and pMK-S-fms-IGFP. Retroviral vectors with long terminal repeats (LTRs) and packaging signal (ψ) are used for the efficient transcription of chimeric receptor and EGFP gene. An immunoglobulin heavy chain secretion signal sequence (S) is located upstream of the chimeric receptor genes to enable their cell surface expression. (**b**) Chimeric receptors construction in this study

fied Eagle's Medium (DMEM) (Nissui Pharmaceutical Co., Ltd.) supplemented with 10% FBS. A retroviral packaging cell line, Plat-E, DMEM supplemented with 10% FBS, 1 μg/ml puromycin (Sigma), and 10 μg/ml blasticidin (Kaken Pharmaceutical Co., Ltd.).

2.3 AMEGA Selection

Ba/F3 and NIH/3T3 were retrovirally transduced with vectors for chimeric receptors with Fugene6 (Roche Diagnostics, Basel, Switzerland) following manufacture's instruction. As for Ba/F3 (Fig. 2a), the cells (2×10^5) were washed once, and seeded into 24-well plates. Selection was performed in the medium containing no factor or 5 μg/ml BSA-FL (Sigma). After selection, cells were analyzed by flow cytometry to estimate transduced cell ratio. As for NIH/3T3 (Fig. 2b), the cells (5×10^3) were detached by trypsin EDTA, and seeded into 24-well plates. Selection was performed in the DMEM supplemented with 3% FBS. After cells became sub-confluent, cells were further subcultured, and remainder of the cells was subjected to flow cytometric analysis to examine transduced cell ratio. This subculture/flow cytometric analysis cycle was repeated for about 2-month selection.

2.4 Flow Cytometry

Ba/F3 cells were washed once with PBS and resuspended in PBS. NIH/3T3 cells were washed once with PBS, detached and resuspended in PBS. Green fluorescence intensity was measured by using FACS Calibur (Becton Dickinson) at 488 nm excitation and fluorescence detection at 530 ± 15 nm.

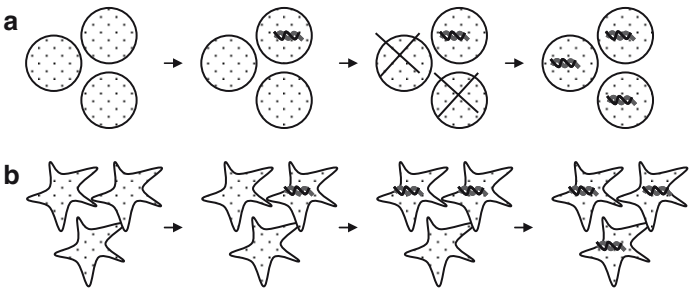

Fig. 2 Concept of this study. (**a**) AMEGA for hematopoietic cells. Since untransduced cells cannot survive, we can get exclusively transduced cells. (**b**) AMEGA for non-hematopoietic cells. Since transduced cells grow faster than untransduced cells during serial subcultures, we can select only transduced cells

3 Result

3.1 AMEGA on Ba/F3

In this study, the EGFP gene was used as a model transgene, and vectors, pMK-S-EGFR-IGFP and pMK-S-fms-IGFP, were employed for subsequent analyses. IL-3-dependent Ba/F3 cells were retrovirally transduced with the vectors, resulting in Ba/S-EGFR and Ba/S-fms, respectively. After the transduction efficiency was analyzed by flow cytometry, AMEGA selection of these cells performed. 5 days later, to examine whether BSA-FL promoted cell growth selectively for those with transgene expression, flow cytometric analysis was performed to compare the EGFP-positive cell ratio before and after the selection (Fig. 3). While initial EGFP-positive cell ratios of Ba/S-EGFR and Ba/S-fms were 1.47% and 1.56%, respectively, after AMEGA selection those became all about 100%. As a result, we successfully achieved AMEGA selection by chimeric EGFR and fms receptors.

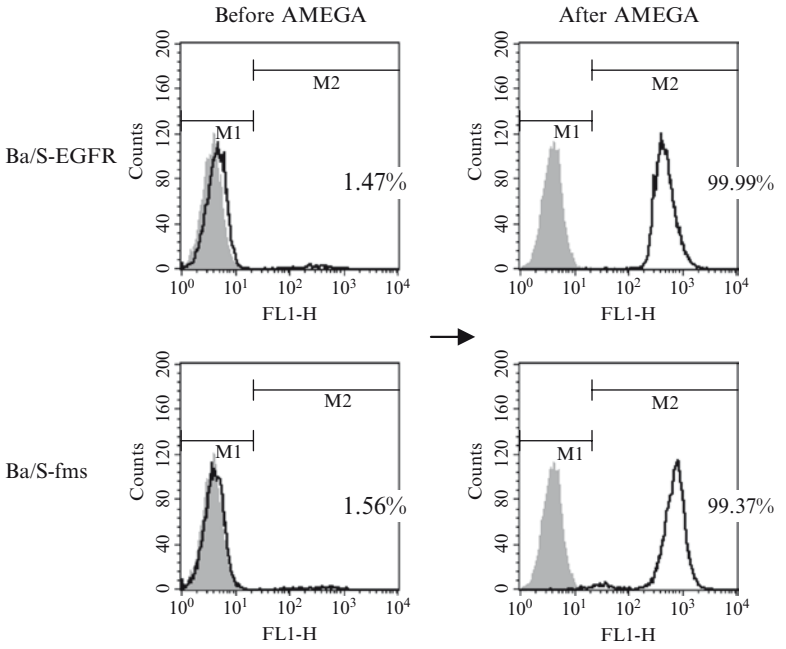

Fig. 3 The results of AMEGA selection on Ba/F3 with chimeric receptors consisting of antibody ScFv and receptor tyrosine kinase. Cells were analyzed by flow cytometry, and cell number was plotted against log green fluorescence intensity. EGFP-negative cells appeared in M1 region and EGFP-positive ones appeared in M2. Values (%) in each diagram represent M2 ratio. Filled space and line indicate parental Ba/F3 (negative control) and transduced cells, respectively

3.2 Growth Assay of Ba/S-EGFR and Ba/S-fms

To determine whether the selected transduced cells show BSA-FL dependent cell growth, growth assay was performed. The BSA-FL-selected Ba/S-EGFR and Ba/S-fms cells were washed and cultured in the medium with various BSA-FL concentrations. Cell density was measured with Cell Counting Kit8 (Dojindo). Ba/S-EGFR and Ba/S-fms cells proliferated in a ligand-dependent manner (Fig. 4), indicating that we can control growth speed by ligand concentration.

3.3 AMEGA on NIH/3T3

We investigated whether these chimeric receptors could promote growth of mouse fibroblast NIH/3T3 cells as a representative of non-hematopoietic cells. NIH/3T3 cells were retrovirally transduced with pMK-S-EGFR-IGFP and pMK-S-fms-IGFP, resulting in NIH/S-EGFR and NIH/S-fms, respectively. After the transduction efficiency was analyzed by flow cytometry, AMEGA selection of these cells was performed by serial subcultures. When subcultured each time, cells were subjected to flow cytometry to analyze EGFP-positive cell ratio. It took about 1 and 2 months selection to give ~100% EGFP-positive cell population for NIH/S-fms and for NIH/S-EGFR, respectively (Fig. 5). This difference indicates S-fms has higher growth-promoting activity than S-EGFR.

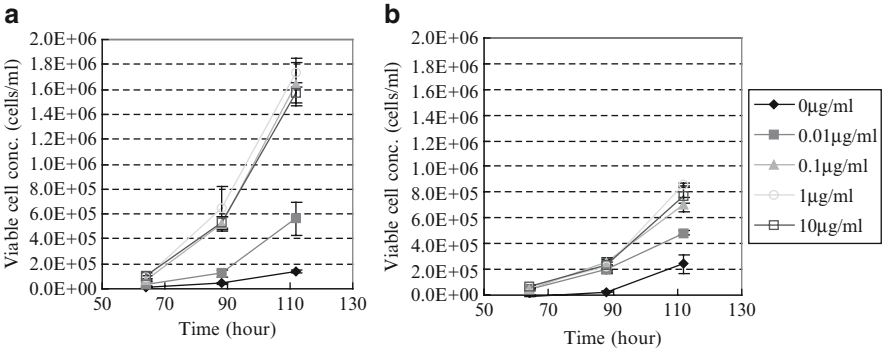

Fig. 4 Growth curves of (**a**) Ba/S-EGFR and (**b**) Ba/S-fms in various BSA-FL concentrations. Initial cell density was set at 4×10^3 cells/ml. Viable cell concentration was plotted against incubation time (hour). In line plot, filled rhombus, filled square, filled triangle, open rhombus, and open square indicate BSA-FL conc. 0, 0.01, 0.1, 1, and 10 μg/ml, respectively

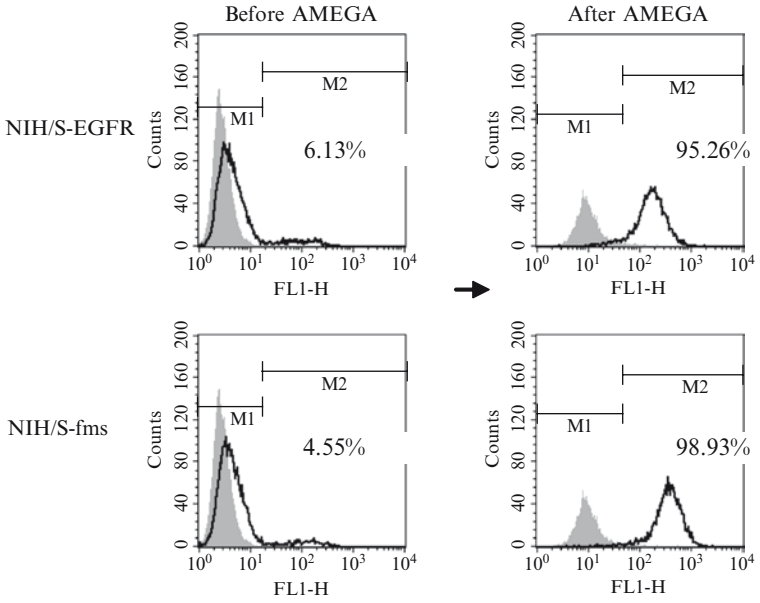

Fig. 5 The results of AMEGA selection on NIH/3T3 with chimeric receptors consisting of antibody ScFv and receptor tyrosine kinase. Values (%) in each diagram represent M2 ratio. Filled space and line indicate parental NIH/3T3 (negative control) and transduced cells, respectively

Fig. 6 An analysis of ligand dependency of S-fms. Initial cell density was 10^4 cells/ml, and 6 days later cell number was analyzed by flow cytometry

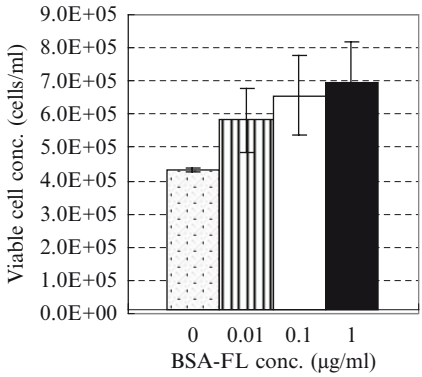

3.4 Growth Assay of NIH/S-fms

To evaluate the growth promotion in various ligand concentrations, growth assay of NIH/3T3 was performed. The BSA-FL-selected NIH/S-EGFR and NIH/S-fms cells were washed and cultured in the medium with various BSA-FL concentrations. NIH/S-fms proliferated faster with increasing ligand concentrations (Fig. 6), concluding that the chimeric receptor could promote growth of non-hematopoietic cells.

4 Discussion

We developed new chimeric receptors consisting of an antibody fragment and a receptor tyrosine kinase functional in hematopoietic and non-hematopoietic cells. So far, although AMEGA was performed only for hematopoietic cells, we could apply AMEGA also to non-hematopoietic cells, which expand application field of AMEGA. We attained promotion of growth around 1.4-fold, which might improve protein productivity. In addition chimeric receptors have one additional advantage. In protein production, there are generally two phases, log growth phase and production phase [5]. Our chimeric receptor can switch ON/OFF of growth promotion depending on phase, leading to more sophisticated production process. There is one problem in our chimeric receptor, especially S-fms, which promoted growth promotion without ligand probably due to preformed dimers. Since S-EGFR exhibited lower residual cell growth without ligand, we had better apply S-EGFR for protein production process when rigid growth regulation is necessary. Since not NIH/3T3 but CHO cells are available now for therapeutic protein production, we should investigate whether these chimeric receptor could promote growth of CHO cells as well as their protein productivity. If these problems are solved, our AMEGA system would be a versatile method to produce more affordable biomedicines, contributing to better therapeutic treatment for many patients.

References

1. Kawahara, M. et al. Bypassing antibiotic selection: positive screening of genetically modified cells with an antigen-dependent proliferation switch. *Nucl. Acids Res.* **31**, e32 (2003)
2. Shinkawa, T. et al. The absence of fucose but not the presence of galactose or bisecting N-acetylglucosamine of human IgG1 complex-type oligosaccharides shows the critical role of enhancing antibody-dependent cellular cytotoxicity. *J. Biol. Chem.* **78**, 3466–3473 (2003)
3. Renner, R. A. et al. Recombinant cyclin E expression activates proliferation and obviates surface attachment of Chinese hamster ovary (CHO) cells in protein-free medium. *Biotechnol. Bioeng.* **47**, 476–482 (1995)
4. Zhu, L. et al. Production of human monoclonal antibody in eggs of chimeric chickens. *Nat. Biotechnol.* **23**, 1159–1169 (2005)
5. Fussenegger, M. et al. Genetic optimization of recombinant glycoprotein production by mammalian cells. *Trends Biotechnol.* **17**, 35–42 (1999)

Efficient Acquisition of Antigen-Specific Human Monoclonal Antibody by Using Peripheral Blood Mononuclear Cells Immunized In Vitro

Efficient Cloning of Human Monoclonal Antibody Gene

Shinei Matsumoto, Makiko Yamashita, Yoshinori Katakura, Kosuke Tomimatsu, Yoshihiro Aiba, Kiichiro Teruya, and Sanetaka Shirahata

Abstract We have developed an in vitro immunization protocol of human peripheral blood mononuclear cells (PBMC) for generating human antigen-specific antibodies. Upon sensitization of PBMC with antigen in vitro according to the protocol, B cells producing antigen-specific antibody can be propagated within a week. In the present study, we tried to establish a strategy to clone variable region genes of antigen specific human monoclonal antibody by applying in vitro immunized PBMC to the phage display method. By using PBMC immunized in vitro as template, heavy and light chain variable region genes were easily amplified by PCR. After generating the combinatorial phage library (1.6×10^5 members), phage antibody library was subjected to panning using biotinylated antigen and streptavidin magnetic beads to select antigen-specific phage antibody. After five rounds of panning, we obtained four antigen-specific clones. We combined variable region genes of these selected clones with human IgG constant region genes, and produced as human IgG format antibody. Among these clones, 1C11 showed a highest reactivity for sensitizing antigen. All these results demonstrate that we could obtain antigen-specific human monoclonal antibody from a relatively small phage antibody library by using in vitro immunized PBMC.

Keywords In vitro immunization • human monoclonal antibody • phage display

S. Matsumoto, Y. Katakura, K. Teruya, and S. Shirahata
Faculty of Agriculture, Kyushu University, Fukuoka, Japan

M. Yamashita, K. Tomimatsu, and Y. Aiba
Graduate School of Systems Life Sciences, Kyushu University, Fukuoka, Japan

K. Ikura et al. (eds.), *Animal Cell Technology: Basic & Applied Aspects*,
Animal Cell Technology: Basic & Applied Aspects 15,
DOI 10.1007/978-1-4020-9646-4_15, © Springer Science+Business Media B.V. 2009

1 Introduction

Human monoclonal antibodies (mAbs) have a great potential for diagnosis and treatments of cancer, allergy and other diseases. However, we cannot immunize human with antigen by ethical problems. Monoclonal antibodies from mouse origin are relatively easy to produce, however, their therapeutic availability is restricted by their antigenicity. At present, human monoclonal antibodies are mainly produced by humanizing mouse monoclonal antibodies using genetic engineering. But it is difficult to completely remove antigenicity derived from mouse. Therefore, we have developed an in vitro immunization (IVI) protocol of human peripheral blood mononuclear cells (PBMC) for generating human antigen specific antibodies (1). By using this protocol, B cells producing antigen specific antibody can be propagated within a week. In the present study, we tried to establish an efficient strategy to clone variable region genes of antigen specific human monoclonal antibody by applying in vitro immunized PBMC to the phage display method.

2 Methods

2.1 In Vitro Immunization

Human PBMC were cultured for 8 days in ERDF medium containing 10% heat inactivated fetal bovine serum, CpG-ODN, IL-2, IL-4, 2-mercaptoethanol and Mite-Extract (ME). Antibody production in the supernatant of cultured PBMC measured by ELISA and the number of antigen-specific cells were estimated by ELISPOT assay.

2.2 Construction of Phage Antibody Library

The VH and VL genes from in vitro immunized PBMC were prepared by RT-PCR (2). The VH and VL DNA fragments were joined with the linker DNA by overlap extension PCR and amplified using restriction site add-on primers by PCR (3). The resulting DNA fragments encoding the scFv repertoires were digested with *Sfi*I and *Not*I, and ligated into the pCANTAB5E phagemid vector. The ligated vector was introduced into competent *E. coli* TG1 cells by electroporation. Phagemid-containing bacterial colonies were infected with M13KO7 helper phage to yield phage-displayed antibody ScFv fragments.

2.3 Detection and Production of ME-Specific Antibody

The phage antibodies were selected by panning against ME. ME-specific phage antibodies bound to biotinylated ME on streptavidin magnetic beads and non-specific

phage were washed off. *E. coli* TG1 cells were infected with the binding phage. After five rounds of panning, 120 individual phage antibodies were picked. Using ME-coated 96 well plates, ME-reactive phage antibodies were detected by ELISA. The VH and VL genes were isolated from the positive clones and the DNA fragments were ligated to the respective vectors. The resulting DNA was co-transfected to the CHO cells. IgG in the supernatant were purified and analyzed.

3 Results and Discussion

20 positive clones were selected from random picked 120 phage clones and clonality analysis was performed using BstNI digestion and sequence analysis. In result, we confirmed that these 20 candidates consist of 4 clones. So, we performed recombination to the human monoclonal antibody expression vector. The phagemid DNA were isolated from the positive clone 1C11, 1F06, 1E04, and 2F07. The VH and VL genes were amplified and joined with the CH and CL genes, and the DNA fragments were ligated to the respective vectors. The resulting DNA was co-transfected to the CHO cells. IgG in the supernatant were purified and analyzed.

Specificity of these antibodies was tested using ELISA. Among these clones, 1C11 showed a highest reactivity for sensitizing antigen.

Next, we estimated the binding constant for 1C11 by competitive ELISA and BIACORE. Der f 1, the major antigen of ME was used as a target protein. The Kd value of 1C11 is about 10^{-5} molar (Fig. 1). The mAb 1C11 did not bind to other proteins. This value is very low, but it is possible that the target of 1C11 is not Der f 1, but other protein contained in ME. We should identify the target of 1C11.

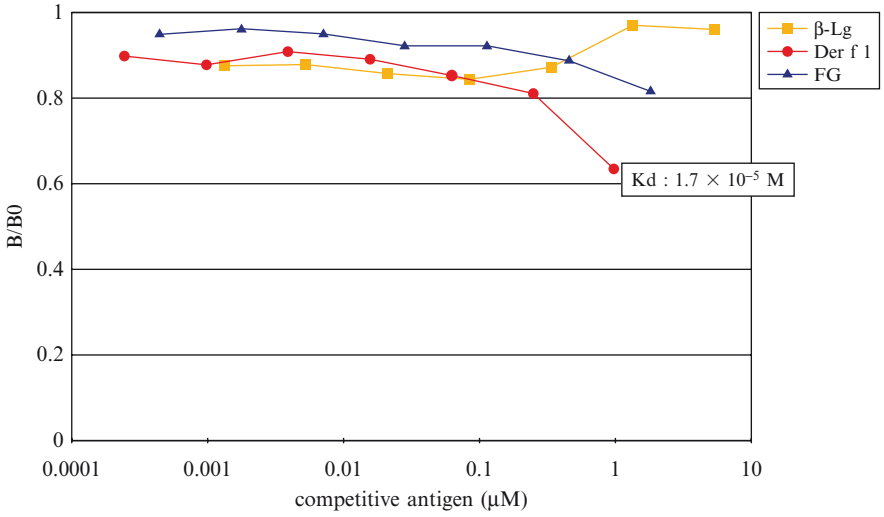

Fig. 1 Affinity of the mAb 1C11 to Der f 1

Our results shown that it is possible to produce antigen-specific human monoclonal antibody from smaller (1.6×10^5) library by using in vitro immunized PBMC. We expect that in vitro immunization and phage display method make a strong combination to produce human monoclonal antibody that have specificity for many kinds of antigens rapidly.

References

1. Ichikawa, A., Katakura, Y., Teruya, K., Hashizume, S., and Shirahata, S. In vitro immunization of human peripheral blood lymphocytes: establishment of B cell lines secreting IgM specific for cholera toxin B subunit from lymphocytes stimulated with IL-2 and IL-4. Cytotechnology (1999) 31, 131.
2. Wang, X. and David Stollar, B. Human immunoglobulin variable region gene analysis by single cell RT-PCR. Journal of Immunological Methods (2000) 244, 217–225.
3. Marks, J.D., Hoogenboom, H.R., Bonnert, T.P., McCafferty, J., Griffiths, A.D., and Winter, G. By-passing immunization. Human antibodies from V-gene libraries displayed on phage. Journal of Molecular Biology (1991) Dec 5; 222(3), 581–597.

Immunomodulatory Effects of Orally Administered *Bifidobacterium* Components on Intestinal Lymphoid Tissues

Yasuhiro Hiramatsu, Akira Hosono, Yusuke Nakanishi, Masamichi Muto, Satoshi Hachimura, Ryuichiro Sato, Kyoko Takahashi, and Shuichi Kaminogawa

Abstract To clarify the immunomodulatory effects of orally administered *Bifidobacterium pseudocatenulatum* 7041 (Bp) as probiotic bacteria, we determined the IgA production and cytokine secretion by lymphocytes derived from each of the intestinal immune tissues (e.g. Peyer's patch, PP; cecal follicle, CF; and mesenteric lymph node, MLN). It was demonstrated that IgA production and cytokine secretion (e.g. IL-5, IFN-γ) by lymphocytes derived from each intestinal immune tissue were significantly increased following the oral administration of Bp to BALB/c mice for 7 consecutive days. In order to clarify the nature of the immunomodulatory mechanisms induced by the oral administration of Bp, we investigated immunohistochemically bacterial migration and localization in vivo after a single-shot oral injection of Bp using Bp fluorescently-labeled with CFSE. CFSE-labeled Bp spots in tissue sections were observed in the PPs 1 h after the single-shot oral administration. These results indicated that orally administered Bp were taken up by the PPs through M cells and suggest that oral injection of Bp induces immunomodulation directly following uptake of bacterial components into the intestinal lymphoid tissues. Additionally, the immunomodulation by Bp acted through the activation of $CD4^+$ cells in the PP.

Keywords Bifidobacterium • bacterial migration • IgA production

1 Introduction

Some probiotic bacteria such as *Lactobacillus* or *Bifidobacterium* have various beneficial functions for our health. We demonstrated that oral administration of *Bifidobacterium* immunomodulator (BIM), derived from sonicated *B. pseudocatenulatum*

Y. Hiramatsu, A. Hosono, Y. Nakanishi, K. Takahashi, and S. Kaminogawa
Department of Food Science Technology, College of Bioresource Sciences, Nihon University, 1866, Kameino, Fujisawa-shi, Kanagawa, 252-8510, Japan

M. Muto, S. Hachimura, and R. Sato
Department of Applied Biological Chemistry, Graduate school of Agricultural and Life Sciences, The University of Tokyo, 1-1-1, Yayoi, Bunkyo-ku, Tokyo, 113-8657, Japan

K. Ikura et al. (eds.), *Animal Cell Technology: Basic & Applied Aspects*,
Animal Cell Technology: Basic & Applied Aspects 15,
DOI 10.1007/978-1-4020-9646-4_16,

7041 (Bp) [1], to BALB/c mice for 7 consecutive days induced IgA production and cytokine (e.g. IL-5, IFN-γ) secretion by Peyer's patch (PP) cells [2]. In particular, $CD4^+$ T cells isolated from PP were activated following oral administration of BIM. These results suggested that oral administration of BIM induced activation of cytokine secretion by $CD4^+$ T cells in PP. However, the immunological mechanisms responsible for the actions of probiotic bacteria have not been clarified.

In the present study, we investigated the influence of the oral administration of Bp on mucosal immune responses in the intestine through the determination of cytokine and IgA production in the small- and large-intestinal lymphoid tissues, especially PP and cecal follicles (CFs). We also investigated bacterial migration and localization following oral administration of Bp.

2 Materials and Methods

2.1 Mice

Female BALB/c mice aged 6–8 weeks were obtained from Clea Japan (Tokyo, Japan) and were housed in a room with a 12 h light-dark cycle. The mice were acclimatized and given MF diet (Oriental Yeast, Tokyo, Japan) for 3 days before experiments. All mice were kept in accordance with Guidelines for the Care and Use of Laboratory Animals by the College of Bioresource Sciences, Nihon University.

2.2 Bacteria and Preparation of Bifidobacterium Immunomodulator (BIM) Derived from Sonicated B. Pseudocatenulatum 7041

B. pseudocatenulatum 7041 (Bp) was obtained from the Japan Bifidus Foundation (Tokyo, Japan). Bp was cultured at 37°C for 20 h in GAM broth (Nissui Seiyaku Co., Tokyo, Japan). Cultured Bp was washed 3 times with sterilized PBS (sPBS). Sonicated *B. pseudocatenulatum* 7041 was prepared by the method described in a previous report [1].

2.3 Culture of Immune Tissue Cells and Cytokine and IgA Determination

Mice (n = 6–8) were orally administered a dose of 1×10^9 CFU/day of Bp in sPBS (200 μl) for 7 consecutive days. The control mice were given sPBS only by the same method.

After 7 days oral administration, cells from each immune tissue (e.g. PPs, CFs and mesenteric lymph nodes; MLNs) were obtained from each experimental group by the method described previously [3]. These cells (2.5×10^6 cells/well in a total volume of 1 ml) were cultured with 0, 10, or 50 μg/ml BIM in RPMI 1640 medium containing 5% FCS in a 48-well plate. The culture supernatants were collected at 24 and 72 h and assayed for IL-12 p40 and for IL-5, IL-6 and IFN-γ. Additionally, culture supernatants were collected after 1 week and assayed for IgA. Levels of cytokines and IgA in the supernatants were measured by the sandwich ELISA method as described previously [2, 3].

2.4 Fluorescent Staining of Bp

Bp (1×10^9 CFU/ml) was cultured at 37°C for 1 h with 5- (and 6-) carboxyfluorescein succinimidylester; CFSE (50 or 100 μg/ml final concentration) in PBS. CFSE-labeled Bp were washed 3 times with sPBS and resuspended to 1×10^9 CFU/200 μl.

2.5 Bacterial Localization in PP Frozen Sections

Mice were fasted for 24 h before a single-shot of CFSE-labeled Bp administered orally. PP from experimental mice was obtained 1 h after the single single-shot administration of CFSE-labeled Bp, and frozen sections were prepared. The detection of CFSE-labeled Bp in frozen PP sections was performed using a confocal laser scanning microscope (FV 500, Olympus, Tokyo, Japan) with FLUOVIEW software (Olympus).

3 Results

3.1 Culture Supernatant IgA and Cytokines from PP, CF and MLN Cells Derived from Experimental Mice After Oral Administration of Bp for 7 Consecutive Days

To clarify the influence of the oral administration of Bp on mucosal immune responses, we determined the IgA production and cytokine secretion by lymphocytes derived from PP, CF and MLN. Culture supernatant IgA levels from PP, CF and MLN cells were significantly increased in the Bp group compared to the control group. Additionally, IL-5 and IFN-γ secretion from PP cells was significantly increased by oral administration of Bp. IL-5 production from CF cells was

Table 1 Effects of oral administration of Bp on IgA production and cytokine secretion by intestinal lymphoid cells

Tissue	IgA production			
PP	+ +			
CF	+ +			
MLN	+			
Tissue	IL-5	IL-6	IL-12	IFN-γ
PP	+ +	±	±	+
CF	+	±	±	+
MLN	Not detected	±	±	±

PP, CF and MLN tissues were obtained and pooled for each experimental group. Cells were then co-cultured with BIM (10 mg/ml) for 24 h, 48 h and 7 days. IgA and cytokines in the culture supernatant were measured by ELISA. + indicated a significant increase. ++, +, ± were judged based on the results of more than three experiments.

also increased by oral administration of Bp. However, IL-6 and IL-12 p40 secretion from each of the immune tissue cells derived from the Bp group were not different from the control group (see Table1).

These results indicated that oral administration of live Bp modulates the IgA production and cytokine secretion in the gut-associate lymphoid tissue (GALT).

3.2 The Bacterial Localization in PP After Single-Shot Oral Administration of Bp

We demonstrated that oral administration of Bp to mice up-regulated IgA production and cytokine secretion on the PP, CF and MLN. However, we could not clarify the immunological mechanisms responsible for the actions of Bp. In particular, the interactions between orally administered Bp and GALT. Therefore, to achieve this we investigated immunohistochemically the uptake and localization of Bp into the intestinal immune tissue after single-shot oral administration.

CFSE-labeled Bp spots in tissue sections were observed in the PP 1 h after the single-shot administration of CFSE-labeled Bp.

This result indicated that orally administered Bp was taken up by the PP through M cells (see Fig. 1).

4 Discussion

Some probiotic bacteria have many beneficial functions, for example, preventing food allergies and enhancing host immune responses. In this study, we demonstrated that live Bp also induce IgA production and cytokine secretion in the GALT after administration for 7 consecutive days. In addition, we previously reported that BIM derived from Bp also modulates the mucosal immune responses.

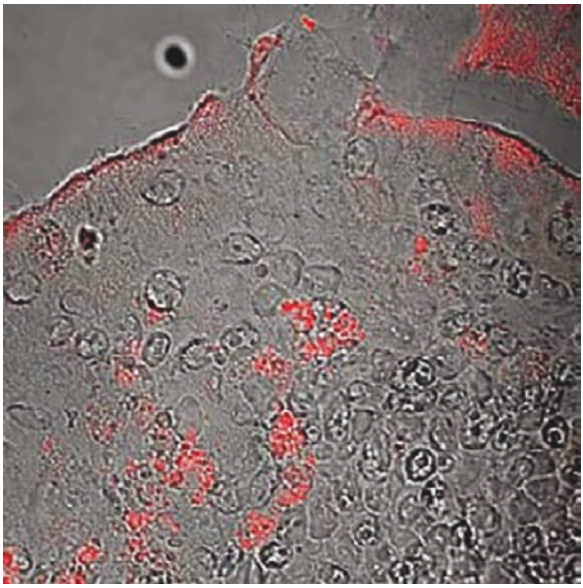

Fig. 1 Localization of Bp in the PP 1 h after oral administration. Bp were fluorescently labeled by CFSE. PP frozen sections were obtained from experimental mice 1 h after oral administration of fluorescently labeled Bp (red spots). The localization of Bp in the PP frozen section was observed using a confocal laser scanning microscope. This picture was evaluated and compared with non-administered control (data not shown)

However, the interactions between probiotic bacteria and mucosal immune cells in the gut are not well understood. In particular, how this interaction between mucosal immune cells in the gut and orally administered probiotic bacteria takes place is not known. Therefore, we investigated the uptake and localization of Bp in the intestinal immune tissue after a single-shot oral administration and subsequently observed some Bp in the PP. These results suggested that oral injection of Bp induced immunomodulation of GALT directly, following uptake of bacterial components into the intestinal lymphoid tissues. Additionally, the immunomodulation by oral administration of Bp was induced via the activation of $CD4^+$ cells in the PP.

References

1. Lee, J., A. Ametani, A. Enomoto, Y. Sato, H. Motosima, F. Ike, and S. Kaminogawa. 1993. Screening for the immunopotentiating activity of the immune response by *Bifidobacterium adolescentis* M101-4. *Biosci. Biotech. Biochem. 57:2127.*
2. Nakanishi, Y., A. Hosono, Y. Hiramatsu, T. Kimura, R. Nakamura, and S. Kaminogawa. 2005. Characteristic immune response in Peyer's patch cells induced by oral administration of Bifidobacterium components. *Cytotechnology 47:69.*
3. Hosono, A., A. Ozawa, R. Kato, Y. Ohnishi, Y. Nakanishi, T. Kimura, and R. Nakamura. 2003. Dietary fructooligosaccharides induce immunoregulation of intestinal IgA secretion by murine Peyer's patch cells. *Biosci. Biotechnol. Biochem. 67:758.*

Murine Intestinal Bacteria Modulate Antigen-Specific Cytokine Production by Intestinal Immune Cells Derived from Germ-Free TCR-Transgenic Mice

Masato Tsuda, Akira Hosono, Tsutomu Yanagibashi, Satoshi Hachimura, Kazuhiro Hirayama, Yoshinori Umesaki, Kikuji Itoh, Kyoko Takahashi, and Shuichi Kaminogawa

Abstract We have previously established germ-free ovalbumin- (OVA) specific T cell receptor transgenic (OVA-Tg) mice to examine the direct effects of intestinal bacteria on intestinal immune responses to dietary antigen. We prepared the intestinal immune cells from Peyer's patches and lamina propria in the small intestine derived from germ-free (GF) or conventional (CV) mice, and demonstrated that the immunocytes from GF mice showed higher cytokine production in response to OVA antigen compared with those from CV mice. This suggested that intestinal bacteria could regulate cytokine production in response to OVA antigen. In this study, we investigated the effects of stimulation of antigen presenting cells (APCs) by intestinal bacteria on antigen-specific immune responses by using germ-free OVA-Tg mice. *Lactobacillus* and *Bacteroides*, which were isolated from murine intestinal bacteria, were inactivated by UV exposure. Thy1.2$^-$ cells, APCs of mesenteric lymph nodes (MLN) representing the gut associated lymphoid tissues, and MLN CD4$^+$ T cells were prepared from GF Balb/c and OVA-Tg mice respectively. These cells were co-cultured with OVA and intestinal bacteria, and cytokines (IFN-γ, IL-10) in the supernatants were then assayed by ELISA. Both *Lactobacillus* and *Bacteroidess* enhanced OVA-specific cytokine production when the cells were stimulated with bacteria and OVA together. On the other hand, the pre-stimulation of APCs with *Lactobacillus* down-regulated OVA-specific cytokine

M. Tsuda, A. Hosono, T. Yanagibashi, K. Takahashi, and S. Kaminogawa
Department of Food Science and Technology, Nihon University, 1866, Kameino, Fujisawa-shi Kanagawa, 252-8510, Japan

S. Hachimura
Department of Applied Biological Chemistry, The University of Tokyo, Japan

K. Hirayama and K. Itoh
Department of Veterinary Public Health, The University of Tokyo, Japan

Y. Umesaki
Yakult Central Institute for Microbiological Research, Japan

K. Ikura et al. (eds.), *Animal Cell Technology: Basic & Applied Aspects*,
Animal Cell Technology: Basic & Applied Aspects 15,
DOI 10.1007/978-1-4020-9646-4_17, © Springer Science+Business Media B.V. 2009

production by CD4+ T cells. However *Bacteroides* did not enhance OVA-specific IFN-γ production significantly. These results suggested that *Lactobacillus* might modulate antigen-specific T cell responses via APCs differently from *Bacteroides*.

Keywords Germ-free (GF) mice • ovalbumin specific T cell receptor transgenic (OVA-Tg) mice • intestinal bacteria • mesenteric lymph nodes (MLN) • antigen-presenting cells (APCs)

1 Introduction

It has been reported that intestinal commensal bacteria interact with intestinal immune systems, and have important roles in the development of mucosal tissues and in maintaining homeostasis of immune responses. However, it has not been clarified exactly how intestinal bacteria modulate the antigen-specific immune responses.

We have previously established germ-free ovalbumin (OVA)-specific T cell receptor transgenic (OVA-Tg) mice to investigate the effects of intestinal bacteria on antigen-specific T cell responses. These mice are characteristic in that their CD4+ T cells respond to OVA specifically as they were transfected with a sequence encoding the T cell receptor recognizing OVA and their immune cells have never been stimulated with intestinal bacteria. As such, we can analyze the immune responses of OVA-Tg mice to intestinal bacteria specifically. We have previously found that, in a comparison of the breeding conditions between conventional (CV) and germ-free (GF) mice, the immunocytes from GF mice showed higher cytokine production in response to OVA stimulation compared with those from CV mice [1]. This suggested that intestinal bacteria could regulate antigen-specific immune responses.

We hypothesized that intestinal bacteria might modulate antigen-specific immune responses via antigen presenting cells (APCs), because APCs were thought to have important roles in antigen-presentation to T cells and recognizing different bacterial components via pattern recognition receptors such as the toll-like receptors (TLR). In this study, we investigated the effects of stimulation of APCs by intestinal bacteria on antigen-specific cytokine production by using intestinal immune cells derived from GF OVA-Tg mice.

2 Materials and Methods

2.1 Preparation of Intestinal Bacteria

Lactobacillus acidophilus 129 (LA) and *Bacteroides acidifaciens* type A43 strain (BA) which were isolated from murine feces were cultured in MRS broth (BD Difco, Sparks, USA) or GAM broth (Nissui, Tokyo, Japan) for 24–48 h. These bacteria were washed with PBS and then inactivated by UV-exposure and lyophilized.

2.2 Mice

OVA-Tg (+/+) and Balb/c GF mice were housed in sterile vinyl isolators. These mice were fed CMF diet (Oriental Yeast, Tokyo, Japan) irradiated with 50 kGy of γ-rays. In this study we prepared immune cells from mice aged 8–11 weeks. All experiments were performed in accordance with the guidelines for the care and use of laboratory animals by the College of Bioresource Sciences, Nihon University and the guidelines of the University of Tokyo for the care of laboratory animals.

2.3 Preparation of $CD4^+$ Cells and $Thy1.2^-$ Cells from Mesenteric Lymph Nodes (MLN)

MLN cells were prepared from GF OVA-Tg mice and Balb/c mice respectively. MLN $CD4^+$ cells from OVA-Tg mice were negatively isolated by using a $CD4^+$ T cell isolation kit and magnetic cell sorting systems (MACS; Miltenyi Biotec, Bergisch Gladbach, Germany) and MLN $Thy1.2^-$ cells were isolated from GF Balb/c mice by using anti-mouse Thy1.2 microbeads.

2.4 Cell Culture

MLN cells (2.5×10^6 cells/well) were added to 48-well flat-bottom plates and cultured in the absence or the presence of OVA (250 μg/ml) and intestinal bacteria (50 μg/ml) in RPMI 1640 containing 5% FCS. $CD4^+$ cells (5×10^5 cells) were cultured in the absence or the presence of OVA and intestinal bacteria with $Thy1.2^-$ cells (2×10^6 cells). Supernatants were collected 48 h later for cytokine analysis.

2.5 Measurements of Cytokine Production

The amounts of interferon (IFN)-γ and interleukin (IL)-10 in the supernatants were assayed by sandwich ELISA. Rat anti-mouse IFN-γ monoclonal antibody (R4–6A2, BD Pharmingen, San Diego, CA, USA) and biotinylated rat anti-mouse IFN-γ monoclonal antibody (XMG1.2, BD Pharmingen) were used for IFN-γ measurement. IL-10 was measured by using the OptEIA mouse IL-10 set (BD Pharmingen).

3 Results and Discussion

In this study, to investigate how the stimulation of intestinal bacteria affects APCs and antigen-specific cytokine production, we designed two groups of experiments, the first consisting of simultaneous stimulation with intestinal bacteria and OVA and the second of pre-stimulation with intestinal bacteria.

Table 1 Effects of stimulation with intestinal bacteria on OVA-specific cytokine production by MLN cells

	Simultaneous Stimulation			Pre-stimulation		
	Without Bacteria	LA	BA	Without Bacteria	LA	BA
IFN-γ	+	+	+++	+	+	+++
IL-10	–	+++	++	–	++++	++

For simultaneous stimulation, MLN cells were co-cultured with 50 μg/ml of LA or BA and 250 μg/ml of OVA simultaneously. For pre-stimulation, MLN cells were pre-stimulated with 50 μg/ml of LA or BA for 24 h before being stimulated with 250 μg/ml OVA. IFN-γ and IL-10 secreted in the culture supernatants were assayed by ELISA. Secretion of cytokines was judged based on the results of two individual experiments.

We first examined the effects of intestinal bacteria on antigen-specific cytokine production by MLN cells representing gut associated lymphoid tissue (Table 1). When MLN cells were co-cultured with OVA and intestinal bacteria simultaneously, *Bacteroides* enhanced OVA-specific IFN-γ production, and *Lactobacillus* and *Bacteroides* enhanced OVA-specific IL-10 production. *Lactobacillus* especially induced higher IL-10 production as compared to *Bac*teroides. On the other hand, when MLN cells were pre-stimulated with intestinal bacteria 24 h before pre-culture with OVA, *Lactobacillus* and *Bacteroides* did not enhance OVA-specific IFN-γ production significantly. *Lactobacillus* did not induce OVA-specific IL-10 production but *Bacteroides* weakly induced OVA-specific IL-10 production. These results suggested that intestinal bacteria induced OVA-specific cytokine production when the immune cells were stimulated simultaneously with bacteria, but pre-stimulation with intestinal bacteria did not enhance OVA-specific cytokine production significantly.

Furthermore, to examine the effects of pre-stimulation of APCs with intestinal bacteria on antigen-specific cytokine production by $CD4^+$ T cells, MLN $CD4^+$ T cells and MLN $Thy1.2^-$ cells as the antigen presenting cells were purified from GF OVA-Tg mice and GF Balb/c mice respectively. When $CD4^+$ T cells, intestinal bacteria and OVA were co-cultured with $Thy1.2^-$ cells simultaneously, *Lactobacillus* and *Bacteroides* enhanced OVA-specific IFN-γ and IL-10 production effectively (Table 2). In particular, *Bacteroides* induced higher cytokine production when compared with *Lactobacillus*. When $Thy1.2^-$ cells were pre-stimulated with intestinal bacteria for 24 h, and then $CD4^+$ T cells and OVA were co-cultured, it was interesting that *Lactobacillus* decreased OVA-specific IFN-γ and IL-10 production compared with the control which had no bacterial stimulation (Table 2). However, *Bacteroides* did not enhance OVA-specific IFN-γ production significantly and only weakly induced OVA-specific IL-10 production. These results suggested that the immunomodulatory effects of *Lactobacillus* on APCs were different from those of *Bacteroides* in so far as the pre-stimulation of APCs with *Lactobacillus* down-regulated OVA-specific cytokine production.

It has been reported that microbial components of gram-positive bacteria such as lipoteichoic acid and peptidoglycan are recognized by TLR2 [2]. On the other

Table 2 Effects of the stimulation of APCs with intestinal bacteria on OVA-specific cytokine production by $CD4^+$ T cells

	Simultaneous Stimulation			Pre-stimulation		
	Without Bacteria	LA	BA	Without Bacteria	LA	BA
IFN-γ	+	++	+++	++	+	++
IL-10	–	++	+++	+	–	++

For simultaneous stimulation, MLN $CD4^+$ T cells from GF OVA-Tg mice and MLN $Thy1.2^-$ cells from GF Balb/c mice were co-cultured with 50 μg/ml of LA or BA and 250 μg/ml of OVA simultaneously. For pre-stimulation, $Thy1.2^-$ cells were pre-stimulated with 50 μg/ml of LA or BA for 24 h before being co-cultured with $CD4^+$ T cells and 250 μg/ml of OVA. The concentrations of IFN-γ and IL-10 secreted in the culture supernatants were measured by ELISA.

hand, lipopolysaccharide (LPS), a major cell wall component of gram-negative bacteria is recognized by TLR4 [3, 4]. Thus, gram-positive and-gram negative bacteria might induce the secretion of different humoral factors and/or the expression of different co-stimulatory molecules by APCs, resulting in differences in modulation of antigen-specific T cell responses.

Taken together, our results suggested that *Lactobacillus* modulates antigen-specific T cell responses via APCs differently from *Bacteroides*. Furthermore, it is possible that *Lactobacillus* has characteristics which enable the down-regulation of excessive antigen-specific immune responses such as food allergy.

Acknowledgements We thank Dr. Sonoko Habu and Dr. Takehito Sato (Tokai University, School of Medicine) for generously providing the TCR-transgenic mice.

References

1. Fujioka, M., S. Hachimura, A. Hosono, R. Nakamura, K. Hirayama, K. Itoh, and S. Kaminogawa. 2004. Establishment and analysis of germ free T cell receptor transgenic mice. *Animal Cell Technology: Basic & Applied Aspects* 13:243.
2. Takeuchi, O., K. Hoshino, T. Kawai, H. Sanjo, H. Takada, T. Ogawa, K. Takeda, and S. Akira. 1999. Differential roles of TLR2 and TLR4 in recognition of gram-negative and gram-positive bacterial cell wall components. *Immunity* 11:443.
3. Poltorak, A., X. He, I. Smirnova, M. Y. Liu, C. Van Huffel, X. Du, D. Birdwell, E. Alejos, M. Silva, C. Galanos, M. Freudenberg, P. Ricciardi-Castagnoli, B. Layton, and B. Beutler. 1998. Defective LPS signaling in C3H/HeJ and C57BL/10ScCr mice: mutations in Tlr4 gene. *Science* 282:2085.
4. Qureshi, S. T., L. Lariviere, G. Leveque, S. Clermont, K. J. Moore, P. Gros, and D. Malo. 1999. Endotoxin-tolerant mice have mutations in Toll-like receptor 4 (Tlr4). *Journal of Experimental Medicine* 189:615.

Spleen Cells Derived from Male Non-Obese Diabetic Mice are Capable of Suppressing the Autoantigen-Specific Production of Interferon-γ of Female Cells *In Vitro*

Atsushi Enomoto, Takumi Ohsaki, Shogo Komine, and Mayuko Hasegawa

Abstract Non-obese diabetic (NOD) mice spontaneously develop insulin-dependent diabetes mellitus with a clear female prevalence. Using Transwell co-culture systems with both female and male splenocytes, we found that spleen cells of male NOD mice suppress autoantigen (glutamic acid decarboxylase, GAD)-specific production of interferon-γ of female cells. In addition, this suppression appeared to be mediated by a soluble factor(s) produced by male cells in response to the similar epitope on GAD molecule. Our experimental systems might be useful for further understanding sex differences in autoimmunity.

Keywords insulin-dependent diabetes mellitus • spleen cells • interferon-γ • autoantigen • female predilection

1 Introduction

It has been recognized for more than 100 years that autoimmune diseases such as systemic lupus erythematosus (SLE), rheumatoid arthritis (RA), and multiple sclerosis (MS) are often more prevalent in females than males [1–3]. Although the incidence of T cell-mediated type 1 diabetes, also known as insulin-dependent diabetes mellitus (IDDM), is similar in men and women, non-obese diabetic (NOD) mice, an animal model for spontaneous IDDM, also show a clear female predilection [2]. To understand the overall mechanisms underlying the gender gap in autoimmunity, a great deal of attention has been focused on enhanced or suppressive effects of sex hormones, mainly estrogen, progesterone, and testosterone, on the development of autoimmune diseases [1, 2], but the precise reasons are not yet clear at present.

A. Enomoto, T. Ohsaki, S. Komine, and M. Hasegawa
Department of Biological and Chemical Engineering, Faculty of Engineering,
Gunma University, 1-5-1 Tenjin, Kiryu, Gunma, 376-8515, Japan

K. Ikura et al. (eds.), *Animal Cell Technology: Basic & Applied Aspects*,
Animal Cell Technology: Basic & Applied Aspects 15,
DOI 10.1007/978-1-4020-9646-4_18,

2 Materials and Methods

Spleen cells were prepared from naïve NOD mice (Clea Japan, Tokyo) and cultured at a concentration of 1.0×10^7 cells/well with or without a peptide fragment of glutamic acid decarboxylase 65, from amino acid residues 524 through 543 (GAD 524–543), in HL-1 medium (Cambrex Bio Science Walkersville, MD) in a flat-bottom 24-well culture plate (Asahi Techno Glass, Tokyo) for 3 days (primary antigenic stimulation). In some experiments, 1.0×10^7 cells/well of male and female spleen cells were co-cultured in a Transwell (no. 3470, Corning, NY) to examine the suppressive effects of male cells. In another experiment, culture supernatants of male or female spleen cells was added to the wells at day 0 (initiation of the culture) and day 3 in place of spleen cells. The use and care of the animals in this study were approved by Animal Care and Experimentation Committee of Gunma University, Kiryu Campus.

The cells were further stimulated by the addition of murine interleukin-2 (IL-2) (Genzyme/Techne, Minneapolis, MN) for another 3 days, and then washed, resuspended, and cultured with or without GAD 524–543, 524–538, or 530–543 in RPMI 1640 medium (Invitrogen, Carlsbad, CA) containing 10% FCS (Invitrogen) in a round-bottom 96-well culture plate (Asahi Techno Glass) for 24 h (secondary antigenic stimulation). In the case of the Transwell experiments, only the splenocytes in lower sites were used for secondary antigenic stimulation. One μg/ml of the anti-CD3ε antibody (BD Biosciences Pharmingen, San Diego, CA) was used as a positive control.

After secondary antigenic stimulation, the culture supernatants were collected and tested for production of interferon-γ (IFN-γ) by ELISA. Both capture and detection anti-IFN-γ antibodies and standard IFN-γ were purchased from BD Biosciences Pharmingen. Student's *t* test was used to determine statistical significance in all experiments. A value of $p < 0.05$ was considered to be significant.

3 Results and Discussion

As shown in Figs. 1 and 2, using co-culture systems with both female and male spleen cells, we found that spleen cells derived from young male NOD mice showing low susceptibility to IDDM suppressed autoantigen (GAD)-induced production of IFN-γ of female cells *in vitro*, which is presumably associated with the induction of IDDM [4, 5]. The spleen cells from 10–12 week-old female NOD mice secreted significantly high amounts of IFN-γ in response to GAD 524–543, an important epitope of the GAD molecules [5]. The young male cells at 8–10 weeks of age were usually shown to reduce the autoimmune response of the female cells to approximately 1/2, as compared with the culture of female cells alone, whereas the male cells derived from 32 week-old mice did not exhibit any such suppressive effects (Fig. 2).

In addition, this suppression appeared to be mediated by a soluble factor(s) produced by male cells in response to the same antigen, because addition of the male

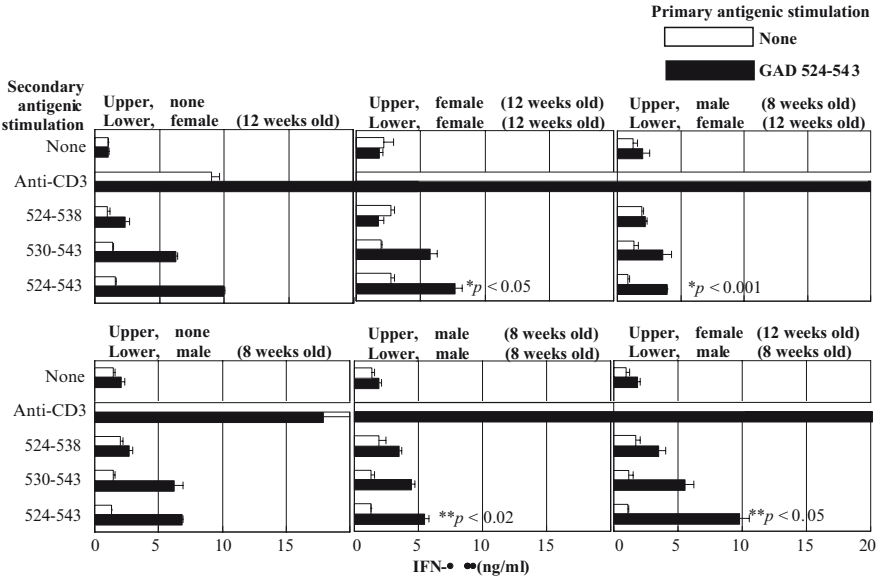

Fig. 1 Suppressive effects of male spleen cells in the upper sites of Transwell on the GAD 524–543-induced production of IFN-γ of female cells in the lower sites. Using the Transwell culture system, spleen cells derived from female (12-week-old) and male (8-week-old) NOD mice were co-cultured in the indicated manner for primary antigenic stimulation. Data are presented as means of triplicates ± SEM. *p values compared with the culture of female cells alone, **p values compared with the culture of male cells alone

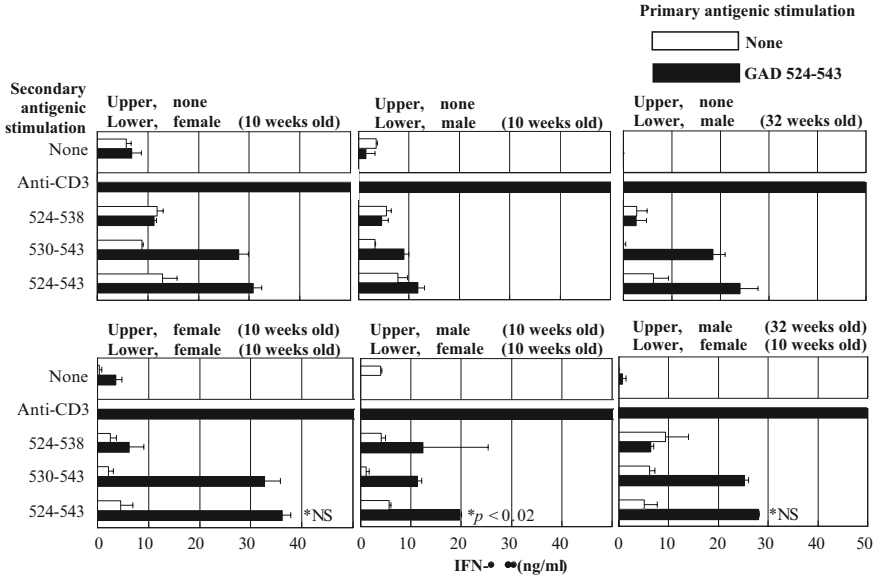

Fig. 2 Comparison of the suppressive effects of male spleen cells at 10 and 32 weeks of age. Using the Transwell culture system, spleen cells derived from female (10-week-old) and male (10- or 32-week-old) NOD mice were co-cultured in the manner indicated for primary antigenic stimulation. Data are presented as means of duplicates ± SEM. *p values compared with the culture of female cells alone, NS, not significant

supernatants to the culture was found markedly to decrease the autoimmune response of female spleen cells to about 1/3, only when the male cells had been cultured in the presence of GAD 524–543, especially GAD 530–543 (Figs. 3 and 4).

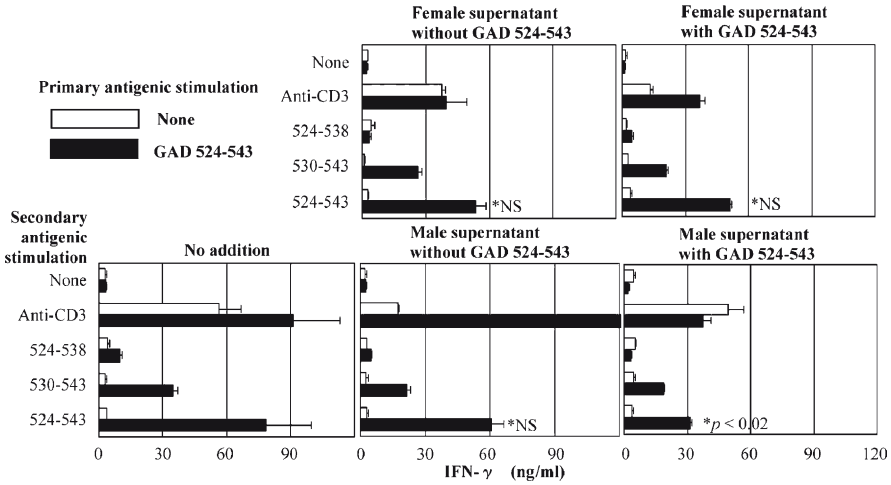

Fig. 3 Suppressive effects of the culture supernatants of male spleen cells on the GAD 524–543-induced production of IFN-γ of female cells. Male (7-week-old) and female (11-week-old) spleen cells were cultured with or without GAD 524–543 for 3 days. The culture supernatants were then collected and 0.1 ml of each supernatant was added to the culture of female cells (12-week-old) at days 0 and 3. Data are presented as means of triplicates ± SEM. *p values compared with the culture of the female cells alone; NS, not significant

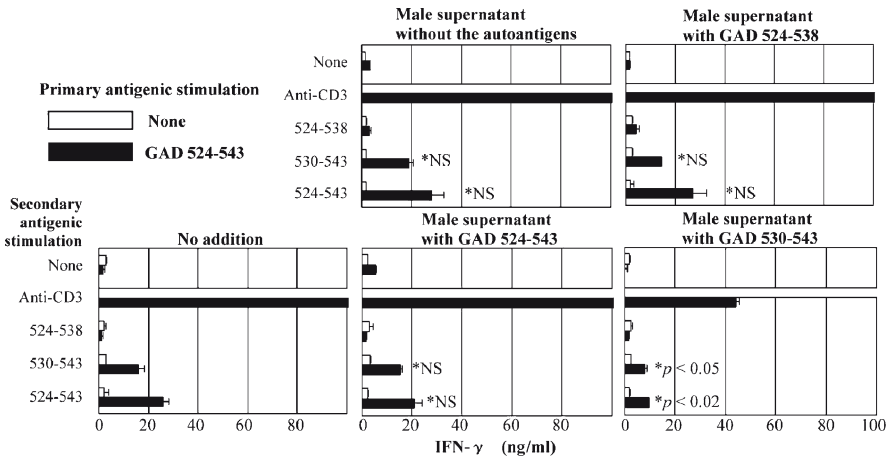

Fig. 4 Comparison of the suppressive effects of male supernatants stimulated with GAD peptides. Male (7-week-old) spleen cells were cultured with GAD 524–543, 524–538 or 530–543 for 3 days. The culture supernatants were then collected and 0.1 ml of each supernatant was added to the culture of female cells (10-week-old) at days 0 and 3. Data are presented as means of duplicates ± SEM. *p values compared with the culture of the female cells alone; NS, not significant

Interestingly, these results suggest that both pathogenic T cells derived from the female mice and protective T cells from the male mice may probably recognize the same epitope on the GAD molecules, from amino acid residues 530 through 543. Our findings and experimental systems might be useful for further understanding sex differences in autoimmunity as well as in the basic immune response, especially in the T cell response to the self-antigen.

Acknowledgments The authors thank Dr. Koko Mizumachi for advice and for help with the peptide syntheses.

References

1. Yu, C. Y. and Whitacre, C. C. Sex, MHC and complement C4 in autoimmune diseases, Trends Immunology 25 (2004), 694–699.
2. Whitacre, C. C. Sex differences in autoimmune diseases, Nature Immunology 2 (2001), 777–780.
3. Fairweather, D. and Rose, N. R. Women and autoimmune diseases, Emerging Infectious Diseases 10 (2004), 2005–2011.
4. Bach, J.-F. and Chatenoud, L. Tolerance to islet autoantigens in type 1 diabetes, Annual Review Immunology 19 (2001), 131–161.
5. Kaufman, D. L., Clare-Salzler, M., Tian, J., Forsthuber, T., Ting, G. S. P., Robinson, P., Atkinson, M. A., Sercarz, E. E., Tobin, A. J., and Lehmann, P. V. Spontaneous loss of T-cell tolerance to glutamic acid decarboxylase in murine insulin-dependent diabetes, Nature 366 (1993), 69–72.

Highly Efficient Antibody Production by Improving Cell Survival Using Sericin

Kazuaki Itoh, Naoki Takada, Akiko Ogawa, Masahiro Sasaki, Hideyuki Yamada, and Satoshi Terada

Abstract The antibody therapeutics, as well as the diagnostic market, in Japan has grown rapidly and has soared to an annual total of 55 billion yen. Industrially, these antibodies are produced by fed-batch or perfusion culture of mammalian cells. We have previously reported that sericin improves cell survival, and in this study, we tried to prolong the culture period of the hybridoma cells by supplementing the culture medium with sericin in order to improve monoclonal antibody productivity. In the presence of sericin, maximum cell density and final monoclonal antibody concentration were lower than those in the presence of 0.1% BSA and 10% FBS, but the specific antibody production rate was higher.

Keywords Cell survival • hybridoma • monoclonal antibody • sericin • serum-free medium

1 Introduction

Monoclonal antibodies play an important role in pharmacotherapy and diagnosis. The antibody therapeutics market has grown rapidly year by year. Most monoclonal antibodies are produced by similar culture processes, mostly using fed-batch culture of mammalian cells [1]. The major advantage of fed-batch culture over other culture methods, including batch, perfusion and continuous cultures, is that monoclonal antibodies are produced in higher concentration, to downstream advantage [2].

We have previously reported that sericin improves cell survival [3, 4]. Sericin is a silk protein and very Ser rich; 31% of the residues are Ser and 19%, 18% and 8%

K. Itoh, N. Takada, and S. Terada
Department of Applied Chemistry and Biotechnology, University of Fukui, 3-9-1, Bunkyo, Fukui, 910-8507, Japan

A. Ogawa, M. Sasaki, and H. Yamada
SEIREN Co. Ltd., 48-113-2, Yonozu, Mikuni-Cho, Sakai, Fukui, 913-0038, Japan

K. Ikura et al. (eds.), *Animal Cell Technology: Basic & Applied Aspects*,
Animal Cell Technology: Basic & Applied Aspects 15,
DOI 10.1007/978-1-4020-9646-4_19,

are Gly, Asp and Thr, respectively. In this study, we used sericin in order to improve monoclonal antibody production.

2 Materials and Methods

2.1 Cell Line and Culture Conditions

2E3-O is a mouse hybridoma cell line derived from myeloma P3X63 AG8U.1 by electric fusion with spleen cells [5]. The hybridoma cells are high producers of an IgG1 antibody specific for a trinitrophenyl hapten. The cells were cultured in Daigo T medium, which was kindly given by Nihon Pharmaceutical (Osaka, Japan). The cells were grown in 24-well plates (Sumitomo Bakelite, Tokyo, Japan) at 37°C in humidified air containing 5% CO_2. The viable and dead cell numbers were determined by counting in a hemocytometer under a phase contrast microscope using the trypan blue exclusion method.

2.2 Determination of Antibody Concentration

The monoclonal antibody concentration was determined by enzyme-linked immunosorbent assay (ELISA). Monoclonal antibody was sandwiched by rabbit antibody to mouse IgG, and horseradish peroxidase (HPR)-conjugated goat antibody to mouse IgG. After addition of the peroxidase substrate, H_2O_2 and *o*-phenylenediamine dihydrochloride, the optical density at 490 nm was measured by a plate reader (SJ Auto Reader; Sanko-Junyaku, Tokyo, Japan).

3 Results and Discussion

A series of cultures with hybridoma cells supplemented with sericin was performed. A representative growth curve is shown in Fig. 1. The cell density of the culture in the presence of 10% FBS was higher than that in the presence of any other supplements, but the cells died quickly after reaching maximum cell density. In contrast, cells treated with 0.1% sericin continued to proliferate, and retained a high viability of 90% during culture.

Table 1 shows the doubling time of the cells during 3 days after seeding. The doubling time of the cells treated with 0.1% sericin was longer than that with 10% FBS, while the cells treated with 0.1% sericin survived longer than with any other supplements.

Representative time profiles of monoclonal antibody production are shown in Fig. 2. Monoclonal antibody concentration in the culture supplemented with 10% FBS was higher than that in all the other cultures. The integral of viable cell density

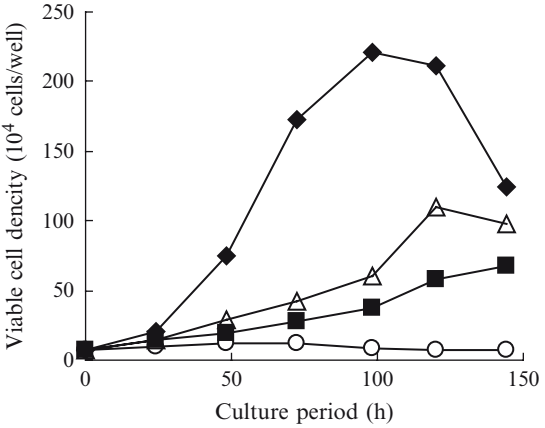

Fig. 1 Effects of various supplements on cell growth. Cells were cultured in basal medium in the absence of supplement (open circles), or in the presence of 0.1% sericin (closed squares), 0.1% BSA (open triangles) or 10% FBS (closed diamonds)

Table 1 Doubling time of cells in the presence of supplements from day 0 to day 3

Supplement	Doubling Time (h)
–	112
0.1% Sericin	41
0.1% BSA	29
10% FBS	16

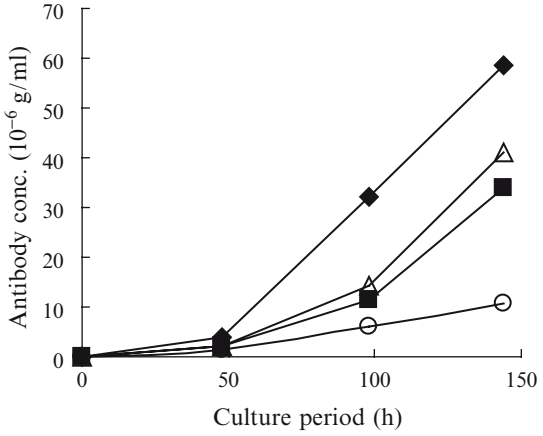

Fig. 2 Effects of various supplements on monoclonal antibody production. Cells were cultured in basal medium in the absence of supplement (open circles), or in the presence of 0.1% sericin (closed squares), 0.1% BSA (open triangles) or 10% FBS (closed diamonds)

with respect to time, defined as IVC, was calculated for each culture. Compared to the ratio of IVC in normalized basal medium, the ratio in 10% FBS was 13, and this was higher than that in any other cultures, but the antibody production efficiency was reduced to 0.43 (Table 2). The ratio of IVC of 0.1% sericin was 3.3, and the antibody production efficiency was 0.96. These results indicate that monoclonal antibody was most efficiently produced in the presence of sericin.

To investigate the effects of supplements on cell morphology, phase contrast microscopy was performed. In general, cell morphology was similar, but larger flocculations of cells were observed in cultures treated with 10% FBS, while smaller flocculations of cells were observed in cultures treated with 0.1% sericin or 0.1% BSA.

Table 2 Population and antibody production. Column A indicates normalized IVC. FAC represents final antibody concentration. Column B indicates normalized FAC

	IVC (10^6 cells × h)	A	FAC (μg/ml)	B	Antibody Production Efficiency (B/A)
–	14	1.0	10.57	1.0	1.00
0.1% Sericin	46	3.3	33.76	3.2	0.96
0.1% BSA	73	5.3	40.96	3.9	0.74
10% FBS	180	13.0	58.58	5.5	0.43

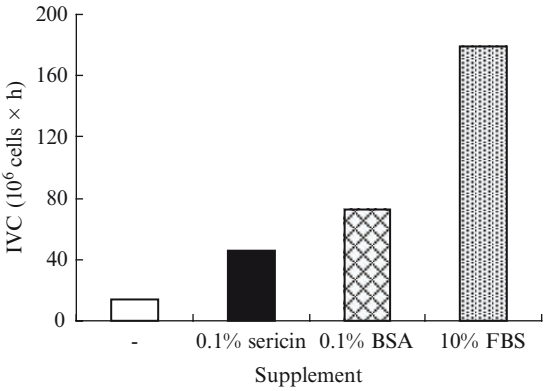

Fig. 3 IVC of the hybridoma cell culture in the presence of various supplements

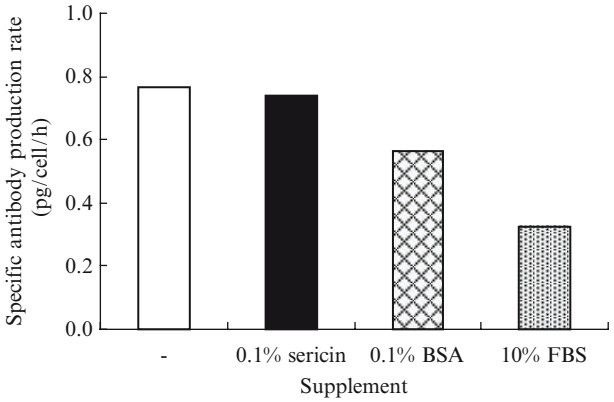

Fig. 4 Specific antibody production rates of the hybridoma cell treated with various supplements

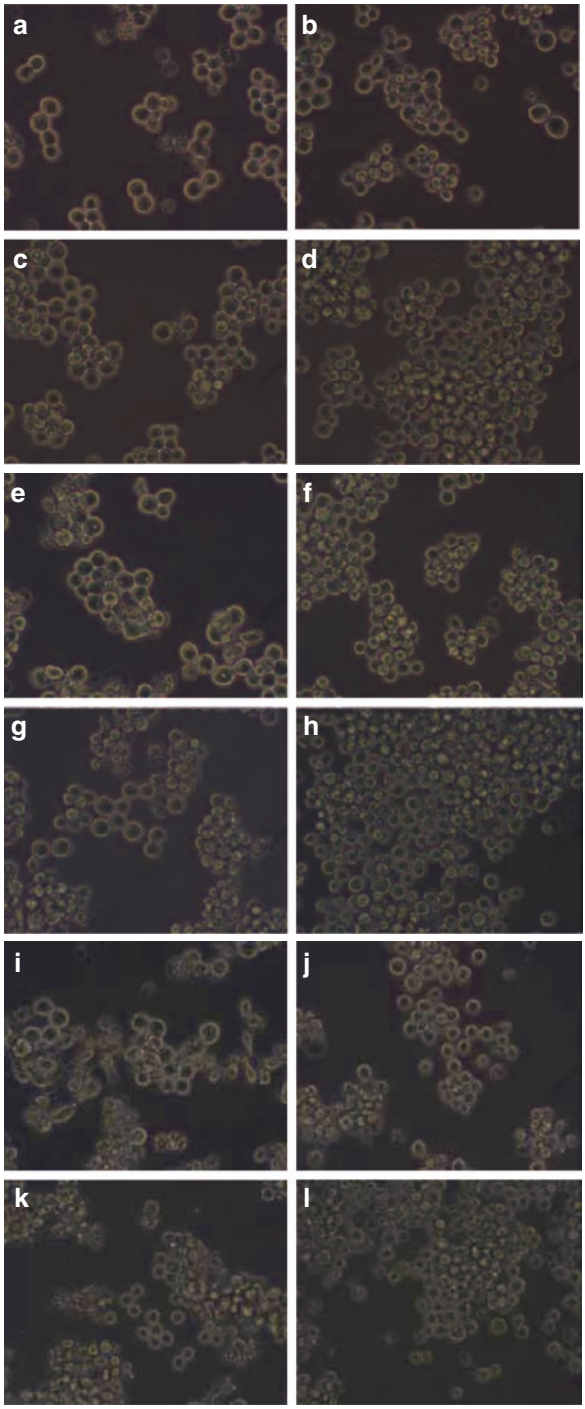

Fig. 5 Phase-contrast microscopic observations of hybridoma 2E3-O cells. Cells were cultured in basal medium in the absence of supplement (**a**, **e**, **i**), or in the presence of 0.1% sericin (**b**, **f**, **j**), 0.1% BSA (**c**, **g**, **k**) or 10% FBS (**d**, **h**, **l**) at 48 (**a**, **b**, **c**, **d**), 98 (**e**, **f**, **g**, **h**) and 144 h (**i**, **j**, **k**, **l**)

References

1. Farid S. S., Process economics of industrial monoclonal antibody manufacture, Journal of Chromatography B, 07, 037–048, 2006.
2. Kuwae S. et al., Development of a fed-batch culture process for enhanced production of recombinant human antithrombin by Chinese hamster ovary cells, Journal of Bioscience and Bioengineering, 100, 502–510, 2005.
3. Terada S. et al., Sericin, a protein derived from silkworms, accelerates the proliferation of several mammalian cell lines including a hybridoma, Journal of Cytotechnology, 40, 3–12, 2002.
4. Terada S. et al., Preparation of silk protein as a mitogenic factor for better mammalian cell culture, Journal of Bioscience and Bioengineering, 100, 667–671, 2005.
5 . Makishima F. et al., Interleukin-6 is antiproliferative to a mouse hybridoma cell line and promotive for its antibody productivity, Journal of Cytotechnology, 10, 15–23, 1992.

Generation of Human Monoclonal Antibody Specific for Propionibacterium Acnes by In Vitro Immunization

Yeon Suk Jung, Makiko Yamashita, Shin-Ei Matsumoto, Yoshinori Katakura, Kosuke Tomimatsu, Yoshihiro Aiba, Kiichiro Teruya, and Sanetaka Shirahata

Abstract *Propionibacterium acnes (P. acnes)* is known to be a main factor of pimple deterioration that occurs in hair follicle. *P. acnes* destroys skin structure and its resultant scars remain for a long time. Recently, bloods kept in blood banks were reported to be contaminated with *P. acnes*, which might cause serious post-transfusion infection in blood donors. The aim of this study is to generate human monoclonal antibody specific for *P. acnes* to treat skin problems caused by *P. acnes* and to apply it to examination for blood contamination. To develop human monoclonal antibody specific for *P. acnes*, we performed in vitro immunization (IVI) of human peripheral blood mononuclear cells (PBMCs). Sonicated or autoclaved *P. acnes* were used as sensitizing antigen in IVI. PBMC were treated with L-leucyl-L-leucine methyl ester (LLME) to remove lysosome-rich cells including monocytes and NK cells, and sensitized with antigen in the presence of IL-2 and IL-4. Cells were cultured for 7 days and supernatants were applied to ELISA and ELISPOT analyses. To select antigen-specific phage antibodies, we performed phage display using solid-panning system. Results demonstrate that in vitro-immunized PBMC produce *P. acnes*-specific antibody, suggesting that IVI protocol is useful for inducing antibody production specific for pathogenic bacteria.

Keywords *Propionibacterium acnes* • in vitro immunization • human monoclonal antibody • phage display

Y.S. Jung, S.-E. Matsumoto, Y. Katakura, Y. Aiba, K. Teruya, and S. Shirahata
Graduate School of Bioresources and Bioenvironmental Sciences, Kyushu University, 6-10-1 Hakozaki, Higashi-ku, Fukuoka, 812-8581, Japan

M. Yamashita, Y. Katakura, K. Tomimatsu, K. Teruya, and S. Shirahata
Graduate School of Systems Life Sciences, Kyushu University, 6-10-1 Hakozaki, Higashi-ku, Fukuoka, 812-8581, Japan

Y. Katakura, K. Teruya, and S. Shirahata
Faculty of Agriculture, Kyushu University, 6-10-1 Hakozaki, Higashi-ku, Fukuoka, 812-8581, Japan

K. Ikura et al. (eds.), *Animal Cell Technology: Basic & Applied Aspects*,
Animal Cell Technology: Basic & Applied Aspects 15,
DOI 10.1007/978-1-4020-9646-4_20,

1 Introduction

Propionibacterium acnes (*P. acnes*), a gram-positive bacillus, is a major inhabitant in skin microflora of human. Several mechanisms have been proposed regarding its role in the disease. First, *P. acnes* damages host tissues, and then cells are degraded by bacterial enzymes. Second, immunogenic factors derived from *P. acnes* such as surface determinants or heat shock proteins might trigger inflammation. Moreover, bloods kept in the blood banks were reported to be contaminated with *P. acnes*, which might cause infectious disease in blood donors. The aim of this study is to generate human monoclonal antibody to treat skin problems caused by *P. acnes* and to apply it to diagnosis of blood contamination.

2 Methods

2.1 Cells and Bacterial Culture

Human peripheral blood mononuclear cells (PBMCs) was collected from human healthy donors and was separated by density-gradient centrifugation with lymphocytes separation medium. On the other hand, *P. acens* was cultivated at 37°C with GAM mediums in an anaerobic culture and was identified by PCR [1]. Sonicated- (SC) and autoclaved- (AC) *P. acnes* were used as sensitizing antigens in in vitro immunization.

2.2 In Vitro Immunization

PBMCs were separated from peripheral blood of healthy donors. PBMCs were diluted with one volume of PBS, were layered on the lymphocyte separation medium and were centrifuged at 400 × *g* for 30 min. The lymphocytes were harvested by pipetting and washed three times with fresh ERDF medium. After washing, PBMCs were treated with 0.25 mM L-leucyl-L-leucine methyl ester (LLME; Bachem, Torrance, CA) to remove immunosuppressive cells [2]. The LLME-treated PBMCs were sensitized with killed *P. acnes* (1 to 10 μg/ml) in the ERDF medium containing 10% fetal bovine serum, 50 μg/ml of 2 ME (Invitrogen, Carlsbad, CA), 10 unit/ml of IL-2 (Genzyme, Cambridge, MA) 10 ng/ml of IL-4 (PeproTech, London, UK), and cultured for 7 days.

2.3 ELISA and ELISPOT

Ninety-six well microtiter plates were coated with 10 μg/ml of *P. acnes* or 1% of fish gelatin (BioFX Laboratories, Owing Mills, MD) in PBS and were incubated at

4°C overnight. The plates were washed three times with PBS, and were blocked with 2% BSA for 2 h at 37°C. Supernatants of PBMCs were added into the plates and placed for 2 h. After the plates were washed three times with PBS, 100 μL of horseradish peroxides conjugated goat anti-human IgM (Biosource, International) were added and the plates were incubated for 2 h. After the plates were washed three times, 100 μl of substrate solution (0.1 M citrate buffer containing 0.003% H_2O_2 and 0.3 mg/ml p-2, 2-azino-diammonium salt) were added. ELISA leader measured absorbance at 405 nm.

Multi Screen 96-well plates (Multi Screen-HA: Millipore, Bedford, MA) were used to detect B cells producing antigen-specific antibodies. Firstly, the plates were coated with 100 μg/ml of sonicated- or autoclaved-*P. acnes* in 0.1 M sodium carbonate buffer (pH 9.6) overnight. As a negative control, the plates were coated with 1% fish gelatin in PBS. After washing three times with PBS, plates were blocked with 200 μl of 1% fish gelatin in PBS for 2 h at 37°C. After washing three times with PBS, 100 μl of the incubated PBMC (1×10^5 cells/well) were seeded and incubated at 37°C overnight. After washing five times with TPBS, diluted horseradish peroxidase-conjugated goat anti-human IgM (BioSource) or IgG (BioSource) antibody were added as capturing antibodies, and subsequently incubated for 2 h at 37°C. Finally, True Blue Peroxidase Substrate (KPL, Inc., Gaithersburg, MD) was added to the plates. After the incubation, the plate was washed with water and dried. We counted the number of spots by using ImageJ, an image analyzing software.

2.4 Generation of Single-Chain Fv Antibody

The purified DNA products (V_H and V_L) were assembled into a single gene using a linker DNA encoding $(Gly_4Ser)_3$ to make scFv DNA fragment by overlap extension PCR.

2.5 Selecton of Antigen-Specific Phage Antibody by Solid-Phase Panning

The scFv DNA was digested with *Sfi*I and *Not*I for subsequent cloning into the pCANTAB5E phagemid (Amersham Biosciences, Buckinghamshire, U.K.) [3]. *E. coli* TG1 cells were transformed with pCANTAB5E, and infected with helper phage M13KO7 to produce phage antibody [4]. Panning was performed on 25 mm T-flask that was coated with autoclaved- or sonicated-*P. acnes*. After thorough washing with PBS, TG1 cells were added to rescue antigen-specific phage antibody, and were spread on SOBAG plates. Colonies were cultured in 2 × YT medium and the production of antigen-specific phage antibody was measured by ELISA.

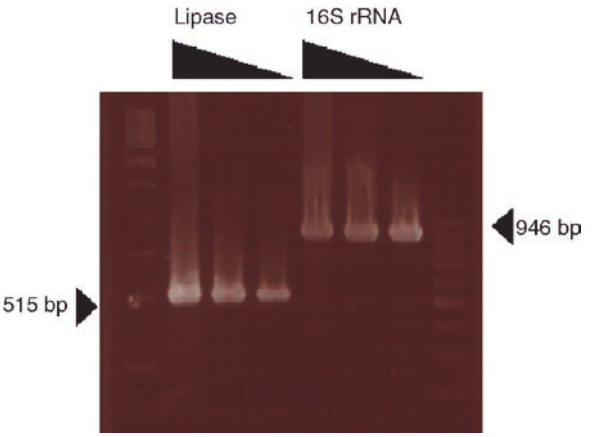

Fig. 1 *P. acnes* was confirmed by PCR that was used to detect 16S rRNA and lipase genes of *P. acnes*

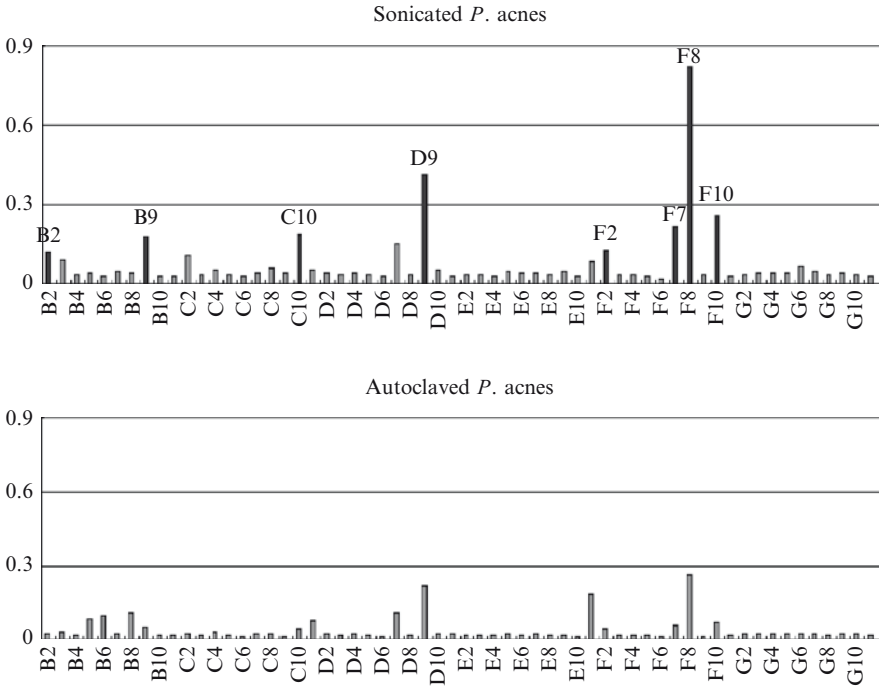

Fig. 2 *P. acnes*-specific clones selected from the second round of panning. Condition of sonicated *P. acnes*; B2, B9, C10, D9, F2, F7, F8, and F10 were detected as high positive signals

3 Results and Discussion

We detected 16S rRNA and lipase gene of *P. acnes* by PCR (Fig. 1), indicating that *P. acnes* were successfully cultivated in our culture system. We first investigated the treatment method of *P. acnes* to be used in IVI. When autoclaved or sonicated *P. acnes* were used, antigen-specific antibody production was efficiently induced upon the addition of sonicated *P. acnes* in IVI. These results suggest that IVI technique is useful for inducing antibody production specific for pathogenic bacteria.

We next generated phage antibodies and selected *P. acnes* specific antibody by panning. After 2nd panning, *P. acnes* specific phage antibody was identified by ELISA (Fig. 2). We are now trying to generate human monoclonal IgG antibody that bound to *P. acnes*.

References

1. Nakamura, M., Kametani, I., Higaki, S., Yamagishi, T., Identification of *Propionibacterium acnes* by polymerase chain reaction for amplification of 16S ribosomal RNA and lipase genes. Clinical Microbiology Anaerobe (2003) 9, 5–10.
2. Ichikawa, A., Katakura, Y., Hashizume, S., Shirahata, S., In vitro immunization of human peripheral blood lymphocytes: establishment of B cell lines secreting IgM specific for cholera toxin B subunit from lymphocytes stimulated with IL-2 and IL-4. Cytotechnology (1999) 31, 131–139.
3. Smith G.P., Petrenko V.A., Phage Display. Chemical Review (1997) 97, 391–410.
4. McCafferty, J., Griffiths, A.D., Winter, G., Chisewll, D.J., Phage antibodies: filamentous phage displaying antibody variable domains. Nature (1990) 348 (6301), 552–554.

Construction of Multi-layered Cell Sheet Using Magnetite Nanoparticles and Magnetic Force

Akira Ito, Hiroyuki Honda, and Masamichi Kamihira

Abstract Novel technologies to establish 3D tissue-like constructs are desired for tissue engineering. In the present study, magnetic force and magnetite nanoparticles were used to construct a layered mesenchymal stem cell (MSC) sheet, a layered cardiomyocyte sheet, and a layered fibroblast sheet involving capillaries. Magnetite cationic liposomes (MCLs), which have a positive surface charge, were taken up by the target cells. When a magnet was set under a tissue culture dish, magnetically labeled target cells were attracted and then adhered to form a layered cell sheet. For MSC sheets, MSCs within the sheets maintained an in vitro multi-differentiation ability into osteoblasts, adipocytes or chondrocytes after a 21-day culture period using each induction medium. By using an electromagnet, MSC sheets were harvested and transplanted into the bone defect in cranium of nude rats. Histological observation revealed that new bones surrounded by osteoblast-like cells were formed in the defect area of rats on 14 days after transplantation with MSC sheets. For cardiomyocyte sheets, the immunofluorescence staining of connexin43 revealed the existence of gap junctions within the cardiomyocyte sheets. Moreover, electrical connection within the cardiomyocyte sheets was confirmed by using extracellular potential mapping. For fibroblast sheets, normal human dermal fibroblasts (NHDFs) sheets contained the major dermal extracellular matrix (ECM) components (fibronectin and type I collagen). Human umbilical vein endothelial cells (HUVECs) were co-cultured with NHDF sheets, resulted in tube-like formation of HUVECs, resembling early capillaries, within NHDF sheets after short-term 3D co-culture. These results suggest that this novel use of magnetite nanoparticles and magnetic force, which we refer to as "magnetic force-based tissue engineering (Mag-TE)", offers a major advancement in tissue engineering.

Keywords Tissue engineering • magnetite nanoparticle • liposome

A. Ito and M. Kamihira
Department of Chemical Engineering, Faculty of Engineering, Kyushu University,
744 Motooka, Nishi-ku, Fukuoka, 819-0395, Japan

H. Honda
Department of Biotechnology, School of Engineering, Nagoya University,
Furo-cho, Chikusa-ku, Nagoya, 464-8603, Japan

K. Ikura et al. (eds.), *Animal Cell Technology: Basic & Applied Aspects*,
Animal Cell Technology: Basic & Applied Aspects 15,
DOI 10.1007/978-1-4020-9646-4_21,

1 Introduction

Tissue engineering holds much promise as means of resolving the various issues surrounding organ transplantation, and several tissue engineering approaches are being explored. The most common approach has been to seed target cells into biodegradable porous synthetic polymers. However, inflammatory reaction due to biodegradation of the scaffolds is remained to be a problem. To solve these problems, novel tissue-engineering methodologies to construct a three-dimensional (3-D) tissue without scaffolds is needed.

We previously developed magnetite cationic liposomes (MCLs), which are cationic liposomes containing 10-nm magnetite nanoparticles (Fe_3O_4), improve the accumulation of magnetite nanoparticles in target cells. We proposed an original tissue engineering methodology using the cells which labeled magnetically by MCLs and magnetic force [1, 2], and have designated this novel methodology as "magnetic force-based tissue engineering (Mag-TE)".

Previously, we applied Mag-TE technique for construction of 3-D multilayered cell sheets without scaffolds [3, 4]. The cells which are magnetically labeled with MCLs are seeded onto ultralow-attachment plates. Subsequently, a magnet is placed under the plates to accumulate the magnetically cells, and then 3-D multilayered cells sheets was constructed. In our previous study, transmission electron microscopy revealed desmosomes which is one of the cell-to-cell adherence proteins were observed within the keratinocyte sheets constructed by Mag-TE [1]. However, further experiments were needed to examine the 'functional' connections within the sheets constructed by Mag-TE. In the present study, we investigated whether functional cell sheets could be constructed by Mag-TE technique.

2 Materials and Method

2.1 Preparation of MCLs

Magnetite (Fe_3O_4; average particle size, 10 nm) used as the core of the magnetite cationic liposomes (MCLs) was obtained from Toda Kogyo (Hiroshima, Japan). MCLs were fabricated according to the previous study [1]. Briefly, colloidal magnetite and a lipid mixture consisting of N-(α-trimethylammonioacetyl)-didodecyl-D-glutamate chloride, dilauroylphos-phatidyl-choline and dioleoylphosphatidyl-ethanolamine in a 1:2:2 molar ratio were used.

2.2 Cell Culture

Human bone marrow mesenchymal stem cells (MSCs) were obtained from Cambrex (Walkersville, MD), and were cultured in MSCGM (Cambrex) containing fetal bovine serum (FBS), L-glutamine, streptomycin sulfate and potassium penicillin

G as antibiotics. Neonatal cardiomyocytes (CMs) were isolated using neonatal cardiomyocyte isolation system (Worthington biochemical, Lakewood, NJ) according to the manufacturer's instructions with some modifications. CMs were cultured using Medium 199 containing 10% FBS, 2.7 mM glucose, 0.1 mg/ml streptomycin sulfate, and 100 U/ml potassium penicillin G. Human umbilical vein endothelial cells (HUVECs) and normal human dermal fibroblast (NHDFs) were provided by Kurabo (Osaka, Japan), and were cultured in HuMedia-EG2 for HUVECs, Medium106S for NHDFs (Kurabo).

2.3 Cell Sheets Construction

The procedures used to construct cells sheets were consisted of two processes. As the first step, MCLs (100 pg-magnetite/cell) were added into cultured target cells, in order to label the cells magnetically. As the second step, after 4 h of incubation, target cells labeled with MCLs were seeded into a 24-well ultra-low-attachment plate (Corning, NY), the surface of which consists of a covalently bound hydrogel layer that is hydrophilic and electrically neutral. A cylindrical neodymium magnet (diameter, 30 mm; height, 15 mm; magnetic induction, 4,000 Gauss) was then placed at the reverse side of the ultra-low-attachment plate, and the cells were cultured for 24 h.

2.4 Transplantation of MSC Sheet

An electromagnet for transplantation of MSC sheets was fabricated by Toyo Jiki Industry (Saitama, Japan). Magnetic field was generated at a tip of the probe (magnetic field intensity, 450 Gauss).

Bone defect was surgically created at the head of F344 nude rats. The pericranium was removed and 5-mm defects were made using an electric drill. After placement of the MSC sheets into the defect by using the electromagnet, the skin was closed. After 14 days of the transplantation, the rats were sacrificed and the pericranium containing the defect site was surgically extirpated. For histological evaluation, the extirpated pericranium accompanying skin tissue was fixed with 3.7% paraformaldehyde and thin (4 μm) slices were stained with hematoxylin and eosin (H&E).

2.5 Electrical Conduction Within CM Sheet

To examine the presence of gap junctions, CMs sheets constructed by Mag-TE were subjected to immunofluorescence staining with connexin43-specific antibody. The CMs sheets were frozen cross-sectioned and were incubated with a rabbit anti-connexin 43 for 30 min, and then they were incubated with an Alexa568 conjugated goat anti-rabbit IgG for 1 h.

Electrical conduction within CM sheets constructed by Mag-TE was examined by extracellular potential mapping by using a specifically designed multi-electrode array system (MED64, Panasonic, Tokyo, Japan).

2.6 Construction of NHDF Sheets Including HUVECs

MCLs (100 pg/cell) were added to both NHDFs and HUVECs and cells were incubated for 24 h. Cells were harvested, and HUVECs (6×10^4 cells) were mixed with NHDFs (1.8×10^6 cells). The mixture was seeded onto ultra-low-attachment plates. A magnet was placed under the plate, and the cells were cultured for 1 day.

Fluorescence microscopy was performed using CellTracker (Molecular Probes, Eugene, OR); HUVECs were pre-stained, fluorescent-stained cells were seeded onto NHDF sheets and the formation of capillaries was periodically observed by fluorescence microscopy.

For immunohistochemistry, the primary antibody used was rabbit anti-von Willebrand factor (vWF; DakoCytomation). Biotinylated goat anti-rabbit immunoglobulin was used as a secondary antibody. Peroxidase activity was visualized after soaking at room temperature for 10 min in 0.02% diaminobenzidine tetrahydrochloride containing 0.005% hydrogen peroxide (brown staining indicates peroxidase activity).

3 Results and Discussion

3.1 MSC Sheets

When human MSCs labeled with MCLs were seeded into 24-well ultralow-attachment plates, cells accumulated rapidly on the plates by magnetic force caused by a magnet placed under the plate. Due to the 3D culture using magnetic force, MSCs formed a sheet-like structure after a 24-h incubation period. MSC sheets had a black-brown color, which is the color of magnetite nanoparticles. The MSC sheets had a somewhat shrunken appearance, and the shrunken MSC sheets had greater mechanical strength in cell–cell interaction than the sheets before shrinking. When the magnet was removed from the underside of the plate, the cell sheets could be easily detached from the bottom of the plates without enzymatic digestion, and were thus harvested. To confirm that MSC layers formed a sheet-like construct, we examined cross-sections of the layers. Phase-contrast microscopy of the cross-sections of the MSC sheets revealed that the sheets were approximately 20-layered cell sheets.

To examine whether MSC sheets could differentiate into osteoblasts and form new bone in vivo, MSC sheets were transplanted into nude rats. A 5-mm defect was made in the cranial bone of nude rats (Fig. 1a). Here, we investigated whether these magnetically labeled sheets could be harvested and transplanted using an electron magnets. Figure 1 shows the procedure for the harvest and transplantation of MSC

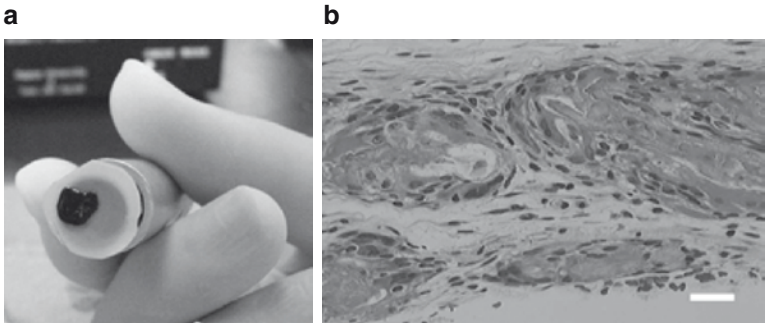

Fig. 1 MSC sheets constructed by Mag-TE [5] were harvested (**a**) and were transplanted into a bone defect by using the electromagnet. (**b**) Histlogical analysis of in vivo bone formation

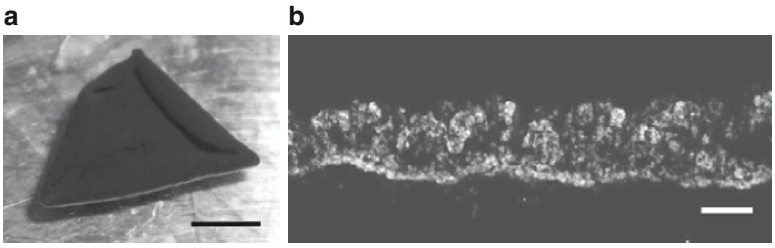

Fig. 2 Cardiomyocyte sheet constructed by Mag-TE [6]; scale bar 5 mm (**a**). The cross-section appearance of immunological stained cardiomyocyte sheet with anti-connexin 43 antibody; scale bar 100 mm (**b**)

sheets constructed by Mag-TE. When the cylindrical neodymium magnet positioned at the reverse side of the 24-well ultra-low-attachment plate was removed, MSC sheets were detached from the culture surface. Then, the electromagnet was positioned at the surface of the culture medium. Due to the magnetic force, the MSC sheets floated up to the surface of the culture medium without disruption, and stuck to the magnet (Fig. 1b). The MSC sheets were delivered to the defect site by use of the electromagnet (Fig. 1c).

At 14 days after the transplantation, the cranial bone sections were stained with hematoxylin and eosin and examined for bone formation (Fig. 1d). New bones surrounded by osteoblast-like cells were observed in the area of the defect of MSC sheet-transplanted rats (Fig. 1d), suggesting that transplantation of MSC sheet constructed by Mag-TE induced new bone formation in the bone defect.

3.2 CM Sheets

After 24 h incubation in the presence of a magnet, CMs accumulated to form a sheet-like structure (Fig. 2a). On the contrary, CMs formed spheroid when CMs cultured without a magnet on an ultra-low attachment plate. When the magnet was

removed, the CM sheets were detached from the surface of ultra-low-attachment dish and somewhat shrank from their edge (Fig. 2a). Immunofluorescence staining of connexin43 revealed the presence of gap junction within the CM sheets, at 24 h after the seeding of CMs onto a magnet (Fig. 2b).

Since the gap junctions were existed within the CM sheet constructed by Mag-TE (Fig. 2b), the electrical conduction was also examined. The electrical conduction of CMs within CM sheets constructed by Mag-TE was measured by a multi-electrode extracellular potential mapping. CM sheets were constructed on the multielectrode by using magnetically labeled CMs and a magnet (4,000 G) and incubated for 48 h. As a result, electric signals widely spread and were recorded from more than half of the 64 electrodes. The conduction velocity across the CM sheet constructed by Mag-TE was 9.1 ± 1.8 cm/s. The electrical spikes were synchronized at 22.6 beat per min (bpm). These results suggest that the electrical conduction was established between CMs within the CM sheets constructed by Mag-TE.

3.3 Fibroblast Sheet Involving Capillaries

In order to produce capillaries within NHDF sheets, magnetically labeled NHDFs and HUVECs were admixed and seeded into ultralow-attachment plate. When the cells were co-cultured in the presence of a magnet for 1 day, NHDF sheets incorporating HUVECs were formed. Figure 3a shows cross-sections of NHDF sheets incorporating HUVECs on day 1. HUVECs formed tube-like structures with lumens of 5-6 μm (Fig. 3b), and some formed connected tube-like structures (Fig. 3c) within the sheets. These results suggest that 3D co-culture of HUVECs within NHDF sheets induced angiogenesis.

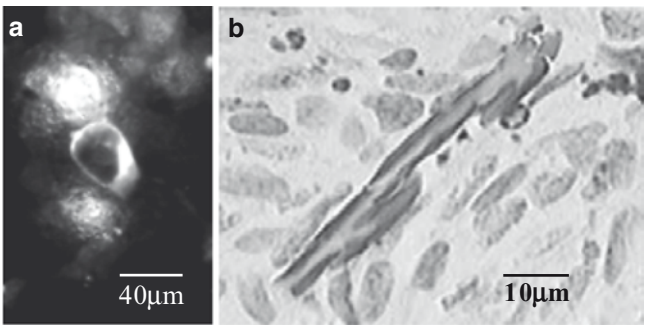

Fig. 3 (**a**) Fluorescence microscopy of HUVECs within NHDF sheets [7]. (**b**) Bright-field micrographs of immuno-staining against vWF in NHDF sheets

References

1. A. Ito, M. Hayashida, H. Honda, K. Hata, H. Kagami, M. Ueda, T. Kobayashi, Construction and harvest of multilayered keratinocyte sheets using magnetite nanoparticles and magnetic force. *Tissue Eng* 10(5-6), 873–880 (2004).
2.. A. Ito, Y. Takizawa, H. Honda, K. Hata, H. Kagami, M. Ueda, T. Kobayashi, Tissue engineering using magnetite nanoparticles and magnetic force: heterotypic layers of cocultured hepatocytes and endothelial cells. *Tissue Eng* 10(5-6), 833–840 (2004).
3. A. Ito, E. Hibino, C. Kobayashi, H. Terasaki, H. Kagami, M. Ueda, T. Kobayashi, H. Honda, Construction and delivery of tissue-engineered human retinal pigment epithelial cell sheets, using magnetite nanoparticles and magnetic force. *Tissue Eng*11(3-4), 489–496 (2005).
4. A. Ito, K. Ino, M. Hayashida, T. Kobayashi, H. Matsunuma, H. Kagami, M. Ueda, H. Honda, Novel methodology for fabrication of tissue-engineered tubular constructs using magnetite nanoparticles and magnetic force. *Tissue Eng* 11(9-10), 1553–1561 (2005).
5. K. Shimizu, A. Ito, T. Yoshida, Y. Yamada, M. Ueda, H. Honda, Bone tissue engineering with human mesenchymal stem cell sheets constructed using magnetite nanoparticles and magnetic force. *J Biomed Mater Res B Appl Biomater* 82(2), 471–480 (2007).
6. K. Shimizu, A. Ito, J.K. Lee, T. Yoshida, K. Miwa, H. Ishiguro, Y. Numaguchi, T. Murohara, I. Kodama, H. Honda, Construction of multi-layered cardiomyocyte sheets using magnetite nanoparticles and magnetic force. *Biotechnol Bioeng* 96(4), 803–809 (2007).
7. K. Ino, A. Ito, H. Kumazawa, H. Kagami, M. Ueda, H. Honda, Incorporation of capillary-like structures into dermal cell sheets constructed by magnetic force-based tissue engineering. *J Chem Eng Jpn* 40(1), 51–58 (2007).

Anti-histone H1 Autoantibody: An Inducible Immunosuppressive Factor in Liver Transplantation

Akiko Katayama, Seiji Kawamoto, Yasushi Yamanaka, Takashi Kiso, Tsunehiro Aki, Toshiaki Nakano, Naoya Ohmori, Takeshi Goto, Shuji Sato, Jenny Chiang, Yayoi Shimada, Shigeru Goto, Chao-Long Chen, and Kazuhisa Ono

Abstract In a rat model of tolerogeneic liver transplantation, serum from the recipient has been shown to exhibit a strong immunosuppressive activity. However, molecular identity of those humoral factors has yet to be elucidated. We previously found that one of major immunosuppressive factors in the recipient serum was transplantation-induced IgG antibodies. Here we identified an antigen recognized by the regulatory IgG as histone H1. Polyclonal antibody raised against histone H1 not only suppressed allogeneic mixed lymphocyte reaction (MLR), but also prolonged allograft survival *in vivo*. To elucidate mechanisms underlying the immunosuppressive activity, we generated murine anti-histone H1 monoclonal antibodies (mAbs) which can suppress allogeneic MLR. One of selected mAbs, termed 16G9, showed a dose-dependent MLR inhibitory activity. Flow cytometric analysis revealed that 16G9 specifically reacted with a part of murine splenocytes including T cells, B cells, and $CD11b^+$ monocytes/macrophages. These results raise a possibility that 16G9 may suppress MLR *via* cross-reaction with target antigens on the leukocytes.

Keywords Liver transplantation • histone H1 • monoclonal antibody

A. Katayama, S. Kawamoto, Y. Yamanaka, T. Kiso, T. Aki, and K. Ono
Department of Molecular Biotechnology, Graduated School of Advanced Science of Matter, Hiroshima University, Higashi-Hiroshima, 739-8530, Japan

T. Nakano, S. Goto, and C-L. Chen
Department of Surgery, Liver Transplant Center, Chang Gung Memorial Hospital-Kaohsiung Medical Center, Kaohsiung, 833, Taiwan

N. Ohmori, T. Goto, S. Sato, J. Chiang, and Y. Shimada
Faculty of Pharmaceutical Sciences, Josai International University, Togane, 283-8855, Japan

S. Goto
Iwao Hospital, Yufuin, 879-5102, Japan

K. Ikura et al. (eds.), *Animal Cell Technology: Basic & Applied Aspects*,
Animal Cell Technology: Basic & Applied Aspects 15,
DOI 10.1007/978-1-4020-9646-4_22, © Springer Science+Business Media B.V. 2009

1 Introduction

In current organ transplantation, administration of immunosuppressant such as tacrolimus (FK506) or cyclosporine A is indispensable for prevention of allograft rejection. However, use of these immunosuppressant includes problems such as permanent medication or serious side effects [1]. Therefore, development of new effective immunosuppressants and/or therapeutic interventions have long been a major focus of organ transplantation research.

The graft survival rate of liver transplantation is well known to be higher than those of other organ transplantations [2]. It has also been demonstrated that allograft rejection could be overcome without using any immunosuppressants in a rat model of orthotopic liver transplantation (OLT) [3]. Moreover, recipient serum after OLT (post-OLT serum) has been reported to prevent allograft rejection [4], suggesting that immunosuppressive factors are induced in the post-OLT serum.

Nakano et al. previously showed that one of major immunosuppressive factors in the recipient serum is OLT-inducible IgG antibody [5]. In the present study, we demonstrated that a target antigen recognized by this immunosuppressive IgG was histone H1. To start elucidating the immunosuppressive mechanisms, here we also generated an anti-histone H1 mAb 16G9, which can neutralize allogeneic MLR.

2 Materials and Methods

2.1 Animals, OLT, and Post-OLT Serum

Male DA rats (major histocompatibility complex haplotype RT1a, 7 to 8 weeks of age) were obtained from Japan SLC (Hamamatsu, Japan). Age matched male PVG (RT1c) and LEW (RT1l) rats were obtained from Seac Yoshitomi (Fukuoka, Japan). BALB/c mice and C57BL/6N (B6) mice (6 to 10 weeks of age) were obtained from Charles River Japan (Yokohama, Japan). All animals were maintained in a specific pathogen-free animal facility. In OLT, DA rat liver was implanted into the PVG recipient by the cuff method as described [6]. Post-OLT sera were obtained from the recipient 14 or 21 days after OLT.

2.2 Evaluation of Immunosuppressive Activity

In vitro immunosuppressive activity of post-OLT serum was evaluated using rat allogeneic MLR as described previously [7]. Briefly, stimulator splenocytes from DA rat were inactivated by treatment with mitomycin C (MMC, Kyowa Hakko Kogyo, Tokyo, Japan). Responder PVG splenocytes (1×10^6 cells in 100 μl) and stimulator cells (8×10^6 cells in 100 μl) were mixed in 96-well round bottom plates

(Nunc, USA). Then post-OLT serum was added at a final concentration of 2%. A control culture consisted of PVG splenocytes mixed with syngeneic, MMC-treated stimulator cells (PVG vs. PVG). These cell samples were cultured in RPMI 1640 medium (Sigma, USA) supplemented with 100 U/ml penicillin, 100 μg/ml streptomycin, 50 μM 2-mercaptoethanol, and 10% fetal calf serum (FCS, BioWest, USA) at 37°C for 84 h. Allogeneic proliferative response was determined using BrdU Labeling and Detection Kit III (Roche Diagnostics, The Swiss). To evaluate the MLR inhibitory activity of anti-histone H1 autoantibody, rabbit anti-histone H1 polyclonal antibody (Santa Cruz Biotechnology, USA) was supplemented into the MLR culture at final concentrations up to 8 μg/ml. *In vivo* immunosuppressive activity of anti-histone H1 antibody was assessed by its administration to a rat model of heterotopic heart transplantation as described [8]. Murine allogeneic MLR was performed by the same protocols as described above, except using MMC-treated BALB/c splenocytes (stimulator) and those from B6 mice (responder). Anti-hisotne H1 mAb 16G9 or isotype control mAb (described below) was supplemented into the MLR culture at final concentrations up to 20 μg/ml.

2.3 SDS-PAGE and Western Blot Analyses

SDS-PAGE was performed as described [5]. Briefly, cell lysate samples were boiled for 5 min, and run on a 12.5% SDS-PAGE gel using a miniature gel apparatus (ATTO, Tokyo, Japan). Protein bands were visualized by Coomassie brilliant blue R-250 staining. To detect specific autoantigens recognized by post-OLT serum IgG, PVG splenocytes were lysed and subjected to SDS-PAGE and western blot assay using post-OLT serum and secondary peroxidase-conjugated goat anti-rat IgG (Cell Signaling, USA).

2.4 Purification and Structural Analysis of Autoantigens Recognized by Post-OLT Serum IgG

To characterize autoantigens recognized by post-OLT serum IgG, the 31 and 34 kDa antigens in PVG splenocyte insoluble fraction were visualized in 10% SDS-PAGE gel by negative staining with 4 M sodium acetate. After excision of these bands, proteins were extracted from gel pieces in PBS containing 1% SDS. For amino acid sequencing, purified 31 and 34 kDa antigens were digested by lysyl endopeptidase (Wako Pure Chemical, Osaka, Japan) or V8 protease (Roche Diagnostics). The 31 kDa antigen was also chemically digested in 500 mM CNBr/70% formic acid. Resulting protein fragments were resolved by SDS-PAGE, and blotted onto Immobilon filters (Millipore, USA). *N*-terminal amino acid sequencing was carried out using 492 protein sequencer (Applied Biosystems, USA).

2.5 Generation of MLR-Neutralizing Anti-histone H1 mAb

BALB/c mice were intraperitoneally immunized with a mixture of calf thymus histone H1 (500 μg/ml, Roche Diagnostics) and complete Freund's adjuvant (Wako Pure Chemical) every 2 weeks. After confirming serum histone H1 titer and MLR inhibitory activity, splenocytes from these mice were fused with P3-X63-Ag8.653 myeloma cells according to standard procedures [7]. We selected a potent MLR-neutralizing anti-histone H1 mAb termed 16G9. The 16G9 secreting hybridoma was maintained in 15% FCS/Iscove's Modified Dulbecco's Medium (Gibco, USA).

2.6 Serum-Free Culture of Hybridoma Cells and Purification of Anti-histone H1 mAb 16G9

The 16G9 hybridoma was adapted to a serum-free medium (CD Hybridoma Medium, Gibco) according to manufacturer's instruction. Then the hybridoma cells were inoculated at a density of 1×10^5 cells/ml, and cultured for 7 days. The supernatant was collected and subjected to 50% ammonium sulfate precipitation. Resulting precipitate was dialyzed in 20 mM sodium phosphate buffer (pH 7.0). After dialysis, mAb was purified using histone H1-immobilized affinity column as described [8].

2.7 Flow Cytometry

B6 splenocytes were incubated with anti-mouse CD16/CD32-blocks Fc (eBiosciences, USA) at 4°C for 20 min in a staining buffer (0.5% FCS/0.1NaN_3 in PBS), followed by staining with biotinylated 16G9 or isotype control (0.5 μg/ml) for 30 min. After washing with a staining buffer, the cells were incubated with streptavidin-conjugated phycoerythrin (0.5 μg/ml, BD Bioscience, USA) for 30 min. After washing, the samples were analyzed by FACSCalibur flow cytometer (BD Biosciences) with CellQuest software. To clarify 16G9-positive cell subset, splenocytes were co-stained with fluorescein isothiocyanate-conjugated anti-mouse CD3ε, anti-B220, or anti-CD11b antibody (BD Biosciences).

3 Results and Discussion

3.1 Anti-histone H1 Autoantibody Identified as a Major Immunosuppressive Factor in Post-OLT Serum

A previous report indicated that IgG was induced in post-OLT sera, and its depletion abrogated their immunosuppressive activity [5]. We hypothesized that the MLR inhibitory activity of the OLT-inducible IgG was executed through its recognition

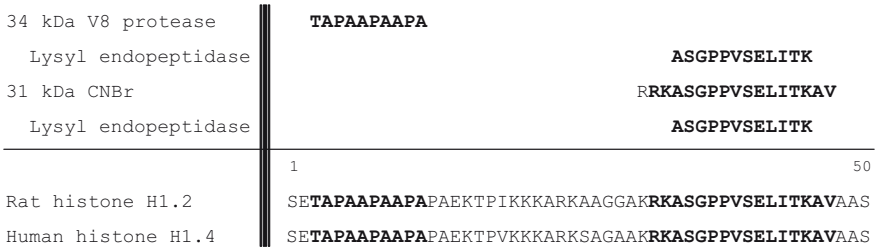

Fig. 1 Identification of antigens recognized by post-OLT regulatory IgG as histone H1

of specific antigens expressed on the immune cells. To test this possibility, we first attempted to detect those antigens. Western blot analysis revealed that early post-OLT serum IgG (14 days) specifically reacted with 31, 34 and 73 kDa autoantigens in splenocytes from PVG rat. We focused on the 31 and 34 kDa antigens, and determined their amino acid sequences. The internal sequences obtained from both antigens coincided with those of histone H1 (Fig. 1). Immunodepletion of histone H1-specific antibody from the early post-OLT serum abrogated its MLR inhibitory activity (data not shown), suggesting that anti-histone H1 autoantibody is a major immunosuppressive factor induced by OLT.

3.2 Immunosuppressive Activity of Anti-histone H1 Antibody In Vitro and In Vivo

We next examined whether rabbit anti-histone H1 polyclonal antibody (pAb) possessed immunosuppressive activity. As expected, anti-histone H1 pAb suppressed rat allogeneic MLR (data not shown). Furthermore, in vivo administration of anti-histone H1 pAb to a rat model of heterotopic heart transplantation prolonged cardiac allograft survival (data not shown). These results established a potent immunosuppressive activity of anti-histone H1 antibody, and its potential usefulness as a new immunosuppressant.

3.3 Generation of MLR-Neutralizing Anti-histone H1 mAb, 16G9

To start elucidating mechanisms underlying the immunosuppressive activity of anti-histone H1 autoantibody, we next generated murine anti-histone H1 mAbs which can suppress allogeneic MLR. One of selected mAbs, here we termed 16G9, showed a dose-dependent MLR inhibitory activity (Table 1). The immunosuppressive potency of 16G9 (added at a concentration of 20 μg/ml) was comparable to that of FK506 (10 nM). Exogenous addition of histone H1 abrogated the immunosuppressive activity (data not shown), suggesting that 16G9 suppresses MLR in an antigen-specific manner.

Table 1 MLR-inhibitory activity of anti-histone H1 mAb 16G9

Stimulator/Responder	Additive	BrdU Incorporation (Mean A405 nm ± SD)
B6/B6	–	0.340 ± 0.053
BALB/c/B6	–	0.703 ± 0.082
Isotype control 10 μg/ml	0.500 ± 0.126	
20 μg/ml	0.512 ± 0.042	
16G910 μg/ml	0.343 ± 0.040[a]	
20 μg/ml	0.256 ± 0.056[a]	
FK506 (10 nM)	0.230 ± 0.055	

[a] Significantly inhibited as compared with respective isotype controls ($p < 0.05$).

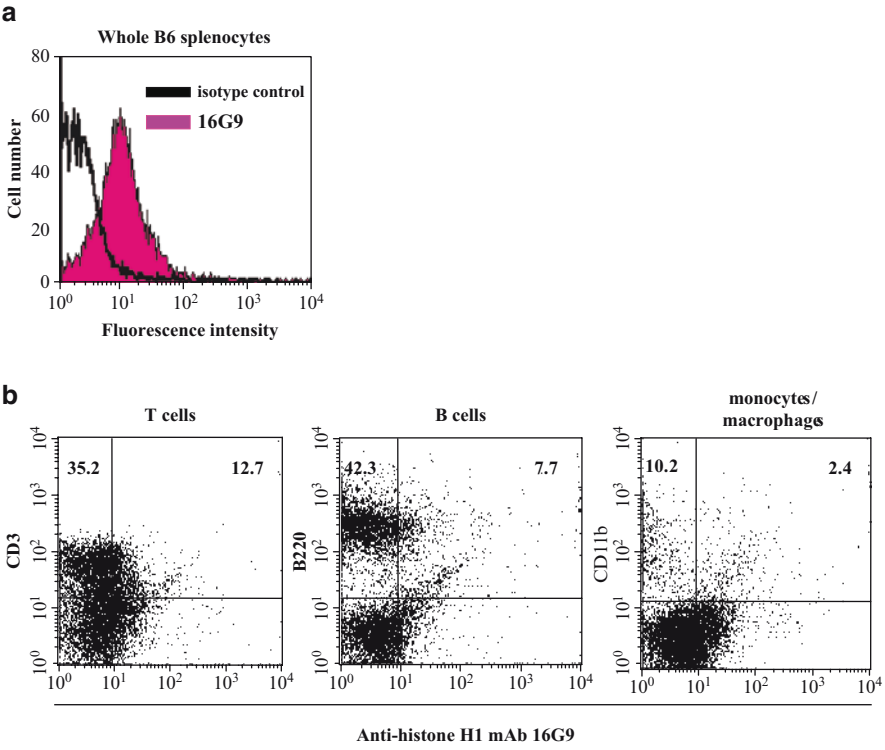

Fig. 2 (**a**) 16G9 specifically reacted with a part of splenocytes. (**b**) Dissection of 16G9-positive leukocytes

3.4 16G9 mAb Specifically Reacts with Murine Leukocytes

We next examined whether 16G9 cross-reacts with the cell surface of splenocytes from B6 mice. Flow cytometric analysis revealed that a fraction of splenocytes were specifically stained with 16G9 (Fig. 2a). We also found that these 16G9

positive cells included $CD3^+$ T cells, $B220^+$ B cells, and $CD11b^+$ monocytes/macrophages (Fig. 2b). These results imply that immunosuppression by 16G9 might occur through cross-reaction with cell surface antigens.

Acknowledgments This work was supported by a grant of Research for Promoting Technological Seeds, which was conducted by Japan Science and Technology Agency. S. K. was also supported by the Uehara Memorial Foundation.

References

1. Hojo M. et al. (1999) Cyclosporine induces cancer progression by a cell-autonomous mechanism. *Nature* 377, 530–534.
2. Kobayashi E. (1997) Immunological tolerance induced by liver grafting: Cellular and humoral factors. *Molecular Medicine* 34, 797–804.
3. Kamada N. et al. (1981) Reversal of transplantation immunity by liver grafting. *Nature* 292, 840–842.
4. Kamada N. et al. (1984) Antigen-specific immunosuppression induced by liver transplantation in the rat. *Transplantation* 38, 217–221.
5. Nakano T. et al (2002) Analysis of immunosuppressive factors expressed in serum of liver transplanted rast. *Animal Cell Technology: Basic & Applied Aspects* 12, 257–261.
6. Kamada N. et al. (1979) Orthotopic liver transplantation in the rat: Technique using cuff for portal vein anastomosis and biliary drainage. *Transplantation* 28, 47–51.
7. John E. C. et al. (1994) *Current Protocols in Immunology*. New York, Wiley.

Anti-histone H1 Autoantibody Directly Acts on T Cells to Exert Its Immunosuppressive Activity

Yasushi Yamanaka, Seiji Kawamoto, Akiko Katayama, Takashi Kiso, Tsunehiro Aki, Toshiaki Nakano, Naoya Ohmori, Takeshi Goto, Shuji Sato, Jenny Chiang, Yayoi Shimada, Shigeru Goto, Chao-Long Chen, and Kazuhisa Ono

Abstract We previously demonstrated that histone H1-specific autoantibody is one of major immunosuppressive factors in a rat model of tolerogeneic liver transplantation. To gain insight into mechanisms underlying the tolerance induction, we generated a murine anti-histone H1 monoclonal antibody (mAb) 16G9, that can block allogeneic mixed lymphocyte reaction. In the present study, we tested whether 16G9 mAb directly acts on T cells to exhibit immunosuppressive activity. 16G9 inhibited cell proliferation and IL-2 production of purified T cells upon stimulation with immobilized anti-CD3 antibody. 16G9 also suppressed pharmacological T cell activation bypassing T cell receptor (TCR) ligation, implying that 16G9 does not affect TCR-membrane proximal signaling event, but rather acts on downstream TCR signaling pathway to exert immunosuppressive activity. Flow cytometric analysis indicated that 16G9 specifically bound to a fraction of T cells. Exogenous addition of histone H1 competitively inhibited the immunoreactivity, suggesting the existence of histone H1-like antigens on the T cell surface. Intriguingly, the 16G9-reactive T cell population was transiently increased upon TCR crosslinking, implicating that 16G9 might also react with activated T cells *via* inducible cross-reactive antigens.

Keywords Histone H1 • immunosuppression • liver transplantation

Y. Yamanaka, S. kawamoto, A. Katayama, T. Kiso, T. Aki, and K. Ono
Department of Molecular Biotechnology, Graduate School of Advanced Sciences of Matter, Hiroshima University, Higashi-Hiroshima, 739-8530, Japan

T. Nakano, S. Goto, and C.-L. Chen
Department of Surgery, Liver Transplant Center, Chang Gung Memorial Hospital-Kaohsiung Medical Center, Kaohsiung 833, Taiwan

N. Ohmori, T. Goto, S. Sato, J. Chaing, and Y. Shimada
Faculty of Pharmaceutical Sciences, Josai International University, Togane, 283-8855, Japan

S. Goto
Iwao Hospital, Yufuin, 879-5102, Japan

K. Ikura et al. (eds.), *Animal Cell Technology: Basic & Applied Aspects*,
Animal Cell Technology: Basic & Applied Aspects 15,
DOI 10.1007/978-1-4020-9646-4_23, © Springer Science+Business Media B.V. 2009

1 Introduction

In current organ transplantation, administration of immunosuppressant (tacrolimus/FK506, cyclosporine A etc.) is essential to prevent allograft rejection [1]. However, use of these immunosuppressive drugs includes various problems such as permanent medication or serious side effects [2]. Thus, development of a new effective immunosuppressant has continuously been desired. In a rat model of orthotopic liver transplantation (OLT) in which DA rat liver is implanted into PVG rat, allograft rejection is overcome beyond the barrier of histoincompatibility [3]. It has also been demonstrated that recipient serum after OLT (post-OLT serum) has immunosuppressive activity [4], although the details of these humoral factors is poorly understood. Recently, we provided evidence that autoreactive antibody against histone H1 is a major immunosuppressive factor induced in early post-OLT serum [5, 6]. To gain insight into the mode of immunosuppressive action, we have generated a murine anti-histone H1 mAb 16G9, which can neutralize allogeneic mixed lymphocyte reaction (MLR) [6]. To start clarification of the immunosuppressive mechanisms, here we examined the effect of 16G9 on purified T cells. We found that 16G9 suppressed T cell activation not only triggered upon stimulation with allogeneic dendritic cells (DCs), but also in response to TCR ligation. In addition, we demonstrated that 16G9 specifically reacted with a fraction of T cells, and that these 16G9-positive T cell population was transiently increased upon TCR crosslinking.

2 Materials and Methods

2.1 Animals and Anti-histone H1 mAb, 16G9

BALB/c and C57BL/6 mice (6 weeks of age, female) were purchased from Charles River Japan (Yokohama, Japan). All mice were bred under specific pathogen-free conditions. The MLR-neutralizing anti-histone H1 mAb 16G9 was generated and prepared as described [6].

2.2 Murine Allogeneic MLR

Stimulator $CD11c^+$ DCs were purified from BALB/c splenocytes by magnetic cell sorting (MACS) using CD11c MicroBeads (Miltenyi Biotec, Germany), and inactivated by treatment with mitomycin C (MMC; Kyowa Hakko Kogyo, Tokyo, Japan). Responder T cells were purified from C57BL/6 splenocytes also by MACS using Pan T Cell Isolation Kit (Miltenyi Biotec). DCs (5×10^3 cells/100 μl) and T cells

(5×10^4 cells/100 μl) were mixed in 96-well round-bottom plates (Nunc, USA). Then, 16G9 or mouse IgM isotype control antibody (clone 11E10; eBioscience, USA) was added at serial concentrations (0.78-50 μg/ml). Control culture consisted of C57BL/6 T cells mixed with syngeneic, MMC-treated DCs (C57BL/6 vs. C57BL/6). These cells were cultured in RPMI 1640 medium (Sigma, USA) supplemented with 100 U/ml penicillin, 100 μg/ml streptomycin, 50 μM 2-mercaptoethanol, and 10% fetal calf serum (FCS; BioWest, USA) at 37°C for 84 h. Before cell harvest, cells were pulsed with 110 μM 5-Bromo-2′-deoxy-uridine (BrdU) for 15 h. Proliferation was determined using BrdU Labeling & Detection Kit III (Roche Diagnostics, The Swiss).

2.3 T Cell Proliferation Assay

Purified T cells from C57BL/6 mice (2×10^5 cells/well, suspended in 10% FCS/RPMI 1640 medium) were seeded in 96-well plates (Becton Dickinson, USA) that were pre-coated with anti-mouse CD3ε [2 μg/ml in phosphate buffered saline (PBS), clone 145-2C11; eBioscience], and cultured in the presence of 16G9 (25 μg/ml) or IgM isotype control antibody for 48 h. T cell proliferation was estimated by BrdU incorporation as described above. Viability of T cells was analyzed by trypan blue dye exclusion assay. In addition, supernatant from the 48 h culture was subject to enzyme-linked immunosorbent assay (ELISA) for determination of IL-2 production by using rat anti-mouse IL-2 mAbs (BD Pharmingen, USA) and recombinant mouse IL-2 (R&D Systems, USA) as a standard. We also stimulated purified T cells with 4α-phorbol 12-myristate 13-acetate (PMA, 400 pg/ml, Sigma) and ionomycin (1.0 μM, Sigma), and assessed immunosuppressive effect of 16G9 as described above.

2.4 Flow Cytometry

Purified T cells (2×10^6 cells/each sample) were washed twice with PBS, and resuspended in a staining buffer (PBS supplemented with 0.5% FCS and 0.1% sodium azide). To block Fc receptor-mediated non-specific binding, we added anti-mouse CD16/32-blocks Fc (clone 93; eBiosciece, 0.5 μg/2×10^6 cells), and incubated for 20 min on ice, followed by further incubation with biotinylated 16G9 or IgM isotype control for 30 min. The samples were washed twice and stained with 0.5 μg/ml of streptavidin-conjugated phycoerythrin (BD Biosciences) for 30 min on ice. After washing twice, each sample was resuspended in 1 ml of staining buffer and analyzed using FACSCalibur flow cytometer (BD Biosciences) with CellQuest software. For competitive inhibition, biotinylated primary antibodies were preincubated with 10 μg/ml of histone H1 or ovalbumin. To analyze 16G9-positive T cell populations, cell samples were co-stained with fluorescein isothiocyanate-conjugated anti-mouse CD8α or anti-CD4 mAbs (BD Biosciences).

2.5 Statistical Analysis

Statistical analysis was performed by Student's t-test. A p-value of <0.05 was considered to have a significant difference.

3 Results and Discussion

3.1 Anti-histone H1 mAb 16G9 Suppresses T Cell Activation upon Stimulation with Allogeneic DCs

We showed that 16G9 mAb can block allogeneic MLR using murine whole splenocytes [6]. To start clarifying the MLR-inhibitory mechanisms, we first examined whether 16G9 can also block MLR in a more defined culture system. To this end, we set up a MLR culture consisting of purified $CD11c^+$ DCs (from BALB/c splenocytes) and purified splenic T cells from C57BL/6 mice. 16G9 significantly inhibited this MLR in a dose-dependent manner (data not shown). The MLR-inhibitory potency was comparable to that obtained by stimulation with immunosuppressant FK506 (10 nM). This suggests that 16G9 acts on T cells and/or DCs to exert its immunosuppressive effect.

3.2 16G9 mAb Suppresses T Cell Activation and IL-2 Production in Response to TCR Ligation

We next tested whether 16G9 can block activation of purified T cells in response to TCR ligation. As shown in Table 1, addition of 16G9 significantly inhibited anti-CD3-triggered T cell proliferation as compared to that of isotype control. We also found that 16G9 suppresses IL-2 secretion from these T cells during the

Table 1 Anti-histone H1 mAb 16G9 suppresses T cell activation in response to TCR ligation

Stimulation	Additive	BrdU Incorporation (Mean A405 nm ± SD)
–	–	0.216 ± 0.033
Anti-CD3	–	0.758 ± 0.094
	Isotype control	0.658 ± 0.146
	16G9	0.174 ± 0.018[a]
	FK506 (10 nM)	0.172 ± 0.022

16G9 mAb or isotype control was supplemented at 25 μg/ml.
[a] Significantly inhibited as compared with isotype control (p< 0.05).

Table 2 16G9 mAb suppresses T cell activation upon stimulation with PMA and ionomycin

Stimulation	Additive	BrdU Incorporation (Mean A405 nm ± SD)
–	–	0.143 ± 0.001
PMA/ionomycin	–	0.593 ± 0.049
	Isotype control	0.483 ± 0.027
	16G9	0.180 ± 0.013[a]
	FK506 (10 nM)	0.196 ± 0.005

16G9 mAb or isotype control was supplemented at 25 μg/ml.
[a]Significantly inhibited as compared with isotype control ($p< 0.05$).

culture period between 24 and 48 h (data not shown). Trypan blue dye exclusion assay indicated that viability of 16G9-stimulated T cells at 48 h culture was comparable to that of isotype control (data not shown), suggesting that immunosuppressive action of 16G9 mAb was not attributable to the induction of apoptosis. 16G9 also suppressed T cell activation upon stimulation with PMA and ionomycin which bypassed TCR ligation (Table 2), implicating that 16G9 does not affect TCR-membrane proximal signaling event, but rather acts on downstream TCR signaling pathway to exert immunosuppressive activity. Taken together, these results indicate that 16G9 can directly act on purified T cells to exert its immunosuppressive activity.

3.3 Specific Binding of Anti-histone H1 mAb 16G9 to Purified T Cells

Previously, we demonstrated that 16G9 specifically reacted with a part of murine splenocytes including T cells, B cells, and $CD11b^+$ monocytes/macrophages [6]. Here we focused on T cells, and verified that 16G9 bound to a fraction of purified splenic T cells (data not shown). The immunoreactivity was competitively inhibited by exogenous addition of histone H1, suggesting the existence of histone H1-like cross-reactive antigens on the surface of T cells. To further dissect 16G9-positive subsets, we stained purified T cells with 16G9 and anti-CD4 or CD8 mAbs. Flow cytometric analysis revealed that about 12.0% or 8.6% of $CD4^+$ or $CD8^+$ T cells are co-stained with 16G9, respectively. This indicates that both $CD4^+$ and $CD8^+$ T cell subsets are partially reactive with the mAb. Intriguingly, anti-CD3-treated $16G9^+$ $CD4^+$ T cell number was transiently increased (up to about 45%), suggesting that 16G9 might also react with activated $CD4^+$ T cells *via* inducible cell surface antigens.

Acknowledgments This work was supported by a grant of Research for Promoting Technological Seeds, which was conducted by Japan Science and Technology Agency. S. K. was also supported by the Uehara Memorial Foundation.

References

1. Oka T. et al. (1996) Immunosuppression in organ transplantation. *Jpn. J. Pharmacol. 71*, 89–100.
2. Platz K. P. et al. (1994) Nephrotoxicity following orthotopic liver transplantation: A comparison between cyclosporine and FK506. *Transplantation 58*, 170–178.
3. Kamada N. et al. (1983) Liver transplantation in the rat. Biochemical and histological evidence of complete tolerance induction in non-rejector strains. *Transplantation 35*, 304–311.
4. Kobayashi S. et al. (1998) Analysis of immunosuppressive proteins in serum of liver-transplanted rats by using an anti-LSF-1 column. *J. Surg. Res. 80*, 58–61.
5. Nakano T. et al. (2004) Liver transplantation-induced antihistone H1 autoantibodies suppress mixed lymphocyte reaction. *Transplantation 77*, 1595–1603.
6. Katayama A. et al. (2009) Anti-histone H1 autoantibody: an inducible immunosuppressive factor in liver transplantation. *Animal Cell Technol.: Basic Appl. Aspects 15*, in press (in this issue).

The Effect of Culture Conditions on Liver Function and Proliferation of Hepatic Cells for Bio-Artificial Liver

Yumi Narita, Kozue Kaito, Takeshi Omasa, and Satoshi Terada

Abstract Bio-artificial liver (BAL) is an effective treatment for serious liver disease. It is thought that a mass of hepatic cells corresponding to 30% of the liver are needed for BALs, and a small size of reactor, at most a few liters in volume, is desired for use at the hospital bedside. Therefore, high-density culture, $\geq 1 \times 10^7$ cells/cm^3, should be employed. However, sufficient oxygen and nutrients are not supplied to all cells in the reactor, resulting in apoptosis and serious impairment to BAL performance. In order to solve these problems, we have previously introduced anti-apoptosis gene *bcl-2* into HepG2 cells, establishing an anti-apoptosis cell line, Hep-Bcl2. The Hep-Bcl2 cell line survived under low oxygen conditions, and had twice the level of albumin productivity than do HepG2 cells. In this study, the Hep-Bcl2 cell line was cultured under high-density conditions, with a change of culture medium twice daily to mimic the circulation. In this way, Hep-Bcl2 successfully maintained a high population for at least 14 days, and the albumin productivity of Hep-Bcl2 was significantly higher than that of HepG2 cells.

Keywords *bcl-2* • bio-artificial liver • HepG2, Hep-Bcl2 • high-density culture

1 Introduction

Due to the shortage of liver donors, development of bio-artificial liver (BAL) is expected to be an alternative to liver transplantation, effective against serious liver disease. Although a variety of BAL devices are being developed, their period of operation is not sufficiently long to support the patients until they recover from their liver disease [1]. Suitable cell lines contribute to the improvement of BALs,

Y. Narita, K. Kaito, and S. Terada
Department of Applied Chemistry and Biotechnology, University of Fukui

T. Omasa
Department of Biotechnology, Graduate School of Engineering, Osaka University

K. Ikura et al. (eds.), *Animal Cell Technology: Basic & Applied Aspects*,
Animal Cell Technology: Basic & Applied Aspects 15,
DOI 10.1007/978-1-4020-9646-4_24,

as well as does the development of BAL reactors. We focused on the former approach, and generated anti-apoptotic hepatic cell lines. HepG2 cells were transduced with the anti-apoptotic gene *bcl-2*, and named Hep-Bcl2 cells. Hep-Bcl2 cells successfully survive under adverse conditions such as hypoxia, and produce more albumin than do HepG2 cells [2].

The number of hepatic cells required by BALs is ~30% of the liver (5×10^{10} cells). The size of culture vessels used in hospital should be limited to a few liters. Therefore, high-density culture, $\geq 1 \times 10^7$ cells/cm^3, must be achieved. Moreover, in high-density culture, there are serious concerns with problems such as lower liver specific functions. To solve these problems, a continuous supply of oxygen and nutrients is needed. Various methods for supplying sufficient oxygen to hepatic cells in BALs have been employed, including perfusion culture and culture carriers [3]. In this study, we tried high-density culture of Hep-Bcl2 cells with frequent medium change twice daily.

2 Materials and Methods

2.1 Cell Lines and Culture Conditions

The human hepatoma cell lines HepG2 and Hep-Bcl2 were used. Hep-bcl2 was established by transfection of HepG2 with the vector BCMG-bcl-2-neo. The medium was Dulbecco's modified Eagle medium containing 0.2% sodium bicarbonate, 10 mM HEPES, 2 mM L-glutamine, 0.06 mg/ml kanamycin, and 10% fetal bovine serum. The cells were grown in 35 mm culture dishes (Sumitomo Bakelite, Japan) at 37°C in 5% CO_2.

2.2 Seeding and Medium Change

HepG2 and Hep-Bcl2 cells were seeded in 35 mm dishes at 2×10^6 and 4×10^6 cells/2 ml medium. One milliliter of spent medium was replaced with the same volume of fresh medium twice daily, and the removed supernatants were stored at −30°C for analysis of albumin productivity.

2.3 Morphology

Morphology of HepG2 and Hep-Bcl2 was observed under phase-contrast microscopy (Olympus, Japan).

2.4 Cell Proliferation

Cell proliferation was assessed by the trypan blue exclusion method. The number of cells was determined by counting under a microscope with a hemacytometer every other day.

2.5 Albumin Productivity

The albumin concentration in the culture supernatant was assessed by ELISA. First, the 96-well plate (BD Falcon, USA) was coated with goat anti-human albumin polyclonal antibody (ICN Biomedicals, USA), and blocked with 5% skimmed milk (NAKALAI TESQUE, Japan). After wells were rinsed, the standard wells were incubated with purified human serum albumin (Sigma, USA) and the remaining wells were incubated with supernatant samples. Finally, the wells were incubated with peroxidase-conjugated sheep anti-human albumin antibody (The Binding Site, UK) and citric acid buffer containing *o*-phenylenediamine. The absorbance was measured at 490 and 630 nm.

3 Results and Discussion

3.1 Morphology

Hepatocytes began to form aggregates at day 2. The cell aggregates grew daily and spread around the dish. After day 10, the growth of the aggregates appeared to stop, and the cells began to detach. Hep-Bcl2 cells formed more aggregates than did HepG2 cells, and Hep-Bcl2 cells peeled off the dishes more readily than did HepG2 cells (Fig. 1).

3.2 Cell Proliferation

To compare proliferation at different initial cell density, hepatocytes were seeded at different densities and cultured. In cultures seeded at 2×10^6 and at 4×10^6 cells/dish, the required cell number of $>1 \times 10^7$ cells/dish was achieved at day 10. After day 10, the viable cell density was stable until the culture termination at day 14 (Fig. 2).

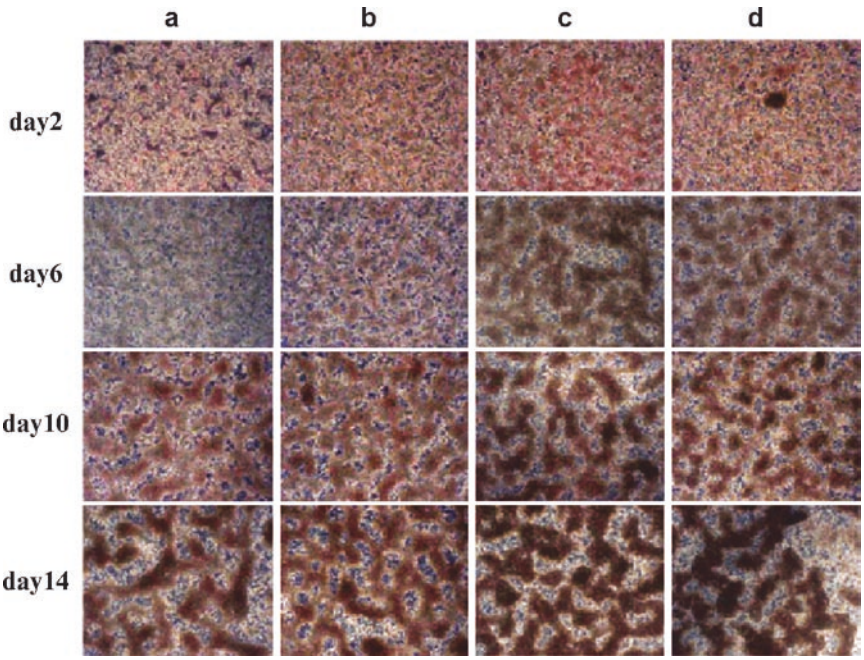

Fig. 1 Morphological study. (**a**) HepG2 (seeded at 2×10^6 cells), (**b**) HepG2 (4×10^6), (**c**) Hep-Bcl2 (2×10^6), and (**d**) Hep-Bcl2 (4×10^6)

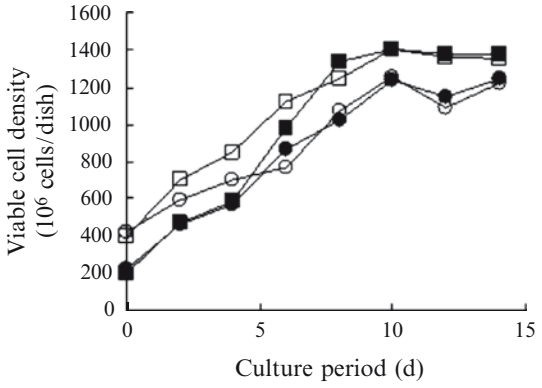

Fig. 2 Time course of viable cell density in high-density culture. Closed circles, HepG2 (seeded at 2×10^6 cells); open circles, HepG2 (4×10^6); closed squares, Hep-Bcl2 (2×10^6); and open squares, Hep-Bcl2 (4×10^6)

3.3 Albumin Productivity

To estimate the liver specific function of hepatocytes, albumin concentration in the supernatants was determined. Hepatocytes continuously secreted albumin during culture. Albumin productivity of Hep-Bcl2 cells was twice as high as that of HepG2 cells. This result suggests that Hep-Bcl2 cells had high liver function (Fig. 3).

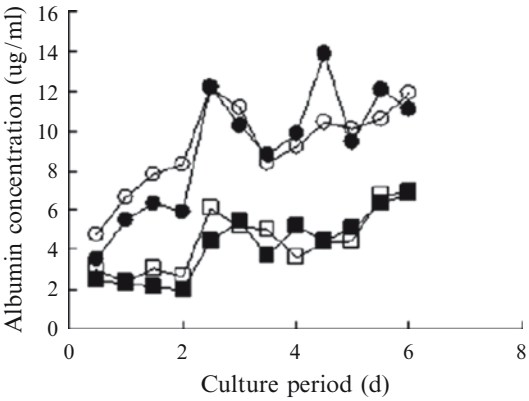

Fig. 3 Time course of albumin productivity in high-density culture. Closed squares, HepG2 (seeded at 2×10^6 cells); open squares, HepG2 (4×10^6); closed circles, Hep-Bcl2 (2×10^6); open circles, Hep-Bcl2 (4×10^6)

References

1. Park, J. K. et al., 2005, Bioartificial liver systems: culture status and future perspective, J. Biosci. Bioeng. **99**: 311–319.
2. Terada, S. et al., 2003, Generation of a novel apoptosis-resistant hepatoma cell line, J. Biosci. Bioeng. **95**: 146–151.
3. Chen, J. P. et al., 2006, High-density culture of hepatocytes in a packed-bed bioreactor using a fibrous scaffold from plant, J. Biochem. Eng. **30**: 192–198.

The Effect of Scaffold on the Morphology and Insulin Secretion of Islet Cells

Takanori Kanayama, Hirofumi Mitsuishi, and Satoshi Terada

Abstract Pancreas islet transplantation is established as a therapeutic option for diabetes. In vitro culture of islets is pivotal, because islet cells often lose their function during culture prior to transplantation. To improve culture and maintain insulin secretion, we focused on the extracellular matrix (ECM). The islet cells were cultured on several ECMs, and we observed their morphology and measured their insulin release in response to changing glucose levels. The cells grown on collagen I and collagen IV were not sharp and had high insulin release, but the cells on non-coat polystyrene and fibronectin were sharp and their insulin release was decreased. These results show that sharpness in cell morphology was related to insulin release, and cells grown on laminin were sharp and showed high level insulin secretion.

Keywords Pancreatic islet • scaffold • collagen • laminin • fibronectin • morphology

1 Introduction

Since the Edmonton protocol for pancreas islet transplantation has been established [1], islet transplantation has been vigorously pursued because it offers patients complete recovery from diabetes, instead of insulin injection. For islet transplantation, in vitro culture of islets is pivotal, because islet cells often lose their function during in vitro culture.

To improve the culture and maintain insulin secretion, we focused on the extracellular matrix (ECM). Under in vivo conditions, islets are surrounded by ECM and interact with it. Bosco and his colleagues have reported that islet β-cells on ECM show a spread morphology and high insulin secretion [2]. By similar but distinct

T. Kanayama, H. Mitsuishi, and S. Terada
Department of Applied Chemistry and Biotechnology, Faculty of Engineering,
University of Fukui, 3-9-1, Bunkyo, Fukui, 910-8507, Japan

K. Ikura et al. (eds.), *Animal Cell Technology: Basic & Applied Aspects*,
Animal Cell Technology: Basic & Applied Aspects 15,
DOI 10.1007/978-1-4020-9646-4_25,

morphological criteria, we classified islet cells on ECMs. Insulin release in response to changing glucose level on the ECMs was also determined, and the relation between morphology and insulin release was studied.

2 Materials and Methods

2.1 Islet Cell Preparation

Rat pancreases were extirpated from male Lewis rats (9 weeks old, 200–250 g weight), and immediately islets were isolated by the conventional collagenase digestion method. Purification was achieved by density gradient separation using Histopaque (Sigma–Aldrich, USA). The purified islets were dispersed with trypsin into individual cells, and the cells were collected by centrifugation, and suspended in culture medium.

2.2 Islet Cell Culture

The culture medium was RPMI 1640 containing 10% FBS, 10 mM HEPES, 0.2% $NaHCO_3$, 2 mM glutamine, and 0.06 mg/ml kanamycin. The culture was performed at 37°C in an atmosphere of 5% CO_2 and 95% air.

2.3 ECM Proteins

Four ECM proteins were purchased from Sigma-Aldrich. Culture dishes (Sumitomo bakelite, Japan) were coated with collagen (CL) I, CL IV, fibronectin (FN) or laminin (LM) at 37°C for 2 h. The dishes were rinsed twice with PBS before seeding with cells.

2.4 Morphological Assay

Morphology of islet cells on the ECMs was assayed as follows. Islet cells were cultured on each ECM component, and photographs were taken of nine areas per dish every day. The cells were classified by their shape into two types: sharp type with sharply defined edges, and non-sharp type with round edges (Fig. 1). These two cell types were counted, and the sharp intensity was calculated by the following equation:

$$\text{Sharp intensity}(\%) = \frac{\text{Sharp type cells}}{\text{Non-sharp type cells} + \text{sharp type cells}} \times 100$$

$$\text{Sharp intensity (\%)} = \frac{\text{Sharp type cells}}{\text{Non-sharp type cells + sharp type cells}} \times 100$$

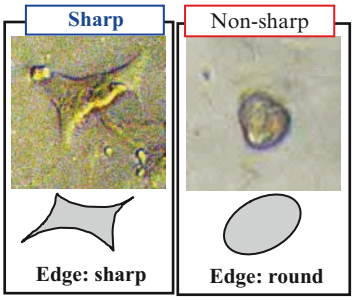

Fig. 1 Islet cells were classified into two types. Cells with sharply defined edges were classified as sharp type, and those with round edges were classified as non-sharp type

2.5 Insulin Secretion in Response to Glucose Level

Glucose stimulation tests were carried out in a glucose-rich (16.7 mM) and a glucose-poor medium (3.3 mM), and insulin release was measured by ELISA using a rat insulin ELISA kit (Sibayagi, Gunma, Japan).

3 Results and Discussion

3.1 Effect of ECM on Morphology

To estimate the morphological characteristics of islet cells grown on ECM, we defined sharp intensity as described above. Figure 2 shows the cell morphology on ECM components. Cells grown on CLs were round, whereas those on the non-coat polystyrene, LM and FN were sharp. Figure 3 shows the sharp intensity on each ECM component. Cells grown on LM had the highest intensity, followed by FN and non-coat polystyrene. Cells grown on CL I and CL IV had lower intensity.

3.2 Effect of ECM on Insulin Release in Response to Glucose Level

To investigate the relationship between morphology and insulin release, glucose stimulation tests were performed. The results are shown in Fig. 4. Stimulation index is the insulin concentration in glucose-rich medium divided by the average

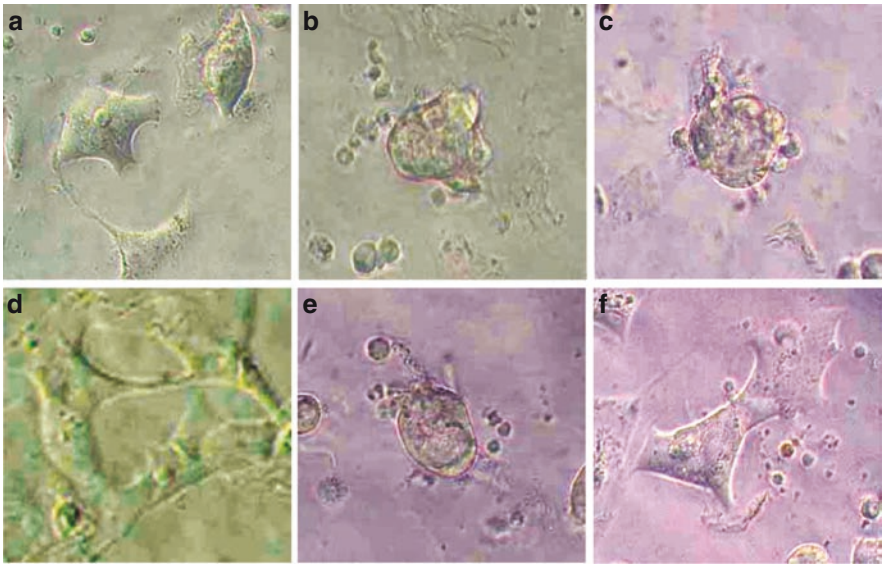

Fig. 2 Morphology of islet cells on ECM components after 2 days culture. Islet cells were cultured on non-coat polystyrene (**a**), 300 μg/ml CL I (**b**), 30 μg/ml CL I (**c**), 30 μg/ml CL IV (**d**), 30 μg/ml LM (**e**), and 30 μg/ml FN (**f**). Magnification ×200

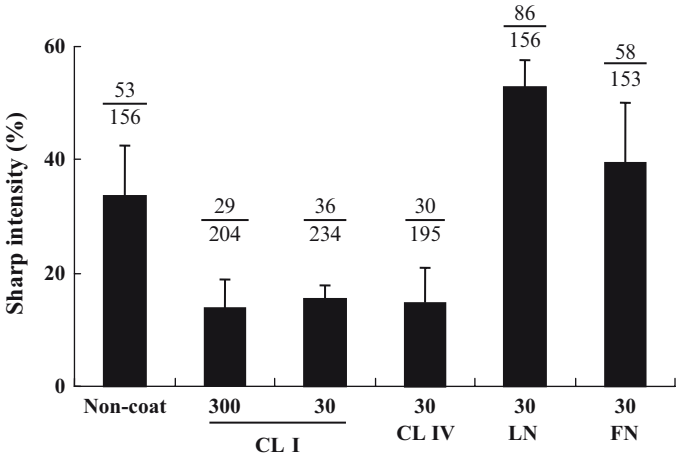

Fig. 3 Sharp intensity of the islet cells cultured on ECM after 2 days culture. Islet cells were seeded at a density of 1.8×10^4 cells per dish, and cultured on non-coat polystyrene, 300 μg/ml CL I, 30 μg/ml CL I, 30 μg/ml CL IV, 30 μg/ml LM, and 30 μg/ml FN

insulin concentration in glucose-poor medium. The cells cultured on CLs and LM showed a high stimulation index, whereas non-coat polystyrene and FN showed a low index.

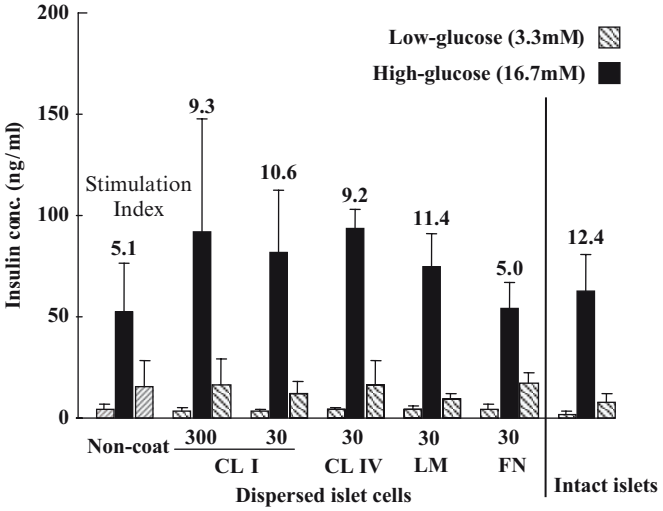

Fig. 4 Insulin secretion in response to glucose level after 3 days culture. Islet cells were seeded at a density of 1.8×10^4 cells per dish, and cultured on non-coat polystyrene, 300 μg/ml CL I, 30 μg/ml CL I, 30 μg/ml CL IV, 30 μg/ml LM, and 30 μg/ml FN. Intact islets shown on the right were cultured for 3 days without dispersion, distinguishing them from dispersed islet cells

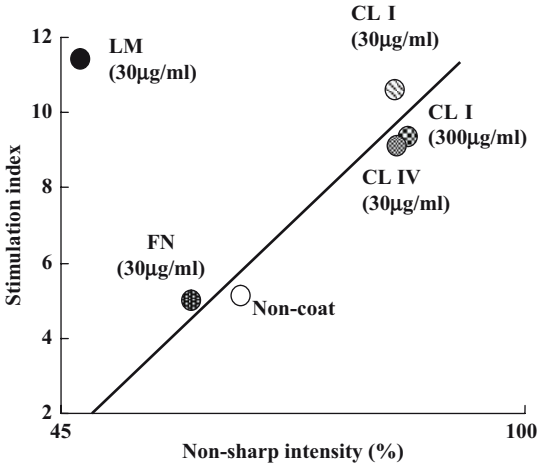

Fig. 5 Relationship between morphology and glucose response. The vertical axis represents glucose stimulation shown in Fig. 4. The horizontal axis represents non-sharp intensity, the reverse of sharp intensity shown in Fig. 3

Figure 5 shows the relationship between morphology and glucose response. The islet cells cultured on a scaffold have a tendency towards higher insulin release, with a weaker sharp intensity. However, on LM, islet cells were sharp but showed high insulin release.

References

1. Shapiro AM, Lakey JR, Ryan EA, Korbutt GS, Toth E, Wornock GL, Kneteman NM, Rajotte RV:Islet transplantation in seven patients with type 1 diabetes mellitus using a glucocorticoid-free immunosuppressive regimen. *N Engl J Med* 343:230–238, 2000
2. Bosco D, Meda P, Halban PA, Rouiller DG:Importance of cell-matrix interactions in rat islet β-cell secretion in vitro: role of α6β1 integrin. *Diabetes* 49:233–243, 2000

Sterilization of Chicken Primordial Germ Cells

Makoto Motono, Hiroyuki Komatsu, Yoshinori Kawabe, Ken-Ichi Nishijima, and Shinji Iijima

Abstract It is important to introduce exogenous genes into germ cells for making transgenic bird efficiently. Primordial germ cells (PGCs) are the progenitor cells for the gametes. If PGCs that have been transfected in vitro are efficiently migrated into the gonads of recipient birds, transgenic progeny can be easily obtained. This is enhanced by depletion of recipient PGCs prior to the transfer of transfected PGCs. By now several methods have been reported to deplete endogenous PGCs, though efficiency of each methods is not directly compared. Avian PGCs are located in the central region of area pellucida in the blastodermal stage of embryo and sensitive to irradiation of X ray or ultraviolet (UV). We have compared methods using UV, γ irradiation, and removal of cells from the center of area pellucida to reduce the number of PGCs in chicken embryos. By careful depletion of the cells of area pellucida, we have obtained a high depletion efficiency of PGCs with relatively low damage to embryos.

Keywords Chicken • primordial germ cell (PGC) • sterilization

1 Introduction

Production of transgenic chickens has a great value in the field of animal biotechnology, which leads to the efficient production of bioactive materials for human pharmaceuticals into eggs [1, 2]. Recently, technology to make transgenic avian species has been greatly improved [3–5]. We reported that injecting retroviral vectors into the heart of developing embryo enabled to make transgenic avian that produced high level of target proteins [5]. Although we confirmed that transgene was successfully transmitted to the progeny with efficiency of approximately 3%, this value is practically low.

M. Motono, H. Komatsu, Y. Kawabe, K.-I. Nishijima, and S. Iijima
Department of Biotechnology, Nagoya University, Furo-cho, Chikusa-ku, Nagoya, 464-8603, Japan

K. Ikura et al. (eds.), *Animal Cell Technology: Basic & Applied Aspects*,
Animal Cell Technology: Basic & Applied Aspects 15,
DOI 10.1007/978-1-4020-9646-4_26,

Primordial germ cells (PGCs) are the precursors of sperm and egg. In avian species, PGCs can be isolated from bloodstream in a specific developmental stage, which allows transfer to other recipient embryos. In 1990s, a number of attempts have been made to produce germline chimeras, which successfully produced donor-derived offsprings in chicken [6–8]. This suggests that PGC can serve as a vehicle for introducing exogenous genes to produce transgenic birds if the genes are stably integrated into the genome. To produce transgenic birds by this method, it is critical to effectively incorporate donor PGCs into the gonadal tissues of recipient embryos. Several methods have been used to remove endogenous PGCs in recipient embryo, sterilization, prior to the transfer, which caused a higher rate of donor-derived gametes [9–11]. These include the radiation of ultraviolet (UV) [9], γ irradiation [10] and removal of cells from the region that contained PGCs at the stage [11]. Effectiveness of sterilization was ranged from 1% to 70%, which largely depends on each experimental conditions and relative effectiveness of these methods has not been directly compared so far.

In this study, we compared the effectiveness of several methods such as ultraviolet, γ irradiation and removal of the center of area pellucida to reduce endogenous PGCs in chicken. Among them, removal of the center of area pellucida is the best way to reduce endogenous PGCs, however survival of the embryo was better with UV irradiation.

2 Materials and Methods

2.1 Sterilization by UV

The fertilized eggs (White Leghorn) were obtained from Chubukagakushizai and preserved at 12°C until use. The embryos used were stage X blastoderm [12] of either freshly laid or unincubated eggs. Before the sterilization, eggshells were cut horizontally with a diamond cutter to make an opening of 35 mm in a diameter at the sharp end. Ultraviolet lamp (15W) was put at 15 cm from the cutting surface and eggs were irradiated for 5–7 s. Immediately after the sterilizations, the opening was sealed with a polytetrafluoroethylene membrane (Milliwrap; Nihon Millipore, Tokyo, Japan) and plastic film (Saran Wrap; Asahi Kasei Kogyo, Tokyo, Japan) using thin albumen as glue [13].

2.2 Sterilization by γ Ray Using ^{60}Co

Freshly laid, unincubated eggs were exposed to approximately 500–700 rad of γ ray from a ^{60}Co source.

2.3 Sterilization by Removal of Cells from the Center of Area Pellucida

Before the sterilization, eggshells were cut horizontally as was mentioned in UV irradiation. A sharp needle (27G, Terumo) attached to a micropipetter was pushed through the yolk mass to reach the subgerminal cavity of the blastoderm. Then, a cell cluster was aspirated from the center of area pellucida. Immediately after the sterilizations, the opening of the eggshell was sealed as was mentioned in UV irradiation.

2.4 Culture of Manipulated Embryos and Count of PGCs

The sterilized eggs were incubated at 39°C under a relative humidity of 65% with rocking through an angle of 90° with 15-min intervals until the stage13–16 based on the staging by Humberger and Hamilton [14]. The blood from the embryos was collected with fine needle and number of PGCs were determined under the microscope according to the shape and size of cells since PGCs are bigger in size comparing to erythrocytes (Fig. 1).

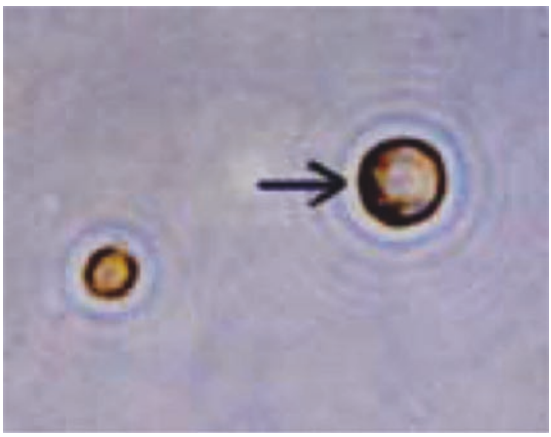

Fig. 1 The morphology of PGC. The size of PGC is larger than that of blood cell thus PGC can be distinguished from blood cell under microscopy. Arrow: PGC

3 Results and Discussion

3.1 Viability of Embryos

Blastodermal stage of chicken egg consists of approximately 60,000 cells [1] and some cells are already committed to differentiate into germ cells. PGCs in this stage exist in the center of area pellucida: depletion of about 1,000 cells from this area significantly reduced the number of PGCs in blood and in gonad at later stages [11]. Germline cells are sensitive to UV or γ irradiation compared with somatic cells, therefore, these methods of irradiation have been used to 'sterile' chicken embryos [8, 9]. The viabilities of sterilized embryos after 2 days were 83.3% (n = 28), 73.3% (n = 12) and 82.3% (n = 21) in UV and γ irradiation, and removal of cells from the center of area pellucida, respectively (Fig. 2). Viable embryos often had abnormalities in the developing allantoic membrane while its shape was circular in non-treated embryos. Furthermore, the development of embryos sterilized by γ irradiation was delayed approximately 12 h, while this was not obvious with the other methods.

3.2 Reduction of the Number of Circulating PGCs in Sterilized Eggs

The number of circulating PGCs per 1μl of blood was counted. The reduction of PGCs are 38.0%, 26.6% and 55.6% in UV irradiation, γ irradiation and removal of cells from the center of area pellucida, respectively (Fig. 3). These results indicated that removal of cells from the center of area pellucida reduces the number of PGCs with a higher percentage compared with other two methods with high viability of treated embryos.

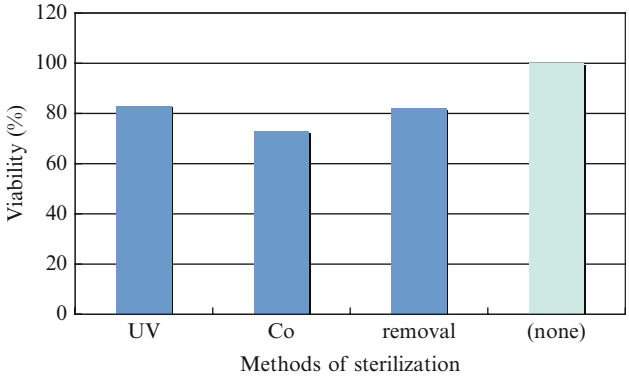

Fig. 2 Viability of embryos. The sterilized embyos were incubated until stages 13–16 (53–56 h), and the number of living embryos was counted

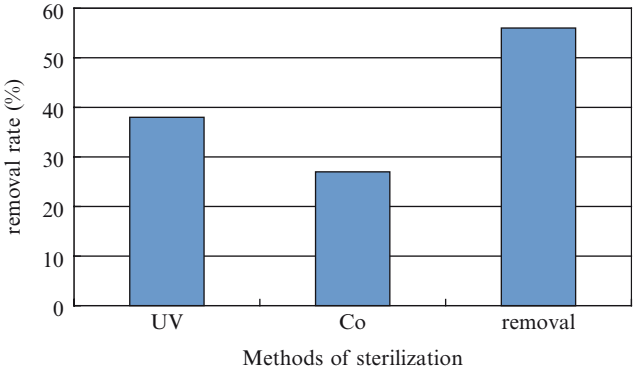

Fig. 3 Reduction of the number of PGC in blood. The sterilized embryos were incubated until stages 13–16, and their blood samples were collected. The number of PGCs was counted under microscopy

Although removal of cells from the center of area pellucida is technically difficult, this method gave better results for sterilization and may contribute to enhancement of the frequency of donor-derived gametes in PGC transfer studies. We are now trying to make transgenic chicken by transferring PGCs that have been infected in vitro with retroviral vector.

Acknowledgments This work was supported in part by the Program for Promotion of Basic Research Activities for Innovative Biosciences (PROBRAIN).

References

1. H. Sang, Transgenic chickens - methods and potential applications, *TIBTECH* **12,** 415–420 (1994).
2. S. G. Lilico, M. J. McGrew, A. Sherman et al., Transgenic chickens as bioreactors for protein-based drugs, *Drug Discov. Today* **10,** 191–196 (2005).
3. H. Sang, Prospects for transgenesis in the chick, *Mech Dev.* **121,** 1179–1186 (2004).
4. J. Petitte, G. Liu, and Z. Yang, Avian pluripotent stem cells, *Mech. Dev.* **121,** 1159–1168 (2004).
5. M. Kamihira, K. Ono, K. Esaka et al., High-level expression of single-chain Fv–Fc fusion protein in serum and egg white of genetically manipulated chickens by using a retroviral vector, *J. Virol.* **79,** 10864–10874 (2005).
6. L. Vick, Y. Li, and K. Simkiss, Transgenic birds from transformed primordial germ cells, *Proc. Biol. Sci.* **251,** 179–182 (1993).
7. M. Naito, A. Tajima, and Y. Yasuda et al., Production of germline chimeric chickens, with high transmission rate of donor-derived gametes, produced by transfer of primordial germ cells, *Mol. Reprod. Dev.* **39,** 153–161 (1994).
8. I. Chang, D. Jeong, Y. Hong et al., Production of germline chimeric chickens by transfer of cultured primordial germ cells, *Cell Biol. Int.* **21,** 495–499 (1997).
9. V. Aige-gil and K. Simkiss, Sterilising embryos for transgenic chimaeras, *Br. Poult. Sci.* **32,** 427–438 (1991).

10. R. Carsience, M. Clark, A. Gibbins et al., Germline chimeric chickens from dispersed donor blastodermal cells and compromised recipient embryos, *Development* **117,** 669–675 (1993).
11. H. Kagami, T. Tagami, Y. Matsubara et al., The developmental origin of primordial germ cells and the transmission of the donor-derived gametes in mixed-sex germline chimeras to the offspring in the chicken, *Mol. Reprod. Dev.* **48,** 501–510 (1997).
12. H. Eyal-Giladi and S. Kochav, From cleavage to primitive streak formation: a complementary normal table and a new look at the first stage of the development of the chicken I. General Morphology, *Dev. Biol.* **49,** 321–337 (1976).
13. M. Kamihira, S. Oguchi, A. Tachibana et al., Improved hatching for in vitro quail embryo culture using surrogate eggshell and artificial vessel, *Dev.. Growth Differ.* **40,** 449–455 (1998).
14. V. Hamburger and H. Hamilton, A series of normal stages in the development of the chick embryo, *J. Morphol.* **88,** 49–92 (1951).

Protein Expression by Human Intestinal Epithelial Cells in Response to Wastewater Constituents

Hiroko Isoda, Junkyu Han, Terence P.N. Talorete, Hiroki Narita, Mikako Takenaka, and Naoyuki Funamizu

Abstract The effects of wastewater constituents, nonylphenol and lipopolysaccharide (LPS) on the intestinal epithelial Caco-2 cells, a human intestinal epithelial cell line derived from a human colon carcinoma, were evaluated. Results of proteomics analysis showed that galectin-3, a galactose-specific lectin, glutathione S-transferase A2 subunit and peroxiredoxin-1 were overexpressed by nonylphenol-treated cells while Hsp90b was overexpressed by LPS-treated cells. From the results of proteomics analysis of human intestinal Caco-2 cells treated with wastewater constituents, we found that the overexpression of specific proteins can be used as biomarkers for the risk assessment of water and wastewater.

Keywords Proteomics • Caco-2 cells • nonylphenol • lipopolysaccharide • biomarkers

1 Introduction

In this study, the effects of wastewater constituents on intestinal epithelial Caco-2 cells, a human intestinal epithelial cell line derived from a human colon carcinoma, was evaluated.

Since the cells lining the alimentary tract serve as the first line of defense against xenobiotics that enter the body orally, the impact of these compounds on these cells should be determined. The human intestinal epithelial cell line Caco-2 is considered a model intestinal epithelium [1], and because Caco-2 cells can be cultured on

H. Isoda, J. Han, and T.P.N. Talorete
Graduate School of Life and Environmental Sciences, University of Tsukuba, 1-1-1, Tennodai, Tsukuba, 305-8572, Japan

H. Narita, M. Takenaka, and N. Funamizu
Department of Environmental Engineering, Graduate School of Engineering, Hokkaido University, Kita-13, Nishi-8, Kita-ku, Sapporo, 060-8628, Japan

K. Ikura et al. (eds.), *Animal Cell Technology: Basic & Applied Aspects*,
Animal Cell Technology: Basic & Applied Aspects 15,
DOI 10.1007/978-1-4020-9646-4_27, © Springer Science+Business Media B.V. 2009

microporous filters and can establish monolayers, the measurement of changes in the paracellular ion flux linked to tight-junction disruption can be carried out [2]. As a target cell type, the intestinal epithelium is a good subject for determining protein expression profiles by proteomics analysis.

Nonylphenol was used because it is a typical component of detergent. LPS, which has the potential to be the main toxic component of the effluent, was used because it is a component of activated sludge bacteria [3].

2 Materials and Methods

2.1 Cell Culture

The human colon adenocarcinoma cell line Caco-2 was kindly provided by Dr. Makoto Shimizu of the University of Tokyo, Japan. The cells were cultured in Dulbecco's modified Eagle's medium (DMEM; Sigma) supplemented with 10% fetal calf serum (FCS), 1% nonessential amino acids (NEAA), 4 mM L-glutamine in a 95% air and 5% CO_2 atmosphere at 37°C. The cells were subcultured at a split ratio of 3 to 8 every 3 days. Only reagent-grade or cell-culture-grade reagents were used in this study.

2.2 Cell Treatment Conditions

For nonylphenol experiments, Caco-2 cells were plated onto Petri plates at 1×10^6 cells per plate and then allowed to attach for 24 h. Nonylphenol was then added to the cells to obtain a final concentration of 1 or 10 μM. The cells were incubated for 6 days, after which, the total proteins were extracted.

In another experiment, lipopolysaccharide (LPS) from *E. coli* O111:B4 (Wako, Japan) was dissolved in 10% methanol, diluted with ultrapure water and then added to 10 ml of cell suspension (1×10^6 cells) in a petri dish. LPS was added to the cells at a final concentration of 220 μg/ml followed by incubation for 1, 2 and 3 h. LPS was also added to the cells at final concentrations of 2.2 and 22 μg/ml followed by 3 h of incubation. The LPS concentrations used in this study were based on the critical micelle concentration of LPS, which is 22 μg/ml; 2.2 and 220 μg/ml are one order of magnitude lower and higher, respectively, than the CMC.

2.3 Proteomics

After incubation, the proteins were extracted by cell lysis in 4% (v/v) 3-[(3-cholamidopropyl)dimethylammonio]-1-propanesulfonate (CHAPS), 7 M urea, 2 M thiourea, 25 mM spermine base (Sigma), 1 M ethylenediaminetetraacetic acid (EDTA), 1 mM dithiothreitol (DTT), and 5 mM 4-(2-aminoethyl) benzene-sulfonylflouride (AEBSF), followed by centrifugation at 100,000 g for 1 h at 15°C.

Protein samples from the treated or nontreated cells were quantified using the 2D Quant Kit (Amersham Biosciences, Uppsala, Sweden) and resuspended at 1 µg/µl in 350 µl of 8 M urea, 2% (w/v) CHAPS, 0.5% (v/v) immobilized pH gradient (IPG) buffer (pH 3–10) (Amersham Biosciences, Uppsala, Sweden), and 10 mM DTT. Solubilized proteins were electrophoresed in the first dimension following the Amersham protocol using a flatbed electrophoresis system (Multiphor II, Amersham Biosciences, Uppsala, Sweden) and 18-cm IPG dry strips (Amersham Biosciences, Uppsala, Sweden) with a pH 3-10 linear range. After isoelectric focusing, the IPG strips were re-equilibrated for 20 min in 2% (w/v) sodium dodecyl sulfate (SDS), 6 M urea, 30% (v/v) glycerol, 0.05 M Tris–HCl (pH 8.8), and 2% (w/v) DTT, and for 20 min in 2% (w/v) SDS, 6 M urea, 30% (v/v) glycerol, 0.05 M Tris-HCl (pH 8.8), and 5% (w/v) iodoacetamide. The strip was placed on a gradient SDS-PAGE gel (12–14% (w/v) polyacrylamide) and run at 1,000 V, 20 mA for 45 min and at 1,000 V, 40 mA for 160 min. The proteins were visualized by Coomassie Brilliant Blue (CBB) staining (using PhastGel Blue R-350, Amersham Biosciences, Uppsala, Sweden) for spot analysis and the gel was analyzed using ImageMaster 2D Elite (Amersham Biosciences, Uppsala, Sweden).

2.4 Mass Spectrometry

The protein spot of interest was excised from the gel, washed and digested in-gel with trypsin (sequencing grade, Boehringer Mannheim, Germany). All matrix-assisted laser desorption/ionization time-of-flight (MALDI-TOF) mass spectra were acquired using a Voyager-DE STR mass spectrometer (Applied Biosystems). The matrix solution was prepared by dissolving 10 mg of α-cyano-4-hydroxycinnamic acid (Sigma, USA) in 1 ml of 50% acetonitrile and 0.1% trifluoroacetic acid in deionized water. The obtained peptide sequence tags were used to identify the protein of interest by searching databases using BLAST (http://www.ncbi.nlm.nih.gov:80/blast) or the Prospector software MS-Tag (http://prospector.ucsf.edu/).

3 Results and Discussion

Galectin-3 is associated with the decrease in cell apoptosis and cell death [4, 5]. Glutathione S-transferase A2 subunit is related to protection against oxidative damage [6, 9]. Peroxiredoxin-1 is associated with cellular defense against oxidative

Table 1 Overexpressed proteins as determined by proteomics analysis

Spot No.	Treatment	Protein	M.W. (kDa)	pI	Spot Density (Untreated)	Spot Density (Treated)
1	Nonylphenol (1 μM)	Galectin-3 (galactose-specific lectin)	33	8.5	4	17
2	Nonylphenol (1 μM)	Glutathione S-transferase A2 subunit	26.8	8.8	6	29
3	Nonylphenol (1 μM)	Peroxiredoxin-1	23	7.5	7	41
4	LPS (220 μg/ml)	Hsp90b	90	4.5	0	23

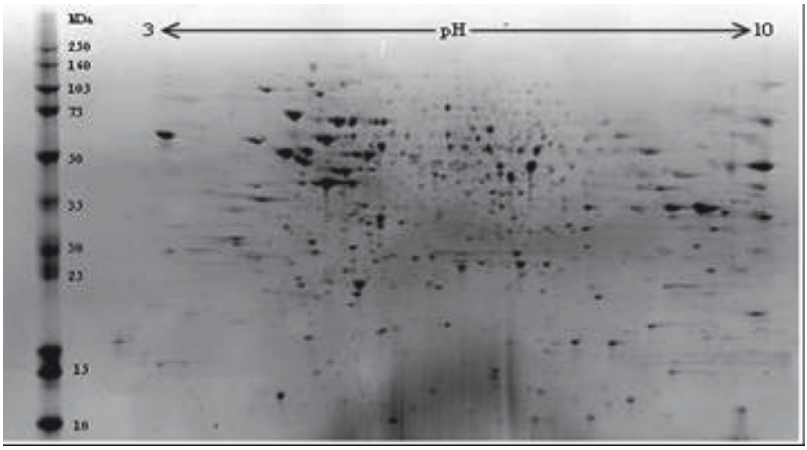

Fig. 1 Typical two-dimensional protein profile of Caco-2 cells (untreated) (Coomassie brilliant blue staining)

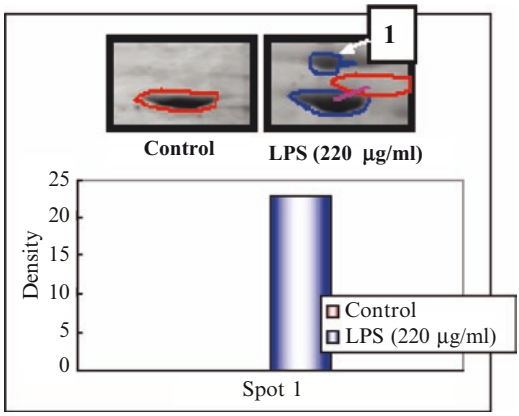

Fig. 2 Spot intensity of spot 1

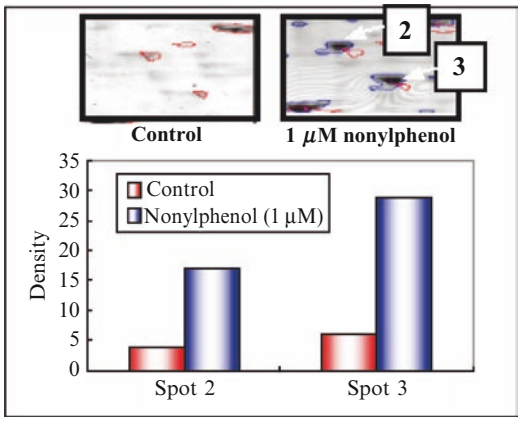

Fig. 3 Spot intensities of spots 2 and 3

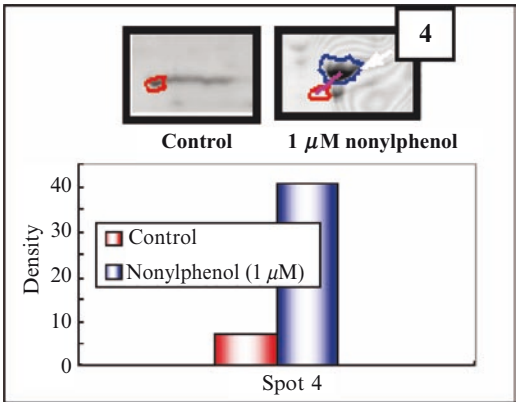

Fig. 4 Spot intensity of spot 4

stress [7, 10]. The expressions of these proteins are considered to be in response to nonylphenol-induced stresses (Table 1).

On the other hand, Hsp90b expression is related to endotoxin activities [8]. Heat shock proteins such as Hsp90 are expressed by various cells, including human cells, when they are stressed by chemicals, toxins or heat [11]. It is considered that stress proteins participate in protective adaptation and help repair damage to the cellular machinery. Thus, the authors hypothesize that the Hsp90 expression by the treated Caco-2 cells also represents a protective mechanism against the LPS-induced stress (Figs. 1–4).

References

1. Pinto M., Rabine-Leon S., Appay M.D., Kedinger M., Triadou N., Dussaulx E., Louroix B., Simon-Assmann P. and Haffeb K. (1983) Enterocyte-like differentiation and polarization of the human colon carcinoma cell line Caco-2 in culture. *Biology of the Cell* **47,** 323–330.
2. Artursson P. and Magnusson C. (1990) Epithelial transport of drugs in cell culture. II: Effect of extracellular calcium concentration on the paracellular transport of drugs of different lipophilicities across monolayers of intestinal epithelia (Caco-2) cells. *Journal of Pharmaceutical Sciences* **79,** 595–600.
3. Narita H., Isshiki I., Funamizu N. and Takakuwa T. (2005) Organic matter released from activated sludge bacteria cells during their decay process. *Environmental Technology* **26,** 433–439.
4. Liu F.-T., Patterson R.J. and Wang J.L. (2002) Intracellular functions of galectins. *Biochimica et Biophysica Acta* **1572,** 263–273.
5. Joo H.G., Goedegebuure P.S., Sadanaga N., Nagoshi M., von Bernstorff T.J. and Eberlein T.J. (2001) Expression and function of galectin-3, a beta-galactoside-binding protein in activated T lymphocytes. *Journal of Leukocyte Biology* **69,** 555–564.
6. Vecchini F., Pringault E., Billiar T.R., Geller D.A., Hausel P. and Felley-Bosco E. (1997) Decreased activity of inducible nitric oxide synthase type 2 and modulation of the expression of glutathione S-transferase alpha, bcl-2 and metallothioneins during the differentiation of Caco-2 cells. *Cell Growth and Differentiation* **8,** 261–268.
7. Manevich Y., Sweitzer T., Pak J. H., Feinstein S. I., Muzykantov V. and Fisher A. B. (2002) 1-Cys peroxiredoxin overexpression protects cells against phospholipid peroxidation-mediated membrane damage. *Proceedings of the National Academy of Sciences USA* **99,** 11599–11604.
8. Gao B. and Tsan M.F. (2003) Recombinant human heat shock protein 60 does not induce the release of tumor necrosis factor from murine macrophages. *Journal of Biological Chemistry* **278,** 22523–22529.
9. Isoda H., Talorete T.P.N., Han J. and Nakamura K. (2006) Expressions of galectin-3, glutathione S-transferase A2 and peroxiredoxin-1 by nonylphenol-incubated Caco-2 cells and reduction in transepithelial electrical resistance by nonylphenol. *Toxicology In Vitro* **20,** 63–70
10. Tang R.B., Chen Y.S., Chou H., Lee S.S., Tai H.Y. and Shen H.D. (2005) cDNA cloning and immunologic characterization of a novel EF-1β allergen from penicillium citrinum. *Allergy* **60,** 366–371.
11. Zhang D., Kian T., Lee W., Chiu L., Sethi S. and Koay E. (2005) Proteomic study reveals that proteins involved in metabolic and detoxification pathways are highly expressed in HER-2/neu-positive breast cancer. *Molecular & Cellular Proteomics* **4,** 1686–1696.

In Vitro Cytotoxic Effects of Tin Compounds on Normal Human Astrocytes

Saifuddin Ahmed, Toshie Tsuchiya, and Rumi Sawada

Abstract Astrocyte proliferation is strictly controlled both during development and in the adult nervous system. Stannous chloride ($SnCl_2$) an inorganic tin, stimulated the nervous system when injected into laboratory animals. It also induced extensive DNA damage. In the present study, we investigated the effects of $SnCl_2$ and stannous 2-ethylhexanoate [Sn(Oct)2] at different concentrations on the proliferation and development of normal human astrocytes (NHA). Cells were cultured with $SnCl_2$ or Sn(Oct)2, and the number of viable cells and the presence of neural cell-specific genes were determined to assess their proliferation, gap-junctional intercellular communication (GJIC) function, and development, respectively. Cell proliferation, GJIC function, and the expression of gap junctional proteins were suppressed when NAH were cultured with $SnCl_2$ and Sn(Oct)2. It was reported that the proliferating cells initially express nestin, a gene specific for neural precursor cell which subsequently give rise to neurons, oligodendrocytes, and astrocytes. Here, we examined the expression of neural cell-specific genes using real-time polymerase chain reaction (PCR). Expression of genes specific for neural precursor cells and astrocytes was decreased, while expression of genes specific for neurons and oligodendrocytes was increased with Sn(Oct)2, but all were decreased with $SnCl_2$ compared with the control culture. Our findings suggest that these tin compounds are neurotoxic to astrocytes, resulting in the suppression of the proliferation and development of NHA.

Keywords In vitro • tin compound • normal human astrocytes

1 Introduction

Tin a heavy metal that is extensively used as a stabilizer in plastic industries, an antifoulant in boat paint, an agricultural biocide, and a hospital disinfectant, has long been known as an environmental contaminant. Human has been exposed to

S. Ahmed, T. Tsuchiya, and Rumi Sawada
Division of Medical Devices, National Institute of Health Sciences, 1-18-1, Kamiyoga, Setagaya ku, Tokyo, 158-8501, Japan

K. Ikura et al. (eds.), *Animal Cell Technology: Basic & Applied Aspects*,
Animal Cell Technology: Basic & Applied Aspects 15,
DOI 10.1007/978-1-4020-9646-4_28,

stannous chloride ($SnCl_2$), an inorganic tin, as a food preservative, in some fluoride toothpastes, and as a reducing agent in some radiopharmaceuticals. It can produce stimulation and depression of the central nervous system when injected into laboratory animals [1]. It was also reported to be neurotoxic and can cause behavioral abnormalities in living organisms [2]. Trimethyltin chloride, which is produced by methylation of inorganic tin in the environment, induced necrosis of neurons in rats [3, 4]. $SnCl_2$ can induce extensive DNA damage in treated Chinese hamster ovary (CHO) cells and is potentially genotoxic [5]. Stannous 2-ethylhexanoate [Sn(Oct)2] is used as a catalyst for polymerizing biodegradable polymers. It is also used as a catalyst in the production of culture dishes.

Astrocyte proliferation is strictly controlled during development and in the adult nervous system. Telencephalic neuroepithelial cells contain neural precursors that give rise to the neuronal lineage and the glial lineage, which includes astrocytes and oliogodendrocytes [6, 7]. In all regions of the central nervous system (CNS), astrocytes are comprehensively coupled by gap junctions [8]. Gap-junctional intercellular communication (GJIC) occurs through clusters of intercellular channels that directly connect the cytoplasm of adjacent cells, allowing selective passage of ions and small molecules between coupled cells [9, 10]. Because of the probability of human exposure and the lack of in vitro toxicity reports, we performed these experiments to determine the effects of $SnCl_2$ and Sn(Oct)2 on normal human astrocytes (NHA). This study showed that both inorganic tins cause decreased development and suppression of the proliferation of NHA, and are potentially neurotoxic to astrocytes.

2 Materials and Methods

2.1 Material Preparation

Stock solutions of $SnCl_2$ (Wako Pure Chemical Industries, Ltd., Osaka, Japan) and Sn(Oct)2 (Sigma-Aldrich Co. Ltd., Irvine, CA, USA) were made directly in astrocyte basal medium (ABM) medium (Cambrex Bio Science, Walkersville, MD, USA) supplemented with 5% fetal calf serum (FCS) and recombinant human epidermal growth factor.

2.2 Astrocyte Cell Culture

Normal human astrocytes (Cambrex Bio Science) were maintained in ABM medium supplemented with 5% FCS, and recombinant human epidermal growth factor, and cultured in a humidified atmosphere of 5% CO_2 in 95% air at 37°C.

2.3 MTT Assay for Cell Proliferation

NHA were seeded into 24-well plates for MTT assay at a density of 1×10^4/well in ABM medium supplemented with 5% FCS and recombinant human epidermal growth factor, and cultured in a humidified atmosphere of 5% CO_2 in 95% air at 37°C. After 1 week culture with 1 or 3 μg/ml $SnCl_2$ or 2.5 or 5 μg/ml Sn(Oct)2, the viability of NHA cells was determined by MTT assay. TetraColor ONE (Seikagaku Kogyo, Tokyo, Japan) was used to measure changes in cell numbers. This assay is a nonradioactive alternative to tritium-thymidine incorporation. The system measures the conversion of tetrazolium salt compound to a soluble formazan product by the mitochondria of living cells. The medium was replaced with 300 μl of fresh medium containing 6 μl TetraColor ONE reagent. After 2 h, samples were measured in a microplate reader.

2.4 Scrape-Loading and Dye Transfer (SLDT) Assay

The Scrape-loading and dye transfer (SLDT) technique was performed by the method of El-Fouly et al. [11]. Confluent monolayer cells in 35-mm culture dishes were rinsed with Ca^{2+}, Mg^{2+} phosphate-buffered saline [PBS(+)], and cell dishes were filled with 0.1% Lucifer Yellow (Molecular Probes, Eugene, OR, USA) in PBS(+) solution and immediately scraped with a sharp blade. After incubation for 5 min at 37°C, cells were washed four times with PBS(+), and the extent of the dye transfer was monitored using a fluorescence microscope equipped with a type UFX-DXII CCD camera and a super-high-pressure mercury lamp power supply (Nikon, Tokyo, Japan).

2.5 Expression of Gap Junctional and Neural Cell Marker Genes

For quantitative RT-PCR, NHA were seeded into 12-well plates at a density of 2×10^4 cells/well in ABM medium (Cambrex Bio Science) supplemented with 5% FCS and recombinant human epidermal growth factor, and cultured in a humidified atmosphere of 5% CO_2 in 95% air at 37°C. After 1 week cell culture with 1 or 3 μg/ml $SnCl_2$ or 2.5 or 5 μg/ml Sn(Oct)2, single-stranded cDNA was prepared from 1 μg of total RNA by reverse transcription (RT) using a commercially available First-Strand cDNA kit (Amersham Pharmacia Biotech, Uppsala, Sweden). Aliquots of the cDNA (1/20) were used as templates for PCR analysis using a Lightcycler system (Roche, Mannheim, Germany). PCR amplification was performed in a total volume of 20 μl mixture including 1 μl of RT reaction mixture, 2 μl Light Cycler-Fast Start Reaction Mix SYBR Green 1 (Roche), 0.5 μM each primer, and 3 mM $MgCl_2$. The PCR program consisted of 40 cycles of 8 s at 94°C, 5 s at 65°C, and 10 s at

72°C. Primer sequences for amplification were 5′-GGGCTAATTACAGTGCAG-3′ and 5′-CATGTCC-AGCAGCTAGTT-3′ for Cx43, 5′-GAGATCAGAGCCCAGG-ATGCT-3′ and 5′-CTGAGGGGTGGTGCCAAGGAG-3′ for nestin, 5′-TCCGCT-GCTCGCC-GCTCCTAC-3′ and 5′-TCATCTCTGCCCGCTCACTGG-3′ for glial fibrillary acidic protein (GFAP), 5′-CACTTCCTCCTCCTCCACGAC-3′ and 5′-GTCC-ATGGCCAGGTTCAGGTC-3′ for oligodendrocyte transcription factor 1 (OLIG1), 5′-CTAAGGAGGAGATTGGACAGG-3′ and 5′-AGTGGTGGC-AGTGATTT-CAGT-3′ for Nurr-1, 5′-AAATCCCATCACCATCTTCCA-3′ and 5′-AATGAGCC-CCAGCCTTCTC-3′ for GAPDH. The RNA preparation and RT-PCR in the present study were performed in triplicate.

2.6 Statistical Analysis

Student's *t* test was used to assess whether differences observed between the $SnCl_2$- and Sn(Oct)2-supplemented and control samples were statically significant. For comparison of groups of means, one-way analysis of variance was carried out. When significant differences were found, Tukey's pairwise comparison was used to investigate the nature of the difference. The confidence level was set at 95% for all tests. Statistical significance was accepted at $p < 0.05$. Values were presented as the mean ± SD.

3 Results and Discussion

$SnCl_2$ can exert biological effects by disrupting a variety of cellular targets including DNA. It can be biomethylated in the environment, which may increase its toxicity to mammalian systems. Some tin compounds can inhibit the immune response in rodents and alter gene expression [12, 13].

In our experiment, NHA were cultured with different concentrations of $SnCl_2$ (1 or 3 μg/ml) or Sn(Oct)2 (2.5 or 5 μg/ml). After 1 week culture, cell proliferation was suppressed with $SnCl_2$ and Sn(Oct)2 and the suppression was significant with Sn(OCT)2 compared to control cultures (Fig. 1a and 1b). The DNA-damaging property of tin compounds is supposed to be the key factor for the suppression of proliferation of NHA.

Astrocytes are believed to play an important role in neuroprotection by providing energy substrates to neurons and by regulating the concentrations of K^+ and neurotransmitters *via* gap junctions. Astrocytes are coupled to a cellular network *via* gap junction channels, predominantly composed of Cx43. Therefore, we measured the GJIC function by SLDT assay. GJIC was significantly decreased in a dose-dependent manner when astrocytes were cultured with $SnCl_2$ but non-significantly with Sn(Oct)2 (Fig. 2a and 2b). The expression of the gap junctional gene Cx43 was also decreased in $SnCl_2$- and Sn(Oct)2-treated cultures, significantly when treated with Sn(Oct)2 (data not shown).

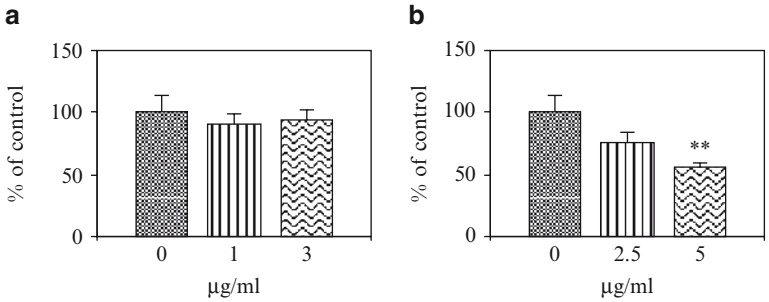

Fig. 1 MTT assay for NHA cell proliferation. In (**a**), cells treated with $SnCl_2$, and in (**b**), cells treated with Sn(Oct)2. ** $p < 0.01$

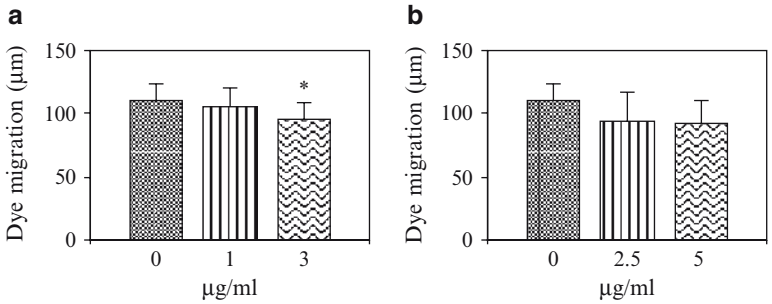

Fig. 2 Statistical analysis of SLDT assay. In (**a**), cells treated with $SnCl_2$, and in (**b**), cells treated with Sn(Oct)2. * $p < 0.05$

Some normal human astrocytes have neural precursor activity which gives rise to new astrocytes, oligodendrocytes, and neurons [14, 15] that express their original specific markers. Neural precursor cells express nestin, a class IV intermediate filament protein. Astrocytes express GFAP, a glial filamentous acidic protein. Oligodendrocytes express OLIG1, and differentiated neurons express Nurr-1, a transcription factor. In our study, culturing NHA with $SnCl_2$ caused a decrease in the expressions of nestin, GFAP, OLIG1, and Nurr-1. In Sn(OCT)2-treated cultures, the expressions of nestin and GFAP were decreased, whereas the expressions OLIG1, and Nurr-1 were increased in a dose-dependent manner (data not shown). This finding suggests that astrocytes may have been differentiated into oligodendrocytes and/or neurons in Sn(Oct)2-treated cultures.

4 Conclusion

In this study, we identified several effects of $SnCl_2$ and Sn(Oct)2 on NHA: a decrease in cell proliferation and inhibition of GJIC function, as well as suppression of the expression of the gap junctional gene. Expression of the specific markers

of certain genes was also suppressed with these materials. Thus, we suggest that both tin compounds are neurotoxic to astrocytes, resulting in the suppression of proliferation and also development of NHA.

Acknowledgments We are grateful for the support of grants for Research on Advanced Medical Technology from the Japanese Ministry of Health, Labour and Welfare and the Japan Health Sciences Foundation.

References

1. Silva, C.R. et al. (2002) Biological effects of stannous chloride, a substance that can produce stimulation or depression of the central nervous system, *Brain Res Bull* **59,** 213–216.
2. Salanki, Y., D'eri, Y., Platokhin, A. and Sh-Rozsa, K. (2000) The neurotoxicity of environmental pollutants: the effects of tin (Sn^{2+}) on acetylcholine-induced currents in greater pond snail neurons, *Neurosci Behav Physiol* **30,** 63–73.
3. Brown, A.W., Aldridge, W.N., Street, B.W. and Verschoyle, R.D. (1997) The behavioral and neuropathologic sequelae of intoxication by trimethyltin compounds in the rat, *Am J Pathol* **97,** 59–82.
4. Bouldin, T.W., Goines, N.D., Bagnell, R.C. and Krigman, M.R. (1981) Pathogenesis of trimethyltin neuronal toxicity. Ultrastructural and cytochemical observations, *Am J Pathol* **104,** 237–249.
5. McLean, J.R.N., Blakey, D.H., Douglas, G.R. and Kaplan, J.G. (1983) The effect of stannous and stannic (tin) chloride on DNA in Chinese hamster ovary cells, *Mutat Res* **119,** 195–201.
6. McKay, R. (1997) Stem cells in the central nervous system, *Science* **276,** 66–71.
7. Gage, F.H. (2000) Mammalian neural stem cells, *Science* **287,** 1433–1438.
8. Rash, J.E. et al. (2000) Immunogold evidence that neuronal gap junctions in adult rat brain and spinal cord contain connexin-36 but not connexin-32 or connexin-43, *Proc Natl Acad Sci USA* **97,** 7573–7578.
9. Yeager, M. and Nicholson, B.J. (1996) Structure of gap junction intercellular channels, *Curr Opin Struct Biol* **6,** 183–192.
10. Yeager, M. and Nicholson, B.J. (2000) Structure and biochemistry of gap junctions, *Adv Mol Cell Biol* **30,** 31–98.
11. El-Fouly, M.H., Trosko, J.E. and Chang, C.C. (1987) Scrape-loading and dye transfer. A rapid and simple technique to study gap junctional intercellular communication, *Exp Cell Res* **168,** 422–430.
12. Dimitrov, N.V., Meyer, C., Nahhas, F., Miller, C. and Averill, B.A. (1981) Effect of tin on immune responses of mice, *Clin Immunol Immunopathol* **20,** 39–48.
13. Kappas, A. and Maines, M.D. (1976) Tin: a potent inducer of heme oxygenase in kidney, *Science* **192,** 60–62.
14. Johansson, C.B., Momma, S., Clarke, D.L., Risling, M., Lendahl, U. and Frisen, J. (1999) Identification of a neural stem cell in the adult mammalian central nervous system, *Cell* **96,** 25–34.
15. Reynolds, B.A. and Weiss, S. (1992) Generation of neurons and astrocytes from isolated cells of the adult mammalian central nervous system, *Science* **255,** 1707–1710.

Effects of Tin Compounds on Human Chondrogenic Activity In Vitro

Nasreen Banu, Toshie Tsuchiya, and Rumi Sawada

Abstract Organotin compounds, particularly tributyltin chloride (TBT) and dibutyltin dichloride (DBT), are widely distributed toxicants. They inhibit cell proliferation and are known to cause neurotoxicity and genotoxicity in animals and humans. DBT is used as a catalyst in biodegradable polymers. We evaluated the effects of TBT and DBT on chondrogenesis of human articular chondrocytes (HAC) under a micromass culture system. In 4 weeks of culture, the lowest dose of TBT caused an increase in cell proliferation and differentiation. When the dose was increased, its effect on cultured chondrocytes was inhibitory compared with the control cultures. DBT produced little change in cell proliferation but it significantly inhibited cell differentiation compared with the control cultures. The expression of cartilage-specific genes, namely collagen type II and aggrecan was inhibited in TBT- and DBT-treated cultured chondrocytes. TBT was significantly toxic to HAC at 0.16 ppb and DBT at 0.75 ppb.

Keywords Tin compound · human articular chondrocytes · in vitro

1 Introduction

The increasing awareness of humans to exposure to different industrial and environmental products has inspired research regarding the effects of organic and inorganic chemicals. Organotin compounds that are widely used in industrial and agricultural sectors cause vast environmental contamination. In the environment, organotin compounds are converted into volatile tin compounds and are dispersed throughout the ecosphere, where they can accumulate in the food chain via the tin geocycle.

N. Banu, T. Tsuchiya, and R. Sawada
Division of Medical Devices, National Institute of Health Sciences, 1-18-1, Kamiyoga, Setagaya ku, Tokyo, 158-8501, Japan

K. Ikura et al. (eds.), *Animal Cell Technology: Basic & Applied Aspects*,
Animal Cell Technology: Basic & Applied Aspects 15,
DOI 10.1007/978-1-4020-9646-4_29,

Organotin compounds from industrial wastes and leaching from PVC water pipes can contaminate human food and water [1]. The commonly used organotin compounds, namely tributyltin chloride (TBT) and dibutyltin dichloride (DBT), are two of the most toxic tin compounds to mammalian cells. They cause inhibition of sex hormone metabolism in humans [2] and are developmental neurotoxicants [3] and teratogens in experimental animals [4]. Recently, TBT was reported to intensify allergic diseases via suppression of Th1 and Th2 development [5] and to be potentially carcinogenic [6].

To the best of our knowledge, no study has reported the effects of TBT and DBT on chondrogenesis yet. Therefore, to obtain insight into the effects of TBT and DBT on chondrogenesis, we cultured human articular chondrocytes (HAC) with these tin compounds under a micromass culture system.

2 Materials and Methods

2.1 Medium and Materials Used for Cell Culture

Chondrocyte growth medium was obtained commercially from BioWhittaker, Inc. (Walkersville, MD, USA). TBT and DBT were purchased from Wako Pure Chemical Industries (Osaka, Japan). TBT (0.016, 0.16 ppb) was dissolved in the growth medium. DBT (0.75, 7.5 ppb) was dissolved in dimethyl sulfoxide (DMSO) (Sigma Chemical Co. St. Louis, MO, USA).

2.2 Cells and Culture Methods

HAC of the knee joint were obtained commercially from BioWhittaker, Inc. High-density micromass cultures were started by spotting 4×10^5 cells in 20 µl of medium onto Costar 24-well tissue culture microplates (Costar type 3,526, Corning Co. Ltd., Corning, NY, USA). After 2 h incubation at 37°C in a CO_2 incubator, 1 ml culture medium was added to each well. The media were supplemented with one of two different concentrations of TBT or DBT. The culture medium alone was used as a control for TBT-treated cultures. DMSO was used as the control for DBT-treated cultured chondrocytes. At least four cultures were performed for each sample. The cultures were continued for 4 weeks with medium change twice a week.

2.3 Cell Proliferation Study

Cell proliferation was quantitatively estimated by crystal violet (Wako Pure Chemical Industries) staining. Briefly, cell fixation with 100% methanol was

followed by application of 0.1% crystal violet in methanol. After washing, cells were again incubated in methanol; 100 µl from each well was transferred to a new 96-well plate, and the absorbance was measured at a wavelength of 590 nm using an ELISA reader (Bio-Tek Instruments, Inc., Winooski, VT, USA). Blank values were subtracted from experimental values to eliminate background readings.

2.4 Cell Differentiation Assay

Cell differentiation was assayed by alcian blue (Wako Pure Chemical Industries) staining. The cells stained with crystal violet were washed with methanol and 3% acetic acid. Cultures were then stained with 1% (w/v) alcian blue in 3% acetic acid, pH 1.0. Guanidine hydrochloride (GH, 4 M) was used to extract the cartilage proteoglycans, and the bound dye was measured at a wavelength of 600 nm using an ELISA reader (Bio-Tek Instruments). Fresh 4 M GH served as the blank. Blank values were subtracted from experimental values to eliminate background readings.

2.5 Real-Time Polymerase Chain Reaction (PCR)

For detection of the presence of proteoglycan genes, namely collagen type II and aggrecan, single stranded cDNA was prepared from 1 µg of total RNA by reverse transcription (RT) using a commercially available First-Strand cDNA kit (Amersham Pharmacia Biotech, Uppsala, Sweden). Subsequently real-time PCR was done using a LightCycler system with LightCycler FastStart DNA Master SYBR Green I (Roche Diagnostics, Penzberg, Germany). A LightCyclerTM-Primer set (Roche Diagnostics) was used for quantitative detection of the collagen type II gene, the aggrecan gene, and a housekeeping gene, glyceraldehyde-3-phosphate dehydrogenase (GAPDH). The quantification data were analyzed with the LightCycler analysis software (Roche Diagnostics).

2.6 Statistical Analysis

Student's *t* tests were used to assess whether differences observed between the material-treated and control samples were statistically significant. For comparison of groups of means, one-way analysis of variance was carried out. When significant differences were found, Tukey's pairwise comparison was used to investigate the nature of the difference. Statistical significance was accepted at $p < 0.05$. Values were presented as the mean ± SD (standard deviation). All experiments were repeated at least twice, and similar results were obtained.

3 Results

3.1 Cell Proliferation

Cell proliferation of chondrocytes was increased 1.7-fold (**p < 0.01) in cultures treated with 0.016 ppb TBT compared with the control culture, but it was significantly decreased (0.45-fold, **p < 0.01) at 0.16 ppb TBT compared with the control (Fig. 1a). In DBT-treated chondrocytes, cell proliferation was similar or slightly increased at 0.75 and 7.5 ppb, respectively, compared to the DMSO control (Fig. 1b).

3.2 Cell Differentiation

Differentiation of cultured chondrocytes was increased 1.2-fold (*p < 0.05) in cultures treated with 0.016 ppb TBT compared with the control, but it was decreased about 0.21-fold (**p < 0.01) when treated with 0.16 ppb of TBT compared with the control (Fig. 2a). Cell differentiation of cultured chondrocytes was significantly inhibited at concentrations of DBT of 0.75 ppb (*p < 0.05) and 7.5 ppb (**p < 0.01) compared to the DMSO control (Fig. 2b).

4 Discussion

General cytotoxic effects of different tin compounds have been observed in rabbit articular cartilage in monolayer culture [7]. Certain tin compounds at low concentrations were reported to enhance chondrocyte proliferation in rat [7]. Disproportionate

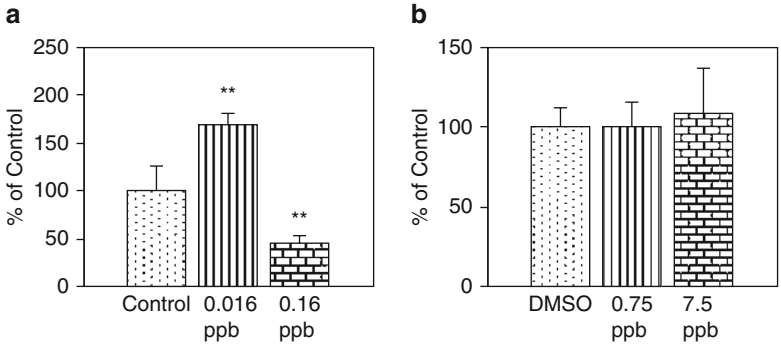

Fig. 1 Assay of HAC proliferation by crystal violet staining. In (**a**), cells were treated with TBT, and in (**b**), with DBT. * p < 0.05, **p < 0.01

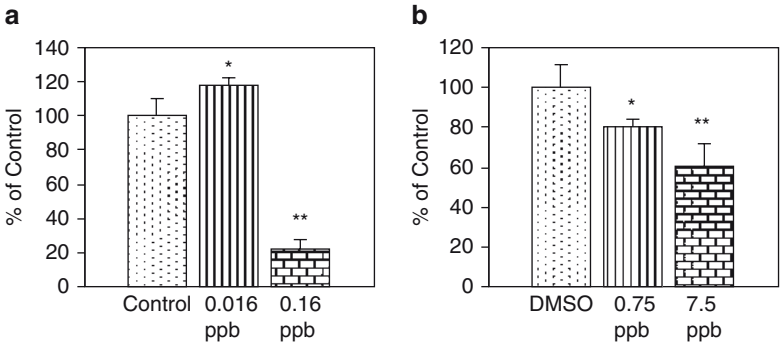

Fig. 2 Assay of HAC differentiation by alcian blue staining. In (**a**), cells were treated with TBT, and in (**b**), with DBT. * $p < 0.05$, **$p < 0.01$

dwarfing syndrome was observed in rats after subcutaneous injection of inorganic tin compounds [8], and Tsukamoto et al. reported that TBT was a critical inhibitor of bone formation in mice both in vivo and in vitro [9]. The aim of this study was to clarify the effects of TBT and DBT on chondrogenesis of HAC in a micromass culture system. Our study showed an increase in cell proliferation and differentiation of TBT-treated chondrocytes at 0.016 ppb in micromass culture (Figs. 1a and 2b), while it showed strong inhibition of chondrogenesis at the higher concentration of TBT. With DBT, our study showed almost no change in the proliferation assay but significant inhibition in the differentiation of HAC in micromass culture. The gene expressions of cartilage- specific proteins, namely collagen type II and aggrecan, were significantly decreased in TBT- and DBT-treated cultures (data not shown). To the best of our knowledge, our study is the first to show the biological effects of TBT and DBT on human articular chondrogenesis in a micromass culture system. Therefore, we speculate that these two inorganic tin compounds might have inhibitory effects on chondrogenesis of HAC. However, more advanced investigations are required to determine their usefulness in the field of regenerative tissue engineering.

Acknowledgements We are grateful for the support of grants for Research on Advanced Medical Technology from the Ministry of Health, Labour and Welfare and the Japan Health Sciences Foundation.

References

1. Snoeij, N.J., Penninks, A.H., and Seinen, W. (1987) Biological activity of organotin compounds-an overview, *Environ Res* 44, 335–353.
2. Heidrich, D.D., Steckelbroeck, S., and Klingmuller, D. (2001) Inhibition of human cytochrome P450 aromatase activity by butyltins, *Steroids* 66, 763–769.

3. Jenkins, S.M., Ehman, K., and Barone, S. Jr. (2004) Structure-activity comparison of organotin species: dibutyltin is a developmental neurotoxicant in vitro and in vivo, *Brain Res Dev Brain Res* 19, 1–12.
4. Farr, C.H., Reinisch, K., Holson, J.F., and Neubert, D. (2001) Potential teratogenicity of di-n-butyltin dichloride and other dibutyltin compounds, *Teratog Carcinog Mutagen* 21, 405–415.
5. Kato, T. et al. (2006) Endocrine disruptors that deplete glutathione levels in APC promote Th2 polarization in mice leading to the exacerbation of airway inflammation, *Eur J Immunol* 36, 1199–1209.
6. Belyaeva, N.N., Bystrova, T.A., Revazova, Y.A., and Arkhangelskii, V.I. (1976) Comparative assessment of the toxic and mutagenic properties of organotin compounds, *Gig Sanit* 5, 10–14.
7. Webber, R.J., Dollins, S.C., Harris, M., and Hough, A.J. Jr. (1985) Effect of alkyltins on rabbit articular and growth-plate chondrocytes in monolayer culture, *J Toxicol Environ Health* 16, 229–242.
8. Chang, L.W. (1984) Hippocampal lesions induced by trimethyltin in the neonatal rat brain, *Neurotoxicology* 5, 205–215.
9. Tsukamoto, Y., Ishihara, Y., Miyagawa-Tomita, S., and Hagiwara, H. (2004) Inhibition of ossification in vivo and differentiation of osteoblasts in vitro by tributyltin, *Biochem Pharmacol* 15, 739–746.

Construction of a Fluorescein-Responsive Chimeric Receptor with Strict Ligand Dependency and Analysis of the Role of Erythropoietin Receptor Domains in Signal Transduction

Wenhai Liu, Masahiro Kawahara, Hiroshi Ueda, and Teruyuki Nagamune

Abstract In our previous study, we designed anti-fluorescein (FL) antibody/receptor chimeras in response to FL-conjugated BSA (BSA-FL). However, considerable background cell proliferation was observed without antigen. Therefore, we tried to redesign chimeric receptor constructs with different combinations of the domains containing anti-FL single chain Fv (ScFv), extracellular D1/D2 domains, transmembrane/intracellular domains of erythropoietin receptor (EpoR) or glycoprotein 130 (gp130), for construction of a strictly fluorescein-dependent chimeric receptor. We also tried to analyze the role of erythropoietin receptor domains in signal transduction. We designed a series of chimeric receptors. Firstly an anti-FL ScFv was fused to full-length EpoR. Next we tried to delete extracellular D1 or D2 domain of EpoR, to mutate transmembrane (TM) domain, to exchange the intracellular domain (ID) into that of gp130, and/or to insert several Ala residues into juxtamembrane domain to modulate the conformation of intracellular domain. Chimeric receptors were expressed in IL-3-dependent Ba/F3 cells to compare their growth characteristics. We found that BSA-FL acted as an inverse agonist at some chimeric receptors, whereas it also acted as an agonist at other chimeric receptors. We also found the effect on cell growth induced by the TM domain mutation and the insertion of Ala residues between TM and intracellular domains of chimeric receptors. Notably, one chimeric receptor, ScFv-EpoRTM-gp130ID, transduced a strict BSA-FL dependent growth signal without any background cell growth. Therefore, this chimera might be promising as a basis for cell growth-based screening of high-affinity ScFvs derived from a randomized antibody library, where simple culture in antigen-containing medium results in growing cells with a high-affinity antibody gene, leading to antibody selection.

W. Liu, M. Kawahara, H. Ueda, and T. Nagamune
Department of Chemistry and Biotechnology, Graduate School of Engineering,
The University of Tokyo, 7-3-1 Hongo, Bunkyo-ku, Tokyo, 113-8656, Japan

M. Kawahara
Department of Pathology, University of Massachusetts Medical School,
55 Lake Avenue North, Worcester, MA, 01655, USA

K. Ikura et al. (eds.), *Animal Cell Technology: Basic & Applied Aspects*,
Animal Cell Technology: Basic & Applied Aspects 15,
DOI 10.1007/978-1-4020-9646-4_30, © Springer Science+Business Media B.V. 2009

Keywords Chimeric receptor · erythrpoietin receptor · fluorescein

1 Introduction

Cytokines are small secreted proteins which mediate and regulate immunity, hematopoiesis, and cell differentiation or proliferation. They generally act in short distances and short time spans at very low concentration. Their action is mediated by binding to specific membrane receptors, which then signal the cell via second messengers, often tyrosine kinases. If we can artificially mimic the characteristics of cytokines, it will be useful for many applications such as artificial control of cell fate. To attain this, we considered to use the relationship between antigen and its antibody which is similar to that between cytokine and its receptor. Concretely we designed a chimeric cytokine receptor whose ligand-binding region is replaced by antibody fragment. By such an engineering we could use the cognate antigen to control cell differentiation or proliferation in place of cytokines.

In this study, we tried to design a chimeric receptor with strict ligand dependency. We selected erythropoietin receptor (EpoR), which is responsible for the regulation of red blood cell (erythrocyte) production. The glycoprotein hormone Epo, which is mainly produced in the kidneys, induces neuronal survival and also differentiation and proliferation of erythroid progenitor cells. To mimic Epo/EpoR signaling, we used FL-conjugated BSA (BSA-FL) and anti-FL single chain Fv (ScFv) clone 31IJ3 [1]. In our previous study, we designed anti-FL antibody/receptor chimeras in response to BSA-FL. However, considerable background cell proliferation was observed without antigen (data not shown) [1]. Therefore, we tried to redesign chimeric receptor constructs with different combinations of the domains containing anti-FL ScFv, extracellular D1/D2 domains, transmembrane/intracellular domains of EpoR or glycoprotein 130 (gp130), for construction of a strictly fluorescein-dependent chimeric receptor. We also tried to analyze the role of erythropoietin receptor domains in signal transduction.

2 Methods and Results

The chimeric receptor gene was cloned in the pMK-IRES-EGFP bicistronic retroviral vector upstream of internal ribosomal entry site (IRES) [2]. The IRES sequence is used to couple the expression levels of the two cistrons,chimeric receptor and enhanced green fluorescent protein (EGFP) [3, 4]. Here, EGFP was used as a marker gene, since FACS analysis readily scores the transduction/selection efficiencies.

We designed a series of chimeric receptors (Fig.1). HA-tag was fused to N-terminus of each chimera to readily analyze cell surface expression levels of chimeras by FACS.

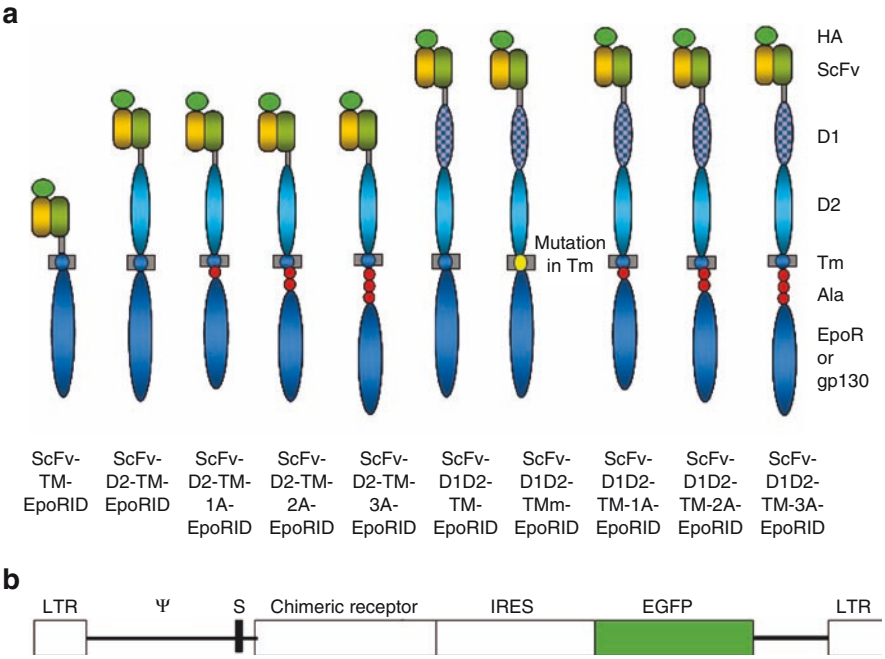

Fig. 1 Scheme of chimeric receptor constructs and vectors. (**a**) Chimeric receptor constructs. HA-tag was appended on the extracellular N-terminus of chimeric receptor, Anti-FL ScFv with a Gly-Ser-Gly tripeptide linker was fused to EpoR domain in each construct. Firstly ScFv was fused to full-length EpoR(ScFv-D1D2-TM-EpoRID). Next we tried to delete extracellular D1 domain (ScFv-D2-TM-EpoRID) or D1D2 domain (ScFv-TM-EpoRID) of EpoR, to mutate transmembrane (TM) domain with double point mutations (L240G L241P) (ScFv-D1D2-TMm-EpoRID), and/or to insert several Ala residues into juxtamembrane domain to modulate the conformation of intracellular domain (from ScFv-D1D2-TM-1A-EpoRID to ScFv-D1D2-TM-4A-EpoRID and from ScFv-D2-TM-1A-EpoRID to ScFv-D2-TM-4A-EpoRID), to exchange the intracellular domain (ID) into that of gp130 (named gp130ID instead of EpoRID in each construct). (**b**) Schematic diagram of vectors. Retroviral vectors with long-terminal repeats (LTRs) and a packaging signal (ψ) are used. An immunoglobulin heavy chain secretion signal sequence (S) is located upstream of the chimeric receptor genes to enable their cell surface expression

To investigate these chimeric receptors can transduce a strictly fluorescein dependent growth signal, cell proliferation assay was performed. We have evaluated that there is no toxicity of BSA-FL to parental BaF3 (data not shown). 100% GFP-positive cells expressing each chimera cultured with 1 ng/ml IL-3 were washed three times by PBS and cultured in various concentrations of BSA-FL, followed by measurement of viable cell concentrations on day 3. Almost all chimeric receptors with EpoR intracellular domain were constitutively active, whereas cells expressing most chimeric receptors with gp130 intracellular domain died except those expressing ScFv-TM-gp130ID. Therefore, in our constructed chimeric receptors, the chimeric receptors with EpoR intracellular domain signaled stronger than those with gp130 intracellular domain.

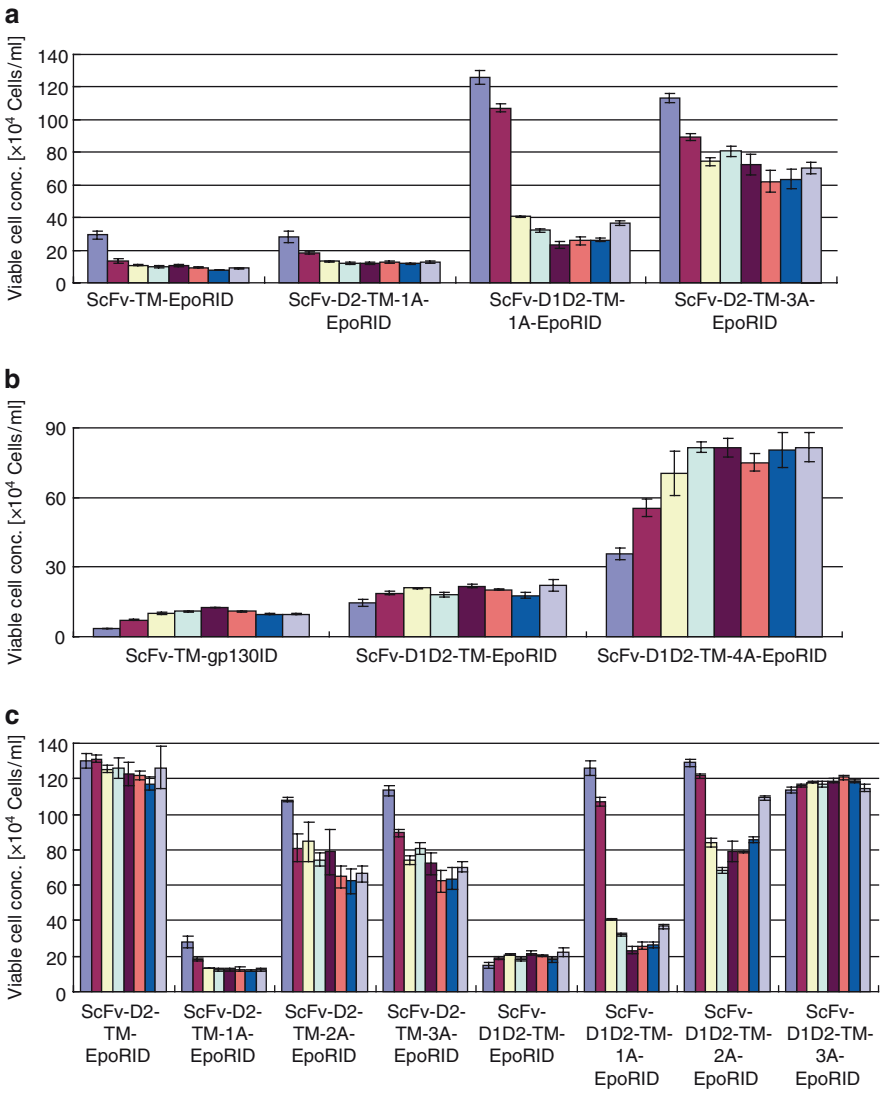

Fig. 2 Cell growth properties of chimeric receptor cells to BSA-FL. Cells (10^4 cells/ml) were inoculated into 96-well plates on day 0 and cultured in the presence of BSA-FL concentrations: 0, 0.1, 0.5, 1, 4, 8, 10, 20 μg/ml (the bar from left to right). Viable cell concentration on day 3 is plotted with average and 1 S.D. (n = 3). Since the proliferation of chimeric receptor ScFv-D1D2-TM-4A-EpoRID was much faster than others, initial cell concentration was set at 5×10^3 cells/ml only for this sample)

Several chimeric receptors of ScFv-TM-EpoRID, ScFv-D2-TM-1A-EpoRID, ScFv-D1D2-TM-1A-EpoRID and ScFv-D2-TM-3A-EpoRID showed inverse agonism to BSA-FL (Fig. 2a). On the other hand, several chimeric receptors of ScFv-TM-gp130ID, ScFv-D1D2-TM-EpoRID and ScFv-D1D2-TM-4A-EpoRID showed agonism to BSA-FL with some residual growth in the absence of BSA-FL (Fig. 2b).

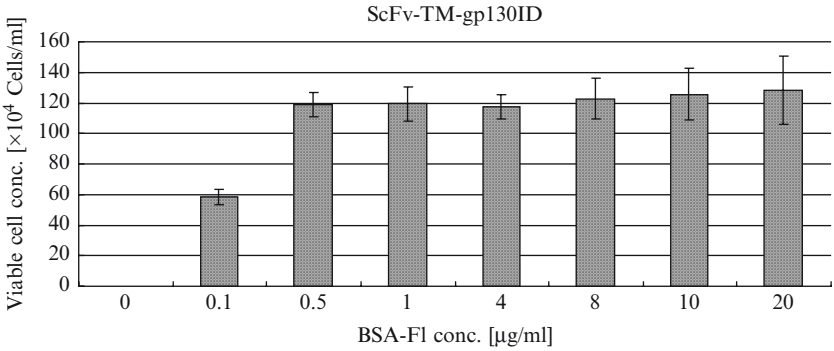

Fig. 3 Cell growth properties of ScFv-TM-gp130ID cells to BSA-FL. Initial cell concentration was 10^4 cells/ml, and viable cell concentration on day 6 is plotted with average and 1 S.D. (n = 3)

The results suggest these chimeric receptors can be dimerized without any ligand and transduce proliferation signal. If BSA-FL addition alters conformation and affinity of chimeras to be better or worse for their signaling, cells would show agonism or inverse agonism to BSA-FL, respectively.

There was great difference in the signaling properties of chimeric receptor ScFv-D2-TM-EpoRID or ScFv-D1D2-TM-EpoRID to BSA-FL with 1 to 3 Ala residues inserted in juxtamembrane domain (Fig. 2c). Inserted Ala residues induced conformational change of intracellular domain, which influenced signal transduction. EpoR activation mechanism is such that Epo induces a close dimer association of both the D1 and D2 domains of EpoR so that their intracellular regions become substrates for phosphorylation by two Jak2 molecules each other. So, those results suggest that the conformation of intracellular domain is very important for Jak2 and other signal transduction molecules.

To mimic the characteristics of cytokine and its receptor, we aimed to design the chimeric receptor with antibody fragment with strict ligand dependency. We found that chimeric receptor ScFv-TM-gp130ID showed strict BSA-FL-dependent cell proliferation (Fig. 3).While cells died without BSA-FL, their proliferation was induced by BSA-FL, even low concentration of 0.1 μg/ml. There is no difference in proliferation activity at the concentration over 0.5 μg/ml BSA-FL, showing this concentration is enough for maximal growth stimulation.

3 Discussion

In addition to the results described above, there was great difference in cell proliferation properties among the following chimeric receptors: ScFv-D1D2-TM-EpoRID, ScFv-D1D2-TMm-EpoRID, ScFv-D2-TM-EpoRID and ScFv-TM-EpoRID (Fig. 4).

Sequence-specific interactions between α-helical transmembrane segment support assembly of EpoR, and a double point mutation (L240G L241P) can abolish it [5]. But in ScFv fusion chimeric receptor, there was not so sizable change after

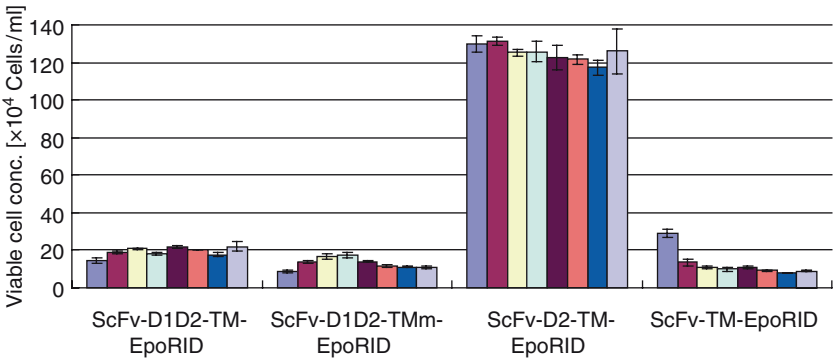

Fig. 4 Cell growth character of ScFv-D1D2-TM-EpoRID, ScFv-D1D2-TMm-EpoRID, ScFv-D2-TM-EpoRID and ScFv-TM-EpoRID cells to BSA-FL. Cells (10^4 cells/ml) were inoculated into 96-well plates on day 0 and cultured in the presence of BSA-FL concentrations: 0, 0.1, 0.5, 1, 4, 8, 10, 20 μg/ml (the bar from left to right). Viable cell concentration on day 6 is plotted with average and 1 S.D. (n = 3)

double point mutations (L240G L241P) were inserted. These results suggest that the fusion of ScFv influenced receptor signaling far more than double point mutations. There are both D1 and D2 extracellular domains in ScFv-D1D2-TM-EpoRID, only D2 domain in ScFv-D2-TM-EpoRID, and no extracellular domain in ScFv-TM-EpoRID. In these receptors, ScFv-D2-TM-EpoRID showed the highest growth activity and the others showed similar growth activity with each other but much lower than ScFv-D2-TM-EpoRID. In the unliganded form EpoR exists as a preformed homodimer in an open scissor-like conformation [6] precluding the activation of signaling. It can be postulated that since there is D1 domain in ScFv-D1D2-TM-EpoRID, the D1 domain might take an open scissor-like conformation, which bothers the binding of ScFv and its antigen BSA-FL, resulting in low growth activity. And since there is no any extracellular domain in ScFv-TM-EpoRID, it can be supposed that since the mobile area of ScFv is limited, and the binding between BSA-FL and ScFv is also limited. But there is only D2 domain in ScFv-D2-TM-EpoRID, there is no open scissor-like conformation and the locomote area of ScFv is just to bind with BSA-FL. Perhaps the D2 domain in ScFv-D2-TM-EpoRID might be helpful to provide mobile area of ScFv. Newly, we are constructing a new series of chimeric receptors whose extracellular domain contains only D1 domain to test the hypothesis.

We constructed a chimeric receptor ScFv-TM-gp130ID, in which cell proliferation showed strict dependency to BSA-FL. In the future we can use this chimeric receptor to randomize the amino acid sequence of ScFv which is fused to chimeric receptor, and this chimera might be promising as a basis for cell growth-based screening of high-affinity ScFvs derived from a randomized antibody library, where simple culture in antigen-containing medium results in growing cells with a high-affinity antibody gene, leading to antibody selection.

References

1. Kawahara M, et al. (2004) Biochem Biophys Res Commun 324, 1165–1172.
2. Gattas IR, et al. (1991) Mol Cell Biol 11, 5848–5859
3. Persons DA, et al. (1997) Blood 90, 1777–1786.
4. Sugimoto Y, et al. (1995) Hum Gene Ther 6, 905–915.
5. Kubatzky KF, et al. (2001) Curr Biol 11, 110–115.
6. Livnah O, et al. (1998) Nat Struct Biol 5, 993–1004.

Nuclear Structures Regulate Liver-Specific Expression of the Tryptophan Oxygenase Gene

Hidenori Kaneoka, Katsuhide Miyake, and Shinji Iijima

Abstract The gene for tryptophan oxygenase (TO) is expressed in a tissue- and development-specific manner and is regulated by glucocorticoid hormone in rat liver. Transcription of the gene is induced 10-fold by glucocorticoids. The TO promoter has two glucocorticoid-responsive elements (GRE), located 450 bp and 1.2 kb upstream from the cap site, and two TATA boxes. Combination of nuclear fractionation and quantitative PCR analysis showed that a putative matrix attachment region, which resides 8.5 kb upstream of the promoter, bound to nuclear matrix in the hormone-treated adult hepatocytes. However, this DNA region was partly released from the nuclear matrix by removing the hormone. These results indicated that binding of MAR to nuclear matrix was also important for regulation of the TO gene expression.

Keywords Tryptophan oxygenase · glucocorticoid receptor · hepatocyte

1 Introduction

In eukaryotic nucleus, active chromatin is arranged in loops composed of 10 to 100 kb of DNA and protruded from the packed chromatin region. In the interphase nucleus, these loops are anchored by scaffold or nuclear matrix. Recent studies suggest that matrix-DNA interaction controls at least partly, gene expression [1, 2]. The matrix-DNA interaction is still ambiguous, but several chromatin-associated proteins such as topoisomerase II, the lamina-associated attachment region-binding protein, and heterogeneous nuclear ribonucleoprotein U (hnRNP U) may be included in the interaction [3–5]. Some of these proteins are capable of binding to the A/T-rich matrix attachment region (MAR).

H. Kaneoka, K. Miyake and S. Iijima
Department of Biotechnology, Graduate School of Engineering, Nagoya University, Furo-cho, Chikusa-ku, Nagoya, 464-8603, Japan

K. Ikura et al. (eds.), *Animal Cell Technology: Basic & Applied Aspects*,
Animal Cell Technology: Basic & Applied Aspects 15,
DOI 10.1007/978-1-4020-9646-4_31, © Springer Science+Business Media B.V. 2009

The glucocorticoid receptor (GR) belongs to the superfamily of steroid hormone receptors, which controls gene expressions in a ligand-dependent manner. In mammals, glucocorticoid hormones play important roles in the control of the response of the organism to various stresses, whereas in developmental process, they prepare various organs for the metabolic adaptations allowing autonomous life after birth. GR interacts with coactivators and corepressor complexes to modulate both chromatin structure and the activity of the basal transcriptional machinery [6]. Furthermore, GR is found to be localized to the nuclear matrix and interacts with the hnRNP U protein [7].

In the liver, the activated GR plays central roles in the expression of tryptophan oxygenase (TO) in postnatal life. The induction of the TO gene is thought to be mediated by regulatory sequences termed glucocorticoid responsive elements (GREs) located at −0.45 and −1.2 kb [8]. Thus, expression of the TO gene is an interesting model system for studying the control mechanism of GR-mediated gene expression. In this study, we analyzed the glucocorticoid-dependant matrix binding of this locus.

2 Materials and Methods

2.1 Isolation and Culture of Rat Hepatocytes

Adult rat hepatocytes were obtained from male Sprague-Dawley rats (6–7 weeks old; Japan SLC) by the collagenase perfusion method [9, 10]. Williams' medium E (Invitrogen), supplemented with 0.1 mM $CuSO_4 \cdot 5H_2O$, 25 nM Na_2SeO_3, 1.0 mM $ZnSO_4 \cdot 7H_2O$, 0.1 μM insulin (Sigma), 1.0 μM dexamethasone (Wako), 48 μg/ml of gentamicin sulfate (Sigma) and 100 μg/ml of chloramphenicol (Wako) was used as the culture medium. Cells were seeded onto collagen type I-coated plastic dishes (Iwaki Glass Works) under a 5% CO_2 atmosphere.

2.2 Nuclear Matrix Isolation

Nuclear matrix was isolated according to previously reported procedures [11]. The isolated nuclear pellets (~10^7) were washed once with 5 ml of cold cell wash buffer (CWB; 5 mM Tris-HCl pH 7.4, 50 mM KCl, 0.5 mM EDTA, 0.05 mM spermine, 0.125 mM spermidine, 0.5% 2-mercaptoethanol, 0.1% digitonin and a protease inhibitor mixture), and nuclei were suspended in 0.5 ml of stabilization buffer (0.5 mM EDTA was replaced by 0.5 mM $CuSO_4$ in CWB). After incubation for 20 min at 37°C, nuclei were extracted for 10 min with 19 volumes of LIS buffer (20 mM HEPES pH 7.4, 10 mM lithium 3, 5-diiodosalicylate, 100 mM Li-acetate, 0.05 mM spermine, 0.125 mM spermidine, 0.5% 2-mercaptoethanol,

0.1% digitonin and a protease inhibitor mixture) at room temperature. Matrices were collected by centrifugation (2,400 *g* for 20 min at 20°C) and were washed once with matrix wash buffer (MWB; 20 mM Tris-HCl pH 7.4, 20 mM KCl, 50 mM NaCl, and 10 mM $MgCl_2$) containing 0.1% digitonin. The sample was then washed twice with MWB and once with the appropriate buffer for restriction-enzyme digestion at 20°C.

Matrices were digested with 1,000 U/ml of restriction enzyme for 3 h at 37°C. Solubilized DNA was separated from nuclear matrix-bound DNA by centrifugation (2,400 *g* for 10 min at 4°C).

DNA was recovered from the matrix fraction after digestion with proteinase K in the 1% SDS and phenol-chloroform extraction, by ethanol precipitation. Then solubilized DNA and nuclear matrix-bound DNA were analyzed by real-time PCR analysis.

2.3 Chromatin Immunoprecipitation (ChIP) Assay

ChIP assay was performed using salmon sperm DNA/protein A agarose beads (Upstate cell signaling solutions) according to the manufacturer's instruction with some modifications. Adult hepatocytes were treated with 1% formaldehyde for 10 min at room temperature. Crosslinking was stopped by adding glycine to 0.125 M. Two microgram of antibodies was used in one reaction. The immunoprecipitated DNA and input DNA were analyzed by PCR using primers for −1.2 kb GRE and −8.5 kb GRE near the MAR (−1.2 kb GRE direct primer; 5′-TCACTCCTTGTCGTTGGCTTCA-3′, -1.2 kb GRE reverse primer; 5′-GCGGTAGTCTTCCAACTTCTGA-3′, GRE near the MAR direct primer; 5′-GCTAGCTGGAGAAGAAAGTACA-G-3′, GRE near the MAR reverse primer; 5′-AGCTCCAGCTGGCTTTAT-TTCC-3′).

3 Results

3.1 A Potential MAR Was Detected Upstream of the TO Gene

The TO gene genomic sequence was analyzed via online-based MAR analyzing program MAR-Wiz (http://www.futuresoft.org/MarFinder/content.html). The result showed that there was a potential MAR in the upstream of the TO gene. The potential MAR was localized at −8.5 kb from transcriptional start site, and this region located just beside a DNase I hypersensitive site. It was reported that an enhancer containing this DNase I hypersensitive site is a key for liver specific expression of the TO gene, since a deletion in this region leads to the loss of the tissue specific expression [12] (Fig. 1).

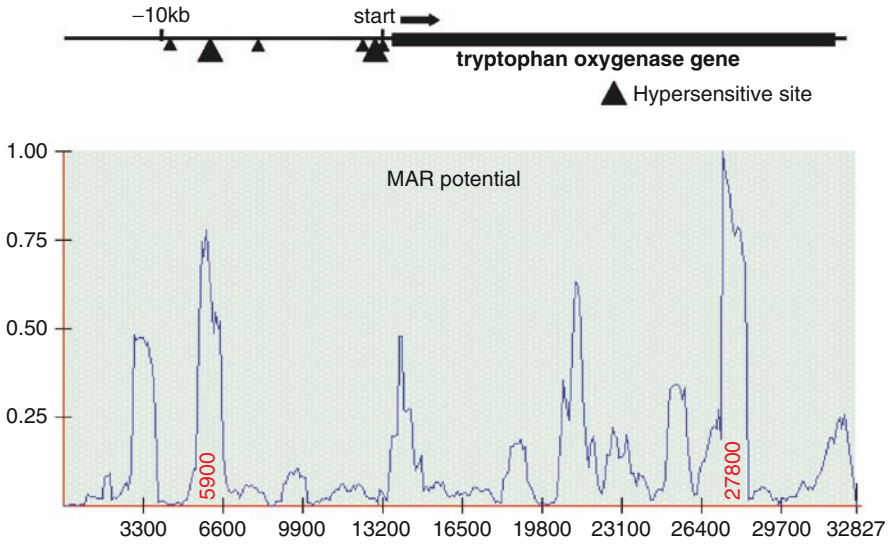

Fig. 1 Mapping of hypersensitive-sites and MARs in the TO regulatory region

3.2 Upstream of the TO Gene Is Specifically Associated with Nuclear Matrices In Vivo

In order to determine if the −8.5 kb region is associated with nuclear matrix in vivo, nuclear matrix-bound DNA and solubilized DNA was extracted and purified from adult rat hepatocytes. Purified DNA was analyzed by real-time PCR analysis. As shown in Fig. 2, the −8.5 kb region strongly interacted with nuclear matrix. Furthermore, this interaction was increased by the treatment of cells with dexamethasone. This result suggests that a GRE of the MAR region controls the matrix attachment of the MAR sequence in a hormone dependent manner.

3.3 GR Is Associated with the Region Near the MAR of the TO Gene In Vivo

TO clear the function of GR to matrix binding, we analyzed receptor binding to GREs at −1.2 and −8.5 kb by ChIP analyses. As shown in Fig. 3, the binding of GR to the −1.2 kb GRE increased after the hormone-treatment and the maximum binding was observed at 16 h after the treatment. This time course is in good accordance with the induction of TO gene expression. As is the case with the −1.2 kb GRE, GR binding was also observed at a putative GRE near the MAR sequence at −8.5 kb in the ChIP analysis (Fig. 3).

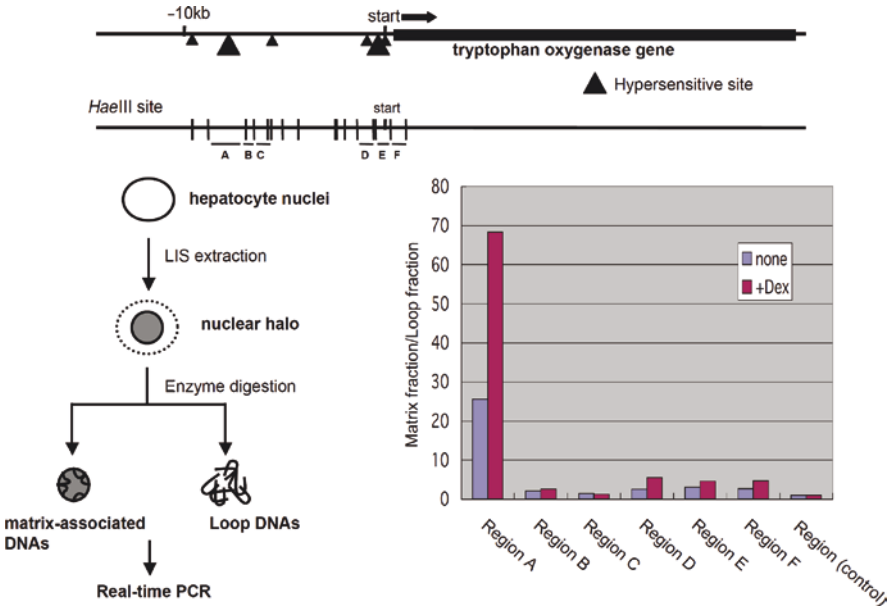

Fig. 2 Localization of the TO regulatory region to matrix fraction

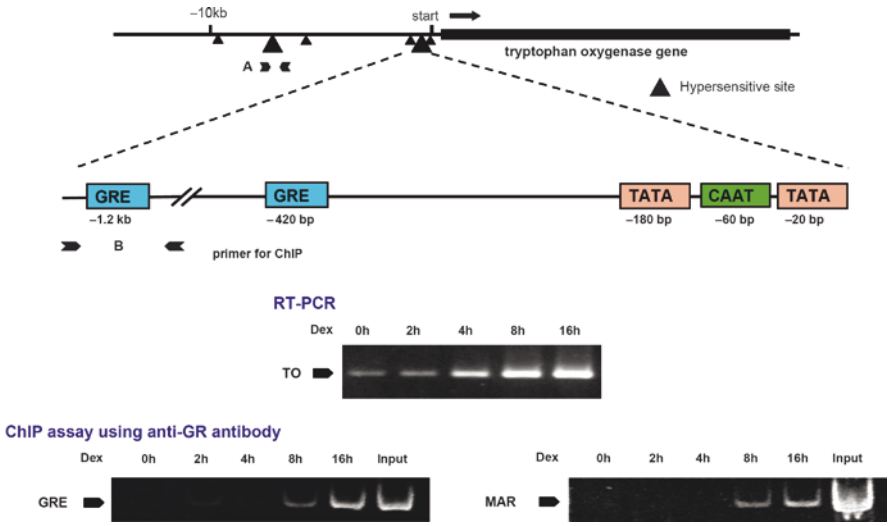

Fig. 3 ChIP analysis on the putative MAR of the TO gene

4 Discussion

It is so far known that nucleus contains several structures such as nucleolus, nuclear body, Cajal body and splicesome, and that these structures have important roles for transcriptional control [13, 14]. In addition, chromosomes occupied a region of nucleus called chromatin territory and active chromatin locus resides in the inter territory space. On the other hand, inactive chromatin is packed inside of the territory and heterochromatin region resides close to nuclear membrane [15]. In interchromosome region, several speckle structures such as transcriptional factory and splicesome have been detected, which suggests that dynamic structural change of chromosomes and their localization in nucleus controls gene expression, in addition to local structural change of chromosome and binding of transcription factors.

In this study, we analyzed the TO gene that expresses in liver specific manner. We found that the TO gene has relatively complex structure in 5′-upstream region. For instance, the gene contains two promoter-like structure within 200 bp of 5′-capping site and several GREs (−450 bp, −1.2 and −8.5 kb), and the most upstream GRE localizes near the putative MAR and DNase I hypersensitive site. It is well known that a matrix component hnRNP U binds both MAR and GR. Thus, cooperative binding of this ribonucleoprotein to MAR DNA sequence and GR may control the location and expression of the TO gene locus by a glucocorticoid dependent manner.

References

1. Iarovaia, O. V., Akopov, S. B., Nikolaev, L. G., Sverdlov, E. D., and Razin, S. V. (2005) Induction of transcription within chromosomal DNA loops flanked by MAR elements causes an association of loop DNA with the nuclear matrix. *Nucleic Acids Res*. **13**, 4157–4163.
2. Heng, H. H., Goetze, S., Ye, C. J., Liu, G., Stevens, J. B., Bremer, S. W., Wykes, S. M., Bode, J., and Krawetz, S. A. (2004) Chromatin loops are selectively anchored using scaffold/matrix-attachment regions. *J. Cell. Sci*. **117**, 999–1008.
3. Cockerrill, P. N. and Garrard, W. T. (1986) Chromosomal loop anchorage of the kappa immunoglobulin gene occurs next to the enhancer in a region containing topoisomerase II sites. *Cell* **44**, 273–282.
4. Luderus, M. E., de Graaf, A., Mattia, E., den Blaauwen, J. L., Grande, M. A., de Jong, L., and van Driel, R. (1992) Binding of matrix attachment regions to lamin B1. *Cell* **70**, 949–959.
5. Romig, H., Fackelmayer, F. O., Renz, A., Ramsperger, U., and Richter, A. (1992) Characterization of SAF-A, a novel nuclear DNA binding protein from HeLa cells with high affinity for nuclear matrix/scaffold attachment DNA elements. *EMBO J*. **11**, 3431–3440.
6. Hebbar, P. B. and Archer, T. K. (2003) Chromatin remodeling by nuclear receptors. *Chromosoma* **111**, 495–504.
7. Eggert, M., Michel, J., Schneider, S., Bornfleth, H., Baniahmad, A., Fackelmayer, F. O., Schmidt, S., and Renkawitz, R. (1997) The glucocorticoid receptor is associated with the RNA-binding nuclear matrix protein hnRNP U. *J. Biol. Chem*. **272**, 28471–28478.
8. Danesch, U., Gloss, B., Schmid, W., Schütz, G., Schüle, R., and Renkawitz, R. (1987) Glucocorticoid induction of the rat tryptophan oxygenase gene is mediated by two widely separated glucocorticoid-responsive elements. *EMBO J*. **6**, 625–630.
9. Hamamoto, R., Yamada, K., Kamihira, M., and Iijima, S. (1998) Differentiation and proliferation of primary rat hepatocytes cultured as spheroids. *J. Biochem*. **124**, 972–979

10. Dohda, T., Nakamura, Y., Kamihira, M., and Iijima, S. (2004) Functional role of RhoA in growth regulation of primary hepatocytes. *J. Biochem*. **135**, 631–637.
11. Mirkovitch, J., Mirault, M. E., and Laemmli, U. K. (1994) Organization of the higher-order chromatin loop: specific DNA attachment sites on nuclear scaffold. *Cell* **39**, 223–232.
12. Kaltschmidt, C., Muller, M., Brem, G., and Renkawitz, R. (1994) DNase I hypersensitive sites far upstream of the rat tryptophan oxygenase gene direct developmentally regulated transcription in livers of transgenic mice. *Mech. Dev*. **45**, 203–210.
13. Cremer, T. and Cremer, C. (2001) Chromosome territories, nuclear architecture and gene regulation in mammalian cells. *Nat. Rev. Genet*. **2**, 292–301.
14. Zaidi, S. K., Young, D. W., Choi, J. Y., Pratap, J., Javed, A., Montecino, M., Stein, J. L., van Wijnen, A. J., Lian, J. B., and Stein, G. S. (2005) The dynamic organization of gene-regulatory machinery in nuclear microenvironments. *EMBO Rep*. **6**, 128–133.
15. Osborne, C. S., Chakalova, L., Brown, K. E., Carter, D., Horton, A., Debrand, E., Goyenechea, B., Mitchell, J. A., Lopes, S., Reik, W., and Fraser, P. (2004) Active genes dynamically colocalize to shared sites of ongoing transcription. *Nat. Genet*. **36**, 1065–1071.

CCAAT/Enhancer-Binding Protein Beta Controls Differentiation-Specific Expression of Chromatin Remodeling Factor BRM

Toshinari Itoh, Katsuhide Miyake, and Shinji Iijima

Abstract The chromatin remodeling complex, SWI/SNF exclusively contains BRG1 or BRM as an ATPase subunit. So far, we have confirmed that the expression of BRM was very low in neural precursor cells and fetal liver cells, and induced to a high level in terminally differentiated neurons and astrocytes, and adult liver cells. The expression of BRM was very low in undifferentiated P19 cells and was induced to a high level during differentiation. In contrast, BRG1 was constantly expressed throughout differentiation. In this study, we analyzed developmental regulation of the brm gene. Luciferase reporter assays showed an increase in the transcriptional activity of the BRM promoter during differentiation of P19 cells. The promoter region of the brm gene contains two putative binding sites for CCAAT/enhancer-binding protein beta (C/EBPβ). Luciferase reporter assays showed that the binding of transcription factors C/EBPβ might stimulate the transcriptional activity of the BRM promoter.

Keywords SWI/SNF • neural cell differentiation • C/EBPβ

1 Introduction

Although the modification of chromatin structure is increasingly recognized as a key factor in transcriptional regulation, the mechanisms by which genomic DNA is packaged into chromatin, and the specific region that is unwound during the process of cellular differentiation have remained obscure. However, recent studies on histone acetyltransferases and deacetylases, histone methyltransferases, chromatin remodeling factors and several heterochromatin-specific DNA binding proteins have suggested

T. Itoh, K. Miyake, and S. Iijima
Department of Biotechnology, Graduate school of Engineering, Nagoya University, Furo-cho, Chikusa-ku, Nagoya 464-8603, Japan

K. Ikura et al. (eds.), *Animal Cell Technology: Basic & Applied Aspects*,
Animal Cell Technology: Basic & Applied Aspects 15,
DOI 10.1007/978-1-4020-9646-4_32, © Springer Science+Business Media B.V. 2009

that cells use various types of cellular machinery to establish and maintain various programs for controlling the state of chromatin and subsequent regulation of gene expression [1–6]. Among them, chromatin remodeling multisubunit complexes alter the organization of the nucleosome structure by hydrolyzing ATP. Mammalian chromatin remodeling complexes contain various ATPase subunits and these ATPases can be divided into three subfamilies, SWI2/SNF2, Mi-2/CHD and ISWI, based on their structures [7].

Mammalian SWI/SNF complexes consist of up to 15 subunits and contain BRG1 or BRM exclusively as the ATPase subunit. The SWI/SNF complex containing either BRG1 or BRM shows chromatin remodeling activity and activates or inactivates gene expression [8–14]. BRM and BRG1 have sequence homology to each other and were reported to have common and distinct roles. Although BRG1-associated factors (BAFs) such as BAF155, BAF170, BAF60 and INI1 are included in all types of complexes studied to date, there are several different complexes containing different combinations of BAFs and/or tissue-specific isoforms of a common subunit [15–18]. Furthermore, BRM and/or BRG1 complexes containing mSin3A and MeCP2, which are related to gene repression, are also detected [19–21]. SWI/SNF has been genetically shown to regulate subsets of inducible genes in yeast [22], and to associate with numerous regulators of gene activation in mammalian cells. These regulators include the glucocorticoid and estrogen receptors [8, 10, 23, 24], the retinoblastoma tumor suppressor protein, pRB [25], cyclin E [26], EKLF [12], CCAAT/enhancer-binding protein β (C/EBPβ) [14] and C/EBPα [27]. The association of these regulators with SWI/SNF directs recruitment of the complex to nucleosomal sites where stable remodeling occurs [28].

We have previously shown that the expression of BRM is upregulated through neural differentiation in mice, although that of BRG1 is downregulated [29]. To shed more light on the activity of SWI/SNF complexes in cell differentiation, we examined the mechanism regulating the transcription of the *brm* gene. We report here that the expression patterns of BRM and BRG1 are different during neural differentiation, and that C/EBPß regulates the expression of BRM.

2 Materials and Methods

2.1 Cell Culture

C33A and SW-13 cells were cultured in Dulbecco's modified Eagle's medium (GIBCO, 31,600-083) supplemented with 10% (v/v) fetal bovine serum. P19 embryonal carcinoma cells were maintained in αMEM (GIBCO, 12,000–063) containing 10% (v/v) fetal bovine serum. For differentiation into neural cells, cells were grown in the medium containing 0.5 μM all-trans retinoic acid (RA) (Wako) at a density of 1×10^6 cells per 100-mm bacteriological-grade petri dish. After 4 days, cell aggregates were transferred into tissue culture dishes and cultured in the

medium without inducers for an additional 6 days. All cultures were maintained at 37°C under humidified 5% CO_2.

2.2 Plasmids

To construct the mBRM promoter-luciferase reporter plasmids, the mBRM promoter regions (-1883- + 1, -1153- + 1, -536- + 1, -49- + 1) were amplified from mouse genomic DNA by PCR using a set of primers (forward primer; 5′-CATACGCGTACTGGCC TATCCTCAGGCAGA-3'' (-1883- + 1), 5′-CA-TACGCGTCTACGTGCAGGCA AATTGCAG-3′(-1153-+1),5′-CA-TACGCGTGCAGGCACACTTAAATTCCA-3′ (-536- + 1) and 5′-CATACG-CGTCGGCTGTCATCAATGAAGTC-3′ (-49- + 1) (*Mlu*I sites are underlined) and a reverse primer; 5′-CATAGATCTTACCTTGCTCG CGAGCAG-TG-3′, *Bgl*II sites are underlined). mBRG1 promoter regions (-1756- + 1, -96- + 1) were amplified from mouse genomic DNA by PCR using a set of primers (forward primer; 5′-CATCTCGAGTTGGGAACGGAATGGAGGT-C-3′ (-1756- + 1), 5′-CATCTCGAGACTAGTACGCGTGCGCACAG-3′ (-96- + 1), *Xho*I sites are underlined,and reverse primer;5′-CATAAGCTTGTAACGG-CGCCGTAACCTTC-3′, *Hin*dIII sites are underlined). These promoter regions were introduced into pGL3-basic vector (Promega).

2.3 Luciferase Reporter Gene Assay

C33A, SW13 and P19 embryonal carcinoma cells were seeded in 24-well plates and transfected with reporter plasmids using Lipofectamine 2000™ reagent (Invitrogen). One hundred nanogram of the luciferase reporter plasmid and 5 ng of the *Renilla* luciferase plasmid were introduced. Reporter gene assays were performed with a dual luciferase assay kit (Promega) according to the manufacturer's instruction. Luciferase activities were measured with a luminometer JNR II (Atto) and normalized to *Renilla* luciferase activity.

3 Results

3.1 Identification of Promoter Regions of the brg1 and brm Gene

Since genome sequences of mouse *brg1* and *brm* are available, transcription start sites for them can be estimated from cDNA sequence of these genes (Fig. 1). According to the results, putative TATA box was identified 17 bp upstream of the

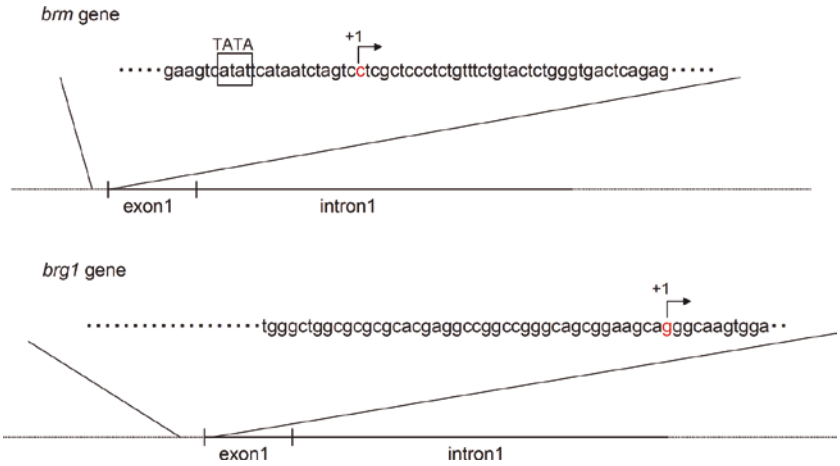

Fig. 1 The transcription start sites of the *brm* and *brg1* genes

transcription start sites for the *brm* gene. On the other hand, no TATA box was identified in the BRG1 promoter.

3.2 Analyses of Promoter Proximal Regions of mbrm and mbrg-1 Genes by Luciferase Reporter Assay

The changes in the expression level of BRG1 and BRM protein during P19 neural differentiation was determined by Western blotting as shown in Fig. 2.

The protein level of BRM increased through the differentiation although BRG1 was constant. To identify transcriptional control region of mouse *brg1* and *brm* genes, several deletion mutants in promoter-proximal-control regions were constructed and fused with the luciferase gene. The structure of the constructs and the results of luciferase assays using these plasmids in differentiated and undifferentiated P19 embryonal carcinoma cells were shown in Fig. 3. With the *brg1* gene, promoter proximal region up to −96 bp gave the highest activity independent on differentiation status of P19 cells. With the *brm* gene, the longest construct which covers over −1.8 kb region gave the highest luciferase activity and the plasmid contains up to −1153 gave a half of the maximum activity. These results suggested that multiple transcription factor binding sites reside in this region and activate the gene expression. Totally, the BRM promoter showed much higher activity in differentiated P19 cells than in undifferentiated cells. By the computer analyses of transcription-factor binding sites in the promoter region of *brm*, we found two putative C/EBPβ binding sites (-786- -774, -1397- -1384). These binding sites were not found in the BRG1 promoter region. Therefore, the transcription factor C/EBPβ may play important roles

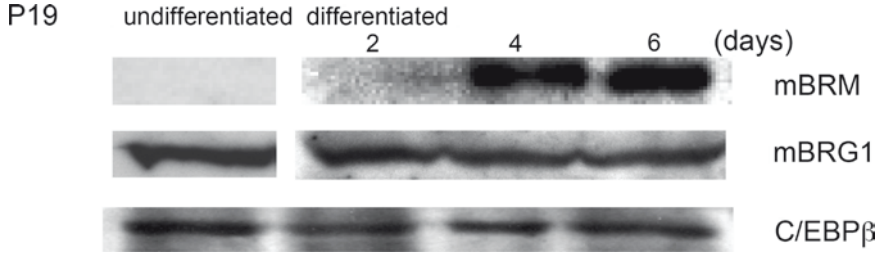

Fig. 2 Expression of mBRM, mBRG1 and C/EBPβ during differentiation of P19 cells

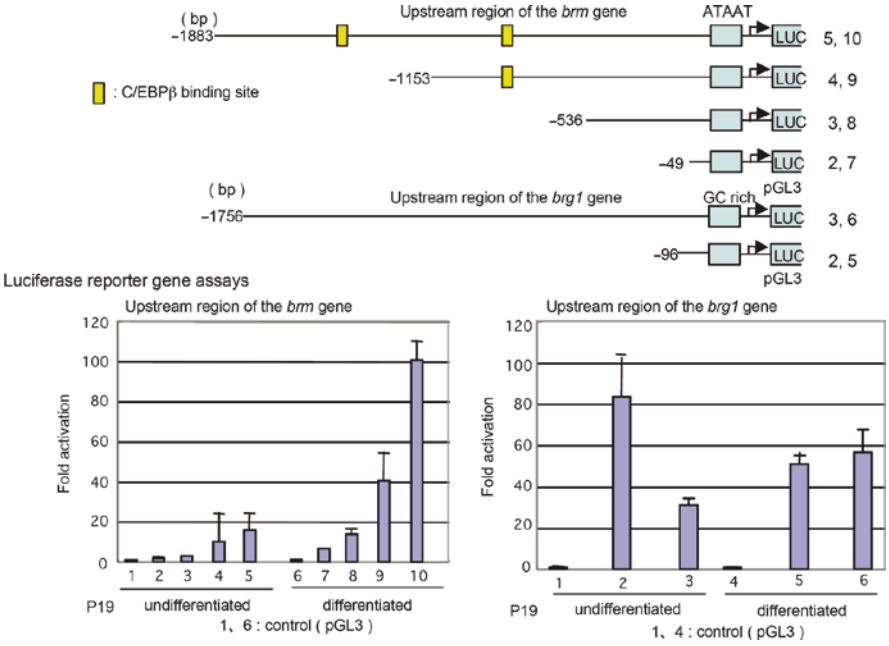

Fig. 3 The transcriptional activity of the mBRM and mBRG1 promoter in P19 cells during differentiation

in specific expression of the *brm* gene in differentiated cells. Indeed, luciferase assays indicated that deletion of the region containing C/EBPβ binding sites showed significant reduction of promoter activity. Furthermore, C/EBPβ is known to be expressed in a wide variety of differentiated cells. However, the expression level of C/EBPβ was constant during differentiation of P19 cells (Fig. 3). Further study will be required for clarifying the role of C/EBPβ.

4 Discussion

It has been speculated that SWI/SNF plays important roles in the induction or maintenance of gene expression through cell differentiation [12, 14]). In neural precursor cells (data not shown) and P19 cells, expression of BRM increased during differentiation to neural cells. This results support the hypothesis that BRM plays an important role in neural differentiation. Increased expression of BRM was also observed in differentiation of P19 cells to other cell types and liver differentiation, suggesting that BRM may generally work in differentiation.

In this study, the results suggested that *brm* expression was partly controlled by C/EBPβ. However, we cannot explain the differentiation specific expression of *brm* just with C/EBPβ since the C/EBPβ level in the differentiation was almost constant as shown in Fig. 2. It is reasonably assumed that other transcription factor also activates or inactivates the *brm* expression in cell type specific manner with the cooperation with C/EBPβ.

References

1. Bird, A. P. and Wolffe, A. P. (1999) Methylation-induced repression-belts, braces, and chromatin. *Cell* **99**, 451–454.
2. Kingston, R. E. and Narlikar, G. J. (1999) ATP-dependent remodeling and acetylation as regulators of chromatin fluidity. *Genes Dev.* **13**, 2339–2352.
3. Knoepfler, P. S. and Eisenman, R. N. (1999) Sin meets NuRD and other tails of repression. *Cell* **99**, 447–450.
4. Kouzarides, T. (1999) Histone acetylases and deacetylases in cell proliferation. *Curr. Opin. Genet. Dev.* **9**, 40–48.
5. Berger, S. L. (2002) Histone modifications in transcriptional regulation. *Curr. Opin. Genet. Dev.* **12**, 142–148.
6. Workman, J. L. and Kingston, R. E. (1998) Alteration of nucleosome structure as a mechanism of transcriptional regulation. *Annu. Rev. Biochem.* **67**, 545–579.
7. Eisen, J. A., Sweder, K. S., and Hanawalt, P. C. (1995) Evolution of the SNF2 family of proteins: subfamilies with distinct sequences and functions. *Nucleic Acids Res.* **23**, 2715–2723.
8. Chiba, H., Muramatsu, M., Nomoto, A., and Kato, H. (1994) Two human homologues of *Saccharomyces cerevisiae SWI2/SNF2* and *Drosophila brahma* are transcriptional activators cooperating with the estrogen receptor and the retinoic acid receptor. *Nucleic Acids Res.* **22**, 1815–1820.
9. Singh, P., Coe, J., and Hong, W. (1995) A role for retinoblastoma protein in potentiating transcriptional activation by the glucocorticoid receptor. *Nature* **374**, 562–565.
10. Ichinose, H., Garnier, J.-M., Chambon, P., and Losson, R. (1997) Ligand-dependent interaction between the estrogen receptor and the human homologues of SWI2/SNF2. *Gene* 188, 95–100.
11. Trouche, D., Chalony, C. L., Muchardt, C., Yaniv, M., and Kouzarides, T. (1997) RB and hbrm cooperate to repress the activation functions of E2F1. *Proc. Natl. Acad. Sci. USA* **94**, 11268–11273.
12. Armstrong, J. A., Bieker, J. J., and Emerson, B. M. (1998) A SWI/SNF-related chromatin remodeling complex, E-RC1, is required for tissue-specific transcriptional regulation by EKLF in vitro. *Cell* **95**, 93–104.
13. Murphy, D. J., Hardy, S., and Engel, D. A. (1999) Human SWI-SNF component BRG1 represses transcription of the c-fos gene. *Mol. Cell. Biol.* **19**, 2724–2733.

14. Kowenz-Leuts, E. and Leutz, A. (1999) A C/EBPβ isoform recruits the SWI/SNF complex to activate myeloid genes. *Mol. Cell* **4**, 735–743.
15. Wang, W., Xue, Y., Zhou, S., Kuo, A., Cairns, B. R., and Crabtree, G. R. (1996) Diversity and specialization of mammalian SWI/SNF complexes. *Genes Dev.* **10**, 2117–2130.
16. Wang, W., Cote, J., Xue, Y., Zhou, S., Khavari, P. A., Biggar, S. R., Muchardt, C., Kalpana, G. V., Goff, S. P., Yaniv, M., Workman, J. L., and Crabtree, G. R. (1996) Purification and biochemical heterogeneity of the mammalian SWI-SNF complex. *EMBO J.* **15**, 5370–5382.
17. Nie, Z., Xue, Y., Yang, D., Zhou, S., Deroo, B. J., Archer, T. K., and Wang, W. (2000) A specificity and targeting subunit of a human SWI/SNF family-related chromatin-remodeling complex. *Mol. Cell. Biol.* **20**, 8879–8888.
18. Debril, M.-B., Gelman, L., Fayard, E., Annicotte, J.-S., Rocchi, S., and Auwerx, J. (2004) Transcription factors and nuclear receptors interact with the SWI/SNF complex through the BAF60c subunit. *J. Biol. Chem.* **279**, 16677–16686.
19. Sif, S., Saurin, A. J., Imbalzano, A. N., and Kingston, R. E. (2001) Purification and characterization of mSin3A-containing Brg1 and hBrm chromatin remodeling complexes. *Genes Dev.* **15**, 603–618.
20. Pal, S., Yun, R., Datta, A., Lacomis, L., Erdjument-Bromage, H., Kumar, J., Tempst, P., and Sif, S. (2003) mSin3A/histone deacetylase 2- and PRMT5-containing Brg1 complex is involved in transcriptional repression of the Myc target gene cad. *Mol. Cell. Biol.* **23**, 7475–7487.
21. Harikrishnan, K. N., Chow, M. Z., Baker, E. K., Pal, S., Bassal, S., Brasacchio, D., Wang, L., Craig, J. M., Jones, P. L., Sif, S., and El-Osta, A. (2005) Brahma links the SWI/SNF chromatin-remodeling complex with MeCP2-dependent transcriptional silencing. *Nat. Genet.* **37**, 254–264.
22. Sudarsanam, P., Iyer, V. R., Brown, P. O., and Winston, F. (2000) Whole-genome expression analysis of *snf/swi* mutants of *Saccharomyces cerevisiae*. *Proc. Natl. Acad. Sci. USA* **97**, 3364–3369.
23. Fryer, C. J. and Archer, T. K. (1998) Chromatin remodeling by the glucocorticoid receptor requires the BRG1 complex. *Nature* **393**, 88–91.
24. Muchardt, C. and Yaniv, M. (1993) A human homologue of *Saccharomyces cerevisiae SNF2/SWI2* and *Drosophila brm* genes potentiates transcriptional activation by the glucocorticoid receptor. *EMBO J.* **12**, 4279–4290.
25. Dunaief, J. L., Strober, B. E., Guha, S., Khavari, P. A., Alin, K., Luban, J., Begemann, M., Crabtree, G. R., and Goff, S. P. (1994) The retinoblastoma protein and BRG1 form a complex and cooperate to induce cell cycle arrest. *Cell* **79**, 119–130.
26. Shanahan, F., Seghezzi, W., Parry, D., Mahony, D., and Lees, E. (1999) Cyclin E associates with BAF155 and BRG1, components of the mammalian SWI-SNF complex, and alters the ability of BRG1 to induce growth arrest. *Mol. Cell. Biol.* **19**, 1460–1469.
27. Pedersen, T. A., Kowenz-Leutz, E., Leutz, A., and Nerlov, C. (2001) Cooperation between C/EBPα TBP/TFIIB and SWI/SNF recruiting domains is required for adipocyte differentiation. *Genes Dev.* **15**, 3208–3216.
28. Kadam, S., McAlpine, G. S., Phelan, M. L., Kingston, R. E., Jones, K. A., and Emerson, B. M. (2000) Functional selectivity of recombinant mammalian SWI/SNF subunits. *Genes Dev.* **14**, 2441–2451.
29. Machida, Y., Murai, K., Miyake, K., and Iijima, S. (2001) Expression of chromatin remodeling factors during neural differentiation. *J. Biochem.* **129**, 43–49.

Involvement of 67 kDa Laminin Receptor on Cellular Uptake of Green Tea Polyphenol Epigallocatechin-3-*O*-Gallate in Caco-2 Cells

Shino Ohta, Yoshinori Fujimura, Koji Yamada, and Hirofumi Tachibana

Abstract The major polyphenol in green tea, (−)-epigallocatechin-3-*O*-gallate (EGCG) has been shown to prevent carcinogenesis. Most recently, we have identified the metastasis-associated 67 kDa laminin receptor (67LR) as a cell surface receptor that mediates the anti-cancer and anti-allergic activities of EGCG. We have established human colon cancer Caco-2 cells expressing elevated or reduced 67LR by transfecting with the 67LR gene or 67LR-specific siRNA. Enhanced expression of 67LR in Caco-2 cells increased the growth inhibitory activity of EGCG correlating with the EGCG binding to the cell surface, whereas the 67LR-downregulated cells have lost the ability to bind EGCG and the response to the EGCG activity. We evaluated the levels of cellular uptake of EGCG in these cells to investigate an involvement of 67LR on EGCG cellular uptake. As a result, the enhanced 67LR-expression reduced the uptake level of EGCG, whereas the 67LR-downregulated cells have increased it. These results suggest that 67LR associates with the cellular uptake of EGCG in Caco-2 cells.

Keywords 67 kDa laminin receptor • EGCG • Caco-2 • uptake

1 Introduction

Tea (*Camellia sinensis*) is one of the most popular beverages worldwide. Among the biological activities of tea, the cancer-preventive activity has attracted the greatest attention. Several epidemiological studies as well as animal studies suggest that green tea has a protective effect against a variety of cancer types, such as lung, prostate and breast [1]. This effect has been attributed to the biologically active polyphenol, EGCG

S. Ohta, Y. Fujimura, K. Yamada, H. Tachibana
Department of Bioscience and Biotechnology, Faculty of Agriculture, Kyushu University, 6-10-1 Hakozaki, Higashi-ku, Fukuoka, 812-8581, Japan

K. Ikura et al. (eds.), *Animal Cell Technology: Basic & Applied Aspects*,
Animal Cell Technology: Basic & Applied Aspects 15,
DOI 10.1007/978-1-4020-9646-4_33,

[2, 3]. EGCG has also been reported to have various biological activities including anti-inflammation [4–6], anti-metastatic [7], and anti-oxidation [8, 9]. However, cellular uptake was poorly understood. Without this knowledge, it is difficult to identify the primary targets of action of these compounds and to elucidate the mechanisms of their actions. We have recently identified the 67 kDa laminin receptor (67LR) as a cell surface receptor that mediates the anti-tumor action of EGCG [10]. Here, to investigate an involvement of 67LR on EGCG cellular uptake, we have constructed both 67LR-overexpressed or -downregulated human colon cancer cell line Caco-2.

2 Materials and Methods

2.1 Reagents

(−)-Epigallocatechin-3-*O*-gallate (EGCG) was purchased from Sigma Co. (St. Louis, MO). Methyl gallate was purchased from Tokyo Kasei Kogyo Co., Ltd. (Tokyo, Japan). Mouse anti-67LR monoclonal antibody (MLuC5) was purchased from NeoMarkers (Fremont, CA). Mouse anti-β-actin monoclonal antibody and FITC-conjugated anti-mouse IgM antibody was from Sigma Co. (St. Louis, MO). Recombinant Mouse IgM and HRP-conjugated anti-mouse IgM or IgG antibody was from Zymed Laboratories Inc. (San Francisco, CA).

2.2 Cell Culture

Caco-2 cells were maintained in Dulbecco's modified Eagle's medium (DMEM) (Cosmo Bio Co., Ltd., Tokyo, Japan) supplemented with 10% fetal calf serum (FCS) (PAA Laboratories GmbH, Austria), 1% non-essential amino acid (Hyclone Inc.), 100 U/ml penicillin G, 100 μg/ml streptomycin and 10 mM HEPES buffer. The cells were cultured at 37°C in a humidified atmosphere with 5% CO2.

2.3 Cell Construction

The 67LR gene expression vector or the 67LR mRNA-targeting short interfering RNA expression vector were transfected into Caco-2 cells by electroporation.

2.4 Western Blot Analysis

Caco-2 cells transfected with the 67LR vector or 67LR-specific siRNA expression vector were washed and lysed in cell lysis buffer containing 50 mM Tris-HCl (pH 7.5), 150 mM NaCl, 1% Triton-X 100, 1 mM EDTA, 50 mM NaF, 30 mM

Na4PO7, 1 mM phenylmethanesulfonyl fluoride (PMSF), 2.0 μg/ml aprotinin, and 1 mM pervanadate. Whole cell lysate samples were loaded onto 10% sodium dodecyl sulfate-polyacrylamide gel, and electrophoresis was done under reducing condition. The samples were then electrotransferred onto a nitrocellulose membrane. The blotted nitrocellulose was probed for 67LR and β-actin using anti-laminin receptor antibody (MLuC5) and anti-β-actin receptor antibody.

2.5 Flow Cytometric Analysis

Caco-2 cells transfected with the 67LR vector or 67LR-specific siRNA expression vector were incubated with anti-67LR specific antibody (MLuC5) followed by FITC-conjugated goat anti-mouse IgM antibody. The cell surface expression of 67LR was assayed using a flow cytometer (FACSCalibur).

2.6 Surface Plasmon Resonance Biosensor Assay

The 67LR-overexpressed or -downregulated Caco-2 cells were fixed on the sensor chip. The binding of EGCG to immobilized cell surface was measured using a surface plasmon resonance (SPR) biosensor SPR670.

2.7 Growth Inhibitory Activity Assay

67LR-overexpressed or -downregulated Caco-2 cells were pre-cultured at cultured with or without EGCG for 72 h. After the culture, adherent cells were counted and indicated as growth inhibition rate.

2.8 Cellular Uptake Analysis

67LR-overexpressed or -downregulated Caco-2 cells were incubated with EGCG (10 μM) for 30 min at 37°C. The cellular uptake of EGCG was analyzed by HPLC with the electrochemical detector (ECD) method. Values are shown as relative peak area under the curve of EGCG normalized with that of internal standard (Methyl gallate).

2.9 Statistical Analysis

All values are expressed as means ± S.D. (n = 3) compared with controls. Statistical analysis was performed by use of the Student *t*-test.

3 Results and Discussion

We established 67LR-overexpressed or -downregulated human colon cancer cells Caco-2 by transfecting with the 67LR gene or 67LR-specific siRNA.

To elucidate whether the expression of 67LR is enhanced or reduced in these transfected cells, the expression of 67LR was examined. Western blot analysis showed that higher expression level of 67LR in the 67LR transfected cells or lower level in the 67LR-specific siRNA transfected cells as compared with each control cells transfected with empty vector. Flowcytometric analysis indicated that the cell surface expression of 67LR was also regulated likewise.

We have previously reported that EGCG can inhibit the cancerous cell growth mediated through the binding to the 67LR [10]. To check the validity, as to cellular functions of EGCG, of the modulation of 67LR expression, the binding of EGCG to these cells was measured by the SPR assay. This analysis demonstrated that the 67LR-overexpressed cells have increased binding of EGCG to the cell surface, whereas such binding was reduced in the 67LR-downregulated cells. In addition to this binding test, as another validity test, the suppressive activity of EGCG on the cell growth in both cells was examined. The control cells transfected with empty vector showed little growth inhibition with EGCG treatment at the concentration of 1 μM (which is physiologically relevant concentration in human after tea drinking), whereas the 67LR-overexpressed cells demonstrated considerable inhibition with the same EGCG treatment. The control cells showed considerable growth inhibition with 5 μM EGCG treatment, on the other hand, in the 67LR-downregulated cells, this growth inhibitory effect of EGCG was disappeared. These results suggested that 67LR is involved in the binding of EGCG to the cell surface and mediates the growth inhibitory effect of EGCG on Caco-2 cells.

To clarify an involvement of 67LR in EGCG cellular uptake, levels of EGCG uptake in both established cells were examined by HPLC-ECD method. As shown in Fig. 1, the amount of EGCG's uptake in 67LR-overexpressed cells was reduced

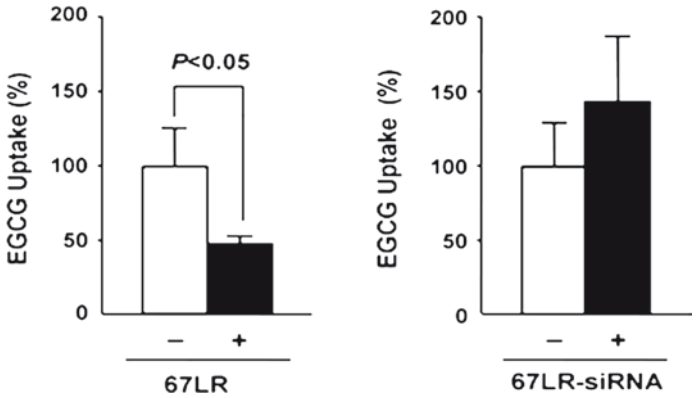

Fig. 1 The EGCG cellular uptake in 67LR-overexpressed or -downregulated Caco-2 cells

as compared to the control cells. On the other hand, the 67LR-downregulation caused an increased uptake of EGCG. These results showed a negative association between the cellular uptake of EGCG and the 67LR expression in Caco-2 cells, suggesting that the 67LR may participate in the cellular uptake process of EGCG.

References

1. Yang, C. S., Maliakal, P. and Meng, X. *Annu. Rev. Pharmacol. Toxicol.* **42**, 25–54 (2002).
2. Katiyar, S. K. and Mukhtar, H. *Int. J. Oncol.* **8**, 221–238 (1996).
3. Yamane, T.et al. *Cancer Res.* **55**, 2081–2084 (1995).
4. Mizushina, Y. et al. *Biochem. Biophys. Res. Commun.* **333**, 101–109 (2005).
5. Kim, S. H. et al. *FEBS. Lett.* **580**, 1883–1890 (2006).
6. Aktas, O. et al. *J. Immunol.* **173**, 5794–5800 (2004).
7. Caltagirone, S. et al. *Int. J. Cancer* **87**, 595–600 (2000).
8. Caturla, N. et al. *Free Radic. Biol. Med.* **34**, 648–662 (2003).
9. Maeda, K. et al. *Atherosclerosis* **166**, 23–30 (2003).
10. Tachibana, H. et al. *Nat. Struct. Mol. Biol.* **11**, 380–381 (2004).

Inositol Derivatives Stimulate Glucose Transport in Muscle Cells

Angeline Yap, Shin Nishiumi, Ken-ichi Yoshida, and Hitoshi Ashida

Abstract Inositol derivatives are natural ingredients found in plants and animals. Some of them have been reported to help the action of insulin, which induces glucose uptake involving the translocation of glucose transporter 4 (GLUT4) to the plasma membrane particularly in muscle tissues. Here, we investigated the effect of eight inositol derivatives on glucose uptake in L6 muscle myotubes, and on GLUT 4 translocation to plasma membrane in ex vivo assay using murine skeletal muscle. At 1 mM, seven inositol derivatives other than *myo*-inositol stimulated glucose uptake in the absence of insulin. However, at 100 μM, only L-*chiro*-inositol, *muco*-inositol and *epi*-inositol increased the glucose uptake compared to control. The ex vivo assay confirmed that D-pinitol, D-*chiro*-inositol, L-*chiro*-inositol, *muco*-inositol and *epi*-inositol stimulated GLUT4 translocation. These results suggest that inositol derivatives can exert insulin-like effect in muscle cells.

Keywords Inositol • glucose uptake • GLUT4 • muscle cells

1 Introduction

The ability of insulin to mediate tissue glucose uptake is important in the maintenance of postprandial glucose homeostasis. Glucose uptake in peripheral cells such as muscle cells is mediated by glucose transporter 4 (GLUT4). GLUT4 is translocated from the endoplasmic reticulum to the plasma membrane upon stimulation by insulin to facilitate the disposal of glucose into the cells [1]. A defect in glucose transport efficiency and GLUT4 activity results in insulin resistance [2].

1,2,3,4,5,6-Cyclohexanehexol, generically called inositol, is a class of compounds which forms nine distinct stereoisomers through epimerization of the six hydroxyl

A. Yap, S. Nishiumi, K. Yoshida, and H. Ashida
Department of Agrobioscience, Graduate School of Agricultural Science, Kobe University, Rokkodai, Nada-ku, Kobe, 657-8501, Japan

K. Ikura et al. (eds.), *Animal Cell Technology: Basic & Applied Aspects*,
Animal Cell Technology: Basic & Applied Aspects 15,
DOI 10.1007/978-1-4020-9646-4_34,

groups. Some of these derivatives have been reported to possess various biological functions for the treatment of diseases such as depression, panic disorder, polycystic ovary syndrome, etc. [3–5]. Furthermore, D-*chiro*-inositol [6] and D-pinitol (3-*O*-methyl-D-*chiro*-inositol) [7–9] have demonstrated to possess insulin mimetic activity, and are effective against insulin resistance. However, the effectiveness of the other inositol derivatives, differing only in the position of the hydroxyl groups, has not been evaluated. Hence, we investigated the effect of eight inositol derivatives on glucose transport in muscle cells.

2 Materials and Methods

2.1 Materials

Modified Eagle's medium (MEM) was obtained from Nissui Pharmaceutical (Tokyo, Japan). Fetal bovine serum (FBS) was purchased from Equitech-Bio, Inc. (Kerrville, TX). D-Pinitol, D-*chiro*-inositol, L-*chiro*-inositol, *muco*-inositol, *epi*-inositol, *allo*-inositol, *scyllo*-inositol and *myo*-inositol were kindly supplied by Hokko Chemical Industry Co., Ltd (Tokyo, Japan). 2-Deoxy-D-[^{3}H]-glucose (2DG) was purchased from American Radiolabeled Chemicals, Inc. (St. Louis, MO). Anti-GLUT4 and anti-goat antibodies were purchased from Santa Cruz Biotechnology (Santa Cruz, CA). ECL plus™ was from GE Healthcare Bio-Sciences Corp. (Piscataway, NJ).

2.2 Cell Culture

L6 myoblasts were maintained in MEM supplemented with 10% FBS at 37°C in a 5% CO_2 atmosphere. Myoblasts were grown to confluence in 24-well plates, and the medium was replaced with MEM containing 2% FBS to induce differentiation into myotubes. Fully differentiated myotubes were serum-starved for 18 h in MEM containing 0.2% bovine serum albumin prior to experiments.

2.3 Glucose Uptake Assay

Differentiated L6 myotubes were exposed to 100 nM insulin or inositol derivatives (1 mM or 100 μM) in Krebs-Ringer HEPES (KRH) buffer (50 mM HEPES, pH 7.4, 137 mM NaCl, 4.8 mM KCl, 1.85 mM $CaCl_2$, and 1.3 mM $MgSO_4$) for 15 min followed by an additional incubation period of 5 min with 2DG (6.5 mM, 0.5 μCi). The cells were washed 4 times with ice-cold KRH buffer, solubilized by adding

250 μl of 0.05 N NaOH and transferred to vials with scintillation cocktail. The radioactivity in the cells was measured by liquid scintillation β counter. Non-specific uptake was measured using the cells pretreated with 20 μM cytochalasin B.

2.4 Ex Vivo Assay

Murine skeletal muscle was enucleated from the hind legs and chopped into small pieces. One hundred mg skeletal muscle was incubated with 1 mM inositol derivatives or 100 nM insulin in 3 ml KRH buffer for 15 min at 37°C with continuous shaking, and then immediately washed twice with ice-cold KRH buffer. The skeletal muscle cells were homogenized in Buffer A (10 mM Tris, pH 7.8, 10 mM KCl, 1.5 mM $MgCl_2$, 1 mM phenylmethylsulfonylfluoride, 0.5 mM dithiothreitol, 5 μg/ml aprotinin and 10 μg/ml leupeptin) containing 0.1% Nonidet® P-40 and passed through 22-gauge needle three times. Homogenates were spun at 1,000 × g for 10 min at 4°C. The pellet was resuspended in Buffer A and spun at 1,000 × g for another 10 min at 4°C. Plasma membrane fraction was obtained by resuspending the resulting pellet in Buffer A containing 1% Nonidet® P-40, and centrifuging at 10,000 × g for 20 min at 4°C. Supernatant was collected and subjected to Western blot analysis.

2.5 Western Blot Analysis

Aliquots of the plasma membrane fraction (10 μg protein) were separated by 10% SDS-polyacrylamide gel electrophoresis (SDS-PAGE), and transferred onto a PVDF membrane. The membrane was blocked with 1% (w/v) non-fat dry milk in TBST (10 mM Tris-HCl, pH 8.0, 150 mM NaCl and 0.05% Tween-20) and incubated with anti-GLUT4 for 1 h at room temperature. The membrane was further incubated with horseradish peroxidase-conjugated anti-goat antibody for 1 h at room temperature and enhanced using ECL plus™ detection kit.

3 Results

3.1 Inositol Derivatives Stimulate Glucose Uptake in L6 Myotubes

Peripheral tissue such as skeletal muscle is important to maintain the postprandial plasma glucose level [1]. Therefore, we investigated the effects of eight inositol derivatives in vitro using murine L6 muscle cells. Seven inositol derivatives other

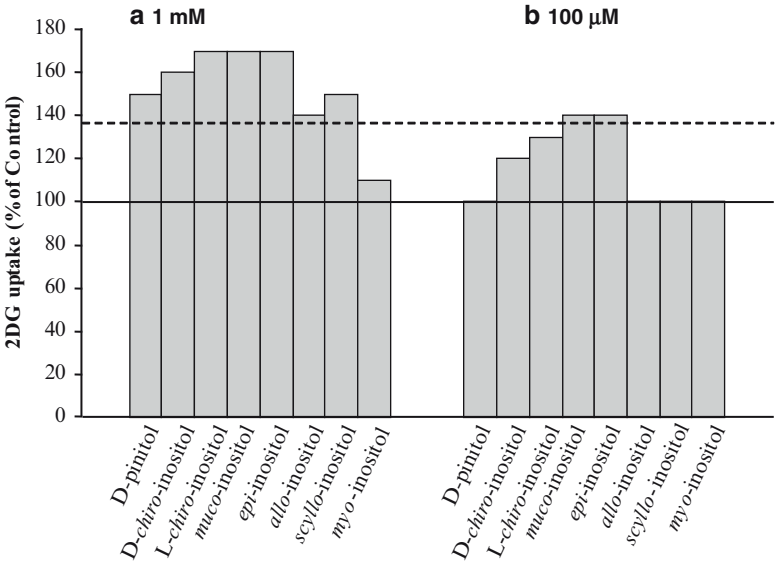

Fig. 1 Effect of inositol derivatives on glucose uptake in L6 myotubes. Treatment of cells with inositol derivatives at (**a**) 1 mM and (**b**) 100 μM. The solid line represents basal glucose uptake while the broken line represents the cells treated with 100 nM insulin. The data shown are mean of results from at least three independent experiments

than *myo*-inositol stimulated glucose uptake in L6 myotubes at 1 mM in the absence of added insulin (Fig. 1a). In addition D-*chiro*-inositol, L-*chiro*-inositol, *muco*-inositol, and *epi*-inositol showed a significant increase in the glucose uptake as compared to insulin (Fig. 1a).

To determine the effect at a lower dose of inositol derivatives, L6 myotubes were then incubated with the derivatives at 100 μM. At the lower dose, only L-*chiro*-inositol, *muco*-inositol and *epi*-inositol significantly exert an increase in glucose uptake as compared to control (Fig. 1b).

3.2 Inositol Derivatives Stimulate Translocation of GLUT4 to the Plasma Membrane Ex Vivo

To determine whether translocation of GLUT4 might be a mechanism by which inositol derivatives increased glucose uptake, we performed the ex vivo assay. Treatment of murine skeletal muscle with 100 nM insulin showed an increase in GLUT4 translocation to the plasma membrane. Furthermore, D-pinitol, D-*chiro*-inositol, L-*chiro*-inositol, *muco*-inositol and *epi*-inositol at 1 mM appeared to

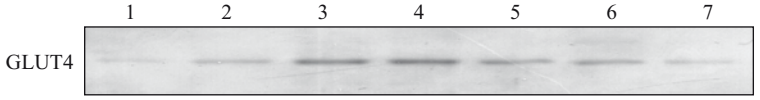

Fig. 2 Effect of inositol derivatives on GLUT4 translocation in murine skeletal muscle: 1, basal; 2, insulin; 3, D-pinitol; 4, D-*chiro*-inositol; 5, L-*chiro*-inositol; 6, *muco*-inositol and 7, *epi*-inositol

induce translocation of GLUT4 to the plasma membrane no less efficiently than insulin (Fig. 2).

4 Discussion

Here, we report that at 1 mM, apart from D-pinitol and D-*chiro*-inositol, L-*chiro*-inositol, *muco*-inositol, *epi*-inositol, *allo*-inositol and *scyllo*-inositol also improved glucose uptake in cultured L6 muscle cells. Our results also showed that at 1 mM, D-pinitol increased glucose uptake 50% over control in L6 myotubes (Fig. 1a) coinciding with previous observation [7]. We observed that *myo*-inositol failed to exert an effect on glucose uptake (Fig. 1a). This result is consistent with the previous results that *myo*-inositol did not possess any hypoglycaemic effect [9, 10]. It has previously been documented that D-pinitol did not exert a significant effect when treated at a lower dose [7, 8]. Hence, we examined the effect of 100 μM inositol derivatives in L6 myotubes. Interestingly, we found that L-*chiro*-inositol, *muco*-inositol and *epi*-inositol exert an effect almost similar to insulin (Fig. 1b). From these results, on top of the reported effective D-pinitol and D-*chiro*-inositol, we selected L-*chiro*-inositol, *muco*-inositol and *epi*-inositol for further analysis.

Treatment with 100 nM insulin increased GLUT4 translocation to the skeletal muscle (Fig. 2) and glucose uptake in the cultured muscle cells (Fig. 1), which is in agreement with previous reports that insulin induces glucose uptake and GLUT4 translocation [11]. The ex vivo assay performed on all five effective inositol derivatives showed that the glucose uptake was indeed stimulated by translocation of GLUT4 to the plasma membrane. However, the ability to stimulate GLUT4 translocation and improve glucose uptake differed among the inositol derivatives. D-Pinitol and D-*chiro*-inositol stimulated GLUT4 translocation to the plasma membrane more obviously than the others. This is consistent with previous reports that both compounds have insulin mimetic activity in vivo [6–9]. On the other hand, GLUT4 translocation stimulated by L-*chiro*-inositol, *muco*-inositol and *epi*-inositol did not correlate with the results from glucose uptake in L6 muscle cells. This inconsistency might be due to the difference in the cells used.

In conclusion, inositol derivatives are able to stimulate glucose transport in muscle cells. However the mechanism of action is still unknown and in the future, we will elucidate the mechanism involved in the effect of inositol derivatives on glucose transport in L6 muscle cells.

References

1. A. Klip and M. Ishiki, Recent developments in the regulation of glucose transporter-4 traffic: new signals, locations, and partners, *Endocrinology* **146**(12), 5071–5078 (2005).
2. K.F. Petersen and G.I. Shulman, Etiology of insulin resistance, *Am J Med* **119**(5A), 10S–16S (2006).
3. J. Benjamin, G. Agam, J. Levine, Y. Bersudsky, O. Kofman, and R.H. Belmaker, Inositol treatment in psychiatry, *Psychopharmacol Bull* **31**(1), 167–175 (1995).
4. M.J. Iuorno, D.J. Jakubowicz, J.P. Baillargeon, P. Dillon, R.D. Gunn, G. Allan, and J.E. Nestler, Effects of D-*chiro*-inositol in lean women with the polycystic ovary syndrome, *Endocr Pract* **8**(6), 417–423 (2002).
5. J. McLaurin, R. Golomb, A. Jurewicz, J.P. Antel, and P.E. Fraser, Inositol stereoisomers stabilize an oligomeric aggregate of Alzheimer amyloid beta peptide and inhibit abeta-induced toxicity, *J Biol Chem* **275**(24), 18495–18502 (2000).
6. J.M. Kawa, C.G. Taylor, and R. Przybylski, Buckwheat concentrate reduces serum glucose in streptozotoxin-diabetic rats, *J Agric Food Chem* **51**(25), 7287–7291 (2003).
7. S.H. Bates, R.B. Jones, and C.J. Bailey, Insulin-like effect of pinitol, *Br J Pharmacol* **130**(8), 1944–1948 (2000).
8. C.E. Weeks and N. Albany, Stimulating transport of glucose into animal tissue by the administration of pinitol, US Patent 6,518,318 B1, 11 Feb 2003.
9. R.E. Ostlund and W.R. Sherman, Pinitol and derivatives thereof for the treatment of metabolic disorders, US Patent **5**,827,896, 27 Oct 1998.
10. H.K. Ortmeyer, L.C. Huang, L. Zhang, B.C. Hansen, and J. Larner, Chiroinositol deficiency and insulin resistance. II. Acute effects of D-chiroinositol administration in streptozotocin-diabetic rats, normal rats given a glucose load, and spontaneously insulin-resistant rhesus monkeys, *Endocrinology* **132**(2), 646–651 (1993).
11. A.H. Khan and J.E. Pessin, Insulin regulation of glucose uptake: a complex interplay of intracellular signaling pathways, *Diabetologia* **45**(11), 1475–1483 (2002).

Hair Growth Regulation by an Aromatic Plant Extract

Mitsuko Kawano, Mohamed Elyes Kchouk, and Hiroko Isoda

Abstract Recently, people are experiencing more stress and some have problems regarding hair growth as a part of the aging process. Resolving this hair growth problem is important for the aging society in the future. This is because not only bodily health but also mental health is important for a healthy life. Thus, we attempted to find plants having hair growth regulation activity.

The Republic of Tunisia is located in North Africa; its northern boundary faces the Mediterranean Sea while its southern side leads to the Sahara Desert. The distance during the Mediterranean Sea and the Sahara Desert is only few kilometers. This environment can be considered that dry inclination is very high. In such environment, plants can accumulate antistress factors in their system. Thus, we collected many plant extracts from Tunisia for bioprospecting purposes. We show that a Tunisian aromatic plant extract has a high activity for promotion of hair growth cycle, or induction of anagen phase from telogen phase.

Keywords Hair growth cycle • dermal papilla • MTT assay • vasodilatation

1 Introduction

The hair growth cycle has three main stages, anagen, catagen and telogen. Anagen is the growth phase of the hair cycle. In this phase, hair follicles grow deep in the dermis, and hairs are made from extracellular matrix cells as melanins are introduced into hair shafts. Anagen hair follicles are long and big, while catagen is the regression

M. Kawano and H. Isoda
Alliance for Research on North Africa (ARENA), Graduate School of Life and Environmental Sciences, University of Tsukuba, 1-1-1 Tennodai, Tsukuba, Ibaraki 305-8572, Japan

M.E. Kchouk
Bordj Cedria Technopark BP95, Hammam-Lif 2050, Tunisie

K. Ikura et al. (eds.), *Animal Cell Technology: Basic & Applied Aspects*,
Animal Cell Technology: Basic & Applied Aspects 15,
DOI 10.1007/978-1-4020-9646-4_35,

phase of the hair cycle. In this phase, hair follicles regress to the shallow portion of the dermis from the epidermis. Telogen is the resting phase of the hair cycle. In this phase, hair follicles do not have any activity, and hair shafts fall out. On the other hand, the falling out of hair shafts is called exogen. These three stages are cycling and hair molt occurs continuously. Normally in humans, anagen continues for 3–4 years in male hair follicles and 4–6 years in female hair follicles [1, 2].

In the hair growth cycle, the most important element of hair follicles and skin is the dermal papilla. Dermal papilla cells are found at the bottom of each hair follicle. Although most hair follicle cell lines are differentiated from the ectoderm, the dermal papilla is differentiated from the mesoderm. The most important role of the dermal papilla is the regulation of hair growth. Signals to regulate hair growth from the dermal papilla stimulate hair follicle cells (such as outer root sheath cells), and then hair growth or hair regression is promoted [3].

The most useful and rapid method for evaluating hair growth promotion is by determining the dermal papilla growth rate as influenced by various samples [4]. After that, more detailed studies should be performed such as in vivo assay [3–11].

We collected many aromatic plants from Tunisia, which is located in North Africa. The northern side of Tunisia faces the Mediterranean Sea while the south leads to the Sahara. From the Mediterranean Sea to the Sahara, the distance is only a few hundred kilometers. This denotes that the dryness gradient is high, and animals and plants living in this region harbor many physiologically active compounds in their body. For the maintenance of skin homeostasis, some physiologically active compounds are useful. Thus, we tried to screen Tunisian aromatic plant extracts for compounds having hair growth regulation activity.

Therefore we also introduce various methods for hair growth research, such as how to search for samples that effectively promote hair growth, and how to investigate the effect of samples in vivo [12].

2 Materials and Methods

2.1 Cells and Cell Culture

Human follicular dermal papilla cells (HFDPCs) were purchased from TOYOBO (Tokyo, Japan) as primary cells and grown in HFDPC growth medium (TOYOBO).

2.2 Sample Extract

Tunisian plants were collected by a Tunisian researcher and extracted in 70% EtOH. Ten grams of dried plant was immersed in 100 ml of 70% EtOH for 1 to 2 weeks. The extract was then filtered to remove plant parts and to sterilize the extract.

2.3 MTT Assay

HFDPCs were used for the 1st screening of Tunisian samples with hair growth promotion ability. Subcultured HFDPCs were used within two passages for the 3-(4,5-dimethyl-2-thyazolyl)-2,5-diphenyl-2H-tetrazolium bromide (MTT) assay and cell growth is evaluated. HFDPCs were trypsinized and plated at a density of 1×10^4 cells per well in 1.0 ml of HFDPC growth medium in collagen type I-coated 24-well plate (SUMILON, Tokyo, Japan). After overnight culture, the medium was changed to starvation medium (Dulbecco's Modified Eagle's Medium (DMEM) containing 0.5% charcoal-absorbed fetal bovine serum). After 96 h, the cells were stimulated with 50 μl of Tunisian aromatic plant samples (70% EtOH extract) at various concentrations for 8 h, after which 50 μl of 5 mg/ml MTT (Dojindo, Tokyo, Japan) was then added to the medium. After 18 h, the cells were washed with PBS, followed by the addition of 0.5 ml of PBS, and then 0.5 ml of 10% SDS was added per well. The SDS was allowed to dissolve the formazan for at least 24 h, and then the absorbance at 570 nm was determined using a plate reader [4, 7]. After the measurement, Tunisian samples that show potential for hair growth regulation were selected for further experiments.

2.4 Cell Cycle Assay

Cultured HFDPCs were subcultured at a density of 4×10^5 cells in collagen type I-coated 100 mm dish (SUMILON, Tokyo, Japan). After overnight culture, medium was changed to starvation medium. After 48 h, the cells were stimulated with Tunisian aromatic plant samples (1/300 dilution) for 12, 24, 48 and 96 h. The treated cells were harvested by trypsinization and washed with PBS, and then fixed in ice-cold 75% EtOH (approximately 1 ml of 75% EtOH for every 1×10^6 cells) at 4 °C for more than 12 h. The fixed cells were stained with Guava Cell Cycle Reagent (GE Healthcare Bio-Science Corp., USA) and the cell cycle kinetics was then determined using the Guava PCA according to the manufacturer's instructions.

2.5 Hair Growth Promotion Assay In Vivo

To evaluate hair growth activity, Tunisian aromatic plant extract should be applied to telogen skin. For this assay, 16 seven-week-old male C3H/He mice were obtained and maintained on a standard laboratory diet and water *ad libitum*. After conditioning for 1 week, all mice were anesthetized with an intraperitoneal injection of pentobarbital and dorsal hair shafts were trimmed to maintain the telogen phase. Tunisian aromatic plant extract or PBS (for negative control) was then injected subcutaneously into the test area (n = 5 in each group). Until results were observed, the mice were maintained normally; they were then sacrificed by CO_2 inhalation and photographed

to detect skin colorization by anagen induction. Their skin was then isolated and the reverse side was photographed to evaluate anagen induction.

3 Results and Discussion

3.1 Effect of Tunisian Aromatic Plant Extract on Human Dermal Papilla Cell Growth

For the 1st screening, the potential of Tunisian aromatic plants to promote the growth of HFDPCs was evaluated by the MTT assay. We evaluated seven extracts using HFDPCs, and found that only one plant has the ability to promote the growth of HFDPCs. During treatment, cell shape was not changed and cytotoxicity was not detected. This result suggested that one Tunisian aromatic plant has for the potential to promote hair growth (Fig. 1).

3.2 Effect of Tunisian Aromatic Plant Extract on HFDPCs Cell Cycle

After the 1st screening, we examined the effect of the Tunisian aromatic plant extract on HFDPCs cell cycle. HFDPCs were treated with the Tunisian aromatic plant extract for 12, 24, 36 and 48 h. While the 24, 36 and 48 h treatments did not show any effect, the 12 h treatment of HFDPCs seemed to stimulate the cell cycle. The G_0/G_1 phase was decreased while the G_2/M phase was increased by the 12 h treatment with the Tunisian aromatic plant extract. This denotes that the Tunisian

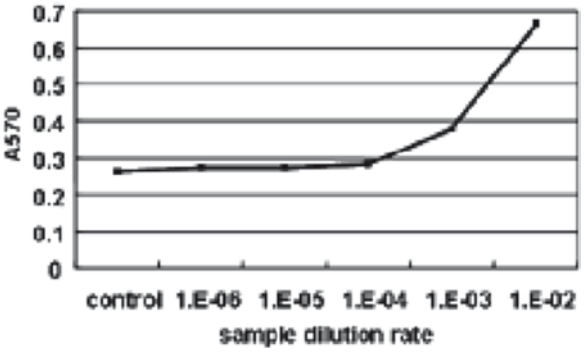

Fig. 1 Growth promotion activity of Tunisian aromatic plant on HFDPCs. Cell growth was stimulated by treatment with Tunisian aromatic plant extract in a concentration-dependent manner

Table 1 Human dermal papilla cell cycle promotion activity of the Tunisian aromatic plant extract. HFDPCs were treated with the Tunisian aromatic plant extract (1/300 dilution) for 12 h. Dermal papilla cell cycle was stimulated and the number of cells at the G_2/M phase was increased

	G_0/G_1	S	G_2/M
Control	72.6%	4.9%	8.2%
Tunisian aromatic plant	68.5%	4.8%	10.0%

aromatic plant extract has the ability to promote dermal papilla cell growth. This result suggested that some factors that can regulate the hair growth cycle via stimulation of dermal papilla cell growth might be included in the Tunisian aromatic plant extract (Table 1).

3.3 Hair Growth Promotion Activity of Tunisian Aromatic Plant Extract

From the cell growth promotion and cell cycle assays using HFDPCs, we confirmed that the Tunisian aromatic plant has the potential to promote the hair growth cycle via dermal papilla cell growth stimulation. We then tried to evaluate the hair growth regulation potential of the Tunisian aromatic plant extract on mouse dorsal skin. Male C3H/HeN mice were selected to eliminate the influence of sex hormones. Because 8-week-old mice are known to be in telogen phase at the same time, mice at this phase were used at the start of this experiment. These mice were anesthetized and their dorsal hair was trimmed to maintain the telogen-phase hair follicle on the back side of their skin even after treatment. After trimming, the Tunisian aromatic plant extract (1/300 dilution) or PBS (negative control) was injected subcutaneously into the test area (trimmed dorsal skin area). After injection, these mice were observed daily to determine whether their dorsal skin color changed to gray from white and whether hair growth was stimulated to the anagen phase from the telogen phase. Gray skin color was detected at 15 days after injection, and then hair growth on skin surface were detected at 3 weeks after injection. The graying skin color denotes that the next anagen phase was induced under the skin but hair on the skin surface was not detected yet. We checked the reverse side of the skin to determine the anagen hair follicle ratio. The reverse side of the dorsal skin of mice injected with the extract showed not only hair follicles at the next anagen stage but also at the next cycled telogen phase. This denotes that normal hair growth cycle was stimulated. Moreover, we observed vasodilation on skin near the anagen-stimulated area. If the anagen stage was stimulated directly by injection of the Tunisian aromatic plant extract, a gray colored skin should be detected 8 to 10 days after. However, in this case, gray colored skin was detected 3 weeks after injection. It suggested that the Tunisian aromatic plant extract stimulated the hair growth cycle indirectly. Because the growth and cell cycle of HFDPCs were promoted, we consider that the Tunisian

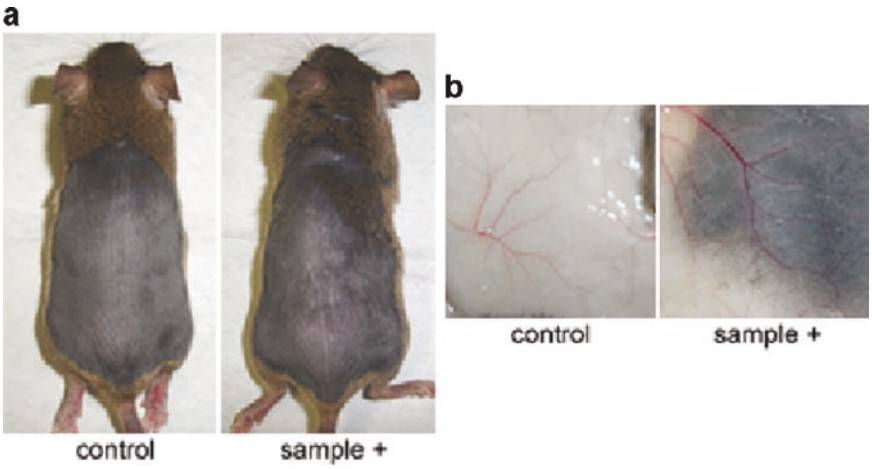

Fig. 2 Hair growth effect of the Tunisian aromatic plant extract. (**a**) Skin surface hair growth was detected on the dorsal skin of mice injected with the Tunisian aromatic plant extract. (**b**) On the reverse side of the skin, dark gray color was detected. This colored skin indicates the presence of anagen-phase hair follicles under the skin. In skin injected with sample, vasodilation was also detected. While control mouse skin showed no vasodilation, vascular thickness was increased in the sample-injected skin

plant extract initially stimulated dermal papilla cell growth, and then some signals were transferred to skin dermis components; vasodilation then occurred and hair growth was stimulated. The reason for the delayed stimulation of hair growth was the indirect stimulation of anagen phase from telogen phase (Fig. 2).

References

1. K. S. Stenn and R. Paus, Control of hair follicle cycling, *Physiol. Rev.*, vol. 81, 2001, pp. 449–494
2. R. Paus and G. Cotsarelis, The biology of hair follicles, *N. Engl. J. Med.*, vol. 341, 1999, pp. 491–497.
3. Y. Ota, Y. Saitoh, S. Suzuki, K. Ozawa, M. Mitsuko, and T. Imamura, Fibroblast growth factor 5 inhibits hair growth by blocking dermal papilla cell activation, *Biochem. Biophys. Res. Commun.*, vol. 290, 2002, pp. 169–176.
4. S.-S. Rho, S.-J. Park, S.-L. Hwang, M.-H. Lee, C. D. Kim, I.-H. Lee, S.-Y. Chang, and M.-J. Rang, The hair growth promoting effect of *Asiasari radix extract and its molecular regulation*, *J. Dermatol. Sci.*, vol. 38, 2005, pp. 89–97.
5. B. G. Howell, N. Solish, C. Lu, H. Watanabe, A. J. Mamelak, I. Freed, B. Wang, and D. N. Sauder, Microarray profiles of human basal cell carcinoma: insight into tumor growth and behavior, *J. Dermatol. Sci.*, vol. 39, 2005, pp. 39–51.
6. T. Midorikawa, T. Chikazawa, T. Yoshino, K. Takada, and S. Arase, Different gene expression profile obsedved in dermal papilla cells related to androgenic alopecia by DNA macroarray analysis, *J. Dermatol. Sci.*, vol. 36, 2004, pp. 25–32.

7. M. Kawano, A. Komi-Kuramochi, M. Asada, M. Suzuki, J. Oki, J. Jiang, and T. Imamura, Comprehensive analysis of FGF and FGFR expression in skin: FGF18 is highly expressed in hair follicles and capable of inducing anagen from telogen stage hair follicles, *J. Invest. Dermatol.*, vol. 124, 2005, pp. 877–885.
8. M. Kawano, S. Suzuki, M. Suzuki, J. Oki, and T. Imamura, Bulge- and basal layer- specific expression of fibroblast growth factor 13 (FHF-2) in mouse skin, *J. Invest. Dermatol.*, vol. 122, 2004, pp. 1084–1090.
9. K. J. McElwee, A. Huth, S. Kissling, and R. Hoffman, Macrophage-stimulating protein promotes hair growth ex vivo and induces anagen from telogen stage hair follicles in vivo, *J. Invest. Dermatol.*, vol. 123, 2004, pp. 34–40.
10. P. Komminoth, Digoxygenin as an alternative probe labeling for in situ hybridization, *Diag. Mol. Pathol.*, vol. 1, 1992, pp. 142–150.
11. C.-M. Huang, K. W. Foster, T. DeSilva, J. F. Zhang, Z. Shi, N. Yusuf, K. R. Van Kampen, C. A. Elmets, and D. C. Tang, Comparative proteomic profiling of murine skin, *J. Invest. Dermatol.*, vol. 121, 2003, pp. 51–64.
12. M. Kawano, T. Imamura, and H. Isoda, Methods for searching and evaluating effective hair growth regulation factors from Tunisian samples, *J. Arid Land Studies*, vol. 15–4, 2006, pp. 443–446.

Screening of Various Tunisian Olive Oils for Their Inhibitory Effect on Beta-Hexosaminidase Release by Basophilic Cells

Parida Yamada, Moktar Zarrouk, and Hiroko Isoda

Abstract In this study, to investigate the antiallergy effect of virgin olive oil samples from seven Tunisian varieties, we used the type I allergy reaction model using rat basophilic leukemia (RBL-2H3) cells and different dilutions of olive oil samples to determine β-hexosaminidase release inhibition at two different response stages, the antibody-antigen binding stage and antibody-receptor binding stage. Moreover, we investigated the effect of olive oil samples on histamine release by activated human basophilic (KU812) cells. Results showed that the Sayali olive oil significantly inhibited β-hexosaminidase release by the IgE-sensitized, antigen-stimulated RBL-2H3 cells at the antibody-antigen binding stage. The Zarrazi olive oil significantly inhibited β-hexosaminidase release by the IgE-sensitized, antigen-stimulated RBL-2H3 cells at the antigen-receptor binding stage. Different dilutions of Zarrazi olive oil dose-dependently inhibited histamine release after stimulation with calcium ionophore A23187 plus phorbol 12-myristate 13-acetate (PMA). They provide evidence that Tunisian olive oils may be beneficial for the treatment or prevention of various types of allergic diseases.

Keywords Olive oil • antiallergy • RBL-2H3 cells • KU812 cells • β-hexosamindase

1 Introduction

The search for functional foods has led to a heightened interest in bioresources from arid and semiarid land. Such bioresources are rich in useful natural components. Plants in the Mediterranean basin, such as vines and olive trees, have developed an

P. Yamada and H. Isoda
Alliance for Research on North Africa (ARENA), Graduate School of Life and Environmental Sciences, University of Tsukuba, Japan

M. Zarrouk
Centre of Biotechnology, Ministry of Scientific Research Technology and Competency Development, Tunisia

K. Ikura et al. (eds.), *Animal Cell Technology: Basic & Applied Aspects*,
Animal Cell Technology: Basic & Applied Aspects 15,
DOI 10.1007/978-1-4020-9646-4_36,

array of antioxidant defenses to protect themselves from environmental stress. The olive tree, *Olea europea* L., is one of the most important fruit trees in Tunisia, a country in North Africa. Recent studies on different olive oil varieties indicate that the cultivar has a significant impact on the phenolic composition of virgin olive oil [1, 2].

Olive oil contains compounds with potent antimicrobial activities against bacteria, fungi, and mycoplasma. In addition, olive oil has antioxidant and anti-inflammatory activities. Animal and in vitro studies suggest that phenolic compounds in virgin olive oil are effective antioxidants. In animal and in vitro studies, hydroxytyrosol and oleuropein have been shown to be strong antioxidants [3, 4]. Considerable data on the polyphenols of olive oil, such as flavonoids, have been reported, but few studies have been published on olive oil antioxidant effects. However, the antiallergy effects of olive oil have not been studied or defined.

A rat mast cell β-hexosaminidase assay has been carried out to quantify the biological activity of a recombinant humanized, monoclonal anti-IgE antibody. Histamine, which is released from mast cells stimulated by an antigen or by degranulation inducers, is usually considered as a degranulation marker in experiments on immediate allergic reaction in vitro. β-hexosaminidase is also stored in secretory granules of mast cells and is released concomitantly with histamine when mast cells are immunologically activated [5, 6]. Thus, the β-hexosaminidase activity in the medium is used as a marker of mast cell degranulation.

The objective of this study was to compare the antiallergy effect of olive oil samples from seven Tunisian cultivars using the type I allergy model and to investigate the in vitro antiallergy activity at the antigen-antibody stage and antibody-receptor stage.

2 Materials and Methods

2.1 Reagents

Dinitrophenylated bovine serum albumin (DNP-BSA) was purchased from Cosmo Biotechnology Co. (LG0017), anti-DNP-IgE (D8406), ketotifen (K2628), and L-glutamine (G7513) were purchased from Sigma Chemical Co. Fetal bovine serum (FBS) was purchased from Hyclone Co. Ltd. Eagle's Minimum Essential Medium (MEM) was purchased from Nissui Pharmaceutical Co., Ltd. RPMI medium 1640 were purchased from Gibco Co., NY, USA. Calcium ionophore A23187 (C7522) and phorbol 12-myristate 13-acetate (PAM, 79346) were obtained from Sigma Japan (Tokyo) and dissolved in DMSO at a concentration of 10 mM.

2.2 Preparation of Olive Oil Sample

Samples of olive oil used in this study were extracted from seven main olive varieties: Chemchali (C_1), Chemlali (C_2), Chetoui (C_3), Sayali (S), Gerboui (G), Zalmati (Z_1),

and Zarrazi (Z_2), grown in various regions of Tunisia. Oil extraction was carried out under similar industrial extraction conditions. Using an Abencor analyzer, 1.5 to 2.0 kg of olives were crushed with a hammer mill and slowly mixed for 30 min. Then the obtained paste was centrifuged for oil extraction. The olive oil samples were then filter-sterilized (0.45 μm Millipore filter), mixed with MEM medium at 10% final concentration, and then sonicated using a supersonic wave machine to obtain an oil emulsion.

2.3 Cell and Cell Culture

RBL-2H3 cells were purchased from Riken Cell Bank, Japan. The cells were maintained in MEM medium supplemented with 10% FBS, 2 mM L-glutamine at 37°C in a 5% CO_2 incubator. KU812 cells were purchased from Riken Cell Bank, Japan. The cells were maintained in RPMI medium 1640 supplemented with 10% FBS at 37°C in a 5% CO_2 incubator.

2.4 β-Hexosaminidase Assay at Different Stages

The β-hexosaminidase release inhibition assay using RBL-2H3 cells was carried out according to the method described by Kawasaki et al. [7] with some modifications. For the β-hexosaminidase inhibition assay at the antigen-antibody binding stage, RBL-2H3 cells were seeded onto 96-well plates (5.0×10^5 cells/ml) in 100 μl of medium for each well. Cells were incubated for 24 h at 37°C and sensitized with 0.3 μg/ml anti-DNP-IgE, then washed twice with PBS (−) to eliminate free IgE. After incubating the cells at 37°C for 10 min in 60 μl per well of releasing mixture (116.9 mM NaCl, 5.4 mM KCl, 0.8 mM $MgSO._4 7\ H_2O$, 5.6 mM glucose, 25 mM HEPES, 2.0 mM $CaCl_2$, 1mg/ml BSA, pH 7.7) containing 5 μl of test samples (olive oil dilutions of 1/100, 1/1,000, and 1/10,000 in medium), the cells were exposed to 0.3 μg/ml DNP-BSA in PBS (-), followed by incubation at 37°C for 1 h. As positive and negative controls, 3 mM ketotifen and MEM medium were used, respectively. The plate was put on ice for 10 min and then 20 μl of the supernatant was taken from each well and transferred to another plate, 80 μl of substrate solution (5 mM 4-Nitrophenyl N-acetyl-β-D-glucosaminide in 50 mM $C_6H_8O_7$ buffer, pH 4.5) was then added to the supernatant followed by incubation at 37°C for 30 min. After adding 100 μl/well of stop buffer (0.1 M $NaHCO_3/Na_2CO_3$, pH 10.0), the absorbance at 405 nm was obtained using a microplate reader (Power Scan HT, Dainippon Pharmaceutical Co., Ltd.). The percent inhibition of β-hexosaminidase release from RBL-2H3 cells by the test sample was calculated using the following equation:

$$\text{Inhibition } (\%) = \{1 - (T - B)/(C - B)\} \times 100$$

Control (C): Cell (+), DNP-BSA (+), test sample (−); Test (T): Cell (+), DNP-BSA (+), test sample (+); Blank (B): Cell (−), DNP-BSA (+), test sample (+).

To determine the effect of the sample at the antibody-receptor binding stage, the test sample was added to the cells before the IgE sensitization stage. The β-hexosaminidase released to the supernatant was measured as in the previous section.

2.5 Histamine Release Assay

KU812 cells (2.0×10^6 cell/ml) were resuspended in 200 μl of Tyrode buffer A (30 mM Tris-HCl, 120 mM NaCl, 5 mM KCl, 1 mM $CaCl_2$, 1 mM $MgCl_2$, 5.6 mM glucose, 0.03% bovine serum albumin) for treatment with olive oil. Then, the cells were incubated without or with 25 μl/well of various concentrations of test sample (olive oil dilutions of 1/100, 1/1000, and 1/10000 in medium) for 15 min, and then stimulated with A23187 (1 μM) plus PMA (20 nM) for 15 min at 37°C. The mixture was incubated at 37°C for 20 min and the reaction was terminated by cooling at 4°C for 15 min. Then the cell suspension was centrifuged at 400 × g for 5 min at 4°C. The supernatant (50 μl) was transferred to a 96-well ELISA plate, and the level of histamine concentration was measured by means of ELISA according to the manufacturer's instructions. Histamine EIA Kit (Oxford Biomedical Research, Inc., USA) was used to detect histamine release.

2.6 Statistical Analysis

Results are expressed as mean ± standard deviation. Statistical comparisons were carried out using Student's T-test for paired values.

3 Results

3.1 Effect of Various Olive Oils on the β-Hexosaminidase Release at the Antigen-Antibody Binding Stage

Seven olive oil samples (obtained from seven olive varieties) commonly used in traditional Tunisian food were screened for their inhibitory effect on β-hexosaminidase release by RBL-2H3 cells. The β-hexosaminidase release from IgE-sensitized RBL-2H3 cells was induced by DNP-BSA as antigen stimulation at the antigen-antibody stage. The inhibition rate of β-hexosaminidase release from RBL-2H3 by

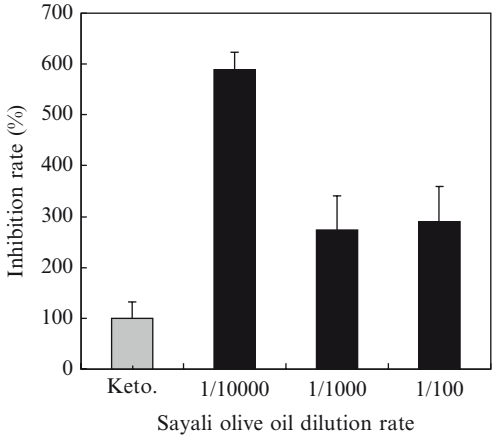

Fig. 1 Inhibitory effect of Sayali olive on the β-hexosaminidase release at the antigen-antibody binding stage

Sayali olive oil is shown in Fig. 1. The Sayali olive oil dose-dependently inhibited the β-hexosaminidase release. At high concentration, all olive oil samples inhibited the β-hexosaminidase release by RBL-2H3 cells (data not shown). The Sayali olive oil was the most potent among the seven extracts tested followed by C_1 and C_2. The Sayali olive oil was found to have high inhibitory effect on β-hexosaminidase release from RBL-2H3 cells at 1/10000 dilution at the antigen-antibody binding stage, showing more than about 600% inhibition compared with ketotifen (Keto.), a standard drug, which caused 100% inhibition (Fig. 1).

3.2 Effect of Various Olive Oils on the β-Hexosaminidase Release at the Antibody-Receptor Binding Stage

The β-hexosaminidase release from IgE-sensitized RBL-2H3 cells was induced by DNP-BSA as antigen stimulation at the antibody-receptor stage. The inhibition rate of β-hexosaminidase release from RBL-2H3 cells caused by Z_2 sample is shown in Fig. 2. The Z_2 sample dose-dependently inhibited the β-hexosaminidase release. At high concentration, S, G, and Z_1 samples also inhibited the β-hexosaminidase release by RBL-2H3 cells (data not shown). The Z_2 sample was the most potent among the seven extracts tested followed by G and Z_1, respectively. The Z_2 sample was found to have a high inhibitory effect on β-hexosaminidase release from RBL-2H3 cells at 1/100 dilution at the antibody-receptor binding stage, showing more than about 150% inhibition compared with ketotifen (Keto.)

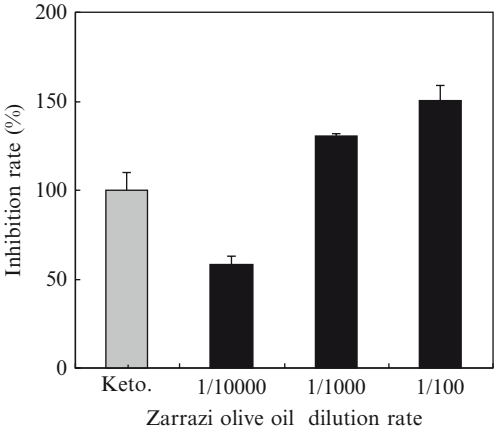

Fig. 2 Inhibitory effect of Zarrazi olive on the β-hexosaminidase release at the antibody-receptor binding stage

3.3 Inhibitory Effect of Olive Oil on Histamine Release from KU812 Cells

We examined the inhibitory effect of olive oil on the A23187 plus PMA-stimulated secretion of histamine from KU812 cells after olive oil addition. The histamine release in A23187 plus PMA-stimulated KU812 cells caused by the Z_2 sample is shown in Fig. 3. The Z_2 sample (dilutions of 1/100, 1/1000, 1/10000) dose-dependently inhibited histamine release from A23187 plus PMA-stimulated KU812 cells, but the S sample did not (data not shown). The histamine release was inhibited by approximately 96.1, 89.0, and 69.8% after treatment with the Z_2 sample at 1/100, 1/1000 and 1/10000 dilutions, respectively. The results showed the same tendency as the β-hexosaminidase release inhibitory effect of the Z2 sample at the antibody-receptor stage.

4 Discussion

Our data demonstrated that the Sayali olive oil dose-dependently inhibited the β-hexosaminidase release from RBL-2H3 cells at the antibody-antigen binding stage. On the other hand, the Zarrazi olive oil dose-dependently inhibited the β-hexosaminidase release from RBL-2H3 cells at the antibody-receptor binding stage. Moreover, the Zarrazi olive oil dose-dependently inhibited histamine release from A23187 plus PMA-stimulated KU812 cells.

Several falconoids, such as apigenin, luteolin, diosmetin and fisetin, which are naturally occurring flavonoids found in many plants, have been reported to potently

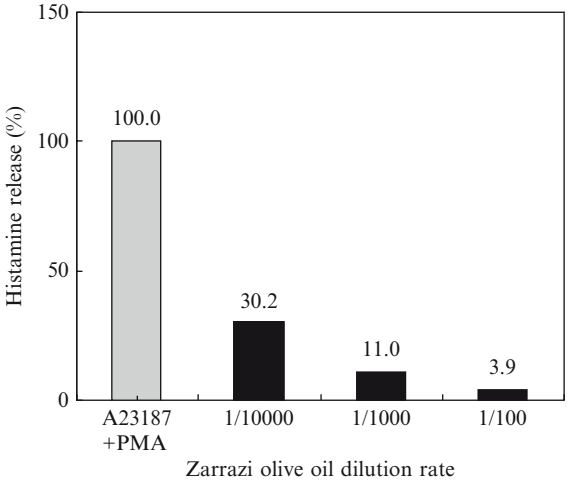

Fig. 3 Inhibitory effect of Zarrazi olive on histamine release from KU812 cells after stimulation with A23187 plus PMA

inhibit β-hexosaminidase release from RBL-2H3 cells. Apigenin and luteolin were also detected in our samples and the amounts vary according to the cultivars. However, phenolic acids, mainly p-coumaric acid are well represented [2]. The apigenin and luteolin contents in the other samples (C_1, C_2, C_2 and Z_1) may also be responsible for their inhibitory effect. Mojca et al. [8] demonstrated that flavones showed antioxidant activity. IgE-specific receptor signaling of mast cells activates intracellular oxidative burst involved in the regulation of calcium signals and degranulation [9]. The inhibitory effect of the Z_2 sample on the degranulation of basophilic cells may be attributable to the antioxidant activity of hydroxytyrosol. The compounds apigenin, luteolin and hydroxytyrosol in olive oil may be the major compounds responsible for the antiallergy effect. The result showed that all of the olive oil samples examined have antiallergy activity. However, this activity is not simply related to the total phenolic compound or flavonoid components in olive oil.

Our studies provide evidence that Tunisian olive oil may be beneficial for the treatment or prevention of various types of allergies. Therefore, it is considered that the consumption of Tunisian olive oil provides protection against allergic diseases.

References

1. Abaza, L., Msallem, M., Daoud, D., Zarrouk, M. (2002) Characterization of the oils from seven Tunisian olive tree varieties. Oleagineux, Corps Gras, Lipides 2(9): 174–179.
2. Abaza, L., Taamalli, W., Ben Temime, S., Daoud, D., Guteirrez, F., Zarrouk, M. (2005) Natural antioxidant composition as correlated to stability of some Tunisian virgin olive oils. *Rivista Italiano Delle Sostanze Gresse* 132: 12–18.

3. Visioli, F., Bellomo, G., Galli, C. (1998) Free radical-scavenging properties of olive oil plyphenols. *Biochemical and Biophysical Research Communication* 247: 60–64.
4. Visioli, F., Galli, C., Plasmati, E., Viappiani, S., Hermandez, A., Colombo, C. (2000) Olive phenol hydroxytyrosol prevents passive smoking-induced oxidative stress. *Circulation* 102: 2169–2171.
5. Schwartz, L.B., Lewis, R.A., Seldin, D., Austen, K.F. (1981) Acid hydrolases and tryptase from secretory granules of dispersed human lung mast cells. *Journal of Immunology* 126: 1290–1294.
6. Marquardt, D.L., Wasserman, S.I. (1983) Modulation of rat serosal mast cell biochemistry by in vivo dexamethasone administration. *Journal of Immunology* 131: 934–939.
7. Kawasaki, M., Toyoda, M., Teshima, R., Sawada, J., Hayashi, T., Arisawa, M., Shimizu, M., Morita, N., Inoue, S., Saito, Y. (1994) In vitro antiallergic activity of flavonoids in histamine release using rat basophilic leukemia (RBL-2H3) cells. *Journal of Food Hygienic Society of Japan* 35: 497–503.
8. Mojca, S., Petra, K., Majda, H., Andreja, R.H., Marjana, S., Zeljko, K. (2005) Phenols, proanthocyanidins, flavones and flavonols in some plant materials and their antioxidant activities. *Food Chemistry* 89: 191–198.
9. Suzuki, Y., Yoshimaru, T., Matsui, T., Inoue, T., Niide, O., Nunomura, S., Ra, C. (2003) Fc epsilon RI signaling of mast cells activates intracellular production of hydrogen peroxide: role in the regulation of calcium signals. *Journal of Immunology* 171(11): 6119–6127.

Leaf Extracts from Tunisian Olive Cultivars Induce Growth Inhibition and Differentiation of Human Leukemia HL-60 Cells

Leila Abaza, Terence P.N. Talorete, Parida Yamada, Mokhtar Zarrouk, and Hiroko Isoda

Abstract Recently a lot of interest is given to the beneficial actions and healthy effects of olive leaves. Thus, this work is an investigation of the antiproliferative activities and other effects of olive leaf extracts (OLEs) from seven principal Tunisian olive varieties on the human promyelocytic cell line HL60.Three in vitro assays were performed for this study: MTT assay to evaluate the cytotoxicity effect of OLE on HL60 cells, double staining esterase assay and nitroblue tetrazolium reduction assay for assessment of cell differentiation. We find that all OLEs exert a cytotoxic effect on HL60 cells which is confirmed by some morphological changes. Despite their apoptotic effect, ethanol extract of Tunisian olive leaves induced differentiation of HL60 cells into granulocytes. The differentiation-inducing activity of G extract was more remarkable than those of the other extracts (NBT reduction greater than 90%). To identify the bioactive components of OLEs the cytotoxicity of oleuropein and luteolin, two major phenols of olive leaves, were tested, nevertheless, no statistically significant difference was observed versus control. These results suggest that OLEs probably contain unknown bioactive components that are present in relatively high amounts in the G sample and are responsible for the cell differentiation, or possibly, cell differentiation is the result of synergism between compounds present in OLEs.

Keywords Olive leaf extracts • human promyelocytic cell line HL60 • cytotoxicity • differentiation

L. Abaza and M. Zarrouk
Laboratoire Caractérisation et Qualité de l'Huile d'Olive, Centre de Biotechnologie, Technopole de Borj Cedria, BP 901, 2050, Hammam-Lif, Tunisia

T.P.N. Talorete, P. Yamada, and H. Isoda
Graduate School of Life and Environmental Sciences, University of Tsukuba, 1-1-1 Tennodai, Tsukuba, Ibaraki 305-8572, Japan

K. Ikura et al. (eds.), *Animal Cell Technology: Basic & Applied Aspects*,
Animal Cell Technology: Basic & Applied Aspects 15,
DOI 10.1007/978-1-4020-9646-4_37, © Springer Science+Business Media B.V. 2009

1 Introduction

Numerous studies have focused on olive oil and in particular on the effects of its minor compounds (phenols, tocopherols, carotenoids) which have strong antioxidant properties. However, although the leaf is the site of primary and secondary plant metabolism, the "secret" of the olive leaf extract is still not yet completely revealed.

The olive leaf is traditionally associated with a wide number of medicinal claims. The first formal report on its medicinal use was made in 1854, when olive leaf extract (OLE) was reported to be effective in treating fever and malaria [1]. OLE was also used to prevent hypertension and hyperglycemia [2, 3], and for overcoming infections. It was also used by herbalists to treat skin rashes and boils [4].The isolation and identification of phenolics in olive leaf have also attracted considerable attention as a source of phenolic compounds. Chemically, olive leaves are characterized by the presence of a wide number of constituents, including oleuropein and its derivatives and several types of flavonoids [5]. Recently, studies have revealed the anti-HIV activity of OLE which is used by some AIDS patients to strengthen their immune system [6].

2 Materials and Methods

2.1 Cell Line and Cell Maintenance

HL-60 cells were obtained from the Riken Cell Bank (Tsukuba, Ibaraki, Japan) and grown in phenol-red-free RPMI 1640 medium (Gibco) supplemented with 10% heat-inactivated fetal bovine serum (FBS, Sigma) and 1% penicillin (5,000 IU/ml) – streptomycin (5,000 μl/ml) solution (ICN Biomedicals Inc.) at 37°C in a 5% CO_2 atmosphere.

2.2 Sampling

The olive leaves used for this study were obtained from seven principal Tunisian varieties, grown in various regions of Tunisia. Dried leaves were extracted with 70% ethanol. The mixture was allowed to stand for at least 1 week at room temperature and then filtered using a 0.45 μm filter (Millipore, Japan).

2.3 Cell Proliferation Assay

HL-60 cells were harvested and seeded onto 96-well plates at 2×10^4 cells per well in 100 μl of medium. After overnight incubation, samples were added to obtain final dilutions of 1/100, 1/500, 1/1000 and 1/10000. The cells were then cultured

for 48 h, followed by the addition of 10 µl of 5 mg/ml 3-(4,5-dimethylthiazol-2-yl)-2,5-diphenyl-2H-tetrazolium bromide (MTT) (Dojindo). After 24 h of incubation, 100 µl of 10% sodium dodecyl sulfate (SDS) was added, followed by another 24 h of incubation. The absorbance was then spectrophotometrically determined at 570 nm using a multidetection microplate reader (Powerscan HT, Dainippon Pharmaceutical, USA).

2.4 Cell Differentiation Assays

HL-60 differentiation was assessed using the NBT assay and the double staining esterase assay. The NBT reduction ability was determined by the method of Takeda et al. [7] , with modifications. For the double staining esterase assay, OLEs were added at 1/100 dilution and the specific and nonspecific activities were determined as described by Isoda et al. [8].

2.5 Neutral Red Assay

The cells at a density of 2.5×10^5 cells/ml were inoculated onto 24-well plates and incubated overnight. The cells were then incubated for 48 h in the presence of samples. This was followed by the transfer of the cells to eppendorf tubes, centrifugation and replacement of the medium with 1 ml neutral red (NR) medium (33 µg NR dye (Sigma) per milliliter of RPMI medium). After incubation for 3 h, the NR medium was removed and the cells washed with 1 ml of fixing solution. Then, 200 µl of NR desorb solution was added and the cells were seeded in 96-well plates. The plates were allowed to stand at room temperature for 10–15 min, agitated on a microplate shaker for 20-30 min, and then the absorbance was determined at 540 nm. This assay was used to study the cytotoxicity effect of oleuropein and luteolin, two major compounds of olive leaf extracts, on HL-60 cells.

3 Results and Discussion

3.1 Growth Inhibition of HL60 Cells by Olive Leaf Extracts

Three independent trials were conducted for this experiment. Figure 1 shows that at 1/100 dilution, all olive leaf extracts (OLEs) expressed a significant ($p < 0.05$) decrease in the proliferation rate of treated cells compared with control. With regards to the data presented, it clearly appears that all olive leaf extracts possess an antiproliferative effect on HL60 cells.

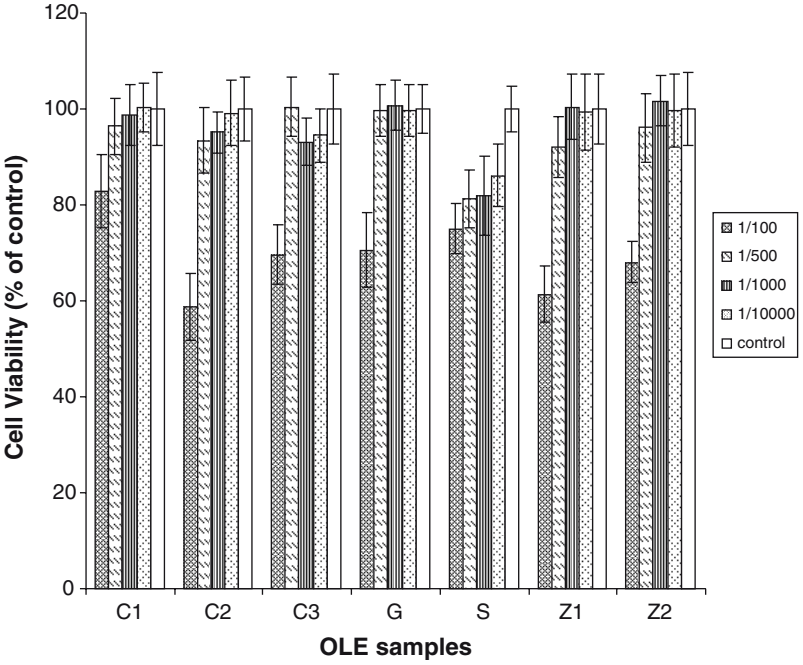

Fig. 1 Viability of HL-60 cells incubated for 48 h with various dilutions of olive leaf extracts (OLEs) from Chemchali (C1), Chemlali (C2), Chétoui (C3), Gerboui (G), Sayali (S), Zalmati (Z1) and Zarrazi (Z2) varieties

3.2 Morphological Examination

The antiproliferative effect exerted by OLEs was confirmed by the morphological changes observed on HL60 cells (Fig. 2). In some cases, the extracts appeared to induce differentiation of cells into monocytes and/or granulocytes. On the other hand, some of these changes were apparently the result of apoptosis or programmed cell death.

3.3 Induction of Differentiation by Olive Leaf Extracts

All cells treated with OLEs showed NBT reduction ability and the values were significantly higher than those of untreated cells. The percentage of differentiated cells treated with the G extract was the most predominant (NBT reduction was greater than 90%) (Fig. 3). HL60 cells treated with OLEs except for C2 and S showed red granulation, which is indicative of differentiation along the granulocyte

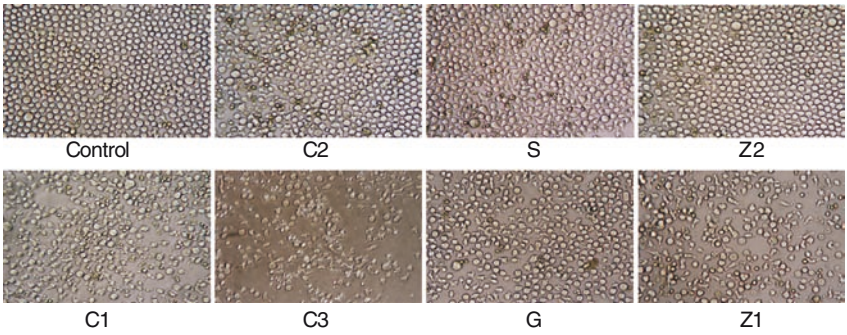

Fig. 2 Morphological changes in HL-60 cells incubated for 48 h with 1/100 dilution of olive leaf extracts from Chemchali (C1), Chemlali (C2), Chétoui (C3), Gerboui (G), Sayali (S), Zalmati (Z1) and Zarrazi (Z2) varieties

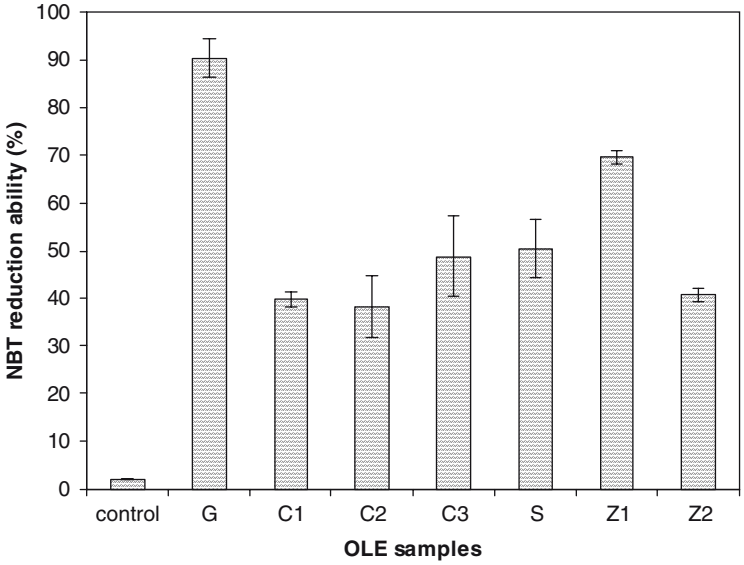

Fig. 3 NBT reduction ability of HL-60 cells incubated for 2.5 h with olive leaf extracts from Chemchali (C1), Chemlali (C2), Chétoui (C3), Gerboui (G), Sayali (S), Zalmati (Z1) and Zarrazi (Z2) varieties. Results represent three independent determinations. Standard deviations were less than 10%

lineage (result not shown). The density and distribution of NCAE-positive cells were very clear.

According to Tai et al. [9], the induction of differentiation may be one of the possible mechanisms of chemoprevention by relatively noncytotoxic agents, and compared to intensive chemotherapy, differentiation therapy and chemoprevention are very attractive alternative approaches to reverse the progression of malignant disease.

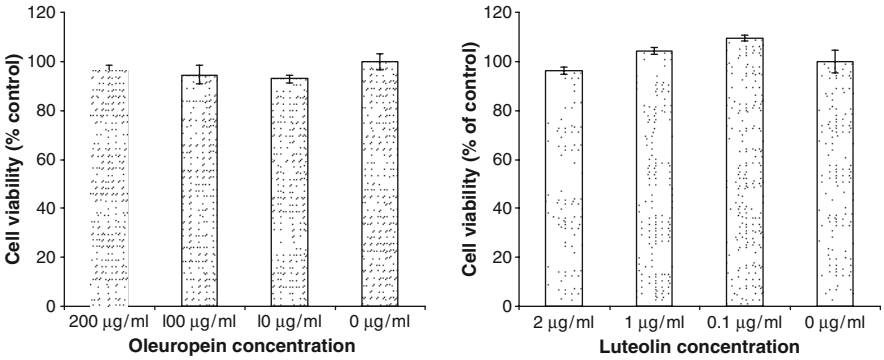

Fig. 4 Cell viability of HL-60 cells incubated for 48 h with various concentrations of oleuropein and luteolin

3.4 Effect of Oleuropein and Luteolin on HL60 Cell Viability

Neither oleuropein nor luteolin showed any significant cytotoxic effects on HL60 cells at concentrations ranging from 10–200 µg/ml and 0.1–2 µg/ml, respectively (Fig. 4).

However, in contrast, Hamdi and Castellon [10] observed an obvious growth inhibition of some cell lines (LN-18, TF-1a, T-47D, MCF-7, RPMI-7951) in a dose-dependent manner by the addition of oleuropein. The disparity of our results with those of these authors may be attributable to the incubation time, oleuropein concentrations as well as the nature of the tested cell lines, since these authors have observed that in the case of 786-O (renal cell adenocarcinoma) and normal fibroblasts, only the highest concentration was effective.

In conclusion, despite their apoptotic effect, ethanol extracts of Tunisian olive leaves (particularly the G extract) induced differentiation of HL60 cells into granulocytes. Further experiments are currently being conducted to understand the mechanism of action of the bioactive component of olive leaves.

References

1. D. Hanbury, On the febrifuge properties of the olive (Olea europea, L.), Pharmaceut. J. Provincial Trans. 1854; pp. 353–354.
2. M. Gonzalez, A. Zarzuelo, M.J. Gamez, M.P. Utrilla, J. Jimenez, I. Osuna, Hypoglycemic activity of olive leaf. Planta Medica. 1992; 58: 513; 515.
3. B. Fehri, J.M. Aiache, A. Memmi, S. Korbi, M.T. Yacoubi, S. Mrad, J.L. Lamaison, Hypotension, hypoglycemia and hypouricemia recorded after repeated administration of aqueous leaf extract of Olea europaea L. *J. Pharm. Belg.* 1994; 49(2): 101108.
4. S. Foster Medicinal Herbs. Loveland, CO: Interweave Press, 1998; 148149.
5. J. Meirinhos, B.M. Silva, P. Valentão, R. M. Seabra, J.A . Pereira, A. Dias, P.B. Andrade, F. Ferreres, Analysis and quantification of flavonoidic compounds from Portuguese olive (Olea Europaea L.) leaf cultivars. Nat. Prod. Res. 2005; 19: 189195.

6. S. Lee-Huang, L. Zhang, P.L. Huang, Y.T. Chang, P.L. Huang, Anti-HIV activity of olive leaf extract (OLE) and modulation of host cell gene expression by HIV1 infection and OLE treatment. Biochem. Biophys. Res. Commun. 2003; 307: 1029–1037.
7. K. Takeda, T. Hosoi, T. Noda, H. Arimura, K. Konno, Effect of fibroblast-derived differentiation inducing factor on the differentiation of human monocytoid and myeloid leukemia cell lines. Biochem. Biophisic Res. *Commun.* 1988; 155: 24–31.
8. H. Isoda, H. Shinmoto, D. Kitamoto, M. Matsumura, T. Ankara, Differentiation of human promyelocytic leucemia cell line HL60 by mitocondrial extracellular glycolipids. Lipids 1997; 32(3): 263–271.
9. J. Tai, S. Cheung, W. Stefan, C. Lowe. In vitro comparaison of Essiac and Flor-Essence on human tumor cell lines. Oncol. Reports 2004; 11: 47–476.
10. H. K. Hamdi, R. Castellon. Oleuropein, a non-toxic olive iridoid, is an anti-tumor agent and cytoskeleton disruptor. Biochem. Biophy. Res. Commun. 2005; 334: 769–778.

In Vitro Observation of the Effect of Intestinal Bacteria on IgA Production by Immunocytes in the Large Intestine: Comparison Between Germ-Free and Conventional Mice

Tsutomu Yanagibashi, Akira Hosono, Masato Tstuda, Satoshi Hachimura, Kazuhiro Hirayama, Kikuji Itoh, Kyoko Takahashi, and Shuichi Kaminogawa

Abstract Previous studies comparing germ-free (GF) and conventional (CV) mice have shown that intestinal commensal microorganisms greatly affect the development of gut-associated lymphoid tissues and mucosal immune responses such as IgA production in the gut. Since there is a large number of intestinal microbiota, particularly in the large intestine, it is supposed that immunocytes in the large intestine are modulated by microbacteria. In this study, we investigated the immunomodulation of IgA production by intestinal microbacteria in the large intestine by comparing immunocytes from CV mice with those from GF mice. In GF mice, there were very few IgA plasma cells in lamina propria isolated from the large intestine (L-LP), but interestingly, greater numbers of IgA plasma cells were identified in lamina propria from the small intestine (S-LP). These findings suggested that IgA plasma cells in S-LP were stimulated by something other than intestinal commensal bacteria. We then found that the level of IgA production by L-LP IgA plasma cells isolated from GF mice was lower than that of CV mice. In addition, we examined the response of $B220^+$ cells isolated from L-LP to LPS, a constituent of gram-negative bacteria. The result was that the $B220^+$ cells from L-LP of GF mice produced IgA at lower levels than $B220^+$ cells of CV mice. These data suggest that the IgA response in the large intestine is strongly induced by stimulation by intestinal microorganisms.

Keywords IgA • lamina propria • germ-free

T. Yanagibashi, A. Hosono, M. Tstuda, K. Takahashi, and S. Kaminogawa
Department of Food Science and Technology, Nihon University, Fujisawa-shi, Kanagawa, 252–8510, Japan

S. Hachimura
Department of Applied Biological Chemistry, The University of Tokyo, 1-1-1, Yayoi, Bunkyo-ku, Tokyo, 113-8657, Japan

K. Hirayama and K. Itoh
Veterinary Public Health, The University of Tokyo, 1-1-1, Yayoi, Bunkyo-ku, Tokyo, 113-8657, Japan

K. Ikura et al. (eds.), *Animal Cell Technology: Basic & Applied Aspects*,
Animal Cell Technology: Basic & Applied Aspects 15,
DOI 10.1007/978-1-4020-9646-4_38,

1 Introduction

Previous studies have shown various interactions between intestinal commensal bacteria and the host physiology. Intestinal microbacteria are considered to regulate various intestinal functions, such as nutrient absorption, allergies, development of the immune system in the gut and so on. In particular, it is well-known that intestinal bacteria interact with intestinal immune systems and have important roles in the development of the mucosal immune system [1–3].

However, most studies of immunological function of the intestine have focused on the small intestine. The relationship between the immunological function of the large intestine and intestinal commensal bacteria is poorly understood. Additionally, intestinal microbacteria are more prominent in the large intestine than in the small intestine. Consequently, in this study, we investigated the immunomodulation of mucosal IgA production by intestinal microbacteria in the large intestine by comparing immunocytes from conventional (CV) mice with those from germ-free (GF) mice.

2 Materials and Methods

2.1 Mice

Conventional and germ-free BALB/c mice (CLEA Japan, Tokyo Japan) were bred under conventional or germ-free conditions for experimental mice and were used at 9–15 weeks of age. In this study, we observed no differences in the immune responses between male and female mice. All experiments were performed in accordance with the guidelines for the care and use of laboratory animals by the College of Bioresource Sciences, Nihon University.

2.2 Cell Preparation

Lymphocytes from the lamina propria of the small intestine (S-LP) and the large intestine (L-LP) were isolated by the method described previously [4]. Briefly, the small intestines were removed, Peyer's patches were excised and were reversed by using a polyethylene tube, then cut into small pieces. The large intestines were removed, isolated lymphoid follicles were excised and were opened longitudinally, and cut into two pieces. Then the small and large intestines were washed three times with 40 ml of Ca^{2+}- and Mg^{2+}-free Hanks' balanced salt solution (Sigma, St. Louis, MO, USA) supplemented with 5% FCS and 5 mM EDTA in 50 ml of tube and incubated at 37°C for 30 min with shaking at 150 rpm. The tissues were cut into smaller pieces, and were incubated with Hanks' balanced salt solution (Sigma) supplemented with 5% FCS, 0.2% $NaHCO_3$ (HBSS+) and 1 mg/ml collagenase

Type I (Sigma) at 37°C for 40–60 min with stirring. Collected cells were placed on the boundary between 44/70% concentrations of Percoll (GE Healthcare UK, Little Chalfont, Buckinghamshire, England) solution and were centrifuged at 1,800 rpm, 20°C for 20 min. After centrifugation, the collected cells were washed and used as lamina propria lymphocytes.

2.3 Flow Cytometric Analysis

S-LP and L-LP lymphocytes were incubated with optimal concentrations of FITC-conjugated anti-mouse IgA, PE-conjugated anti-mouse Syndecan-1, APC-Cy7-conjugated anti-mouse B220 (BD Biosciences, Franklin Lakes, NJ, USA) and Propidium Iodide (Sigma). Flow cytometric analysis was then performed using FACScanto (BD Biosciences). Analysis was performed using FlowJo software (Tree Star, Ashland, OR, USA).

2.4 Enzyme-Linked Immunospots

An enzyme-linked immunospot (ELISPOT) assay was used to detect cells producing IgA antibody. 96-well Multi-Screen HA plates (Millipore, Bedford, MA, USA) were coated with anti-mouse IgG $F(ab')_2$ fragment antibody (Sigma) at 20 μg/ml. After overnight incubation at 4°C, plates were blocked with RPMI 1640 containing 10% fetal bovine serum. L-LP lymphocytes from CV mice were plated at 2.5×10^3 cells/well, and those of GF mice were plated at 5×10^3 cells/well for 3 h at 37°C. Bound antibody was detected with Alkaline Phosphatase- (AP) conjugated anti-mouse IgA antibody (Southern Biotec, Birmingham, AL, USA) for 2 h at room temperature. AP was developed using Fast blue BB (Sigma) for 40 min.

2.5 Detection of IL-6 Products

L-LP lymphocytes were cultured in 96-well plates at 2.5×10^6 cells/ml for 72 h and co-cultured with 0 or 10 μg/ml LPS in RPMI 1640 medium containing 2.5% fetal bovine serum. IL-6 production by L-LP lymphocytes was measured by Cytokine Beads Array System (BD Biosciences) following the manufacturer's instructions.

2.6 Isolation of $B220^+$ Cells and IgA-Plasma Cells

S-LP and L-LP lymphocytes blocked with anti-FCγRII/III (BD Biosciences) were divided into $B220^+$ cells and $B220^-$ cells by magnetic cell sorting (MACS; Miltenyi Biotec, Bergisch Gladbach, Germany) with anti-mouse B220-conjugated magnetic

microbeads. Furthermore, IgA-plasma cells were isolated from the $B220^-$ fraction by subsequent reaction with PE-conjugated anti-IgA antibody (Southern Biotec), and anti PE-conjugated magnetic microbeads (Milteny Biotec).

2.7 Measurement of Total IgA

$B220^+$ cells were cultured in 96-well plates at 2.5×10^6 cells/ml for 5 days and co-cultured with 0 or 10 μg/ml LPS in RPMI 1640 medium containing 2.5% fetal bovine serum. IgA-plasma cells were cultured for 1 week in 96-well plates at 5×10^5 cells/ml in RPMI 1640 medium containing 2.5% fetal bovine serum. Total IgA in the culture supernatant was measured by sandwich ELISA as described previously [5].

3 Results

3.1 The Frequency of IgA-Plasma Cells and IgA-Secreting Cells in L-LP

To demonstrate the differentiation of $B220^+$ cells into IgA-plasma cells as stimulated by intestinal commensal bacteria, we compared the frequencies of IgA^+ $B220^-$ Syndecan-1^+ cells in the L-LP of CV and GF mice. In the L-LP of CV mice, there were small numbers of IgA^+ $B220^-$ Syndecan-1^+ cells. However, in the L-LP of GF mice, these cells were scarcely detected. Interestingly, in the S-LP of GF mice, these cells were very few. Furthermore, to confirm whether IgA^+ $B220^-$ Syndecan-1^+ cells were IgA-plasma cells or not, we determined the ratio of IgA-secreting cells by ELISPOT assay. The frequency of IgA-secreting cells in L-LP correlated well with that of IgA^+ $B220^-$ Syndecan-1^+ cells. IgA^+ $B220^-$ Syndecan-1^+ cells were considered to be IgA-plasma cells (Table 1).

Table 1 The frequency of IgA^+ $B220^-$ Syndecan-1^+ cells detected by flow cytometry and IgA-secreting cells measured by ELISPOT assay

	CV		G.F	
	S-LP	L-LP	S-LP	L-LP
IgA^+ $B220^-$ Syndecan-1^+ cells	++	+	+	–
IgA-secreting cells	++	+	+	–

The frequency of IgA^+ $B220^-$ Syndecan-1^+ cells in S-LP and L-LP of CV and GF mice determined by flow cytometry correlated well with that of IgA-secreting cells in S-LP and L-LP of CV and GF mice measured by ELISPOT assay. ++, +, – were judged based on the results on three separate experiments.

3.2 L-LP Lymphocytes' IL-6 Production

Previous studies have shown that IL-6 plays important roles in IgA production and secretion [6]. We measured IL-6 production levels in L-LP and found that levels in L-LP from GF mice were lower than those from CV mice (Table 2).

3.3 IgA Production by IgA-Plasma Cells and B220$^+$ Cells Isolated from L-LP

We tried to evaluate the effect of intestinal commensal bacteria on IgA production by IgA-plasma cells using ELISA to assay total IgA production. The IgA production levels of IgA-plasma cells isolated from L-LP of GF mice were lower than that of CV mice (Table 3).

In addition, the IgA production levels by B220$^+$ cells were measured. B220$^+$ cells did not include IgA-plasma cells; therefore measurement of IgA production by B220$^+$ cells reflected the differentiation of B220$^+$ cells into IgA-plasma cells. We compared the IgA production by B220$^+$ cells from L-LP between CV mice and GF mice and found that in GF mice the IgA production was very low, whereas in CV mice the levels were high (Table 3).

Table 2 The levels of IL-6 production by L-LP lymphocytes

	CV	GF
IL-6 production	++	+

The levels of IL-6 production by L-LP lymphocytes of CV were higher than that of GF mice. These were determined by ELISA. ++, +, – were judged based on the results on three separate experiments.

Table 3 The levels of IgA production by IgA-plasma cells and B220$^+$ cells isolated from L-LP

	CV	GF
IgA-plasma cells	++	+
B220$^+$ cells	++	+

The levels of IgA production by IgA-plasma cells from L-LP of CV mice were higher than those of GF mice. Also, the levels of IgA production by B220$^+$ cells from L-LP of CV mice were higher than those of GF mice. These were determined by ELISA. ++, +, – were judged based on the results on three separate experiments.

4 Discussion

In GF mice, the frequency of IgA-plasma cells in L-LP was lower than that in S-LP. It is suggested that the differences in numbers and species of the enterobacteria might induce the immunological developmental differences between the large intestine and the small intestine in CV mice. Also, lymphocytes in L-LP may be more affected by intestinal bacteria than that in S-LP, because the microbiota in the large intestine is more varied than that in the small intestine. Furthermore, in S-LP, it is plausible that the differentiation into IgA-plasma cells was affected by factors other than intestinal commensal bacteria.

In addition, IL-6 production by L-LP lymphocytes from CV mice was higher than that from GF mice. It is considered that intestinal bacteria might enhance IgA production by IgA-plasma cells and might induce the differentiation of $B220^{+}$ cells into IgA-plasma cells.

Taken together, the IgA response in the large intestine was strongly induced by intestinal commensal bacteria.

Acknowledgements We thank Dr. Yoshimasa Takahashi (National Institute of Infectious Diseases) for advice on the detection of IgA-plasma cells and ELISPOT assay.

References

1. Umesaki, Y., H. Setoyama, S. Matsumoto, A. Imaoka, and K. Itoh. 1999. Differential roles of segmented filamentous bacteria and clostridia in development of the intestinal immune system. *Infect Immun 67*:3504.
2. Sudo, N., S. Sawamura, K. Tanaka, Y. Aiba, C. Kubo, and Y. Koga. 1997. The requirement of intestinal bacterial flora for the development of an IgE production system fully susceptible to oral tolerance induction. *J Immunol 159*:1739.
3. Schultz, M., C. Veltkamp, L. A. Dieleman, W. B. Grenther, P. B. Wyrick, S. L. Tonkonogy, and R. B. Sartor. 2002. Lactobacillus plantarum 299V in the treatment and prevention of spontaneous colitis in interleukin-10-deficient mice. *Inflammatory Bowel Diseases 8*:71.
4. Fagarasan, S., K. Kinoshita, M. Muramatsu, K. Ikuta, and T. Honjo. 2001. In situ class switching and differentiation to IgA-producing cells in the gut lamina propria. *Nature 413*:639.
5. Nakani, Y., A. Hosono, Y. Hiramatsu, T. Kimura, R. Nakamura, and S. Kaminogawa. 2005. Characteristic immune response in Peyer's patch cells induced by oral administration of bifidobacterium components. *Cytotechnology 47*:49.
6. Bromander, A. K., L. Ekman, M. Kopf, J. G. Nedrud, and N. Y. Lycke. 1996. IL-6-deficient mice exhibit normal mucosal IgA responses to local immunizations and Helicobacter felis infection. *J Immunol 156*:4290.

Differentiation of Human Leukemia Cell Line HL-60 by a Polyacetylenic Compound from Hedera Rhombea

Yui Kurita, Parida Yamada, Hideyuki Shigemori, and Hiroko Isoda

Abstract A novel polyacetylenic compound, Compound **1**, was isolated and purified using a SiO_2 column and ODS HPLC from an acetone extract of Japanese ivy (*Hedera rhombea*). The differentiation-inducing effects of Compound **1** were then determined using the human promyelocytic leukemia cell line HL-60, which is considered useful for studying cellular and molecular events involved in differentiation by chemical agents. The effects of Compound **1** on HL-60 cell viability and proliferation were determined at different treatment times using the MTT assay. The results showed a decrease in cell viability after 48 h of treatment, followed by an increase; however, morphological changes were also observed. Differentiation was assessed by specific and nonspecific esterase double staining. Microscopic observation showed that Compound **1** induced HL-60 cells to differentiate into granulocytes. In addition, the effects of Compound **1** on HL-60 cell cycle kinetics were determined at different treatment times by flow cytometry. Compound **1** induced changes in cell cycle kinetics and induced G1 phase arrest. We report on the HL-60 cell differentiation effect of the novel polyacetylenic compound, Compound **1**, from Japanese ivy (*Hedera rhombea*).

Keywords Keywords • HL-60 • differentiation • cell cycle • polyacetylenic compound

1 Introduction

Galls are made by plants in response to parasitism by insects or fungi. The pharmacological activity of some galls has been reported; however, galls from many other plants have not yet been thoroughly studied. Therefore, bioactive substances in

Y. Kurita, P. Yamada, H. Shigemori, and H. Isoda
Graduate School of Life and Environmental Sciences, University of Tsukuba,
Tennodai 1-1-1, Tsukuba, Ibaraki, Japan

K. Ikura et al. (eds.), *Animal Cell Technology: Basic & Applied Aspects*,
Animal Cell Technology: Basic & Applied Aspects 15,
DOI 10.1007/978-1-4020-9646-4_39,

galls of *Hedera rhombea* were explored, and 4 novel polyacetylenic compounds were isolated. Moreover, 2 novel polyacetylenic compounds were also isolated from flower buds of *Hedera rhombea.* One of the polyacetylenic compounds, 3-hydroxyheptadeca-1,9-dien-4,6-diyn-8yl-11(1H-indol-3-yl)acetate (Compound **1**) from flower buds of *Hedera rhombea* has a polyacetylenic chain and IAA in one structure and it is the first time that such compound is reported; therefore, we examined the biological activity of Compound **1**.

The biological activity of some polyacetylenic compounds has been reported [1, 2, 3]. Some polyacetylenic compounds in *Panax ginseng* inhibited the growth of various cell lines in a dose-dependent manner, and the cell growth inhibitory activity is much stronger against malignant cells than against normal cells. Moreover, the proliferation of human renal carcinoma cell lines was inhibited by a polyacetylenic compound from *Panax ginseng* roots by blocking the cell cycle progression at the G_1 to S phase transition. A spongean polyacetylene induced neuronal cell differentiation in a neuroblastoma cell line, Neuro 2A, and the cell cycle of Neuro 2A cells was found to be specifically blocked at the G_1 phase by a spongean polyacetylene.

HL-60, a human promyelocytic leukemia cell line, is useful for studying cellular and molecular events involved in differentiation by chemical agents. It also has the bipotential to differentiate into mature granulocytes and monocytes [4]. In this study, we determined whether a novel polyacetylenic compound from the flower buds of *Hedera rhombea* can induce differentiation in HL-60 cells.

2 Materials and Methods

2.1 Cell Culture

HL-60 cells were grown in the RPMI 1640 medium supplemented with 10% fetal bovine serum (FBS) and 1% penicillin/streptomycin. The cells were kept in an incubator at 37°C in a humidified atmosphere of 5% CO_2 in air.

2.2 Materials

Flower buds of *Hedera rhombea* were collected from Tsuchiura City, Japan and 140 g were homogenized using a blender, then extracted with acetone (500 ml) and concentrated in vacuo to obtain an acetone extract (3.99 g). The MeOH-soluble portion was eliminated from the acetone extract (3.99 g) and subjected to silica gel column chromatography (2.0 × 20 cm) eluted with a $CHCL_3$-EtOAc solvent system with increasing polarity ($CHCL_3$/EtOAc, 9:1→1:1) to afford 10 fractions (fr. 1 –fr. 10). Fraction 7 (60.5 mg, $CHCL_3$/EtOAc, 6:1) was further applied to a silica gel column (1.0 × 13 cm) eluted with n-hexane/EtOAc (9:1→1:2) to 9 fractions. The fraction (4.3 mg) eluted with n-hexane/EtOAc (6:1) was separated by reversed-phase HPLC [Atlantis dC18 5 μm, 4.6 mm × 25.0 cm, Waters, flow rate 1.0 ml/min,

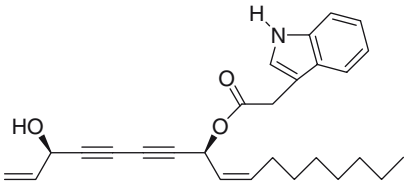

Fig. 1 Chemical structure of compound **1**

CH_3CN/H_2O, 85:15 v/v, UV detection (195, 214, 254, 280, and 300 nm)] to yield Compound 1 (0.7 mg) (Fig.1).

2.3 MTT Assay

The time-dependent change in cell viability and proliferation was determined using the MTT tetrazolium assay. HL-60 cells were seeded onto a 96-well plate at 10^3 cells per well in 50 μl of RPMI 1640 medium (Gibco) and then preincubated for 24 h. Compound 1 diluents were added at 50 μl per well, followed by incubation for 24, 48, 72, 96, and 120 h at 37°C in a humidified atmosphere of 5% CO_2 in air. MTT (5 mg/ml) was then added at 10 μl per well, followed by 24 h of incubation at 37°C; 100 μl of 10% SDS was added to each well to solubilize the MTT formazan product. After 24 h of incubation at 37°C, the absorbance at 570 nm was determined with a POWERSCAN HT multidetection microplate reader

2.4 Specific and Nonspecific Esterase Double Staining

HL-60 cell differentiation was determined by the specific and nonspecific esterase double staining method. HL-60 cells were plated onto 8-well chamber slides at 10^4 cells per well in 200 μl of RPMI 1640 medium (Gibco) and preincubated for 24 h. Compound 1 diluents were added at 100 μl per well, followed by incubation for 48 h. The diluents were then removed, the cells fixed with 300 μl of fixing solution (acetone:citric acid:formaldehyde = 65:25:8), and specific and nonspecific esterase double staining was performed. First, 300 μl of α-naphtyl acetate esterase staining reagent was added to each well, followed by incubation for 30 min at 37°C, and then rinsing with MilliQ. Next, 300 μl of As-D-chloroacetate esterase staining reagent was added to each well, followed by incubation for 15 min at 37°C, and then rinsing with MilliQ. Finally, 300 μl of hematoxylin was added, followed by incubation for 2 min at room temperature, and then thorough rinsing. Slides were observed using a phase-contrast microscope. Photographs of stained cells were taken at the same magnification for each concentration, and the numbers of differentiated and undifferentiated cells were counted. The differentiation rate was calculated by dividing the number of differentiated cells by the total cell number.

2.5 Time-Dependent Change in Cell Cycle Kinetics

The time-dependent change in HL-60 cell cycle kinetics was analyzed by flow cytometry. A 10-ml suspension of HL-60 cells (2×10^4 cells/ml) was treated with Compound 1 for 24, 48, 72, and 96 h at 37°C in a 5% CO_2 incubator. After treatment, 1 ml of treated HL-60 cells was washed with PBS and fixed with 70% ethanol, and then allowed to stand at 4°C for more than 12 h. The fixed cells were centrifuged (500 × g) at 25°C for 5 min, the supernatant was then removed, and the cells washed with PBS. Cell Cycle Reagent was added at 200 µl, followed by incubation in darkness for 30 min. Cell cycle kinetics was then determined by flow cytometry (Guava PCA).

3 Results and Discussion

3.1 Time-Dependent Change in HL-60 Cell Viability

The time-dependent change in HL-60 cell viability was determined using the MTT assay. The viabilities of cells incubated with a high concentration of Compound **1** (10 µg/ml) were low for every treatment time; therefore, it was considered that 10 µg/ml is cytotoxic. On the other hand, cells incubated at lower concentration (0.1 and 1 µg/ml) showed low viability after 48 h of treatment, while those incubated for 72, 96, and 120 h showed higher cell viability. Therefore, it is suggested that HL-60 cells undergo differentiation during the first 48 h of treatment with Compound **1**, after which, the differentiated cells proliferate (Fig. 2).

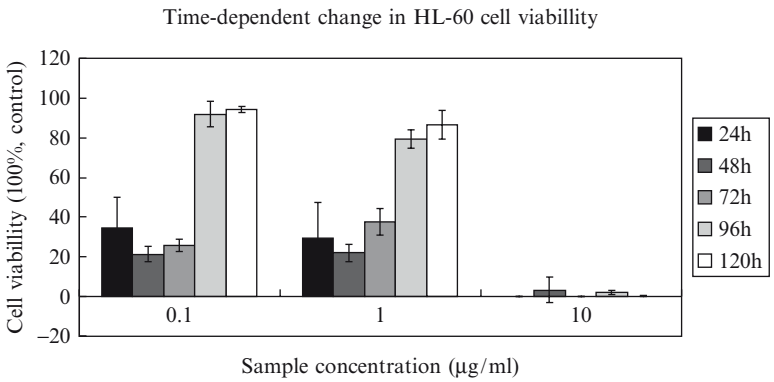

Fig. 2 The time-dependent effect of compound 1 on HL-60 cell viability

3.2 Specific and Nonspecific Esterase Double Staining

We performed specific and nonspecific esterase double staining to determine whether treated HL-60 cells differentiate into granulocytes or monocytes. Granulocytes are positively stained by naphtol As-D chloroacetate to yield red granules, while monocytes are positively stained by α-naphtyl acetate to yield black granules. HL-60 cells incubated with Compound **1** were double-stained with specific and nonspecific esterases followed by microscopic observation. Results showed morphological changes in many cells, as well as red granulation. Therefore, it was revealed that Compound **1** can induce HL-60 cells to differentiate into granulocytes. Moreover, from dose-dependent and time-dependent experiments, it was found that cells incubated with 1 μg/ml of Compound **1** showed the highest differentiation rate (88.5%) after 48 h of incubation (Fig. 3).

3.3 Time-Dependent Change in Cell Cycle Kinetics

Because it has been reported that the differentiation of HL-60 cells is associated with G_1 arrest [5], we determined the effect of Compound **1** on the time-dependent cell cycle kinetics of HL-60 cells. The cell cycle kinetics of HL-60 cells incubated with Compound **1** showed G_0/G_1 phase arrest (after 24, 48, and 96 h of treatment). It is suggested that G_0/G_1 phase arrest induced HL-60 cell differentiation. The cell cycle kinetics of cells incubated for 72 h with Compound **1** was different from those of cells incubated for 24, 48 and 96 h. It is suggested that the cell cycle kinetics changed after 48 h of incubation as a result of differentiation (Fig. 4).

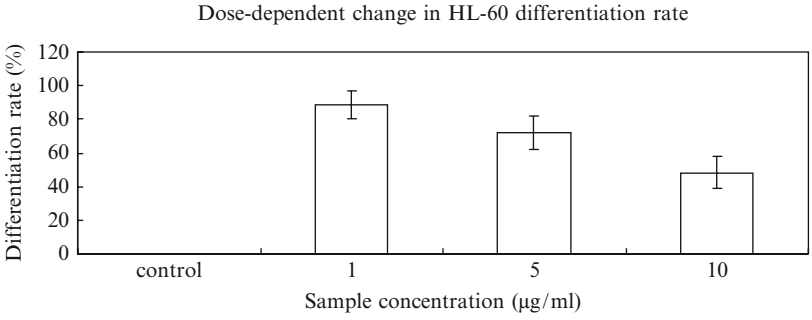

Fig. 3 The dose-dependent effect of compound 1 on HL-60 differentiation rate

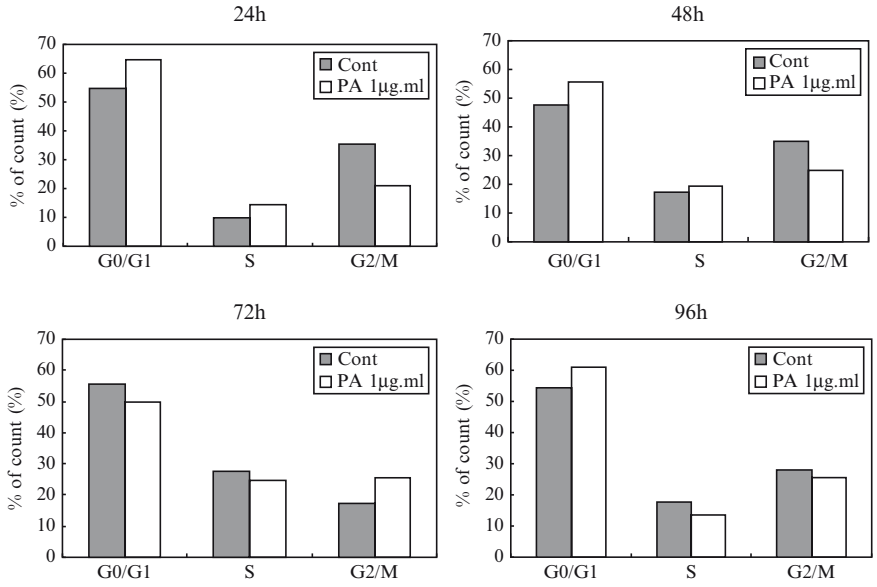

Fig. 4 Effect of Compound 1 on the time-dependent cell cycle kinetics on HL-60 cells

References

1. H. Matsunaga, M. Katano, H. Yamamoto, H. Fujito, M. Mori, and K. Takata, 1990, Cytotoxic activity of polyacetylene compounds in Panax finseng C. A. Meyer, Chemical and Pharmaceutical Bulletin, 38(12), 3480–3482.
2. J. Sohn, C. Lee, D. Chung, S. Park, I. Kim, and W. Hwang, 1998, Effect of petroleum ether extract of Panax ginseng roots on proliferation and cell cycle progression of human renal cell carcinoma cells, Experimental and Molecular Medicine, 30(1), 47–51.
3. S. Aoki, K. Matsui, T. Takata, W. Hong, and M. Kobayashi, 2001, Lembehyne A, a spongean polyacetylene, induces neuronal differentiation in meuroblastoma cell, Biochemical and Biophysical Research Communications, 289, 558–563.
4. H. Isoda, H. Shinmoto, D. Kitamoto, M. Matsumura, and T. Nakahara, 1997, Differentiation of human promyelocytic leukemia cell line HL60 by microbial extracellular glycolipids, Lipids, 32(3), 263–271.
5. H. Kuo, W. Kuo, Y. Lee, C. Wang, and T. Tseng, 2006, Enhancement of caffeic acid phenethyl ester on all-trans retinoic acid-induced differentiation in human leukemia HL-60 cells, Toxicology and Applied Pharmacology, 216, 80–88.

Effect of Tunisian Plant Extract on Melanogenesis

Kyoko Matsuyama, Mitsuko Kawano, Mohamed Kchouk, Hiroshi Shinmoto, and Hiroko Isoda

Abstract In this study, we determined whether Tunisian aromatic plants can induce melanogenesis in the cultured mouse melanoma cell line, B16. The cells were cultured with or without Tunisian aromatic plant extracts. We found that melanogenesis was enhanced by Tunisian aromatic plant extract without affecting cell growth and cell shape. This denotes that Tunisian aromatic plant can induce melanogenesis in B16 cells without causing transformation. In succeeding experiments, we found that Tunisian aromatic plant promoted melanogenesis without affecting tyrosinase protein expression. Moreover, we did not detect the phosphorylation of extracellular signal-regulated kinase 1 and 2 (ERK1/2), which are related to inhibition of melanogenesis.

Keywords Tunisian aromatic plant • B16 • melanogenesis • tyrosinase • ERK1/2

1 Introduction

Pigmentation of the epidermis is caused by excessive melanin synthesis, and melanin plays a major role in photoprotection. Melanin biosynthesis is regulated by melanogenic enzymes, such as tyrosinase, tyrosinase-related protein 1 (TYRP-1) and TYRP-2. Above all, tyrosinase is a very important enzyme in melanin synthesis. Tyrosinase catalyzes the first two steps in melanin synthesis: the hydroxylation of tyrosine to 3-(3,4-dihydroxyphenyl)-alanine (DOPA) and the oxidation of DOPA to dopaquinone [1]. Thus, melanin production is mainly dependent on tyrosinase expression and activation.

K. Matsuyama, M. Kawano, and H. Isoda
Alliance for Research on North Africa (ARENA), Graduate School Life and Environmental Science, University of Tsukuba, 1-1-1 Tennodai, Tsukuba, Ibaraki, 305-8572, Japan

M. Kchouk
Technopole de Borj-Cedria-Centre de Biotechnologie, BP 901, Hammam-Lif 2050, Tunisia

H. Shinmoto
National Food Research Institute (NFRI), 2-1-12 Kannondai, Tsukuba Ibaraki 305-8642, Japan

K. Ikura et al. (eds.), *Animal Cell Technology: Basic & Applied Aspects*,
Animal Cell Technology: Basic & Applied Aspects 15,
DOI 10.1007/978-1-4020-9646-4_40, © Springer Science+Business Media B.V. 2009

Extracellular signal-regulated kinase (ERK) is a key signaling mediator of cell proliferation and differentiation. Recently, it has been reported that ERK signaling pathway is related to melanogenesis. When melanogenesis is inhibited, ERK1/2 is phosphorylated [2].

Essential oils of aromatic plants are valuable natural products used as raw materials in many fields, including perfumes, cosmetics, aromatherapy, phototherapy, spices and nutrition. Recently, many papers on the biological and pharmacological activity of aromatic plants have been published [3].

In this study, we investigated the effects of Tunisian aromatic plants on melanin synthesis, cell growth and tyrosinase activity in the mouse melanoma cell line, B16. In addition, we examined the Tunisian aromatic plant's effects on signaling pathway and protein expression in relation to melanogenesis.

2 Materials and Methods

2.1 Cell Culture

B16 mouse melanoma cells were provided by Dr. Hiroshi Shinmoto, National Food Research Institute (NFRI), 2-1-12 Kannondai, Tsukuba Ibaraki 305-8642, Japan.

The cells were cultivated at 37°C under 5% CO_2 atmosphere in DMEM (9.5 mg/ml Dulbecco's Modified Eagle Medium, 0.1% $NaHCO_3$, 4 mM L-glutamine) containing 10% FBS and 1% penicillin-streptomycin.

2.2 Measurement of Melanin Content and Microscopic Examination

B16 mouse melanoma cells were seeded at 1.0×10^6 cells in 10 ml of medium in a 100-mm dish and grown for 5 days. On days 1 and 3, the medium was replaced with fresh medium containing the Tunisian aromatic plant extract (1:1,000 dilution). The melanin content of cells was measured by the method of Hosoi et al. [4] with slight modifications. B16 mouse melanoma cells grown in a 100-mm dish were washed with Mg^{2+}-, Ca^{2+}-free phosphate-buffered saline [PBS(−)]. The cells were harvested by trypsinization, and precipitated by centrifugation at 2,300 ***g*** for 5 min at 20°C. After centrifugation, the cells were sonicated in 0.5 ml of 1% Triton X-100/PBS (−) on ice. For a quantitative measurement of melanin, acid-insoluble materials were obtained by extracting the pellet twice with 10% trichloroacetic acid. The precipitate was washed once with 100% ethanol, dried and then solubilized by incubating with 1 ml of 1 N NaOH-10% dimethyl sulfoxide at 80°C for 2 h. Standard melanin was also solubilized and used to generate a standard curve (0–50 μg/ml). The absorbance of the solutions was measured at 470 nm using a DR/4,000 spectrophotometer (HACH Co., USA), and the melanin content was calculated as μg/10^6 cells.

Before measuring the melanin content, B16 cells were observed under a phase-contrast microscope and photographed.

2.3 Cell Viability

B16 mouse melanoma cells were seeded at 1.0×10^6 cells in 10 ml of medium in a 100-mm dish and grown for 5 days. On days 1 and 3, the medium was replaced with fresh medium containing the Tunisian aromatic plant extract (1:1,000 dilution). Cell viability was determined using the Guava ViaCount assay system (Guava Technologies, Inc., CA) according to the manufacturer's instructions.

2.4 Western Blot Analysis

For western blot analysis of tyrosinase, ERK1/2 or phospho-ERK1/2, B16 mouse melanoma cells were seeded at 3.0×10^6 cells in 10 ml of medium in a 100-mm dish. After overnight culture, the cells were treated with the extract for 5 h. The cells were lysed in RIPA buffer (SIGMA, USA) and whole proteins were extracted by the freeze-thaw method. Fifteen micrograms of protein were loaded in a single lane and separated by SDS-polyacrylamide gel electrophoresis and blotted onto nitrocellulose membranes (Bio-Rad Laboratories, Inc., CA), which were blocked with 5% skim milk in Tris-buffered saline. After blotting, the membrane was incubated with the appropriate primary antibodies for tyrosinase (Santa Cruz Biotechnology, USA), ERK1/2 (SIGMA, USA) and phospho-ERK1/2 (SIGMA, USA). After washing with TBST buffer (0.05% Tween 20/TBS), the membrane was incubated with horseradish peroxidase-conjugated secondary antibody. After washing with TBST buffer, the membrane was reacted with ECL reagent (Amersham Pharmacia Biotech, UK) or Immobilon Western Chemiluminescent HRP Substrate (Millipore Corporation, USA) and photographed using an ECL camera (Amersham Pharmacia Biotech, UK).

3 Results and Discussion

3.1 Tunisian Aromatic Plant Does Not Induce Cell Morphological Change

Five days after treatment with the Tunisian aromatic plant extract (1:1,000 dilution), we did not observe cell morphological changes. However, we observed that the cells treated with the Tunisian aromatic plant extract contained more melanin than the nontreated cells. The Tunisian aromatic plant induces cell growth and melanin synthesis in B16 cells.

3.2 Tunisian Aromatic Plant Promotes Melanin Synthesis by B16 Cells

B16 cells were cultured in medium containing the Tunisian aromatic plant extract (1:1,000 dilution) for 5 days to determine its effect on melanin synthesis. The amount of melanin was quantitatively measured by the method of Hosoi et al. [4]. As shown in Fig. 1, the extract significantly increased the melanin content in B16 cells.

3.3 Effects of Tunisian Aromatic Plant on B16 Cell Viability

To exclude the possibility that the above promotion effects of the Tunisian aromatic plant extract on melanin synthesis might be related to cell growth inhibition, we compared the number of cells grown in the presence or absence of the Tunisian aromatic plant extract. B16 cells were cultured in medium containing the extract (1:1,000 dilution) for 5 days. As shown in Fig. 2, the extract did not seem to inhibit cell viability. These results indicate that the extract promoted melanin synthesis without cytotoxicity.

3.4 Tunisian Aromatic Plant Does Not Influence the Signaling Pathway Related to Melanogenesis

It has been reported that MAPK (mitogen-activated protein kinase) is related to melanogenesis. When melanogenesis is inhibited, one of the MAPK signaling molecules, ERK1/2, is phosphorylated [2, 5]. Thus, to determine ERK 1/2 phosphorylation, we extracted protein from B16 cells cultured for 5 h in medium containing the extract. We then performed western blotting analysis to detect the activated form of ERK1/2 using a specific antibody.

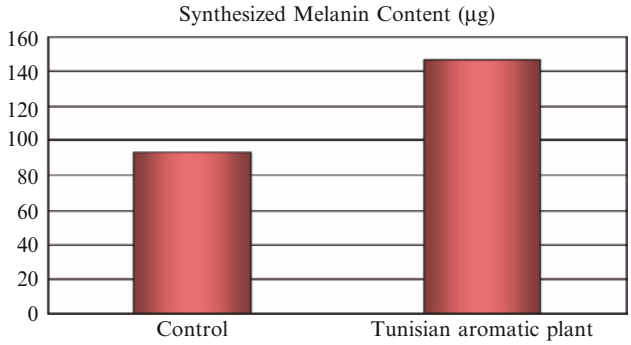

Fig. 1 Effect of Tunisian aromatic plant on melanin synthesis

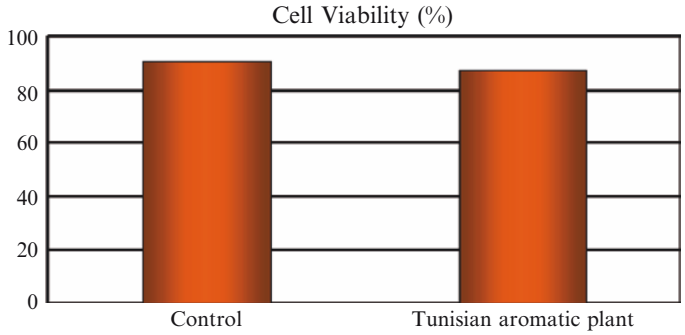

Fig. 2 Effect of Tunisian aromatic plant on cell viability

Results from the western blotting analysis reveal that the extract did not induce ERK1/2 phosphorylation. Thus, we confirm that the promotion effect of the Tunisian aromatic plant on melanin synthesis is not related to the ERK signaling pathway.

3.5 Tunisian Aromatic Plant Does Not Affect Tyrosinase Protein Expression in B16 Cells

To examine the mechanism underlying the promotion effect of the Tunisian aromatic plant extract on melanin synthesis, we determined the tyrosinase protein expression in B16 cells. The cells were cultured in medium containing the extract for 5 h. Then we extracted the proteins from B16 cells and performed western blotting analysis.

Results from the western blotting analysis reveal that the extract did not affect tyrosinase protein expression after 5 h of treatment, suggesting that the extract promotes melanin synthesis in B16 cells by activating other enzymes or signaling pathways [1, 6, 7].

In conclusion, we confirmed that the Tunisian aromatic plant extract promotes melanin synthesis without affecting cell growth and without upregulating tyrosinase protein expression in B-16 cells. The detailed mechanism of the melanin synthesis promotion activity in B16 cells will be reported in the future. This is the first report on the effect of Tunisian aromatic plants on melanin synthesis by mouse melanoma cells.

References

1. Kim, Y.J., Uyama, H., 2005, Tyrosinase inhibitors from natural and synthetic sources: structure, inhibition mechanism and perspective for the future. CMLS 62: 1707–1723.
2. Kim, D.S., Park, S.H., Kwon, S.B., Park, E.S., Huh, C.H., Youn, S.W., Park, K.C., 2005, Sphingosylphosphorylcholine-induced ERK activation inhibits melanin synthesis in human melanocytes. Pigment Cell Res. 19: 146–153.
3. Lahlou, M., 2004, Methods to study the phytochemistry and bioactivity of essential oils. Phytother. Res. 18: 435–448.

4. Hosoi, J., Abe, E., Suda, T., Kuroki, T., 1985, Regulation of melanin synthesis of B16 mouse melanoma cells by 1 alpha, 25-dihydroxyvitamin D3 and retinoic acid. Cancer Res. 45: 1474–1478.
5. Kim, D.S., Kim, S.Y., Park, S.H., Choi, Y.G., Kwon, S.B., Kim, M.K., Na, J.I., Youn, S.W., Park, K.C., 2005, Inhibitory effects of 4-n-Butylresorcinol on tyrosinase activity and melanin synthesis. Biol. Pharm. Bull. 28: 2216–2219.
6. Sugimoto, K., Nishimura, T., Nomura, K., Sugimoto, K., Kuriki, T., 2004, Inhibitory effects of α-Arbutin on melanin synthesis in cultured human melanoma cells and a three-dimensional human skin model. Biol. Pharm. Bull. 27: 510–514.
7. Kawano, M., Imamura, T., Isoda, H., 2006, Methods for searching and evaluating effective hair growth regulation factors from Tunisian samples. J. Arid Land Studies 15: 443–446.

"Nordenau Phenomenon" – Application of Natural Reduced Water to Therapy

Follow-Up Study upon 411 Diabetes Patients

Zbigniew Gadek, Takeki Hamasaki, and Sanetaka Shirahata

Abstract This prospective observation study examines changes in the relevant tests parameters of 411 diabetes patients drinking natural reduced water from the "Nordenau Spring", as well as a correlation of these changes with the fluctuation of the reactive oxygen species in their blood. The average age of the test persons is 71.5 years and the daily consumption of reduced water is as much as two liters. The average duration of stay in Nordenau is 6 days. The diagnostic parameters such as blood sugar, HbA1c, cholesterol, LDL, HDL, and serum creatinine concentration are tested twice - at the beginning and at the end of the participants stay in Nordenau. Additionally a random sample of reactive oxygen species in the blood of 136 patients is taken in order to find out its possible causal connections to the diabetes relevant test parameters.HbA1c has been considered as the substantial test parameter in order to break down the whole group into responder and non-responder categories. One hundred and eighty six tested persons or 45% of the total have been assigned to the responder group, meaning that the patients' HbA1c and blood sugar improved significantly. Furthermore we evaluated among the responder group a portion of patients who in the same time significantly improved their cholesterol, LDL, HDL and serum creatinine concentration average value. This stage of our follow up study regarding type II diabetes patients estimates number needed to treat on four patients in order to achieve the significant improvement of all diabetes relevant parameters. This is a very good quotient; moreover it could be achieved entirely without side effects. The significant improvement of diabetes relevant parameters like blood fats and creatinine can be also beneficial to other diseases like high blood pressure, circulatory disturbance, renal insufficiency or atherosclerotic dementia. In addition to our previous tests, we administered to a random sample group of 136 patients a blood free oxygen radicals test (FORT). The test resulted in a decrease of the ROS of

Z. Gadek
Center for Holistic Medicine and Naturopathy, 57392 Nordenau, Germany

T. Hamasaki and S. Shirahata
Department of Genetic Resources Technology, Faculty of Agriculture,
Kyushu University, Fukuoka 812-8581, Japan

K. Ikura et al. (eds.), *Animal Cell Technology: Basic & Applied Aspects*,
Animal Cell Technology: Basic & Applied Aspects 15,
DOI 10.1007/978-1-4020-9646-4_41, © Springer Science+Business Media B.V. 2009

70.6% of the group or 96 patients. Taking account of the fact that the natural reduced water as well as the electrolyzed reduced water obviously improves in a very short time and entirely without side effects very important metabolic parameters, it can be said that the reduced water shall be considered a useful supplement to the usual orthodox medication of ROS-associated diseases.

Keywords Diabetes • Noredenau water • reactive oxygen species • reduced water

1 Introduction

Reactive oxygen species (ROS) are known to cause various diseases including diabetes mellitus [1–6]. In the type II diabetes they cause reduction of glucose uptake by inhibiting the insulin-signaling pathway in muscle cells and adipocytes [7]. The anti-oxidative waters (reduced waters) such as electrolyzed reduced water and several natural reduced waters e.g. Nordenau water in Germany, Hita Tenryosui water in Japan scavenge ROS are expected to prevent or improve various oxidative stress-related diseases [8–12]. Electrolyzed reduced water, Nordenau water and Hita Tenryosui water stimulated uptake of 2-deoxy-D-glucose into both L6 myotubes and 3T3/L1 adipocytes in the presence or absence of insulin [13]. This insulin-like activity is mediated by the activation of PI-3 kinase, resulting in stimulation of translocation of glucose transporter GLUT4 from microsome to plasma membrane [13]. Insulin secretion from beta cells of pancreas (HIT-T15 cell line derived from Syrian hamster) shown in the medium containing Nordenau water and Hita Tenryosui water was 2.9 and 2.2 times higher than control, respectively [14]. Animal experiments using type II diabetes model mice (C57BL/Ks.J.Db+/Db+) exhibited the significant improved results in the sugar tolerance tests under administration of natural waters such as Nordenau water and Hita Tenryosui water [15]. This prospective observation has been done to find out if an antioxidant operating mechanism of reduced water could really be in a position to suppress the concentration of reactive oxygen species in the blood of diabetes patients and by it to improve their diabetes relevant blood test parameters. Furthermore this study searched for if the results of clinical trials correlate with those of the basic researches and animal experiments.

2 Material and Method

All the participants of the study were patients who had already been diagnosed by specialists and were receiving adequate medication as well as suitable diet guidelines. The inclusive criteria were defined only so far that all the tested persons were suffering by diabetes type II, no matter to age, sex, form of medication and diet. The average age of the test persons is 71.5 years and the daily consumption of reduced water is as much as two liters. The average duration of stay in Nordenau

is 6 days. The test persons were particularly reminded to continue the medication prescribed by their specialists, to stick to their individual diet plans and not to alter any of their behavioral patterns. During their stay in Nordenau the patients drank two liters natural reduced water from "Nordenau spring" daily. We were looking after the patients diagnostically within the scope of what is known as "course control". The investigators strictly kept to the requirements of neutrality and didn't alter either regular medication of the tested persons or their diet instruction. The diagnostic parameters such as blood sugar, HbA1c, cholesterol, HDL, LDL and serum creatinine concentration were tested twice. Once at the beginning and once at the end of the participants stay in Nordenau. Parallel to that the random sample of reactive oxygen species concentration in the blood of 136 patients had been additionally taken to find out the possible causal connections between the alteration of diabetes relevant parameters and the changes of their blood ROS.

The free oxygen radicals monitoring, which were applied, is based on so-called Haber-Weiss reaction. This method is due to the fact that the peroxides, which come into being by lipid peroxidation as an interim product, create in the presence of free transition metals (not bound on proteins) high aggressive hydroxyl radicals. These products can be measured in the presence of N, N-diethyl-para-phenylendiamin on the photometric way. The oxygen species level (ROS) in the blood had been stressed in FORT Units. Here 1 FORT Unit = 0.26 mg H_2O_2 /l blood. The values between 250 and 310 FORT Units are considered to be normal.

The statistical interpretation of this clinical data contains:

- The descriptive statistics of the whole group and of both subgroups
- A pairing-directed T-Test
- A proportional evaluation of the entire group and of both subgroups
- Variance and co-variance analyses

The allowance for error probability was set at 2.5%.

3 Results and Discussion

HbA1c has been considered as the substantial test parameter in order to break down the whole group into responder and non-responder categories (Fig. 1). One hundred and eighty six tested persons or 45% of the total have been assigned to the responder group, meaning that the patients' HbA1c and blood sugar improved significantly.

The data evaluation focuses exclusive on this group, although the significant improvement of cholesterol, LDL, HDL and serum creatinine concentration values has been registered among over 50% of total collective.

This restrictive criterion diminished in numbers the remaining patient's to 186, but the results of the database analysis of this smaller group win through this restriction much more evidence. Furthermore we evaluated among the responder group a portion of patients who in the same time significantly improved their cholesterol, LDL, HDL and serum creatinine concentration average value.

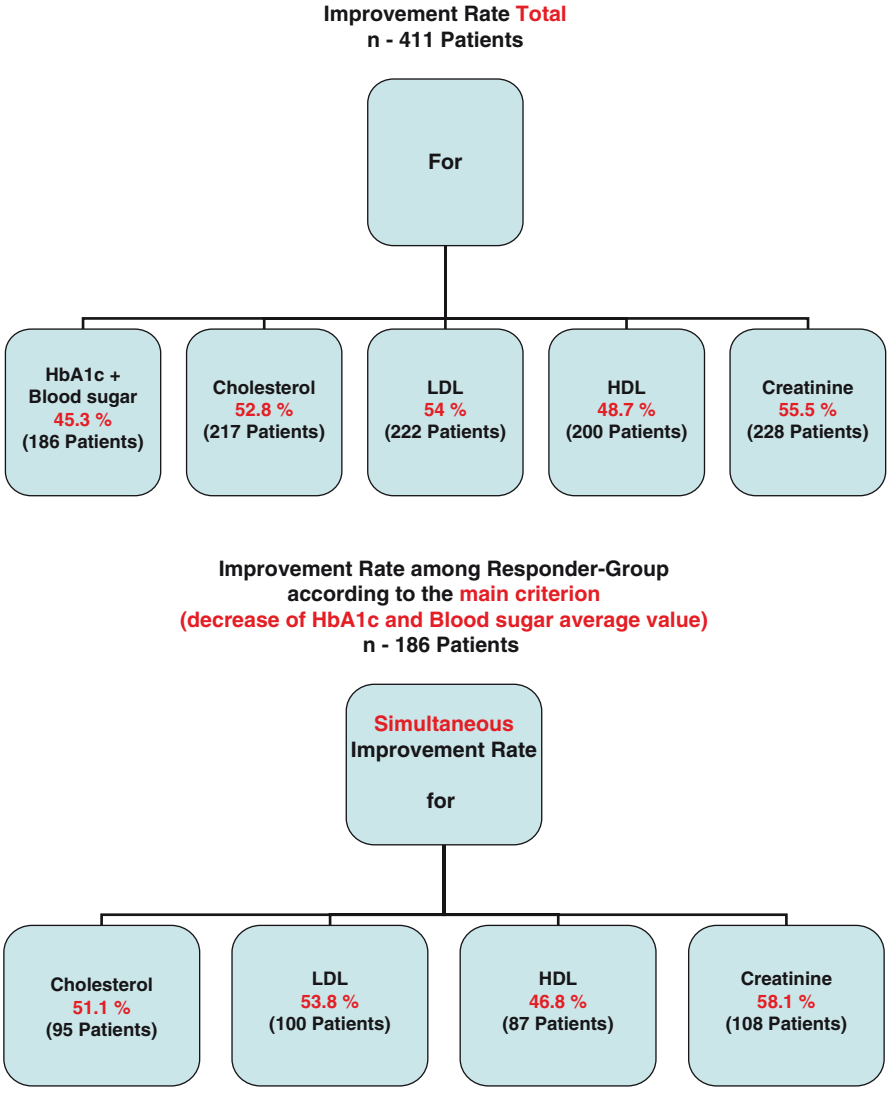

Fig. 1 Improvement rate among total and responder groups

The statistical significant improvement of cholesterol value had been observed among 51% (95 patients) of responder group. As a group, 54.0% of the responders (comprised of 100 persons) demonstrated a significant downward trend of the LDL average value.The average value of HDL increased significantly among 87 patients (47.0%) of the responder group.

The serum creatinine concentration was reduced significantly by among108 patients (58%) of the responder group.

At the next step we tried to find out if the length of therapy period, that also means the quantity of consumed reduced water, can scale up the improvement.

The following Fig. 2 confirm the certain regularity which can be defined as follows:

Except the changes of the serum creatinine concentration, the improvement scales up parallel to the lengths of the therapy period.

In addition to our previous tests, we administered to a random sample group of 136 patients a blood free oxygen radicals test (FORT). The test resulted in a decrease of the ROS of 70.6%.of the group or 96 patients. However, the downward trend of ROS in the blood of the patients (a decrease by 2.3%) was below statistical significance.

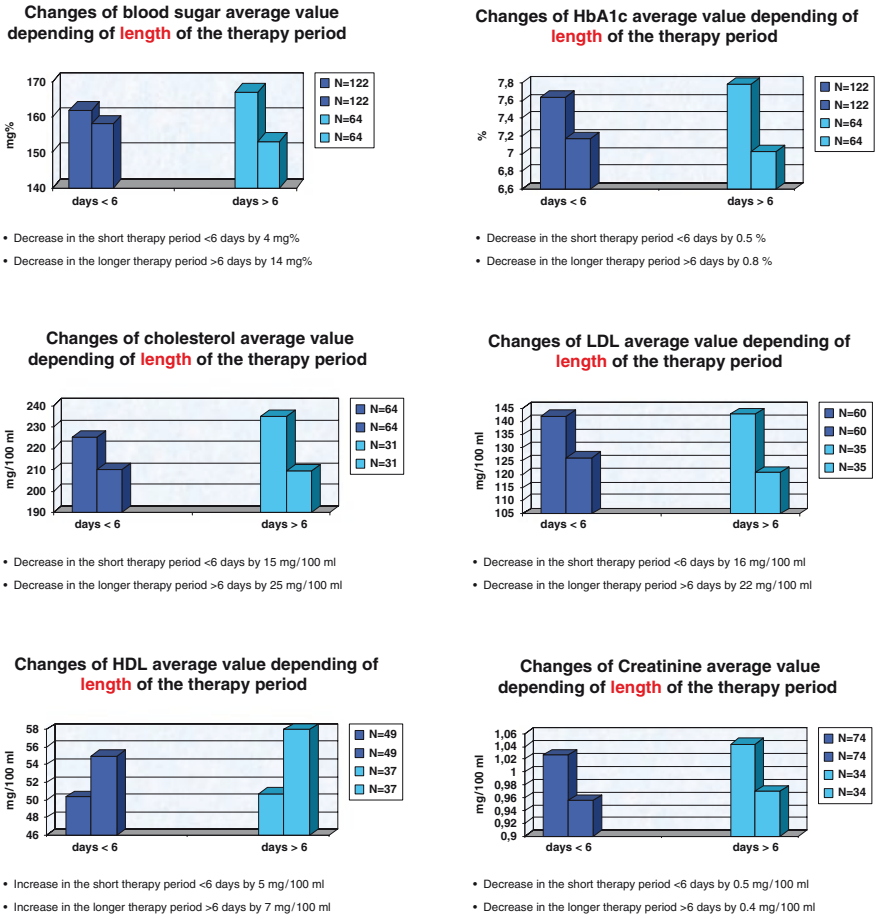

Fig. 2 Changes of blood sugar, HbA1c, cholesterol, LDL, HDL and creatinine average values depending of length of the therapy period

4 Conclusion

- Given the results of the clinical follow up studies on 411 diabetes II patients, it can be said that reduced water consumption seems to have a beneficial effect upon the most important diabetes parameters.
- The evaluation of the clinical data estimates number needed to treat on four patients in order to achieve the significant improvement of all diabetes relevant parameters. This is a very good quotient; moreover it could be achieved entirely without side effects.
- This improvement scales up parallel to the quantity of consumed reducer water.
- The significant improvement of diabetes relevant parameters like blood fats and creatinine can be also beneficial to other diseases like high blood pressure, circulatory disturbance, renal insufficiency or atherosclerotic dementia.
- Taking account of the fact that the natural reduced water as well as the electrolyzed reduced water obviously improves in a very short time and entirely without side effects very important metabolic parameters, it can be said that the reduced water shall be considered a useful supplement to the usual orthodox medication of ROS-associated diseases

References

1. Halliwell B and Gutteridge JMC (1990) Role of free radicals and catalytic metal ions in human disease: an overview. Methods in Enzymol 186: 1–85.
2. Borg LA, Eide SJ, Anderson A and Hellerstrom C (1979) Effect in vitro of alloxan on the glucose metabolism of mouse pancreatic ß-cells. Biochem J 182: 797–802.
3. Kim H, Rho H, Park B, Park J, Kim J and Kim UH (1994) Role of Ca^{2+} in alloxan-induced pancreatic ß-cell damage. Biochim Biophys Acta 1227: 87–91.
4. Malaisse WJ and Lea MA (1982) Alloxan toxicity to the pancreatic ß-cell. A new hypothesis. Biochem Pharmacol 31: 3527–3534.
5. Rho H, Lee J, Kim H, Park B and Park J (2000) Protective mechanism of glucose against alloxan-induced ß-cell damage: pivotal role of ATP. Exp Mol Med 32: 12–17.
6. Takasu N, Asawa T, Komiya I, Nagasawa Y and Yamada T (1991) Alloxan-induced DNA strand breaks in pancreatic islets: Evidence for H2O2 as an intermediate. J Biol Chem 266: 2112–2114.
7. Masumoto N, Tasaka K, Miyake A and Tanizawa O (1990) Superoxide anion increases intracellular free calcium in human myometrial cells. J Biol Chem 265: 22533–22536.
8. Shirahata S, Kabayama S, Nakano M, Miura T, Kusumoto K, Gotoh M, Hayashi H, Otsubo K, Morisawa S and Katakura Y (1997) Electrolyzed-reduced water scavenge active oxygen species and protects DNA from oxidative damage. Biochem Biphys Res Commun 234: 269–274.
9. Shirahata S (2000) Regulation of functions of animal cells by reduced water and its medical application. Nippon Nogei Kagaku Kaishi 74: 994–998.
10. Shirahata S (2002) Reduced water for prevention of diseases. Animal Cell Technology: Basic & Applied Aspects, Volume 12, pp. 25–30, Kluwer Academic, the Netherlands.
11. Hanaoka K (2001) Antioxidant effects of reduced water produced by electrolysis of sodium chloride. J Appl Electrochem 31: 1307–1313.

12. Tashiro H, Kitahora H, Fujiyama Y, Baba T and Itokawa Y (1999) Clinical examination of alkaline ion water. Abstract book of Symposium "Electrolyzed functional water in therapy" in 25th Meeting of Japanese Medical Society, pp. 6–7.
13. Oda M, Kusumoto K, Teruya K, Hara T, Maki T, Kabayama Y, Katakura Y, Otsubo K, Morisawa S, Hayashi H, Ishii Y and Shirahata S (1999) Electrolyzed and natural reduced water exhibit insulin-like activity on glucose uptake into muscle cells and adipocytes. Animal cell Technology: Products from Cells, Cells as Products (eds. Bernard A et-al), pp. 425–427, Kluwer Academic, the Netherlands.
14. Li Y, Nishimura T, Teruya K, Maki T, Komatsu T, Hamasaki T, Kashiwagi T, Kabayama S, Shim S-Y, Katakura Y, Osada K, Kawahara T, Otsubo K, Morisawa S, Ishii Y, Gadek Z, Shirahata S (2003) Cytotechnology 40: 139–149.
15. Shirahata S, Nishimura T, Kabayama S, Aki D, Teruya K, Otsubo K, Morisawa S, Ishii Y, Gadek Z and Katakura Y (2001) Anti-oxidative water improves diabetes. Animal Cell Technology: From Target to Market (eds. Linder-Olsson E et-al), pp. 574–577, Kluwer Academic, the Netherlands.

Anti-melanogenic Activity of Ergosterol Peroxide from *Ganoderma lucidum* on a Mouse Melanoma Cell Line

Toshiyuki Mukaiyama, Noriyuki Tsujimura, Shoko Otaka, Yasuyuki Kosaka, Keishi Hata, Kazuyuki Hori, and Kenji Sakamoto

Abstract MeOH extracts of *Ganoderma lucidum* showed an inhibitory effect on melanin biosynthesis of a mouse melanoma cell line, B16 10F7. We isolated an active compound from the extract. Physical and chemical data of the active compound were identical to those of ergosterol peroxide. Ergosterol peroxide decreased melanin pigment accumulation over 1 μg/ml by the suppression of melanogenic enzyme in B16 10F7 cells. However, ergosterol, a typical steroid in mushrooms, did not show a marked inhibitory effect on B16 10F7 cell melanogenesis at the same concentrations.

Keywords Melanin • *Ganoderma lucidum* • ergosterol peroxide • whiteness • B16 cells

1 Introduction

Melanin pigments, produced by melanocytes in the epidermis, are responsible for shielding skin tissues from ultraviolet beams; however, these pigments are also known to cause skin stains, freckles and sunburn. Therefore, intensive search for naturally occurring inhibitory substances of melanin pigmentation have been performed [1, 2]. We previously reported that alcoholic extracts of *Ganoderma lucidum* exhibited anti-melanogenic effects on B16 10F7 mouse melanoma cells [3]. In this study, we isolated ergosterol peroxide as an anti-melanogenic compound

T. Mukaiyama, N. Tsujimurt, S. Otaka, Y. Kosaka, and K. Sakamoto
Sakamoto Bio Co., Ltd., 25 Kourokuzawa, Yuuwa-Memeki, Akita 010-1233, Japan

K. Hata and K. Hori
Akita Research Institute for Food & Brewing (ARIF), 4-26 Sanuki, Araya-machi, Akita 010-1623, Japan

K. Ikura et al. (eds.), *Animal Cell Technology: Basic & Applied Aspects*,
Animal Cell Technology: Basic & Applied Aspects 15,
DOI 10.1007/978-1-4020-9646-4_42,

from *G. lucidum*, and studied its action on the levels of tyrosinase-related protein (TRP)-1, a melanogenic enzyme in B16 10F7 cells.

2 Materials and Methods

2.1 Isolation of Active Compounds from Ganoderma lucidum

Methanol extracts of *G. lucidum* were partitioned with $CHCl_3$-MeOH-H_2O (4:4:3). $CHCl_3$ extracts exhibited high levels of anti-melanogenic activity, and were separated by chromatography on silica gel. The active fraction was subjected to further fractionation on Cosmosil $75C_{18}$ silica gel. These steps yielded ergosterol peroxide as the active compound (Fig. 1). The structure of ergosterol peroxide was identified by IR, ^{1}H-NMR and ^{13}H-NMR spectrometry.

2.2 Effect of Triterpenes on Melanogenesis and Cell Growth

Aliquots of 1 mL of B16 2F2 cells (1×10^5 cells) were incubated with various concentrations of ergosterol peroxide for 3 days, and the melanin contents and viable cell number were measured as described previously [4].

2.3 Fluorescence Microscopy

Cells grown on glass coverslips pre-coated with fibronectin were cultured with or without stimulants for 72 h. The cells were rinsed twice with PBS, fixed in formaldehyde, and permealized with Triton X-100. TRP-1 in the cells was visualized with anti-TRP-1 antibody and FITC-labeled secondary antibody.

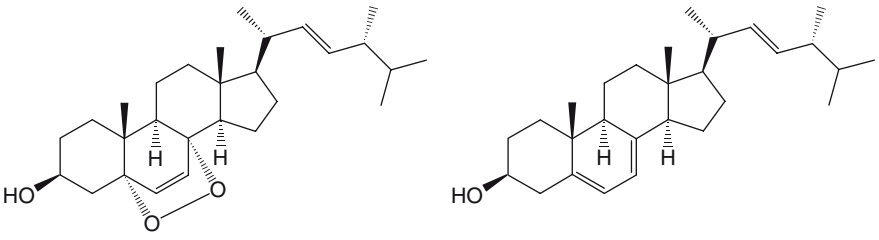

Ergosterol peroxide Ergosterol

Fig. 1 Chemical structures of ergosterol peroxide and ergosterol

3 Results and Discussion

3.1 Anti-Melanogenic Compound from Ganoderma lucidum

We previously selected a B16-derived highly pigmented sub-clone (B16 10F7), which expresses a high level of tyrosinase and TRP-1 (Fig. 2). Using this cell line, we screened for anti-melanogenic activity in food materials. As the alcoholic extracts of *G. lucidum* exhibited marked activity, we isolated ergosterol peroxide as an anti-melanogenic compound by bioassay-guided fractionation of the methanol extract. To study the structure-activity relationship, ergosterol, an analogue of ergosterol peroxide, was examined for the anti-melanogenic activity toward B16 10F7 cells. Ergosterol peroxide at 2 μg/ml inhibited the melanin synthesis of B16 10F7 cells by 9.2% when compared to untreated cells (Fig. 3a); however, ergosterol did not inhibit the melanogenesis of B16 10F7 cells (Fig. 3b). The results suggested that the peroxy moiety between C-5 and C-8 of ergosterol peroxide plays an important role in the anti-melanogenic effect.

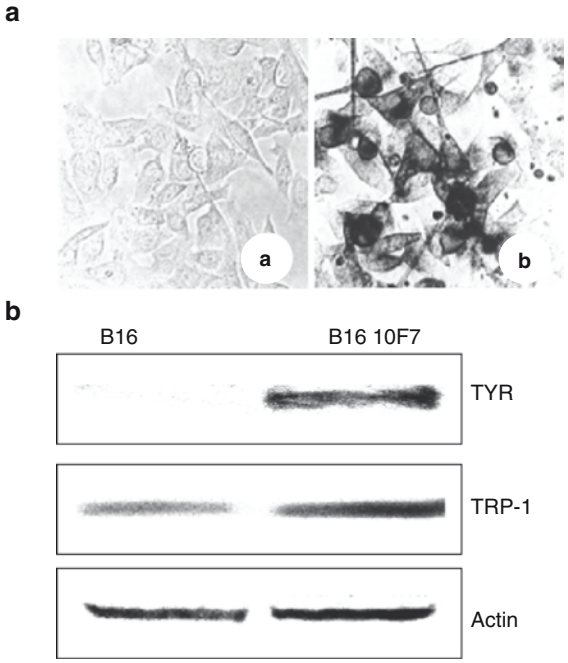

Fig. 2 B16-derived highly pigmented sub-clone, B16 10F7. (**a**) Microscopic observations of B16 (a) and B16 10F7 (b) cells. (**b**) Levels of tyrosinase (TYR) and TRP-1 in B16 and B16 10F7 cells

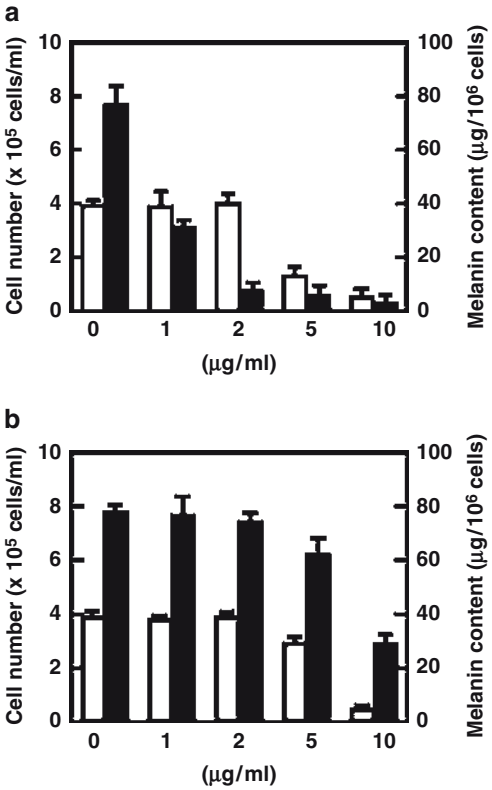

Fig. 3 Effects of ergosterol peroxide (**a**) and ergosterol (**b**) on B16 10F7 cell melanin synthesis. Following the treatment of B16 10F7 cells with various concentrations of each compound for 72 h, the cell growth (▭) and melanin content (▬) were measured

3.2 Effect on the Level of TRP-1 in B16 10F7 Cells

We examined the levels of TRP-1 in B16 10F7 cells stimulated with ergosterol peroxide. Fluorescence microscopic observation revealed that the level of TRP-1 in B16 10F7 cells was decreased by ergosterol peroxide. It was suggested that three melanogenic enzymes (tyrosinase, TRP-1 and TRP-2) were regulated by the same transcriptional factor, MITF [5]. The anti-melanogenic effect of ergosterol peroxide might occur via the suppression of melanogenic enzymes in B16 10F7 cells (Fig. 4).

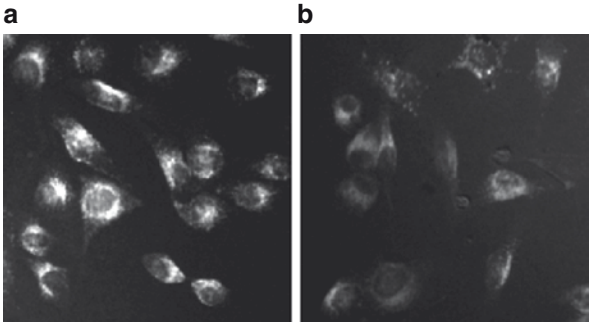

Fig. 4 Fluorescence microscopic observations of B16 10F7 cells treated without (**a**) and with 2 μg/ml ergosterol peroxide for 72 h (**b**)

References

1. Funasaka, Y., Komoto, M., and Ichihashi, M, 2000, Depigmenting effect of alpha-tocopheryl ferulate on normal human melanocytes, *Pigment Cell Res.* **13:**170–174.
2. Lee, S. H., Choi, S. Y., Kim, H., Hwang, J. S., Lee, B. G., Gao, J. J., and Kim, S. Y., 2002, Mulberroside F isolated from the leaves of Morus alba inhibits melanin biosynthesis, *Biol. Pharm. Bull.* **25:**1045–1048.
3. Miura, N., Hata, K., Tsujimura, N., and Sakamoto, K., 2000, Studies on Ganoderma lucidum-I: The methanol extract from antler-shape fruiting body of Ganoderma lucidum inhibits melanin synthesis in B16 melanoma, *Res. Commun. Pharmacol. Toxicol.* **5:**176–178.
4. Hata, K., Iwahori, Y., Hori, K., Okada, Y., and Okuyama Y., 2000, Inhibitory effect of some wild plants in Akita on melanin biosynthesis, *Natural Med.* **54:**144–147.
5. Hearing, V. J., and Tsukamoto, K., 1991 Enzymatic control of pigmentation in mammals, *FASEB J.* **5:**2902–2909

Differentiation-Inducing Activities by Lupane Triterpenes from *Lactuca indica* on a Mouse Melanoma Cell Line

Keishi Hata, Toshiyuki Mukaiyama, Noriyuki Tsujimura, Yusuke Sato, Yasuyuki Kosaka, Kenji Sakamoto, and Kazuyuki Hori

Abstract We isolated 4 lupane triterpenes as differentiation-inducing agents on B16 2F2 melanoma cells from *Lactuca indica*. In the study of structure-activity relationships, the differences of the lupane skeleton at C-3 played a key role in their melanogenic activities. SB203580, a selective inhibitor of p38 MAPK, completely blocked the melanogenesis of B16 2F2 cells induced by lupeol (**1**), a lupane triterpene. Western blot analysis revealed that **1** transiently activated p38 MAPK. Furthermore, **1** was found to induce dendritic formation, a morphological indicator of B16 2F2 cell differentiation. **1** attenuated actin fiber assembly in B16 2F2 cells, and this attenuation caused dendrite outgrowths of the cells. SB203580 blocked the induction of tyrosinase by **1**, but did not block the rearrangement of actin cytoskeleton in B16 2F2 cells stimulated with **1**.

Keywords Melanoma cell differentiation • lupane triterpenes • melanogenesis • dendritic formation • signaling mechanism

1 Introduction

A mouse melanoma cell line, B16 2F2, differentiates into mature melanocyte-like cells by cAMP-elevating agents such as α-melanocyte stimulating hormone (α-MSH). Melanogenesis and dendritic formation of the cells are induced through cell differentiation; however, information concerning melanoma cell differentiation inducers is quite limited. In this study, we found lupane triterpenes to stimulate

K. Hata and K. Hori
Akita Research Institute for Food & Brewing (ARIF), 4-26 Sanuki, Araya-machi, Akita 010-1623, Japan

T. Mukaiyama, N. Tsujimura, Y. Sato, Y. Kosaka, and K. Sakamoto
Sakamoto Bio Co., Ltd., 25 Kourokuzawa, Yuuwa-Memeki, Akita 010-1233, Japan

K. Ikura et al. (eds.), *Animal Cell Technology: Basic & Applied Aspects*,
Animal Cell Technology: Basic & Applied Aspects 15,
DOI 10.1007/978-1-4020-9646-4_43, © Springer Science+Business Media B.V. 2009

melanoma cell differentiation. Moreover, we examined the signaling mechanisms involved in the induction of melanogenesis and dendritic formation of the cells.

2 Materials and Methods

2.1 Isolation of Active Compounds from Lactuca indica

Methanol extracts of *L. indica* were partitioned with $CHCl_3$-MeOH-H_2O (4:4:3). $CHCl_3$ extracts exhibited high levels of differentiation-inducing activity, and were separated by chromatography on silica gel. The active fractions were subjected to further fractionation on Cosmosil $75C_{18}$ silica gel. By these steps, we isolated four active compounds (Fig. 1). The structures of these compounds were identified by IR, ^{1}H NMR and ^{13}H NMR spectrometry.

2.2 Effect of Triterpenes on Melanogenesis and Cell Growth

Aliquots of 1 mL of B16 2F2 cells (1×10^5 cells) were incubated with various concentrations of lupane triterpenes for 3 days, and the melanin contents and viable cell number were measured as described previously [1]. ED_{50} values for melanin biosynthesis were calculated from the results of dose-response studies for the up-regulation of melanogenesis. IC_{50} values, representing the concentration that inhibited melanoma cell growth by 50%, were measured [2].

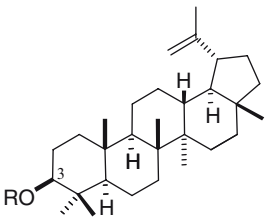

Compound	R	ED_{50} (μM)	IC_{50} (μM)
1 (lupeol)	α-H, β-OH	9.9	38.0
2 (lupeone)	=O	0.35	25.4
3 (lupenyl acetate)	α-H, β-OAc	7.5	22.7
4 (lupenyl palmitate)	α-H, β-$OCOC_{15}H_{31}$	24.7	26.9

Fig. 1 Chemical structures of lupane triterpenes. ED50 values were determined from the results of dose-response experiments in which the up-regulation of melanogenesis by the compound were monitored. IC50 value represents the concentration that inhibited cell growth by 50%

2.3 Western Blotting

Aliquots (10 ml) of B16 2F2 cells (1×10^5 cells/ml) were incubated with or without stimulants for an appropriate period. The cells were collected by pipetting and then lysed with 5 mM Tris-HCl buffer, pH6.8, containing 1% SDS, 1 mM EDTA and 10% sucrose. The proteins were separated by SDS-polyacrylamide gel electrophoresis and then transferred to a nitrocellulose membrane. The membrane was incubated with primary antibodies for 2 h at room temperature and incubated with HRP-conjugated secondary antibodies for 1 h at room temperature. The signals were visualized using enhanced chemiluminescence reagents.

2.4 Fluorescence Microscopy

Cells grown on glass coverslips pre-coated with fibronectin were cultured with or without stimulants for 12 h. The cells were rinsed twice with PBS, fixed in formaldehyde, and permealized with Triton X-100. For the detection of stress fibers, the cells were stained with Alexa-Fluor 488-conjugated phalloidin.

3 Results and Discussion

3.1 Active Compounds

Briefly, we screened the differentiation-inducing activity of the food material on B16 2F2 cells. As the alcoholic extracts of *L. indica* showed strong activity, we isolated lupeol (**1**), lupeone (**2**), lupenyl acetate (**3**) and lupeny palmitate (**4**) as active compounds by bioassay-guided fractionation of the methanol extract. In studies of the structure-activity relationships, it was found that acetylation at C-3 of **1** shows no effect on the activity (Fig. 1). However, oxidation of the OH-group at C-3 enhanced the activity, and the long fatty acid group at C-3 decreased the activity. These results suggested that the differences of the chemical structure at C-3 played an important role in the induction of B16 2F2 cell melanogenesis by lupane triterpenes.

3.2 Signaling Mechanisms

Recently, the activation of p38 MAPK was demonstrated to trigger the B16 cell differentiation induced by α-MSH [3]. Therefore, we studied whether the activation of p38 MAPK was involved in **1**-induced B16 2F2 cell differentiation using a selective

inhibitor of p38 MAPK and Western blotting (Fig. 2). 10 μM **1** elevated the melanogenesis of B16 2F2 cells 6.4-fold when compared to untreated cells. SB203580, a p38 MAPK inhibitor, blocked the up-regulation of melanin synthesis of B16 2F2 cells by **1** in a dose-dependent manner. Western blotting revealed that the level of p38 MAPK in B16 2F2 cells was constant with 10 μM **1** for 240 min; however, the phosphorylation of p38 MAPK was induced by 10 μM **1** for 120 min, and then the level decreased. These results showed that **1** induced the melanogenesis of B16 2F2 cells via the p38 MAPK pathway.

Following treatment with 10 μM 1 for 12 h, dendritic outgrowths in B16 2F2 cells were observed. Recently, it was reported that the dendritic outgrowth in melanocyte/melanoma cells accompanies the remodeling of cytoplasmic filaments [4]. Therefore, we examined whether the rearrangement of cytoskeletal components, such as microfilaments and microtubules, was involved in the formation of dendrites in B16 2F2 cells. In untreated B16 2F2 cells, actin appeared organized in stress fibers crossing the cytoplasm (Fig. 3A-a). By treatment with 10 μM **1** for 12 h, stress fiber assembly in the cytoplasm was disrupted, leaving phalloidin-labeled F-actin only in the dendrites (Fig. 3A-b); however, **1** did not influence the remodeling of the microtubular network. Western blotting demonstrated that **1** did not change the expression levels of actin and tubulin in B16 2F2 cells. These results show that

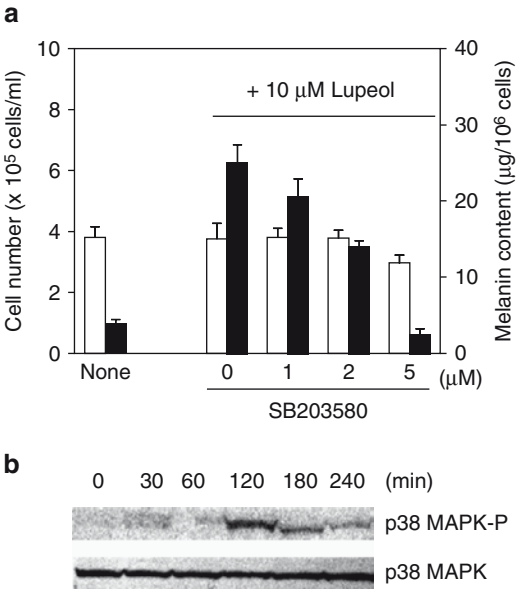

Fig. 2 Activation of p38 MAPK by **1**. (**a**) B16 2F2 cells were incubated with various concentrations of SB203580 in the absence (**a**) or presence of (**b**) 10 μM **1** for 72 h and the cells growth (▭) and melanin content (▬) were measured. (**b**) B16 2F2 cells were incubated with 10 μM **1** for 0–240 min, and the cell lysates were analyzed by Western blotting using anti-phospho p38 MAPK (p38 MAPK-P) antibody or anti-p38 MAPK antibody

the rearrangement of actin cytoskeleton by **1** results in the formation of dendrites in B16 2F2 cells. Recently, it was reported that the inactivation of cofilin, an actin depolymerization factor, was involved in the assembly of actin stress fibers as a downstream target of Rho signaling [5, 6]. We therefore examined the level of phospho-cofilin in untreated or **1**-treated B16 2F2 cells. The levels of cofilin in **1**-treated B16 2F2 cells remained constant, but phospho-cofilin (inactive form) in B16 2F2 cells decreased by treatment with 10 μM **1** in a time-dependent manner (Fig. 3B). We demonstrated that activation of the p38 MAPK pathway by **1** results in the induction of melanogenesis in B16 2F2 cells. Therefore, we studied whether the activation of p38 MAPK promotes remodeling of the actin cytoskeleton. Stress fiber assembly in B16 2F2 cells was disrupted by **1**. The actin cytoskeleton in B16 2F2 cells treated with SB203580 was maintained, and SB203580 did not block the actin cytoskeleton disruption by **1**. Western blotting revealed that **1** induced the expression of tyrosinase in B16 2F2 cells as compared with untreated cells (Fig. 4). SB203580 did not influence the expression of tyrosinase in B16 2F2 cells, and blocked the induction by **1**. Furthermore, we examined the levels of phosho-cofilin in B16 2F2 cells treated with 10 μM **1**. Treatment with 10 μM **1** for 12 h decreased the levels of phospho-cofilin in B16 2F2 cells when compared to untreated cells. Moreover, SB203580 did not influence the levels of phospho-cofilin, and did not abolish the dephosphorylation of cofilin by **1**. These results suggest that both melanogenesis and dendritic formation are hallmarks of melanoma cell differentiation, but they were regulated separately by the activation of p38 MAPK signaling and down- regulation of the Rho pathway, respectively.

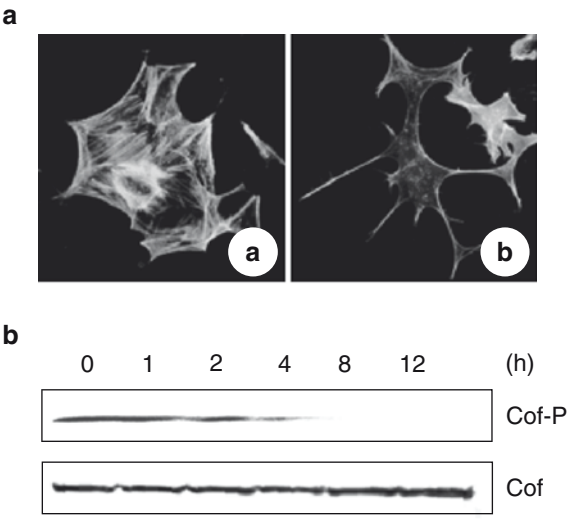

Fig. 3 Effect of **1** on the remodeling of microfilaments and the activation of cofilin. (**a**) B16 2F2 cells were cultured without (a) or with 10 μM **1** (b) for 12 h, stress fibers were stained with Alexa-Fluor 488 phalloidin. (**b**) B16 2F2 cells were incubated with 10 μM **1** for 0–12 h, and then cell lysates were analyzed by Western blotting using anti-phospho cofilin

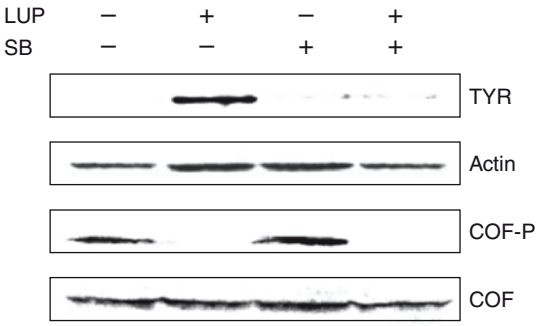

Fig. 4 Effects of a p38 MAPK inhibitor on markers of B16 2F2 cell differentiation

It has been reported that the assembly and disassembly of actin fiber control the cancer cell motility and invasion [7]. In our previous research, **1** suppresses the migration of melanoma and neuroblastoma cells [8]. Furthermore, it was shown that **1** exhibits an anti-angiogenic effect through the inhibition of HUBEC tube formation [9]. These findings suggest that **1** could be an effective compound to prevent tumor metastasis.

B16 2F2 cells were incubated alone, or with 10 μM **1** (LUP), 5 μM SB203580 (SB) or **1** + SB203580 for 12 h, and the cell lysates were analyzed by Western blotting using anti-tyrosinase antibody (TYR), anti-actin antibody, anti-phospho cofilin (COF-P) antibody or anti-cofilin (COF) antibody.

Acknowledgments This research was supported in part by a grant from the Department of Academic and International Affairs, Akita Prefecture Government.

References

1. Hata, K., Ishikawa, K., Hori, K., and Konishi, T., 2000, Differentiation-inducing activity of lupeol, a lupane triterpene from Chinese dandelion root (Hokouei-kon) on a mouse melanoma cell line, *Biol. Pharm. Bull.* **23:**962–967.
2. Hata, K., Hori, K., and Takahashi, S., 2002, Differentiation- and apoptosis-inducing activities of pentacyclic triterpenes on a mouse melanoma cell line, *J. Nat. Prod.* **65:**645–648.
3. Smalley, K. and Eisen, T., 2000, The involvement of p38 mitogen-activated protein kinase in the α-melanocyte stimulating hormone (α-MSH) induced melanogenic and anti-proliferative effects in B16 melanoma cells, *FEBS Lett.* **476**:198–202.
4. Busca, R., Bertolotto, C., Abbe, P., Engalo, W., Ishizaki, T., Narumiya, S., Boquet, P., Ortonne, J.P., and Ballotti, R., 1998, Inhibition of Rho is required for cAMP-induced melanoma cell differentiation, *Mol. Biol. Cell.* **9**:1367–1378.
5. Sumi, T., Matsumoto, K., Takai, Y., and Nakamura, T., 1999, Cofilin phosphorylation and actin cytoskeletal dynamics regulated by rho- and Cdc42-activated LIM-kinase 2, *J. Cell Biol.* **147:**1519–1532.

6. Buchan, A.M., Lin, C.Y., Choi, J., and Barber, D.L., 2002, Somatostatin, acting at receptor subtype 1, inhibits Rho activity, the assembly of actin stress fibers, and cell migration, *J. Biol. Chem.* **277**:28431–28438.
7. Byers, H.R., Etoh, T., Vink, J., Franklin, N., Gattoni-Celli, S., and Mihm, M.C. Jr., 1992, Actin organization and cell migration of melanoma cells relate to differential expression of integrins and actin-associated proteins, *J. Dermatol.*, **19**:847–852.
8. Hata, K., Hori, K., Murata, J., and Takahashi, S., 2005, Remodeling of actin cytoskeleton in lupeol-induced B16 2F2 cell differentiation, *J. Biochem.* **138**:467–472.
9. You, Y.J., Nam, N.H., Kim, Y., Bae, K.H., and Ahn, B.Z., 2003, Antiangiogenic activity of lupeol from Bombax ceiba, *Phytother. Res.* **17**:341–344.Triterpenes from *Lactuca indica* on a Mouse Melanoma Cell Line

Immunoglobulin Production Stimulating Effect of Soy-Derived Proteins

Norihide Maeda, Kazuma Yoshimi, Hirofumi Tachibana, and Koji Yamada

Abstract We found that a novel and potent immunoglobulin production stimulating factor (IPSF) was contained in soybean trypsin inhibitor (STI) preparation. The IPSF significantly enhanced IgM production by mouse spleen lymphocytes. To clarify the mechanism of the IPSF activity, the effect of the IPSF on the expression of some cytokines was examined. The IPSF promoted the expression of interleukin-6 (IL-6) and IL-10 mRNA. The IgM production stimulating activity was partially but significantly suppressed by IL-6 neutralization antibody. These data suggest that the IPSF stimulates IgM production, at least partially, via the enhancement of IL-6 production. To reveal the IPSF is not STI, STI preparation was fractionized by anion-exchange chromatography and the IPSF activity of each fraction was analyzed. Active fraction was eluted distinct fraction containing STI. Active fraction contained some proteins whose molecular weights were about 29 kDa. These suggest that IPSF in STI preparation is not STI itself but contaminants. Taken together, the about 29 kDa protein and/or its complexes with several proteins exist in STI preparation could have a potent IPSF activity and the activity was exerted, at least partially, via stimulation of IL-6 production.

Keywords Soy-derived protein • immunoglobulin production stimulating factor • mouse spleen lymphocyte • interleukin-6

N. Maeda, K. Yoshimi, H. Tachibana, and K.Yamada
Laboratory of Food Chemistry, Division of Applied Biological Chemistry, Department of Bioscience and Biotechnology, Faculty of Agriculture, Kyushu University, 6-10-1 Hakozaki, Higashi-ku, Fukuoka, 812-8581, Japan

H. Tachibana
Laboratory of Functional Food Design, Department of Functional Metabolic Design, Bio-Architecture Center, Kyushu University, 6-10-1 Hakozaki, Higashi-ku, Fukuoka, 812-8581, Japan

K. Ikura et al. (eds.), *Animal Cell Technology: Basic & Applied Aspects*,
Animal Cell Technology: Basic & Applied Aspects 15,
DOI 10.1007/978-1-4020-9646-4_44,

1 Introduction

Humoral Immune responses are mediated by immunoglobulin (Ig) s produced by B lymphocytes and protect us from foreign substances such as pathogen. Among Ig classes, IgA, IgG and IgM are mainly involved in the immunodefensive system. Particularly, IgM is produced first when antigens invade to play a important role in the frontier of host defense. Therefore enhancement of Ig production can lead to immunopotentiation.

B cells interact with each other and with various immune cells such as T cells. These immune cells produce various cytokines by which the immune functions are controlled [1]. Humoral immunity is stimulated by the cytokines such as interleukin-4 (IL-4), IL-5, IL-6 and IL-10 [2–4]. We have previously reported that some dietary proteins such as lactoferrin (LF), β-Casein and lysozyme stimulated Ig production via a promotion of such cytokines and called them immunoglobulin production stimulating factor (IPSF) [5, 6]. In the course of the study about their activity and the mechanism of their action, we found that novel IPSF exist in soybean trypsin inhibitor (STI) preparation. Here, we investigated about their activity and the mechanism of their action and attempted to characterize it.

2 Materials and Methods

2.1 Reagents and Cells Culture

STI type II-S and ovomucoid (OVM) were purchased from SIGMA (St. Louis, Mo., USA). These proteins were dissolved at 10 mg/mL in phosphate-buffered saline (PBS, pH 7.4) and sterilized by filtration with syringe filter (pore size 0.2 μm) before use. C57BL/6N mice were used for isolation of spleen lymphocytes. Isolation of spleen lymphocytes were performed according to the method of Yamasaki and others [7]. Briefly, spleen was excised from mice and then homogenized immediately using a ground glass. Splenocytes were obtained centrifuging the homogenates and washed three times with RPMI 1640 medium. The suspension of splenocytes was stratified on Lympholyte-mouse (Cedarlane, Ontario, Canada), and centrifuged at 1000 × *g* for 30 min. After centrifuging, interfacial layer was harvested as lymphocytes. The remainders of erythrocytes were lysed using 155 mM NH4Cl, 10 mM KHCO3 and 10 mM EDTA (pH 7.4). After two times washing, cell density was adjusted to 2×10^6 cells/mL. These cells were cultured in 5 fetal bovine serum (FBS) containing RPMI 1640 medium (5% FBS-RPMI 1640 medium).

2.2 Enzyme-Linked Immunosorbent Assay (ELISA)

Ig level in the culture supernatant was measured by sandwich ELISA reported previously [7]. Rabbit Anti-Mouse IgA (Zymed, San Francisco, CA), F(ab')2 Goat

Anti-Mouse IgG (H + L) (Zymed) and F(ab')2 Goat Anti-Mouse IgM (μch. sp) (Zymed) were used to fix each Ig. These antibodies were diluted using 50 mM carbonate buffer (pH 9.6), and added to a 96-well plate, and incubated for 1 h at 37°C. 25% Block Ace (Dainihon Pharmaceutical, Co., Osaka, Japan) was added and kept at 4°C overnight or 37°C for 1 h. Then 50 μL of samples were added to each well, and the plates were incubated for 1 h at 37°C. Each well was treated with a solution of either horse radish peroxidase (HRP)-Goat Anti-Mouse IgA (Zymed), HRP-F(ab')2 Goat Anti-Mouse IgG (H + L) (Zymed) or HRP-Rabbit Anti-Mouse IgM (Zymed) and incubated for 1 h at 37°C. The plates were rinsed with PBS containing 0.05% polyethylene sorbitan monolaurate (Nacarai Tsque, Kyoto, Japan) between each step. Then, a 10:9:1 mixture of 1.8 mM H2O2 in 200 mM citrate buffer (pH 4.0), H2O, and 11.7 mM of 2,2′-azinobis(3- ethylbenzothiazolinesulfonic acid) diammonium salt was added 100 μL/well and absorbance at 415 nm was measured.

2.3 Neutralization of Interleukin-6

Mouse spleen lymphocytes are cultured in 5% FBS-RPMI 1640 medium in the presence of 1μg/mL IL-6 neutralization antibody (BD Biosciences Pharmingen, San Jose, CA) or isotype control antibody: rat IgG1 (Genzyme/Techne, Minneapolis, MN). After 72 h, the supernatant was harvested and the IgM level was measured by ELISA.

2.4 Reverse Transcription–Polymerase Chain Reaction (RT-PCR)

To analyze the expression of cytokine mRNA, a reverse transcription-polymerase chain reaction (RT-PCR) was performed. Total cellular RNA was isolated using Trizol (Invitrogen, Carlsbad, CA) according to the manufacture's instructions. For cDNA synthesis, 10 μg of total RNA was reversely transcribed using (dT)20 primer and 20 U of moloney mouse leukemia virus (MMLV)-reverse transcriptase (Amersham Pharmacia Biotech; Piscataway, NJ, USA). The resultant cDNA samples were subjected to PCR amplification in the presence of specific sense and antisense primers (1 μM) and 0.17 U of Taq DNA polymerase (Fermentas, Ontario, Canada). Nucleotide sequence for the PCR primers were as follows: for the IL-6 (GenBank Acc. No. MN031168), sense 5′-CTGGTGACAACCACGGCCTTCCCT-A-3′, and antisense 5′-ATGCTTAGGCATAACGCACTAGGTT-3′; for IL-10 (Gen-Bank Acc. No. MN010548), sense 5′-ATGCAGGACTTTAAGGGTTACTTGGGT-T-3′, and antisense 5′-ATTTCGGAGAGGGTACAAACGAGGTTT-3′; for β-actin (GenBank Acc. No. MN007393), sense 5′-TGGAATCCTGTGGCATCCATGAAA-C-3′, and antisense 5′-TAAAACGCAGCTCAGTAACAGTCCG-3′. The amplified PCR products were subjected to electrophoresis on a 1.5% agarose gel. After ethidium bromide staining, amplified DNA fragments were detected under ultraviolet irradiation.

2.5 Anion-Exchange Chromatography

STI was subjected to HPLC equipped with TSK-gel DEAE-5PW column (21.5 mm I.D. × 150 mm) (TOSOH). STI (10 mg) was applied to the column equilibrated with 10 mM NaPB containing 100 mM NaCl and eluted with 100-200 NaCl gradients. Finally, the solution was eluted with 500 mM NaCl in 10 mM NaPB.

2.6 Sodium Dodecyl Sulfate–Poly Acrylamide Gel Electrophoresis

Active fraction was assayed by SDS-PAGE and protein detection was performed by silver staining. Briefly, the fraction mixed 1:1 with SDS-sample buffer (4% 2-mercaptoethanol, 0.05 M Tris, 8% glycerol, 1.6% SDS, 0.02% Bromophenol Blue) and heated at 100°C for 5 min. These samples were loaded onto 10% SDS-PAGE gel, and electrophoresis was done under reducing condition.

3 Results and Discussions

Figure 1 shows the effect of STI preparation on Ig production by mouse spleen lymphocytes. OVM was used as the control of serine protease inhibitor. STI stimulated IgG and IgM production. Particularly, IgM production was markedly up-regulated in a dose-dependent manner, whereas OVM had no effect on Ig production. These suggest that the IPSF in STI preparation stimulate Ig production, particularly in IgM production, and the activity is independent of the function of STI as serine protease inhibitor.

To clarify the mechanism of the action of IPSF, the effect of IPSF on the expression of IL-6 and IL-10 mRNA was investigated. The expression of them was remarkably enhanced when mouse spleen lymphocytes were cultured with STI preparation for

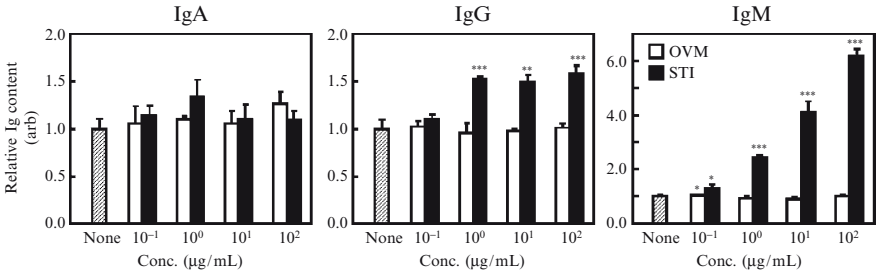

Fig. 1 Dose-dependent enhancement of IgM production by IPSF in STI preparation

24 h (data not shown). We confirmed the time course analysis of enhancement of IL-6 mRNA expression and that of IgM production. Mouse spleen lymphocytes were cultured with or without for 3, 6, 12, 24 and 48 h and analyze the expression level of IL-6 and IL-10 mRNA and IgM level in culture supernatant (Fig. 2a and b). IL-6 mRNA expression was detected in presence of STI after 6 h, and gave a maximal expression at 12 h and the up-regulation was remained at 24 h (Fig. 2a). IL-10 mRNA expression was enhanced after 6 h in the presence of STI and gave a maximal at 24 h and the enhancement was remained at 48 h (data not shown). Whereas, there was no significant difference in IgM level between in the absence and presence of STI until 12 h, and at 48 h, IgM level was prominently raised in the presence of STI (Fig. 2b). IL-6 is a pleiotropic cytokine secreted by various cells such as monocyte, B cell and T cell [8, 9], and it acts as a B cell activator [2]. To ensure the involvement of IL-6, we analyzed the IPSF activity of STI in the presence of IL-6 neutralization antibody. The enhancement of IgM production was suppressed significantly by IL-6 neutralization antibody compared with isotype control antibody (Fig. 2c). These data suggest that STI stimulates the production of IL-6 by which the IgM production is enhanced. But the suppression by the neutralization antibody was incomplete (Fig. 2), suggesting that STI promotes not only the expression of IL-6 but also that of other B cell activator such as IL-10 to enhance IgM production.

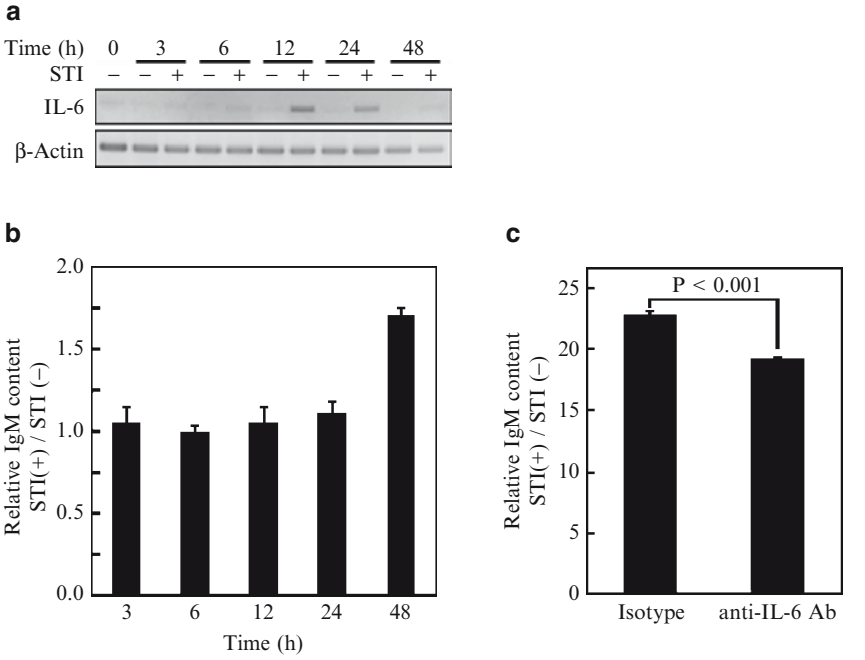

Fig. 2 Involvement of IL-6 in enhancement of IgM production by the IPSF in STI preparation

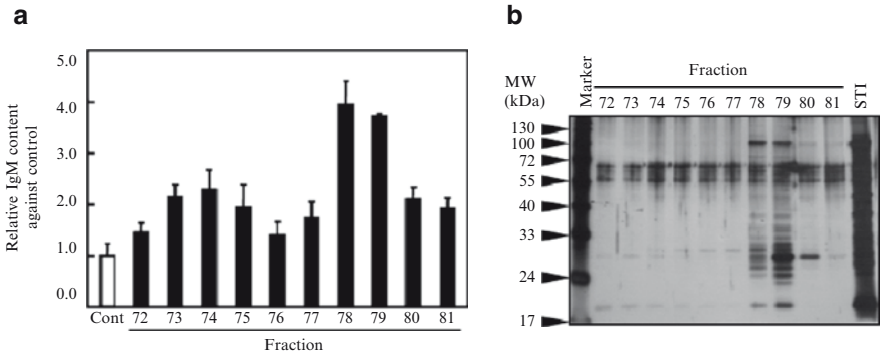

Fig. 3 Isolation of IPSF in STI preparation by anion-exchange chromatography

To clarify whether the IPSF is STI itself or not, STI preparation was subjected to anion exchange chromatography. The maximum IPSF activity was observed at fraction 78 (F78) (Fig. 3a). Each fraction indicated Fig. 3c was subjected to SDS-PAGE. Active fraction F78 and F79 containing several proteins with various molecular weight (Fig. 3b). It is noteworthy that active fraction contained a small amount of proteins (Fig. 3b). The main band in F78 was detected at about 29 kDa and several minor bands with various molecular weights. These data suggest that the IPSF in STI preparation is not STI itself but could be 29 kDa protein or its complexes with other several proteins.

In conclusion, potent IPSFs exist in STI preparation and it could be about 29 kDa protein. In addition, the IPSF exerts IgM production stimulating activity, at least partially, via enhancement of IL-6 production.

References

1. Tagoh H and Muraguchi A.. 1992. Nippon Rinsho 50: 1718–1723.
2. Muraguchi A, Hirano T, Tang B, Matsuda T, Horii Y, Nakajima K and Kishimoto T. 1988. J Exp Med 167: 332–344.
3. Ochel M, Vohr Hw, Pfeiffer C and Gleichmann E. 1991. J Immunol 146: 3006–3011.
4. Itoh K and Hirohata S. 1995. J Immunol 154: 4341–4350.
5. Yamada K, Ikeda I, Nakajima H, Shirahata S and Murakami H. 1991. Cytotechnology 5: 279–285.
6. Okamoto T, Tachibana H and Yamada K. 2002. Animal Cell Technol: Basic Appl Aspects 13: 399–404.
7. Yamasaki M, Chujo H, Hirao A, Koyanagi N, Okamoto T, Tojo N, Oishi A, Iwata T, Yamauchi-Sato Y, Yamamoto T, Tsutsumi K, Tachibana H and Yamada K. 2003. Linoleic acid. J Nutr 133: 784–788.
8. Horii Y, Muraguchi A, Suematsu S, Matsuda T, Yoshizaki K, Hirano T and Kishimoto T. 1988. J Immunol 141: 1529–1535.
9. Matsuzaki N, Saji F, Kameda T, Yoshizaki K, Okada T, Sawaki K and Tanizawa O. 1990. Clin Immunol Immunopathol 55: 305–314.

Immunostimulation Effect of the Jellyfish Collagen

Takuya Sugahara, Masashi Ueno, Yoko Goto, Koichi Akiyama, Satoshi Yamauchi, Ryusuke Shiraishi, and Mikiharu Doi

Abstract The jellyfish extract enhanced IgM production of human hybridoma HB4C5 cells 34-fold. IgM and IgG production of human peripheral blood lymphocytes (hPBL) were also accelerated 2.8- and 1.4-fold, respectively. Moreover, IFN-γ and TNF-α production by hPBL were stimulated 100- and 17-fold, respectively. Collagenase treatment inactivated the immunostimulation activity of the jellyfish extract. In addition, purified collagen from bovine Achilles' tendon accelerated IgM production of hybridoma cells. These facts mean that collagen has immunostimulation effect, and the active substance in jellyfish extract is collagen. As the result of the investigation about the mode of action, collagen stimulates both transcription and translation activities to enhance Ig production.

Keywords Collagen, cytokine production • immunoglobulin production • jellyfish • peripheral blood lymphocytes

1 Introduction

We have screened immunoglobulin (Ig) production stimulating factors (IPSFs), which enhance Ig production of hybridoma cells and lymphocytes. As a result of investigations, several substances were identified as the IPSF in foodstuffs.

T. Sugahara, M. Ueno, Y. Goto, and S. Yamauchi
Faculty of Agriculture, Ehime University, 3-5-7 Tarumi, Matsuyama
Ehime 790-8566, Japan

K. Akiyama
Integrated Center for Sciences, Ehime University, 3-5-7 Tarumi, Matsuyama, Ehime 790-8566, Japan

R. Shiraishi and M. Doi
Marutomo Co. Ltd., 1696 Kominato, Iyo, Ehime 799-3192, Japan

K. Ikura et al. (eds.), *Animal Cell Technology: Basic & Applied Aspects*,
Animal Cell Technology: Basic & Applied Aspects 15,
DOI 10.1007/978-1-4020-9646-4_45,

For instance, we reported that proteose-peptone component 3 enhanced Ig and cytokine production of human peripheral blood lymphocytes (hPBL) [1].

Jellyfish are planktonic marine members of a group of invertebrate animals composed of about 200 described species of the class *Scyphozoa* (phylum *Cnidaria*) or the class *Cubozoa*. Jellyfish is a very important foodstuff in Asia, especially in China and Japan. Only jellyfish belonging to the order Rhizostomeae are harvested for food. The rhizostomes are favored because they are typically larger and have more rigid bodies than other scyphozoan orders. The edible jellyfish are composed of five to seven species, including *Lobonema smithi*, *Lobonemoides gracilis*, *Rhopilema esculentum*, *Rhopilema hispidum*, and *Nemopilema nomurai*. Regardless of their size or shape, most jellyfish are very fragile containing more than 95% water.

In this study, we focused on the immunostimulation activity of an extract of edible jellyfish *Nemopilema nomurai*, because the jellyfish is an unknown subject as a source of substances possessing biological functions.

2 Materials and Methods

2.1 Preparation of Jellyfish Extract

The extraction procedure was designed to obtain collagen and collagen-like substances from jellyfish. Five g of the exumbrella part of jellyfish (*Nemopilema nomurai*) was cut into small pieces and extracted with 50 ml of diluted hydrochloric acid (pH 3.0) for 12 h, and heated at 121°C for 20 min. Insoluble substances were removed by centrifugation at 8,000 × g for 20 min. The supernatant was collected and dialyzed against 10 mm sodium phosphate buffer (NaPB) (pH = 7.4), and sterilized by filtration. Concentration of the jellyfish extract was indicated as protein content.

2.2 Cells and Cell Culture

Human-human hybridoma HB4C5 cells producing lung cancer specific monoclonal IgM were used for the assay of the Ig production stimulating activity. HB4C5 cell line was a fusion product of a human B lymphocyte from lung cancer patient and a human fusion partner, NAT-30 cells. HB4C5 cells were cultured in ERDF medium (Kyokuto Pharmaceutical, Tokyo, Japan) supplemented with 10 μg/ml of insulin, 20 μg/ml of transferrin, 20 μM ethanolamine, and 25 nM selenite (ITES-ERDF) at 37°C under humidified 5% CO_2-95% air.

Human peripheral blood lymphocytes (hPBL) were obtained from peripheral blood of a healthy male donor. Peripheral blood diluted with equal volume of phosphate

buffered saline was centrifuged at room temperature for 30 min on lymphocyte separation medium (Nycomed Pharma, Oslo, Norway).

2.3 Assay of the Immunostimulating Activity

The immunoglobulin (Ig) production stimulating activity was examined by measuring the amount of Ig secreted by HB4C5 cells or hPBL in culture media. HB4C5 cells and hPBL were inoculated in ITES-ERDF medium containing jellyfish extract. The assay of the Ig production stimulating activity was performed in a 96-well culture plate. HB4C5 cells and hPBL were inoculated at 5×10^4 cells/ml and 1×10^6 cells/ml, respectively. After cultivation in CO_2 incubator at 37°C, the amount of Ig secreted in each culture medium was determined by enzyme-linked immunosorbent assay (ELISA).

The assay of cytokine production stimulating activity was performed in a 48-well culture plate. Human PBL were inoculated at 1×10^6 cells/ml in ITES-ERDF containing jellyfish extract and 5.0 μg/ml of LPS. Following cultivation, IFN-γ and TNF-α concentrations in the culture medium were measured by using of each determination kit (Biosource International, CA, USA) on the basis of ELISA.

3 Results and Discussion

3.1 The Effect of Jellyfish Extract on IgM Production of HB4C5 Cells

HB4C5 cells were inoculated at 5×10^4 cells/ml in ITES-ERDF medium supplemented with various concentrations of the jellyfish extract. After cultivation for 6 h, the amount of IgM in each culture medium was measured by ELISA. The jellyfish extract did not affect the determination of the amount of Ig by ELISA. As a result, the jellyfish extract dose-dependently stimulated IgM production of HB4C5 cells. IgM production of hybridoma cells was enhanced 34-fold at 85 μg/ml of protein concentration against the control medium. IgM production stimulating activity of jellyfish extract was maintained for 7 d. Jellyfish extract also stimulated cell growth of HB4C5 cells. By the addition of the jellyfish extract, the lag phase of cell growth at the beginning of culture was canceled. The doubling time of HB4C5 cells at growth phase between the second and the fifth d after inoculation was 26.7 h in jellyfish extract-supplemented medium, and that in the control medium was 30.0 h. The jellyfish extract stimulated growth ratio at growth phase. These results mean that jellyfish extract possesses growth promoter activity.

3.2 *Effect of Jellyfish Extract on Ig and Cytokine Production of hPBL*

The immunostimulating effect of jellyfish extract on Ig production by hPBL was examined under 5.0 μg/ml of LPS stimulation. IgM production by hPBL was facilitated 2.8-fold by 450 μg/ml of jellyfish extract as against the control medium. IgG production was also enhanced 1.4-fold at same concentration. This result means that jellyfish extract is effective not only on cell line, but also on Ig production of primary cultured hPBL.

The effect on typical cytokine production by hPBL was examined. As shown in Fig. 1, jellyfish extract stimulated IFN-γ production about 100-fold at 250 μg/ml of jellyfish extract at 2 days after inoculation. Jellyfish extract also stimulated TNF-α production of hPBL about 17-fold under LPS stimulation, and this effect was observed for 3 days. These results suggest that jellyfish extract stimulates not only Ig producers, but also IFN-γ and TNF-α producers, such as helper-T cells.

3.3 *The Active Substance in Jellyfish Extract*

Because of the extraction condition (pH = 3.0, temperature = 121°C), it is expected that the active substance in the jellyfish extract is collagen or a collagen-related substance. Hence the activity of the jellyfish extract treated with collagenase was investigated. As indicated in Table 1, the immunoglobulin production stimulating effect of jellyfish extract treated with 25 μg/ml of collagenase was reduced by half, and that treated with 250 μg/ml was completely inactivated. These results suggest that the active substance in jellyfish extract is collagen.

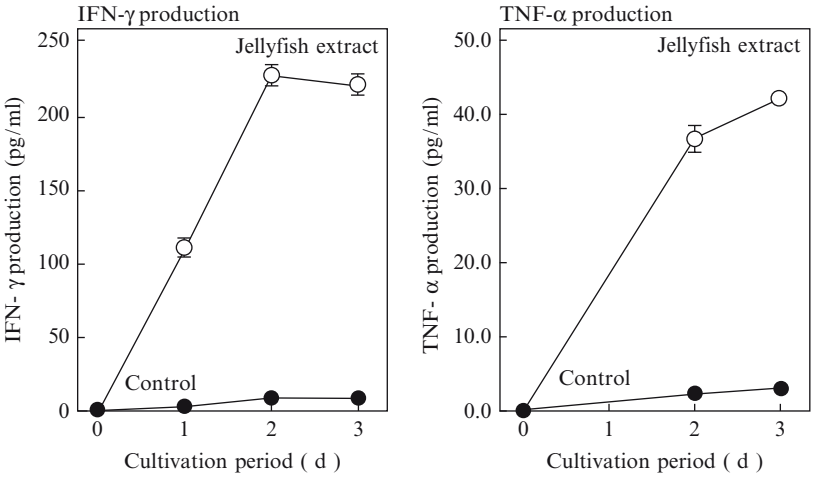

Fig. 1 Effect of jellyfish extract on cytokine production of hPBL

Table 1 Effect of collagenase treatment on Ig production stimulating activity of jellyfish extract

	IgM Production (ng/ml)
None	14.8 ± 0.4
Intact jellyfish extract	173.1 ± 4.9
Collagenase-treated jellyfish extract (25 μg/ml of collagen)	88.8 ± 1.6

Table 2 Effect of collagen on IgM production of HB4C5 cells

	IgM Production (ng/ml)
None	0.8 ± 0.0
Jellyfish extract	154.0 ± 18.3
Bovine Achilles' tendon collagen	25.5 ± 0.0

The IgM production stimulating activities of jellyfish extract and collagen from bovine Achilles' tendon were examined. As shown in Table 2, bovine collagen from Achilles' tendon also stimulated IgM production of HB4C5 cells. However, the specific activity of bovine collagen was about 1/6 than that of jellyfish extract. These results suggest that the active substance in jellyfish extract is collagen.

3.4 Effects of Jellyfish Collagen on mRNA Expression Level for Ig and Cytokines

The effect of jellyfish collagen on transcription was examined by reveres transcription-polymerase chain reaction (RT-PCR). HB4C5 cells were stimulated with 500 μg/ml of jellyfish collagen for 6 h, and the mRNA expression level for IgM was examined. As the result of that, the expression levels of mRNAs for μ-chain and λ-chain were up-regulated. In addition, it was investigated that the effect of collagen on the expression of mRNAs for several cytokines. Human PBL were incubated for 36 h in ITES-ERDF medium supplemented with or without 500 μg/ml of jellyfish collagen, and the mRNA expression levels for TNF-α, IFN-γ and TGF-β were examined. The expression levels of mRNA for these cytokines were also enhanced by collagen stimulation. These results suggest that collagen up-regulates transcription process to accelerate Ig and cytokine production.

3.5 Effects of Jellyfish Collagen on Post-transcription Process

3.5.1 The Stimulation Effect of Collagen on Transcription-Suppressed HB4C5 Cells

The effect of collagen on protein synthesis of HB4C5 cells was investigated. At first, the IPSF effect of collagen on transcription-suppressed HB4C5 cells was determined. HB4C5 cells were treated with 4 μg/ml of actinomycin D (Act D) for

2 h. Following Act D treatment, HB4C5 cells were inoculated in ITES-ERDF medium supplemented with jellyfish collagen and cultured for 12 h. As summarized in Table 3, IgM production of HB4C5 cells which were not treated with Act D was enhanced about 30-fold by collagen. On the other hand, the stimulating effect of collagen on Act D-treated HB4C5 cells was decreased. Even though the IPSF effect of collagen on Act D-treated HB4C5 cells was decreased, collagen still enhanced IgM production of transcription-suppressed HB4C5 cells about 8-fold. This fact suggests that collagen accelerates post-transcription activity of the cell.

3.5.2 The Stimulation Effect of Collagen on Translation-Suppressed HB4C5 Cells

The effect of collagen on translation-suppressed HB4C5 cells was investigated to confirm whether collagen stimulates post-transcriptional process or not. At first, the effect of collagen on HB4C5 cells treated with NaF was examined. NaF is reversible inhibitor repressing the formation of the initiation complex of ribosomes and mRNA. After pre-culture with 4 mM NaF, HB4C5 cells were inoculated in ITES-ERDF medium with or without the same concentration of NaF for 12 h along with 500 μg/ml of jellyfish collagen. If collagen acts on the transcription process at initiation step, the activity of collagen against NaF-treated HB4C5 cells would be reduced or disappeared. However, the IgM production of NaF-treated HB4C5 cells was stimulated as much as that of control cells (Table 3).

Cycloheximide was employed to suppress the peptide-chain elongation activity. After pre-incubation of HB4C5 cells with 10.0 μg/ml of cycloheximide, the stimulating effect of collagen was examined. As indicated in Table 3, the stimulation activity of collagen against control HB4C5 cells was 10.6-fold, and that against cycloheximide-treated cells was 2.5-fold. This result indicates that the effect of collagen on cycloheximide-treated HB5C5 cells was obviously reduced.

These results suggest that collagen stimulates translation activity, especially the stage of peptide-chain elongation step, in addition to the transcription activity.

Table 3 Effect of jellyfish collagen on IgM production of HB4C5 cells treated with protein synthesis inhibitors

Protein Synthesis Inhibitor		Jellyfish Collagen (–)	Jellyfish Collagen (+)	Activity
Actinomycin D	(–)	5.1 ± 0.3	150.6 ± 4.8	29.5
	(+)	1.6 ± 0.1	12.6 ± 0.4	7.9
NaF	(–)	2.6 ± 0.3	36.3 ± 2.1	14.0
	(+)	2.2 ± 0.3	29.4 ± 3.1	13.4
Cycloheximide	(–)	3.3 ± 0.4	35.0 ± 2.4	10.6
	(+)	1.7 ± 0.1	4.2 ± 0.3	2.5
Monensin	(–)	3.0 ± 0.1	53.0 ± 3.0	17.7
	(+)	3.3 ± 0.2	16.1 ± 0.4	4.9

3.5.3 The Stimulation Effect of Collagen on HB4C5 Cells Suppressed the Post-translation Activity

Monensin was used for the suppression of post-translation process of HB4C5 cells. After pre-culture with 10 mM monensin, HB4C5 cells were cultured in ITES-ERDF medium supplemented with or without 10 mM monensin along with 500 μg/ml of collagen for 12 h. By comparison with the amount of IgM produced in the culture medium, the stimulation effect of collagen on HB4C5 cells was reduced by the suppression of post-translation activity (Table 3). However, by comparison with the intracellular amount of IgM of HB4C5 cells treated with monensin was obviously increased by collagen treatment (data not shown). This fact means that IgM synthesis in monensin-treated HB4C5 cells is accelerated by collagen, even though IgM secretion is suppressed by monensin.

We proposed here the putative mode of the action of collagen as an immunostimulation factor. We expected from the results shown here that collagen stimulates Ig and cytokine synthesis by promoting both transcription and translation activity.

References

1. Sugahara, T., Onda, H., Shinohara, M., Horii, M., Akiyama, K., Nakamoto, K., and Hara, K., 2005, Immunostimulation effects of proteose-peptone component 3 fragment on human hybridomas and peripheral blood lymphocytes, *Biochim. Biophys. Acta*, 1725:233–240.

Mycotoxin Nivalenol Induces Apoptosis and Intracellular Calcium Ion-Dependent Interleukin-8 Secretion but Does Not Exert Mutagenicity

Hitoshi Nagashima, Hiroyuki Nakagawa, and Keiko Iwashita

Abstract To elucidate the mechanism underlying the toxicity of nivalenol, we investigated the cytotoxicity of this mycotoxin to the human promyelocyte-derived cell line HL60 after 24-h exposure. Internucleosomal DNA fragmentation, a hallmark of apoptosis, was apparent at 3 and 10 μg/ml nivalenol. The DNA fragmentation at these concentrations was proportional to the morphologic damage they induced in our previous studies, indicating that apoptosis led to the changes in morphology. In addition,1,2-bis(2-aminophenoxy)ethane-N,N,N′,N′-tetraacetic acid tetraacetoxymethyl ester (BAPTA-AM), which chelates intracellular calcium ion, considerably attenuated nivalenol-induced interleukin (IL)-8 secretion from HL60 cells, thereby indicating that this induction is calcium ion-dependent. Further, even at 50 μg/ml, nivalenol failed to induce mutagenesis in *umu* test regardless of treatment with S9 fraction of rat liver homogenate (which is rich in drug-metabolizing enzymes). Therefore, nivalenol is unlikely to be mutagenic.

Keywords Nivalenol • apoptosis • interleukin-8 • BAPTA-AM • mutagenicity

1 Introduction

Nivalenol, a trichothecene mycotoxin, is a secondary metabolite produced by various *Fusarium* fungi. In Japan, nivalenol contamination of wheat and barley is as prevalent as that of deoxynivalenol, another trichothecene mycotoxin [1, 2]. Although the acute toxicity of nivalenol is thought to be equivalent to, or more potent than, that of deoxynivalenol, the paucity of reports suggests that nivalenol has garnered far less interest than deoxynivalenol. In light of these circumstances, the study of

H. Nagashima, H. Nakagawa, and K. Iwashita
National Agriculture and Food Research Organization, National Food Research Institute,
2-1-12 Kannondai, Tsukuba, Ibaraki, 305-8642, Japan

K. Ikura et al. (eds.), *Animal Cell Technology: Basic & Applied Aspects*,
Animal Cell Technology: Basic & Applied Aspects 15,
DOI 10.1007/978-1-4020-9646-4_46,

nivalenol toxicity deserves more attention in Japan. Trichothecene mycotoxins are extremely toxic to rapidly dividing cells including leukocytes [3], and one of the leading symptoms of trichothecene toxicosis is the leukopenia known as alimentary toxic aleukia (ATA) [4]. Therefore, to elucidate the mechanism underlying the toxicity of nivalenol, we investigated its cytotoxicity to the human promyelocyte-derived cell line HL60.

We previously reported that nivalenol causes morphologic change and induces interleukin (IL)-8 secretion in HL60 cells [5]. In addition, treatment with a chelator of intracellular calcium ion attenuated nivalenol-caused retardation of cell proliferation, suggesting that intracellular calcium ion plays a role in exerting nivalenol toxicity [5]. Here, we further investigated potential mechanisms for nivalenol-caused morphologic change and the contribution of intracellular calcium ion to nivalenol toxicity. We also examined nivalenol's mutagenicity, an important aspect of its toxicity.

2 Materials and Methods

2.1 Chemicals and Cells

Nivalenol (M.W. 312) and 1,2-bis(2-aminophenoxy)ethane-N,N,N′,N′-tetraacetic acid tetraacetoxymethyl ester (BAPTA-AM) were purchased from Sigma-Aldrich Corporation (St. Louis, MO, USA) and Wako Pure Chemical Industries, Ltd. (Osaka, Japan), respectively, and dissolved in dimethyl sulfoxide. The human promyelocytic leukemia cell line HL60 was purchased from the RIKEN Cell Bank (Tsukuba, Japan) and cultured in RPMI 1640 medium containing 10% fetal calf serum.

2.2 Examination of DNA Fragmentation

The method used to study DNA fragmentation was identical to that of Nagashima and Goto [6].

2.3 Determination of IL-8 Levels

Approximately 1×10^5 cells in 0.5 ml medium containing chemical(s) were cultured for 24 h in each well of a 24-well culture plate. Media were collected and centrifuged at $5{,}000 \times g$ for 5 min to remove cells and debris, and the levels of IL-8 in the culture supernatants were quantified using the Quantikine Human IL-8 Immunoassay (R&D Systems, Inc., Minneapolis, MN, USA) according to the manufacturer's recommended procedure.

2.4 Evaluation of Mutagenicity (umu Test)

Mutagenicity of nivalenol was evaluated using the Umulac AT (JIMRO Co., Ltd., Takasaki, Japan) according to the manufacturer's recommended procedure. Umulac AT is an *umu* test-based kit, and mutagenicity to *Salmonella typhimurium* is expressed as the optical density at a wavelength of 620 nm. Nivalenol with or without treatment with rat liver homogenate S9 fraction (rich in drug-metabolizing enzymes) underwent mutagenicity testing, because some non-mutagenic chemicals convert to mutagens after S9 treatment (activation). As defined previously [7], the threshold for defining a compound as mutagenic was an optical density that was at least twice that of vehicle-treated control.

2.5 Statistics

Data are expressed as means ± standard deviation. Logarithmically transformed data were statistically analyzed. Differences between groups were analyzed using Tukey's test. A P value of <0.05 was considered to be significant.

3 Results and Discussion

Nivalenol-induced apoptotic DNA fragmentation in HL60 cells has been reported previously [8]. We similarly found that 3 μg/ml (9.7 μM) and 10 μg/ml nivalenol led to prominent internucleosomal DNA fragmentation (DNA ladder) (Fig. 1; lanes 5, 6), confirming that nivalenol induces apoptosis in HL60 cells. Faint DNA laddering occurred at 1 μg/ml nivalenol (Fig. 1; lane 4). The concentrations at which nivalenol caused DNA fragmentation and the amounts of fragmentation induced (Fig. 1) were

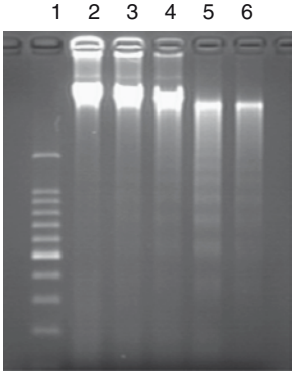

Fig. 1 Agarose gel electrophoresis of DNA from nivalenol-treated HL60 cells. Lane 1: molecular weight marker (100-bp DNA ladder). Lane 2: negative control (treated with vehicle only). Lanes 3–6: treated with 0.3, 1, 3, and 10 μg/ml nivalenol for 24 h

similar to those that led to morphologic damage [5](pronounced damage at 3 and 10 μg/ml, slight at 1 μg/ml nivalenol), indicating that nivalenol-caused morphologic change is due to apoptosis. Although Ueno et al. [8] reported that 0.01 μg/ml nivalenol led to DNA fragmentation in HL60 cells, we were unable to detect DNA fragmentation even at 0.3 μg/ml (Fig. 1; lane 3); this apparent discrepancy may be due to differences in experimental conditions.

Because treatment with BAPTA-AM, a chelator of intracellular calcium ion, decreases the nivalenol-associated retardation of HL60 cell proliferation [5], we investigated the chelator's effect on nivalenol-induced IL-8 secretion. Whereas exposure of HL60 cells to BAPTA-AM alone moderately induced IL-8 secretion, the chelator clearly reduced nivalenol-induced secretion (59.1% of nivalenol-treated alone; Table 1). That BAPTA-AM evidently impaired the effect of nivalenol indicates that IL-8 secretion is dependent on intracellular calcium ion. Nozawa et al. [9], Marino et al. [10] and Matsubara et al. [11] also reported that BAPTA-AM decreased *Helicobacter pylori*-, endozepine triakontatetra-neuropeptide- and histamine-induced IL-8 secretion, respectively.

The genotoxicity of a compound—its ability to induce mutations (mutagenicity), chromosomal aberrations and fragmentation, and aneuploidy—is an important characteristic, because it is well known that damage to genomic DNA can lead to cancer, one of the leading causes of death. We focused here on the mutagenicity of nivalenol, which we investigated in the absence and presence of S9 fraction. The optical densities of nivalenol-treated samples in *umu* test were almost the same as those of corresponding negative controls (0 μg/ml; Table 2) even at 50 μg/ml (161 μM) nivalenol. In light of these results and given that the positive control reactions (-S9, furylfuramide; +S9, 2-aminoanthracene; Table 2) functioned properly, nivalenol is unlikely to be a mutagen. Nivalenol was similarly non-mutagenic in Ames tests and S9-induced chemiluminescence assays [12]. In contrast, Tsuda et al. [13] used alkaline single-cell gel electrophoresis (comet assay) to conclude that nivalenol is a direct mutagen in CHO cells. However, comet assays merely show whether DNA fragmentation has occurred; whether that fragmentation is due to mutagenesis or apoptosis is beyond the scope of the assay. Therefore, the nivalenol-induced DNA fragmentation noted by Tsuda et al. [13] may have been apoptotic, not mutagenic, in origin.

Table 1 Effect of BAPTA-AM on nivalenol-induced secretion of IL-8 in HL60 cells

	Nivalenol (1 μg/ml)			
	−		+	
None	16.8	±0.7[a]	100	±14.9[a,c]
BAPTA-AM (1.5 μM)	25.9	±1.2[b]	59.1	±.9[b,c]

Results are given as means ± SD (n = 4). The value for nivalenol-treated samples was defined as 100%.

[a,b,c] $P < 0.05$ (Tukey's test) between values labeled with the same letter.

Table 2 Mutagenicity testing of nivalenol

		μg/ml	Optical Density at 620 nm		%
−S9	Nivalenol	0	0.21	±0.01	100
		0.5	0.20	±0.02	97
		5	0.20	±0.01	95
		50	0.21	±0.02	98
	AF-2	0	0.18	±0.03	100
		0.01	0.70	±0.05	381
+S9	Nivalenol	0	0.17	±0.01	100
		0.5	0.18	±0.02	107
		5	0.17	±0.02	104
		50	0.18	±0.02	106
	2-AA	0	0.19	±0.01	100
		0.003	0.45	±0.04	242

AF-2, furylfuramide; 2-AA, 2-aminoanthracene. Results are given as means ± SD (n = 6).

We showed that nivalenol induces apoptosis in HL60 cells and that intracellular calcium ion plays a role in the nivalenol-induced secretion of IL-8 from this cell line. We also determined that nivalenol appears to be non-mutagenic. However, further studies are needed to elucidate the detailed mechanisms by which nivalenol leads to cytotoxicity and stimulates IL-8 secretion.

Acknowledgements This work was supported by the Integrated Research Program for Functionality and Safety of Food toward an Establishment of Healthy Diet from the Ministry of Agriculture, Forestry and Fisheries, Japan.

References

1. Sugiura, Y., Fukasaku, K., Tanaka, T., Matsui, Y., and Ueno, Y., 1993, *Fusarium poae* and *Fusarium crookwellense*, fungi responsible for the natural occurrence of nivalenol in Hokkaido, *Appl. Environ. Microbiol.* **59:**3334–3338.
2. Yoshizawa, T. and Jin, Y. Z., 1995, Natural occurrence of acetylated derivatives of deoxynivalenol and nivalenol in wheat and barley in Japan, *Food Addit. Contam.* **12:**689 694.
3. Ryu, J-C., Ohtsubo, K., Izumiyama, N., Nakamura, K., Tanaka, T., Yamamura, H., and Ueno, Y., 1988, The acute and chronic toxicities of nivalenol in mice, *Fund. Appl. Toxicol.* **11:**38–47.
4. Joffe, A. Z., 1971, Alimentary toxic aleukia, in: Microbial Toxins VII, S. Kadis, A. Ciegler, and S. J. Ajl, eds., Academic Press, New York, pp. 139–189.
5. Nagashima, H., Nakagawa, H., and Iwashita, K., 2006, Cytotoxic effects of nivalenol on HL60 cells, *Mycotoxins* **56:**65–70.
6. Nagashima, H. and Goto, T., 1998, Rubratoxin B induces apoptosis in HL-60 cells in the presence of internucleosomal fragmentation, *Mycotoxins* **46:**17–22.
7. Oda, Y., Nakamura, S., Oki, I., Kato, T., and Shinagawa, H., 1985, Evaluation of the new system (*umu*-test) for the detection of environmental mutagens and carcinogens, *Mutat. Res.* **147:**219–229.

8. Ueno, Y., Umemori, K., Niimi, E., Tanuma, S., Nagata, S., Sugamata, M., Ihara, T., Sekijima, M., Kawai, K., Ueno, I., and Tashiro, F., 1995, Induction of apoptosis by T-2 toxin and other natural toxins in HL-60 human promyelotic leukemia cells, *Nat. Toxins* **3:**129–137.
9. Nozawa, Y., Nishihara, K., Peek, R. M., Nakano, M., Uji, T., Ajioka, H., Matsuura, N., and Miyake, H., 2002, Identification of a signaling cascade for interleukin-8 production by *Helicobacter pylori* in human gastric epithelial cells, *Biochem. Pharmacol.* **64:**21–30.
10. Marino, F., Cosentono, M., Fietta, A. M., Ferrari, M., Cattaneo, S., Frigo, G., Lecchini, S., and Frigo, G. M., 2003, Interleukin-8 production induced by the endozepine triakontatetraneuropeptide in human neutrophils: role of calcium and pharmacological investigation of signal transduction pathway, *Cell Signal* **15:**511–517.
11. Matsubara, M., Tamura, T., Ohmori, K., and Hasegawa, K., Histamine H1 receptor antagonist blocks histamine-induced proinflammatory cytokine production through inhibition of Ca^{2+}-dependent protein kinase C, Raf/MEK/ERK and IKK/IκB/NF-κB signal cascades, *Biochem. Pharmacol.* **69:**433–449.
12. Takahashi, H., Osada, K., Yazaki, H., and Kimura, S., 1992, Detection of mutagenic activity of mycotoxins by *Salmonella typhimurium*/microsome assay and ultra-weak chemiluminescence, *J. Jpn. Soc. Nutr. Food Sci.* **45:**169–173.
13. Tsuda, S., Kosaka, Y., Murakami, M., Matsuo, H., Matsusaka, N., Taniguchi, K., and Sasaki, Y. F., 1998, Detection of nivalenol genotoxicity in cultured cells and multiple mouse organs y the alkaline single-cell gel electrophoresis assay, *Mutat. Res.* **415:**191–200.

Development of an In Vitro System for Screening the Ligands of a Membrane Glycoprotein CD36

H. Inagaki, S. Tsuzuki, T. Iino, K. Inoue, and T. Fushiki

Abstract It has well been known that human and rodents exhibit a preference for oils. This suggests the existence of an orosensory system responsible for the detection of dietary lipids. A plasma membrane glycoprotein CD36, besides the role in the uptake of oxidized low-density lipoprotein (OxLDL) by a variety of cells, has been postulated to be a candidate lipid taste receptor on the tongue. This notion is supported by the expression in taste bud cells, the binding to long-chain fatty acids (LCFAs) as well as OxLDL, the lack of preference for LCFAs in the CD36-knockout mice, and the activation of MAP kinases by the binding of the ligands such as OxLDL. Therefore, molecules, irrespective of being occurred naturally or artificially, that stimulate CD36 to cause intracellular signaling but have poor calories would have been expected to be substitutes for dietary lipids. In this study, we developed an in vitro system for screening such ligands of CD36. The full-length human and mouse CD36 cDNAs were obtained and subcloned into pcDNA3.1, a mammalian expression vector. Each construct was transfected into Chinese hamster ovary-K1 (CHO-K1) cells, and a few lines stably expressing human or mouse CD36 were selected by means of Western blotting and immunofluorescence with anti-CD36 antibodies. Much stronger signals were shown in the selected lines by the addition of OxLDL labeled with fluorescence dye to the cultured media relative to those in the non-transfected CHO-K1 cells, confirming the cell surface localization of CD36. Incubation of the lines with non-labeled OxLDL resulted in the phosphorylation of ERK1/2 MAP kinase of the cells. This is the first report showing that the binding of the ligands to exogenously expressed CD36 causes MAP kinase activation. The expression system using CHO-K1 cells would be a powerful tool to screen the novel agonists of CD36.

H. Inagaki, S. Tsuzuki, K. Inoue, and T. Fushiki
Laboratory of Nutrition Chemistry, Division of Food Science and Biotechnology, Graduate School of Agriculture, Kyoto University, Oiwake-cho, Kitashirakawa, Sakyo-ku, Kyoto, 606-8502, Japan

T. Iino
Pharmafoods International Co. Ltd., 24-5, Donoato-Nishimachi, Kisshoin-Ishihara, Minami-ku, Kyoto, 601-8357, Japan

K. Ikura et al. (eds.), *Animal Cell Technology: Basic & Applied Aspects*,
Animal Cell Technology: Basic & Applied Aspects 15,
DOI 10.1007/978-1-4020-9646-4_47, © Springer Science+Business Media B.V. 2009

Keywords CD36 • ligand • OxLDL • LDL • binding • MAP kinase

1 Introduction

CD36 is an 88-kDa plasma membrane glycoprotein that functions as a scavenger receptor. It is expressed in a range of cells and tissues including platelets, monocytes/macrophages, vascular endothelial cells, and adipose tissues [1]. CD36 recognizes a variety of ligands including collagen, thrombospondin-1 (TSP-1), long-chain fatty acids (LCFAs), oxidized low-density lipoprotein (OxLDL), anionic phospholipids, *Plasmodium falciparum*-infected erythrocytes and apoptotic cells [1–4]. It was reported that the membrane fatty acid transporter (FAT/CD36) protein and its mRNA, originally expressed in adipose tissue, were detected in the tongues of rats. Immunohistochemical staining revealed that immunoreactivity for FAT/CD36 is specifically localized in the apical parts of the taste bud cells, possibly the gustatory cells in the circumvallate papillae [5]. The inactivation of the CD36 gene completely eliminated the preference for LCFA-enriched solutions and solid diet observed in wild-type mice. Further, in rats and wild-type mice with esophageal ligations, the deposition of unsaturated LCFA on the tongue led to a rapid and sustained increase in the flux and protein content of the pancreatobiliary secretions [6]. These findings demonstrate that CD36 is involved in oral LCFA recognition, however the mechanism of its signal transduction is not clear. The aim of this study is elucidation of the mechanism of signal transduction involving fatty acid association with CD36 and development an in vitro system for screening such ligands of CD36 for development fat substitutes using two methods, binding and ERK1/2 MAP kinase activation assay.

2 Materials and Methods

2.1 Materials

Penicillin G (1,650 IU/mg), streptomycin sulfate (750 IU/mg), Phosphate-Buffered Salines, Ham's F-12 medium and polyclonal fluorescein isothiocyanate (FITC)-labelled goat anti-mouse IgG antibody were purchased from Invitrogen (Carlsbad, CA, USA). Fatty acid-free bovine serum albumin (BSA) was purchased from Sigma (St. Louis, MO, USA). G418 was purchased from Wako (Tokyo, Japan). Polyclonal goat anti-human CD36 antibody (Cat. #AF1955) and Polyclonal goat anti-mouse CD36 antibody (Cat. #AF2519) were purchased from R&D Systems, Inc. (Minneapolis, MN, USA). Monoclonal mouse anti-mouse CD36 antibody (Clone 63, Cat. #ABM5525) was purchased from Cascade Bioscience, Inc. (Winchester, IN, USA). Monoclonal mouse anti-human CD36 antibody (FA6-152, Cat. #HM2122) was purchased from HyCult biotechnology B.V. (Uden, Netherlands). Polyclonal HRP(horseradish peroxidase)-conjugated rabbit anti-goat IgG antibody (Cat. #P0449)

was purchased from Dako (Kyoto, Japan). OxLDL was purchased from Biotium, Inc. (Hayward, CA, USA). LDL was purchased from Calbiochem (San Diego, CA, USA). Other chemicals were of the best grade available from commercial sources.

2.2 Cell Culture and Establishment of Stable Transformant

CHO-K1 cells were maintained at 37°C in medium A (Ham's F-12 medium supplemented with 100 units/ml penicillin and 100 units/ml streptomycin) containing 10% fetal calf serum. The cDNAs of human and mouse CD36 were amplified from human and mouse spleen cDNA libraries by polymerase chain reaction using the following primers, respectively: human; sense, 5′-ACCATGGGC TGTGACCG-GAAC-3′; and antisense, 5′-GTTTATTTTATTGTTTTCGATCTGCA TGC-3′ mouse; sense, 5′-ACCATGGGCTGTGATCGGAACTGC-3′; and antisense, 5′-ACTTATT-TTCCATTCTTGGATTTGCAAG-3′. The amplified human and mouse CD36 cDNAs were sequenced, subcloned into a mammalian expression vector, pcDNA3.1, and transfected into CHO-K1 cells by lipofection. To select clones expressing CD36, cells were cultured in medium B (medium A supplemented with 10% fetal calf serum and 0.5 mg/ml G418). Positive clones were selected by Western Blotting with polyclonal goat anti-CD36 antibodies. CHO-K1 clones expressing human CD36 or mouse CD36 were designated as CHO-hCD36 or CHO-mCD36, respectively.

2.3 Western Blotting Analysis

Cells were washed with ice-cold PBS and lysed in SDS sample buffer and boiled for 5 min. Equal amounts of proteins were subjected to SDS-polyacrylamide gel electrophoresis (PAGE) (8% separating gel and 4.5% stacking gel). After electrophoresis, the proteins were transferred to PVDF membranes by electrotransfer. Membranes were blocked in 5% skim milk in PBST (PBS containing 0.1% Tween 20) for 1 h at room temperature, and washed three times with PBST. Then membranes were incubated overnight at 4°C with the primary polyclonal goat anti-CD36 antibodies (Cat. #AF2519, #AF1955, 1:1,000 dilution) in PBST. Membranes were subsequently washed three times and incubated in the secondary HRP-conjugated anti-goat IgG antibody for 1 h at room temperature. Immunoreactive bands were detected by chemiluminescence.

2.4 Immunofluorescence

For immunofluorescence, cells (5×10^4) of the each transformant were seeded on 96-well plates, and cultured for 24 h at 37°C. Cells were washed with PBS and fixed with 3% formaldehyde in PBS for 20 min at room temperature, washed twice with PBS.

Washed cells were blocked in 2% BSA in PBS for 1 h at room temperature. Then cells were washed twice with PBS, incubated with the primary anti-human/mouse CD36 monoclonal antibody (dilution 1:1,000) with 2% BSA in PBS for 1 h at room temperature. After 1 h, cells were washed three times with PBS and incubated with FITC-labeled polyclonal goat anti-mouse IgG antibody (dilution 1:1,000) for 1 h at room temperature. After further twice wash in PBS, cells were observed under confocal laser scanning microscope FLUOVIEW/LSM (Olympus).

2.5 Binding

Binding was performed to measure bound OxLDL after binding to CD36 [7]. OxLDL was labeled using Alexa Fluor® 488 Protein Labelling Kit purchased from Invitrogen. After labeling, Alexa Fluor488-labeled-OxLDL (designated as AF488-OxLDL) was dialyzed against PBS, 0.01% NaN3. Cells (5×10^4) were seeded on 96-well plates, and cultured for 24 h at 37°C before experiment. Cells were incubated with 100 μg/ml AF488-OxLDL in the presence or the absence of 10-fold excess of unlabeled ligand (OxLDL or LDL) for 30 min at 37°C. Cells were then washed twice with PBS containing 0.01%BSA. Washed cells were then fixed with 3% formaldehyde for 20 min. After further twice wash in PBS, cells were analyzed by confocal laser scanning microscope FLUOVIEW/LSM (Olympus). We define this procedure binging.

2.6 MAP Kinase Activation Assay

Cells (5×10^4) were seeded on 96-well plates, cultured for 24 h at 37°C, and stimulated with 0.1 mg/ml OxLDL or 0.1 mg/ml LDL for 10 min. MAP kinase activation assay was performed using Cellular Activation of Signaling ELISA CASETM kit for ERK1/2 purchased from SuperArray Bioscience Corporation (Frederick, MD, USA) following the instruction of manufacturer. This kit is a cell-based ELISA that directly measures the amount of phosphorylated ERK1/2 protein and total ERK1/2 protein of cells cultured in 96 well plate.

3 Results and Discussion

3.1 Establishment of Stable Transformants Expressing hCD36 or mCD36

Clones expressing hCD36 (CHO-hCD36) or mCD36 (CHO-mCD36) were selected by Western blot analysis. Western blot analysis using polyclonal goat anti-CD36 antibodies showed that each CD36 with molecular weigh of 88kDa was present in

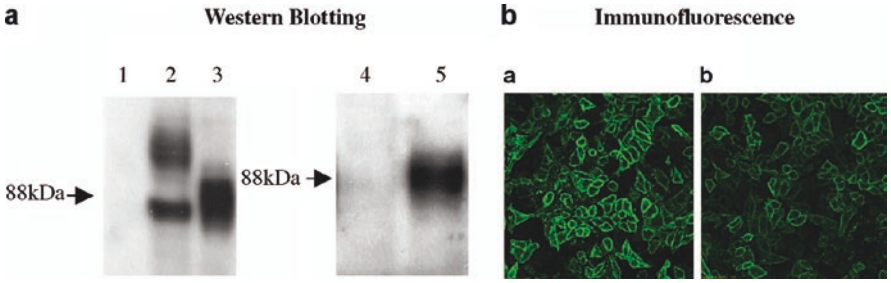

Fig. 1 Characterization of CD36-expressing stable transformants. (A) Western blot analysis of cell lysates from CD36-expressing transformants: Cell lysate proteins were separated by SDS-PAGE, transferred to PVDF membrane, probed with polyclonal goat anti-CD36 antibodies (AF1955 or AF2519), and detected by chemiluminescence. Lanes; 1: parental CHO-K1 cell, 2: THP-1 cell, 3: CHO-hCD36 cell, 4: parental CHO-K1 cell, 5: CHO-mCD36 cell, THP-1 cell was used as positive control. (B) Immunofluorescence of CD36-expressing transformants: Cells were washed, fixed with 3% formaldehyde, incubated with monoclonal anti-CD36 antibodies (HM2122 or ABM5525) for 1 h at room temperature, washed, then incubated with polyclonal FITC-labeled goat anti-mouse IgG antibody for 1 h at room temperature, washed again, and observed under confocal laser scanning microscope FLUOVIEW/LSM

transfected CHO-K1 cells. No detectable CD36 was found in the control parental CHO-K1 cell (Fig. 1). Moreover, the expression of each CD36 on the cell surface was confirmed by immunofluorescence microscopy with anti-human (Fig. 1B(a)) /mouse (Fig. 1B(b)) CD36 monoclonal antibody.

3.2 Binding of OxLDL to the CD36-Expressing Transformants

By analysis using confocal laser scanning microscope FLUOVIEW/LSM, it was shown that CD36-expressing transformants bound AF488-OxLDL, and 10-fold excess of unlabeled OxLDL greatly reduced the binding (Fig. 2A, C, D). On the other hand, the parental CHO-K1 cell also bound some OxLDL, however, its maximal binding was lower compared with that of CD36-expressing transformants (Fig. 2A, B, E). We speculate that the reason why the parental CHO-K1 cell also incorporates AF488-OxLDL is that the cell line expresses some OxLDL-related receptors.

3.3 Binding of LDL to the CD36-Expressing Transformants

It was shown that the binding of AF488-OxLDL was competed by 10-fold excess of unlabeled LDL (Fig. 2A–C). This result strongly suggests that in addition to OxLDL, LDL can interact with CD36 expressed on the cell surface of transformants. On the other hand, the parental CHO-K1 cell also interact some LDL, however, its

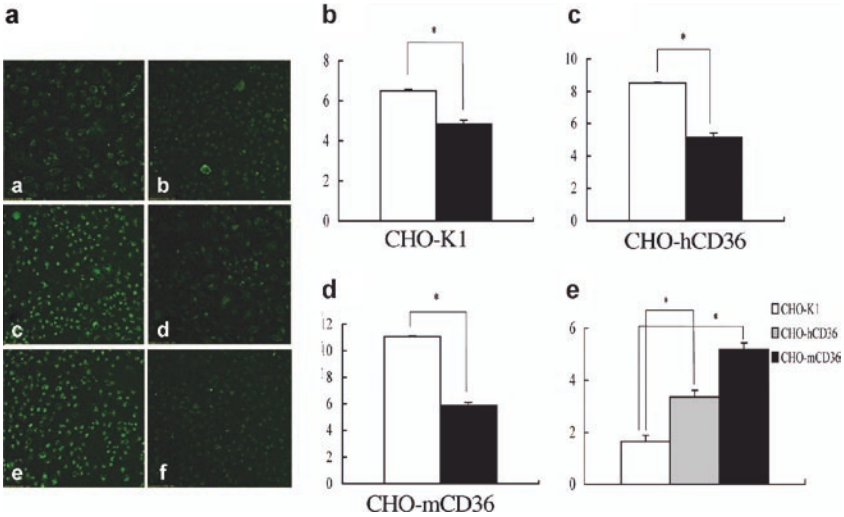

Fig. 2 OxLDL uptake by parental CHO-K1 cell and CD36-expressing ransformants. (A) Parental CHO-K1 cell and CD36-expressing transformants seeded on 96-well plates were incubated with 100 μg/ml AF488-OxLDL for 30 min at 37°C in the presence (b, d, f) or the absence (a, c, e) of 10-fold excess of unlabeled OxLDL, respectively, to measure OxLDL uptake. Then, cells were washed twice with PBS containing 0.01% BSA, fixed with 3% paraformaldehyde. (a), (b) parental CHO-K1 cell, (c), (d) CHO-hCD36 cell, (e), (f) CHO-mCD36 cell. Vertical axis shows the AF488-OxLDL uptake. Each value represents the mean ± S.D. of three independent experiments. (B), (C), (D) Open column means AF488-OxLDL uptake in the absence of 10-fold excess of unlabeled OxLDL. Closed column means AF488-OxLDL uptake in the presence of 10-fold excess of unlabeled OxLDL. (E) AF488-OxLDL uptake among parental CHO-K1 cell and CD36-expressing transformants in the absence of 10-fold excess of unlabeled OxLDL

maximal interact was lower compared with that of CD36-expressing transformants (Fig. 2D). Agnes Boullier et al. reported that LDL does not compete for the binding of OxLDL to the CD36-expressing transformants [8], while S. Frieda et al. reported that LDL does [9]. Our study supports the latter result, however, we can not conclude that LDL is really agonist or antagonist for CD36 by this experiment (see Fig. 3).

3.4 MAP Kinase Activation

The ERK1/2 MAP Kinase (MAPK), a member of the MAPK superfamily, is known to participate in the signal transduction cascades controlling cell growth and differentiation [10, 11], as well as cellular responses to cytokines and stress [12, 13]. It has been previously reported that signaling events induced by β-amyloid include activation of MAPK [14]. To test whether OxLDL and LDL is associated with activation of MAPK, we compared the degree of ERK1/2 MAPK phosphorylation in parental CHO-K1 cell and CD36-expressing transformants after CD36 ligands stimulation.

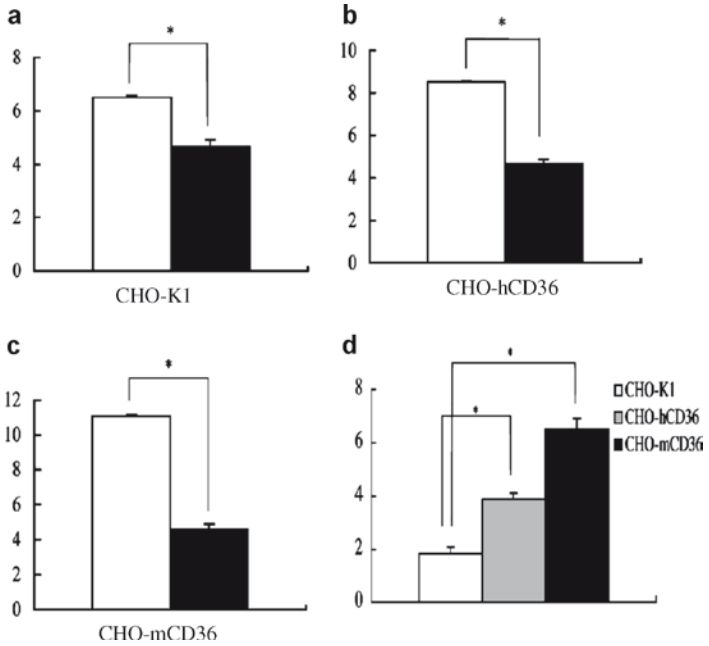

Fig. 3 Interaction with LDL by parental CHO-K1 cell and CD36-expressing transformants. Parental CHO-K1 cell and CD36-expressing transformants were incubated with 100 μg/ml AF488-OxLDL for 30 min at 37°C in the presence or the absence of 10-fold excess of unlabeled LDL, respectively, to measure the interaction with LDL. Vertical axis show the AF488-OxLDL uptake. Open column means AF488-OxLDL uptake in the absence of 10-fold excess of unlabeled LDL. Closed column means AF488-OxLDL uptake in the presence of 10-fold excess of unlabeled LDL. Each value represents the mean ± S.D. of three independent experiments

Figure 4 shows a higher level of ERK1/2 activation in CD36-expressing transformants after stimulation with OxLDL or LDL for 10 min, compared with the parental CHO-K1 cell. Incubation of CD36-expressing transformants with OxLDL or LDL resulted in the phosphorylation of ERK1/2 MAP kinase of the cells, whereas incubation of the parental CHO-K1 cell resulted in the phosphorylation, also. However, the amount of phosphorylated ERK1/2 in CD36-expressing transformants were significantly high compared with that of parental CHO-K1 cell. We speculate that the reason why the ERK1/2 MAPK is activated in the parental CHO-K1 cell is that the cell line expresses some OxLDL-related receptors as shown in binding experiments. These results suggest that OxLDL and LDL are implicated in signal transduction and that these are agonists for CD36. This is the first report showing that the binding of CD36 agonists to exogeneously introduced CD36 causes MAP kinase activation. These results strongly suggest that the expression system using CHO-K1 cells would be a powerful tool to screen the novel agonists of CD36, because the difference can be compared between parental CHO-K1 cell and its transformants.

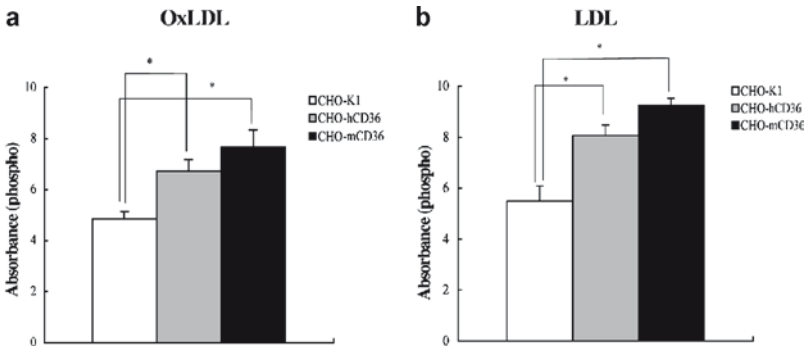

Fig. 4 MAP K activation by parental CHO-K1 cell and CD36-expressing transformants. The amount of phospholylated ERK1/2 MAPK in parental CHO-K1 cell and transformants after stimulation with (**a**) OxLDL or (**b**) LDL. Each value represents the mean ± S.D. of four independent experiments

Acknowledgments This study has been supported by Program for Promotion of Basic Research Activities for Innovative Bioscience.

References

1. Febbraio, M., Hajjar, D.P. and Silverstein, R.L. (2001) CD36: A Class B Scavenger Receptor Involved in Angiogenesis, Atherosclerosis, Inflammation, and Lipid Metabolism. J. Clin. Invest., 108, 785–791.
2. Abumrad, N.A., El-Maghrabi, M.R., Amri, E.Z., Lopez, E. and Grimaldi, P.A. (1993) Cloning of a Rat Adipocyte Membrane Protein Implicated in Binding or Transport of Long-Chain Fatty Acids That Is Induced during Preadipocyte Differentiation. Homology with Human CD36. J. Biol. Chem., 268, 17665–17668.
3. Tandon, N.N., Kralisz, U. and Jamieson, G.A. (1989) Identification of Glycoprotein IV (CD36) As a Primary Receptor for Platelet-Collagen Adhesion. J. Biol. Chem., 264, 7576–7583.
4. Greenwalt, D.E., Lipsky, R.H., Ockenhouse, C.F., Ikeda, H., Tandon, N.N. and Jamieson, G.A. (1992) Membrane Glycoprotein CD36: A Review of Its Roles in Adherence, Signal Transduction, and Transfusion Medicine. Blood, 80, 1105–1115.
5. Fukuwatari, T., Kawada, T., Tsuruta, M., Hiraoka, T., Iwanaga, T., Sugimoto, E. and Fushiki, T. (1997) Expression of the Putative Membrane Fatty Acid Transporter (Fat) in Taste Buds of the Circumvallatepapillae in Rats. FEBS Lett., 414, 461–464.
6. Laugerette, F., Passilly-Degrace, P., Patris, B., Niot, I., Febbraio, M., Montmayeur, J.P., Besnard, P. (2005) CD36 Involvement in Orosensory Detection of Dietary Lipids, Spontaneous Fat Preference, and Digestive Secretions. J. Clin. Invest., 115, 3177–3184.
7. Malaud, E., Hourton, D., Giroux, Lm, Ninio, E., Buckland, R., Mcgregor, J.I. (2002) The Terminal Six Amino-Acids of the Carboxy Cytoplasmic Tail Of CD36 Contain a Functional Domain Implicated in the Binding and Capture of Oxidized Low-Density Lipoprotein. Biochem. J., 364, 507–515.
8. Boullier, A., Gillotte, K.I., Horkko, S., Green, Sr., Friedman, P., Dennis, Ea., Witztum, J.I., Steinberg, D., Quehenberger, O. (2000) The Binding of Oxidized Low Density Lipoprotein to Mouse Cd36 Is Mediated in Part by Oxidized Phospholipids That Are Associated with Both the Lipid and Protein Moieties of the Lipoprotein. J. Biol. Chem., 275(13), 9163–9169.

9. Pearce, Sf., Roy, P., Nicholson, Ac., Hajjar, Dp., Febbraio, M., Silverstein, R.I. (1998) Recombinant Glutathione S-Transferase/CD36 Fusion Proteins Define an Oxidized Low Density Lipoprotein-Binding Domain. J. Biol. Chem., 273(52), 34875–34881.
10. Hill, C.S. and Treisman, R. (1995) Transcriptional Regulation by Extracellular Signals: Mechanisms and Specificity. Cell, 80, 199–211.
11. Marshall, C.J. (1995) Specificity of Receptor Tyrosine Kinase Signaling: Transient Versus Sustained Extracellular Signal-Regulated Kinase Activation. Cell, 80, 179–185.
12. Kyriakis, J.M. and Avruch, J. (2001) Mammalian Mitogen-Activated Protein Kinase Signal Transduction Pathways Activated by Stress and Inflammation. Physiol. Rev., 81, 807–869.
13. Tibbles, L.A. and Woodgett, J.R. (1999) The Stress-Activated Protein Kinase Pathways. Cell. Mol. Life Sci., 55, 1230–1254.
14. Moore, K. J., El Khoury, J., Medeiros, L. A., Terada, K., Geula, C., Luster, A. D., and Freeman, M. W. (2002) A CD36-Initiated Signaling Cascade Mediates Inflammatory Effects of Beta-Amyloid. J. Biol. Chem., 277, 47373–47379.

MTT Reduction by Flavonoids in the Absence of Cells: Influence of Medium Type and Serum

Terence P.N. Talorete, Mohamed Bouaziz, Sami Sayadi, and Hiroko Isoda

Abstract The MTT (3-(4, 5-dimethylthiazolyl-2)-2, 5-diphenyltetrazolium bromide) assay is widely accepted as a simple and reproducible method for determining cell proliferation or cytotoxicity in vitro. In this study, we show that the flavonoids quercetin, rutin and luteolin but not apigenin can reduce MTT in the absence of live cells in the following order: quercetin >> rutin > luteolin > apigenin. The final concentrations of the flavonoids used were 200, 100, 50, 25 and 12.5 μg/ml. Results further show that MTT reduction in Dulbecco's Modified Eagle's Medium (DMEM) is statistically higher than those in RPMI 1640 and F12 media, which are generally similar. Particularly for luteolin, MTT reduction is considerably higher with serum than without serum. In the case of quercetin at 50 μg/ml, a serum concentration of even only 0.01% is sufficient to significantly enhance MTT reduction versus that at 0% ($P < 0.05$, Student's T-test). The authors hypothesize that flavonoid structure, nutrient concentration in the culture medium as well as serum components directly affect MTT reduction by flavonoids in the absence of cells.

Keywords MTT reduction • flavonoids • culture medium • serum

1 Introduction

The reduction of tetrazolium salts such as MTT (3-(4, 5-dimethylthiazolyl-2)-2, 5-diphenyltetrazolium bromide) by live cells has been widely accepted as a reliable means of measuring cell proliferation in vitro. In principle, mitochondrial

T.P.N. Talorete and H. Isoda
Graduate School of Life and Environmental Sciences, University of Tsukuba,
1-1-1 Tennodai, Tsukuba, Ibaraki, 305-8572, Japan

M. Bouaziz and S. Sayadi
Laboratoire des Bio-procédés, Centre de Biotechnologie de Sfax, BP « K »,
3038, Sfax, Tunisia

K. Ikura et al. (eds.), *Animal Cell Technology: Basic & Applied Aspects*,
Animal Cell Technology: Basic & Applied Aspects 15,
DOI 10.1007/978-1-4020-9646-4_48,

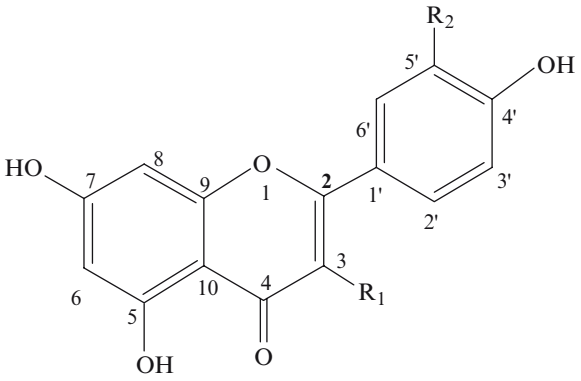

Fig. 1 Structure of flavonoids used in this study. Luteolin (R 1 = H, R 2 = OH), apeginin (R 1 = H, R 2 = H), quercetin (R 1 = OH, R 2 = OH), rutin (R 1 = O-rutinose, R 2 = OH)

dehydrogenases of viable cells cleave the tetrazolium ring of the yellow MTT to yield purple formazan crystals which are insoluble in aqueous solutions. The crystals can then be dissolved using a suitable solvent and the resulting purple solution is measured spectrophotometrically.

Recent studies, however, have shown that MTT can be reduced in the absence of live cells. Shoemaker et al. [1] have shown that botanical extracts can reduce MTT in the absence of live cells and that treatment of these extracts with iodoacetic acid to alkylate free thiol groups inhibited their ability to reduce MTT. Peng et al. [2] have also shown that the flavonoids luteolin and quercetin can also reduce MTT in the absence of live cells. Previous studies have likewise shown that some flavonoids inhibit cell growth but enhance MTT reduction [3, 4].

In this study, we use the flavonoids quercetin, luteolin, rutin and apigenin (Fig. 1) to determine the influence of medium type and serum on MTT reduction in the absence of cells.

2 Materials and Methods

2.1 Materials

Luteolin, quercetin, rutin, Dulbecco's modified Eagle's medium (DMEM) and fetal bovine serum (Lot no. 44K3398) were purchased from Sigma (Japan). Apigenin was obtained from Fluka (Germany). RPMI 1640 medium (RPMI) and F12 Nutrient Mixture (F12) were purchased from Gibco (Invitrogen Corp., USA). 3-(4,5-Dimethyl-2-yl)-2,5-diphenyl tetrazolium bromide (MTT) was obtained from Dojindo (Japan). Sodium dodecyl sulfate (SDS) and 99.5% ethanol were purchased from Wako (Japan).

2.2 Preparation of Flavonoids

Luteolin, quercetin, rutin and apigenin were dissolved in 99.5% ethanol at 1 mg/ml and then filtered using a 0.45 μm filter (Millipore, Japan). The flavonoid solutions were then stored at −80°C until use.

2.3 MTT Assay

The MTT assay is based on the protocol first described by Mossman [5]. To determine the influence of medium type and serum on MTT reduction by flavonoids in the absence of cells, DMEM, RPMI and F12, with or without 10% serum, were added onto 96-well plates and the flavonoids were then added at final concentrations of 200, 100, 50, 25 and 12.5 μg/ml. The final volume per well was 100 μl. MTT was dissolved in ultrapure water at 5 mg/ml final concentration, filter-sterilized, and then added at 10 μl per well (0.45 mg/ml final concentration). The plates were then covered with aluminum foil and incubated at 37°C for 1.5 h, 3 h or 6 h. SDS (10%) was then added at 100 μl per well followed by overnight incubation (18 h) at 37°C to completely dissolve the formazan crystals. Absorbances were obtained at 570 nm using a microplate reader (Powerscan HT, Dainippon Pharmaceutical, USA). Blanks containing only medium (with or without serum), MTT and SDS were used to correct the absorbances.

To determine the effect of serum concentration on MTT reduction by quercetin in the absence of cells, DMEM, RPMI and F12 were added onto 96-well plates and serum was then serially added at final concentrations ranging from 0-5%. Quercetin was then added at a final concentration of 50 μg/ml. Final volume per well was 105 μl. MTT was then added as described earlier and the plates incubated for 24 h. SDS (10%) was then added at 100 μl per well followed by overnight incubation (18 h) at 37°C. Absorbances were then obtained as described earlier. Blanks containing only medium, MTT and SDS were used to correct the absorbances. Differences between means were compared using Student's T-test, with significance pegged at $P < 0.05$.

3 Results

The MTT reduction potential of the flavonoids in DMEM, RPMI and F12 follows this order: quercetin >> rutin > luteolin > apigenin (Figs. 2–4). Apigenin cannot reduce MTT. Results further show that in the case of quercetin and rutin, the MTT reduction is dose-dependent in all types of media, with or without serum, and at all incubation times. On the other hand, MTT reduction by luteolin is dose-dependent only until 100 μg/ml; interestingly, at 200 μg/ml, MTT reduction decreases as shown by the decrease in absorbance. This is true for all types of media, with or without serum, and at all incubation times.

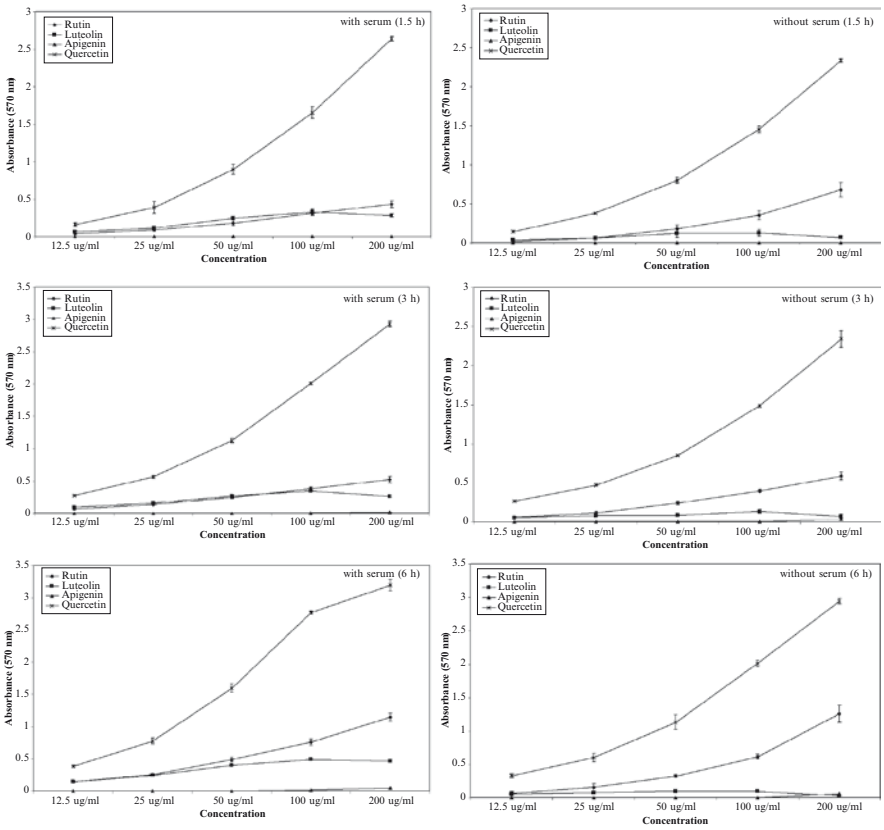

Fig. 2 MTT reduction in the absence of cells by flavonoids in Dulbecco's Modified Eagle's Medium (with or without serum) at different concentrations and incubation times. The mean absorbances ± SD have been corrected using blanks. Results represent the average of two independent experiments with three trials each

Results further show that MTT reduction by flavonoids in DMEM is statistically higher ($P < 0.05$, Student's T-test) than those in RPMI and F12, which are generally similar. In the case of quercetin, MTT reduction is time-dependent in the presence of serum for all types of media, whereas in the absence of serum, the absorbances at 1.5 h and 3 h are generally similar, particularly at 100 and 200 µg/ml.

The influence of serum on MTT reduction is clearly shown in the case of luteolin. Results reveal that absorbances are considerably higher with serum than without serum for all luteolin concentrations, all types of culture media and at all incubation times.

Because quercetin showed the highest MTT reduction potential, it was used at a final concentration of 50 µg/ml to determine the dose-dependent effect of serum. Results show that a serum concentration of even only 0.01% is sufficient to significantly enhance MTT reduction versus that at 0% ($P < 0.05$, Student's T-test) for all types of media (Fig. 5).

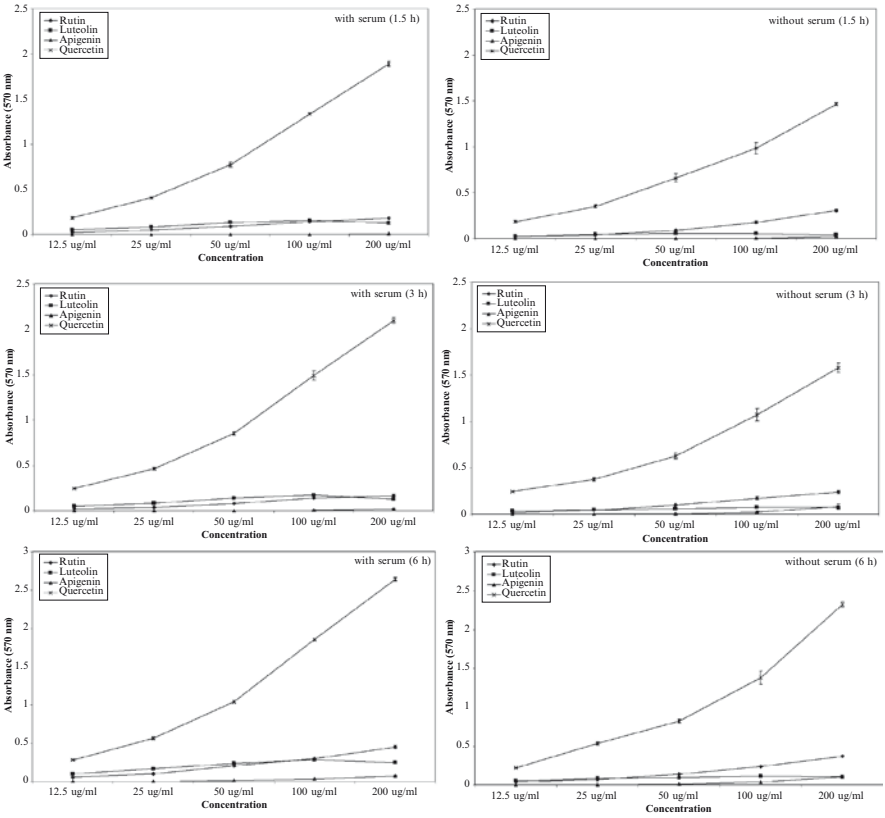

Fig. 3 MTT reduction in the absence of cells by flavonoids in F-12 Nutrient Mixture (with or without serum) at different concentrations and incubation times. The mean absorbances ± SD have been corrected using blanks. Results represent the average of two independent experiments with three trials each

4 Discussion

In this study, the authors have shown that some flavonoids can reduce MTT in the absence of cells and that this reduction is influenced by the type of medium and serum concentration. The MTT reduction potential of the flavonoids used in this study has also been shown to be of the following order: quercetin >> rutin > luteolin >apigenin.

The authors hypothesize that the structure of the flavonoids is directly related to their MTT reduction potential. The foremost consideration is the extent and nature of the hydroxylation pattern of the aromatic rings. Figure 1 shows that in the case of quercetin, the C-5′ (R_1) and C-3 (R_2) positions are both hydroxylated and this is responsible for both its high antioxidant and MTT reduction potentials.

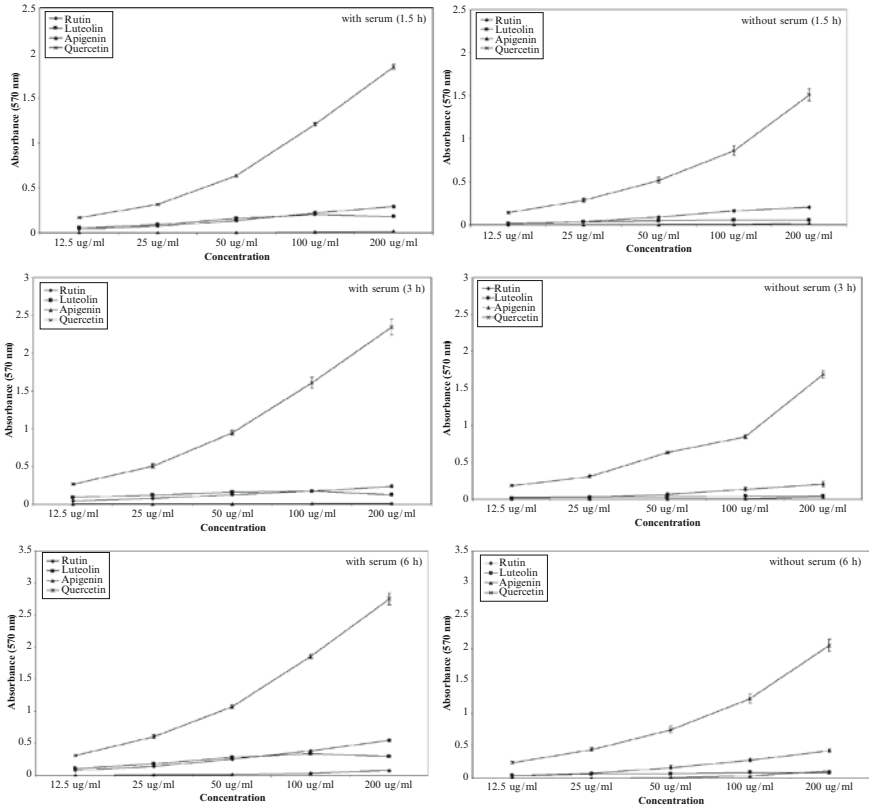

Fig. 4 MTT reduction in the absence of cells by flavonoids in RPMI 1640 Medium (with or without serum) at different concentrations and incubation times. The mean absorbances ± SD have been corrected using blanks. Results represent the average of two independent experiments with three trials each

The differences in MTT reduction in relation to medium type may be attributable to the differences in the concentrations of nutrients found in DMEM, F12 and RPMI. Nutrient concentrations are low in F12 and high in DMEM. Vistica et al. [6] have shown that the MTT assay is significantly influenced by the D-glucose concentration in the growth medium, which is 2.5-fold higher in DMEM than in F12 and RPMI.

Various enzymes that may be found in serum, such as glutathione S-transferase, as well as other energy sources required for Na^+ pumping may also affect MTT reduction [7, 8].

In conclusion, this study has shown that MTT can be reduced by flavonoids in the absence of cells and that reduction potential may be related to flavonoid structure. We have also shown that medium type and serum have a significant effect on MTT reduction by flavonoids in the absence of cells. Thus MTT assay results must be

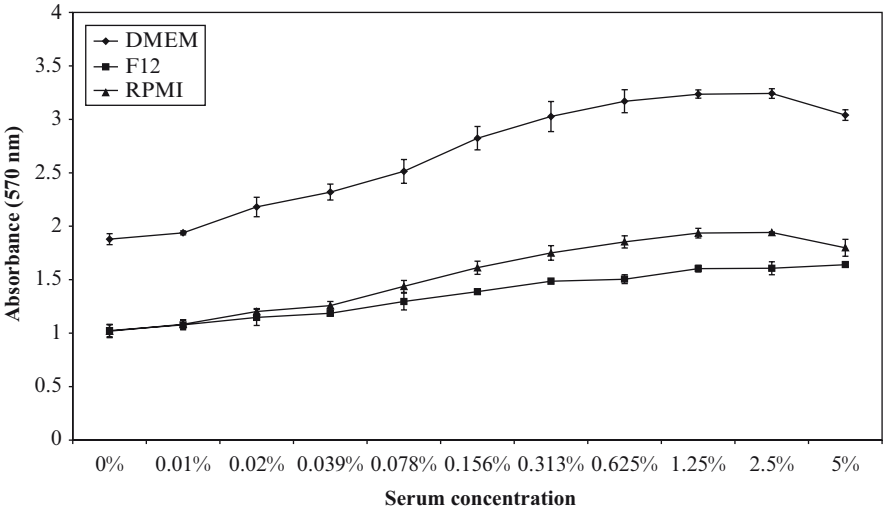

Fig. 5 Effect of serum concentration on MTT reduction in the absence of cells by quercetin (50 µg/ml) in Dulbecco's Modified Eagle's Medium, RPMI 1640 Medium and F12 Nutrient Mix after 24 h of incubation. The mean absorbances ±SD have been corrected using blanks. Results represent the average of three independent experiments. Absorbances starting at 0.01% serum concentration are statistically significant ($P < 0.05$, Student's T-test) versus those at 0%

interpreted with caution and should take into account all factors that may influence the results, particularly when it is used to measure cytotoxicity.

Acknowledgements The authors express their sincere gratitude to the Japan Society for the Promotion of Science (JSPS) for financial support under the Grants-in-Aid for Scientific Research (Scientific Research (A) No.17255011).

References

1. Shoemaker, M., Cohen, I., Campbell, M., 2004. Reduction of MTT by aqueous herbal extracts in the absence of cells. *Journal of Ethnopharmacology* **93:** 381–384.
2. Peng, L., Wang, B., Ren, P., 2005. Reduction of MTT by flavonoids in the absence of cells. *Colloids and Surfaces. B, Biointerfaces* **45:** 108–111.
3. Pagliacci, M.C., Spinozzi, F., Migliorati, G., Fumi, G., Smacchia, M., Grignani, F., Riccardi, C., Nicoletti, I., 1993. Genistein inhibits tumor cell growth in vitro but enhances mitochondrial reduction of tetrazolium salts: a further pitfall in the use of the MTT assay for evaluating cell growth and survival. *European Journal of Cancer* **29A:** 1573–1577.
4. Bernhard, D., Schwaiger, W., Crazzolara, R., Tinhofer, I., Kofler, R., Csordas, A., 2003. Enhanced MTT-reducing activity under growth inhibition by resveratrol in CEM-C7H2 lymphocytic leukemia cells. *Cancer Letters* **195:** 193–199.
5. Mossman, T., 1983. Rapid colorimetric assay for cellular growth and survival: application to proliferation and cytotoxicity assays. *Journal of Immunological Methods* **65:** 55–63.

6. Vistica, D., Skehan, P., Scudiero, D., Monks, A., Pittman, A., Boyd, R., 1991. Tetrazolium-based assays for cellular viability: a critical examination of selected parameters affecting formazan production. *Cancer Research* **51:** 2515–2520.
7. York, J. L., Maddox, L. C., Zimniak, P., McHugh, T. E., Grant, D. F., 1998. Reduction of MTT by glutathione S-transferase. *BioTechniques* **25:** 622–628.
8. Newman, J.M.B., DiMaria, C.A., Rattigan, S., Steen, J.T., Miller, K.A., Eldershaw, T.P.D., Clark, M.G., 2000. Relationship of MTT reduction to stimulants of muscle metabolism. *Chemico-Biological Interactions* **128:** 127–140.

Characterization of Highly Reactive Sequences for Transglutaminase 2 and Factor XIIIa

Yoshiaki Sugimura, Miyako Kitamura, Masayo Hosono, Hideki Shibata, Masatoshi Maki, and Kiyotaka Hitomi

Abstract Transglutaminases (TGase) are enzymes that catalyze the Ca^{2+} dependent cross-linking reaction between a γ-carboxyamide group of glutamine and an ε-amino group of lysine or other primary amine. Among these isozymes, TGases 2 and Factor XIII are major isozymes, which have been investigated since they are involved in various physiological functions.

We developed a screening system to identify highly reactive sequences for TGase substrate using M13 phage-displayed random peptide library. Using the method, we identified several amino acid sequences that were preferred as glutamine-donor substrates on the catalytic reaction of TGase 2 and Factor XIIIa (active form of Factor XIII). In these sequences, there was a tendency of the sequence around the reactive glutamine residues. Furthermore, the highly reactive substrate sequences were quite different between TGase 2 and Factor XIII.

We further confirmed the reactivity of the sequences by producing fusion proteins with glutathione-S-transferase (GST) as histidine-tagged peptide-GST. Most of the fusion proteins exhibited a significant increase in incorporation of fluorescent primary amines over that of GST protein alone. Moreover, among the obtained sequences, we selected the peptide sequences that demonstrated higher specificity and inhibitory activity in the cross-linking reaction by TGase 2 and Factor XIIIa.

Keywords Transglutaminase • substrate • phage library

1 Introduction

Transglutaminases (TGase) are enzymes that catalyze the Ca^{2+} dependent cross-linking reaction between a γ-carboxyamide group of glutamine and an ε-amino group of lysine or other primary amine [1]. To date, eight human TGase isozymes

Y. Sugimura, M. Kitamura, M. Hosono, H. Shibata, M. Maki, and K. Hitomi
Graduate School of Bioagricultural Sciences, Nagoya University,
Chikusa, Nagoya, 464-8601, Japan

K. Ikura et al. (eds.), *Animal Cell Technology: Basic & Applied Aspects*,
Animal Cell Technology: Basic & Applied Aspects 15,
DOI 10.1007/978-1-4020-9646-4_49,

(Factor XIII, TGases 1-7) have been found comprising a large protein family. Among these isozymes, TGase 2 and Factor XIII are major isozymes that are involved in multifunctional biological events such as apoptosis, extracellular matrix formation, and blood coagulation [2].

However, the mechanisms by which TGase recognize substrates remain poorly understood. During the first step, TGases are selective with regard to which glutamine residues in the substrate protein take part in the reaction; they are much less selective with regard to the lysine residue or primary amines. Although a variety of in vivo and in vitro substrate proteins have been reported for various tissues and organisms, less consensus sequence and/or structures have been identified around the reactive glutamine residues [3].

In order to clarify the amino acid sequences around reactive glutamine residue(s) that are preferred by TGases, we used an unbiased phage display random peptide library [4]. In this system, peptides are expressed as fusions with the M13 bacteriophage coat protein pIII, displaying the random peptide sequence on the surface of the phage. We screened a phage-displayed random peptide library using avidin-affinity purification of phage clones that incorporated a biotin-labeled primary amine in catalytic reactions with TGase 2 or Factor XIIIa. Furthermore, we investigated the reactivity of these sequences as recombinant fusion proteins and chemically synthesized peptides.

2 Materials and Methods

2.1 Screening Using Phage-Displayed Random Peptide Library (Fig. 1)

An M13 Ph.D.-12 phage display system was used for screening of preferred substrate sequences both in the TGase 2 and Factor XIIIa catalytic reactions. Approximately 1×10^{11}–1×10^{12} phage clones were incubated at 37°C with TGases containing 1 mM DTT, 5 mM $CaCl_2$ and 5 mM biotinylated cadaverine (Bio-Cd). In each screening round, TGase reaction was performed for 2 min -15 min. The reacted phage particles were precipitated to remove unbound Bio-Cd. Next, phage clones that covalently incorporated Bio-Cd were selected by affinity chromatography using mono-avidin gel. The bound phage clones were eluted competitively using biotin. The entire eluate was used to infect early log phase ER2738 host bacteria and the phages were amplified. The phage clones were concentrated by precipitation, and then used for following rounds. After panning totally five times, DNA sequences encoding the displayed peptide of selected phage clones were determined.

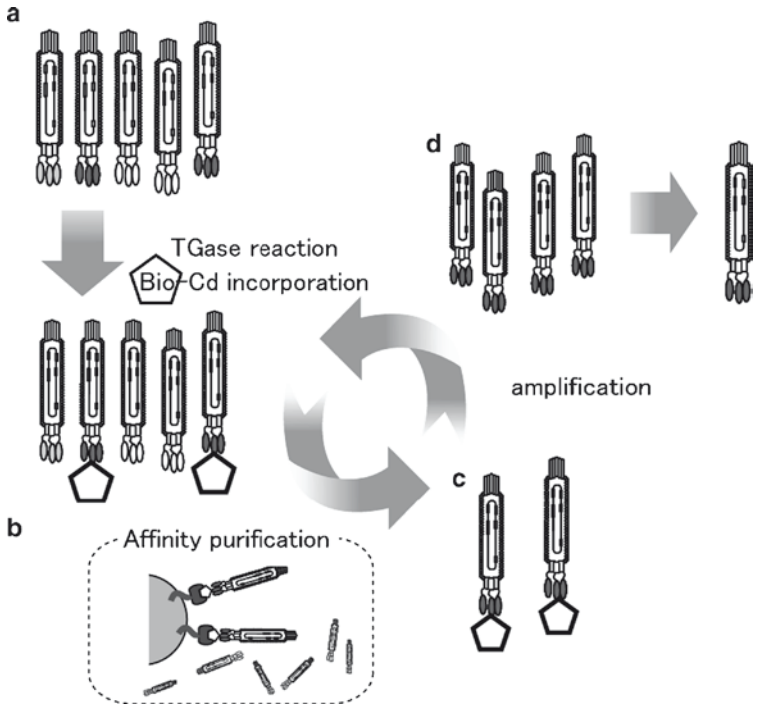

Fig. 1 Screening procedure for substrate sequences preferred by TGases using a phage clones displaying system. (**a**) Incubation of phage clones displaying a 12-mer peptide sequence with Biotin-labeled amine and TGases in an appropriate reaction buffer. (**b**) Affinity purification of phage clones that incorporated Bio-Cd using mono-avid column chromatography. (**c**) Amplification of selected phage clones in host bacteria. (**d**) Sequence analysis of DNA isolated from each phage clone

2.2 Production of Peptide-GST Fusion Proteins

GST cDNA was amplified by PCR method using an expression vector pGEX4T-1 (Novagen) as a template. DNA fragment encoding GST excised from the constructed plasmid was inserted into the pET24d vector (Novagen). The resulting plasmid pET24d-GST was used to express modified GST-fusion proteins attached with hexahistidine-tag at the C-terminus. Phage DNA fragment encoding displayed 12-mer peptide sequences were amplified by PCR. *E. coli* BL21(DE3)LysS was transformed with each constructed expression plasmid for GST-fusion protein. Production in bacteria was induced with IPTG, and the recombinant proteins were purified from soluble fraction of the extract using TALON Metal Affinity Resin.

2.3 Assessments of Substrate Preference in TGase Reaction

TGase reactivities of recombinant GST-fusion proteins were evaluated by incorporation of monodansylcadaverine (Dansyl-Cd) (Sigma), a fluorometric labeled cadaverine. The assay mixture contained 10 mM Tris-HCl (pH 8.0), 150 mM NaCl, 5 mM $CaCl_2$, 1 mM DTT, 200 ng/ul recombinant protein and 0.5 mM Dansyl-Cd in the presence of either TGase 2 (0.5 ng/ul) or Factor XIIIa (5 ng/ul). Reaction mixture was incubated at 37°C and then separated on 12.5% SDS-PAGE. A fluorograph of the gel was obtained on a UV lightbox to detect the Dansyl-Cd incorporation.

2.4 Assessments of Synthetic Peptide as TGase Substrate

Two representative 12-mer peptides, (pepT26: HQSYVDPWMLDH) and (pepF11KA: DQMMLPWPAVAL), were synthesized. To evaluate substrate reactivity and specificity as synthetic peptides, the effect of peptides were examined. Bovine casein and human fibrinogen were used as appropriate substrates for TGase 2 and Factor XIIIa, respectively. Each substrate proteins (200 ng/μl) were incubated with TGase 2 (0.5 ng/μl) or Factor XIIIa (5 ng/μl) in TBS buffer containing 1 mM DTT and 5 mM $CaCl_2$ in the presence or absence of the peptides, pepT26 and pepF11KA. The reaction products were subjected to SDS-PAGE followed by Coomassie brilliant blue staining.

3 Results and Discussion

3.1 Screening of the Preferred Substrate Sequence Using a Phage-Displayed Peptide Library

In order to identify the preferred sequences of each TGase substrate, screening was performed from a total of 1.5×10^{11} phage clones (displaying 12-mer peptides) as shown in Fig. 1. Several clones were identified in each catalytic reaction of TGase 2 and Factor XIIIa, respectively, by totally five transamidation reaction/ selection/ amplification cycles. When the peptide sequences were aligned in relation to the potential reactive glutamine residue, consensus sequences was found in TGase 2 catalytic reaction: TGase 2, Q-x-P-ϕ-D-(P) (where ϕ represents a hydrophobic amino acid); Q-x-P-ϕ; Q-x-x-ϕ-D-P. In the case of Factor XIIIa reaction, half of the clones included the sequence Q-x-x-ϕ-x-W-P.

As expected, identification and analysis of the obtained sequences indicated that the preferred sequences were unique to TGase 2 and Factor XIIIa. Particularly part of the consensus sequence for TGase 2 were consistent with that in the obtained result of studies on coeliac disease [5, 6] (Fig. 2).

T1				W	G	Q	Q	P	I	D	P	A	L	W	M	
T2					F	Q	Q	P	L	D	P	W	T	S	P	I
T8	S	N	G	N	W	Q	F	P	V	D	P	S				
T12			H	V	W	Q	H	P	V	D	P	A	T	F		
T16					W	Q	H	P	L	H	D	W	F	D	L	V
T30				M	W	Q	K	P	L	V	V	H	W	P	T	
T26					H	Q	S	Y	V	D	P	W	M	L	D	H
T29				R	E	Q	L	Y	L	D	Y	N	V	F	S	
T20					W	Q	L	H	Y	E	P	F	S	V	N	P
T32		T	H	M	Y	Q	S	I	Y	V	P	D	I			
T5			Y	P	Y	Q	H	H	L	T	Y	N	M	W		
Ctrl			W	G	H	T	I	Y	H	L	H	P	T	I		

F11		D	Q	M	M	L	P	W	P	A	V	K	L
F19		D	Q	W	M	M	A	W	P	S	L	T	L
F16	S	E	Q	H	L	L	K	W	P	P	W	H	
F12		S	Q	H	P	L	P	W	P	V	L	M	L
F6		S	Q	I	P	M	A	W	P	L	L	S	L
F13		W	Q	I	P	V	D	W	P	P	L	P	P
F17		E	Q	F	P	I	A	F	P	R	Y	S	I

Fig. 2 Alignment of preffered substrate peptide sequences for the phage clones selected. Amino acid sequences of peptides displayed on the phage clones that were selected by screening with TGase 2 (*upper*) and Factor XIIIa (*lower*) are aligned according to the potential reactive glutamine residues are shaded. Glutamines and commonly observed amino acid residues are shaded. The hydrophobic amino acid in the +3 positive is heavily shaded. Ctrl means sequence as negative control that does not contain glutamine residue

3.2 Evaluation of Identified Peptide Sequence as GST Fusion Protein and Labeled Primary Amine

To examine whether the identified sequences were highly reactive as the preferred substrate. We produced the recombinant fusion protein constituting GST and each peptide. Evaluation of selected sequence as GST-fusion proteins revealed that all analyzed sequences were favorable glutamine-donor substrates (Fig. 3). However, among identified clones, the levels of reactivities were various in some sequences that do not correspond to the major sequence motifs.

Comparison of the levels of incorporation between GST-fusion proteins indicated that T1-GST, T5-GST, and T8-GST incorporated less Dansyl-Cd than either T26-GST or T29-GST, which reacted strongly. In the case of the obtained sequences for Factor XIIIa reaction, F11-GST exhibited the greatest level. Although F17 sequence partly coincided with the sequence motif in the major group, both showed also considerable levels. These results suggested that screening system by phage-displayed work successfully to identify the preferred substrate sequences.

Since this screening system is applicable for other TGases, we will clarify other human isozymes and TGase in lower organisms [7, 8].

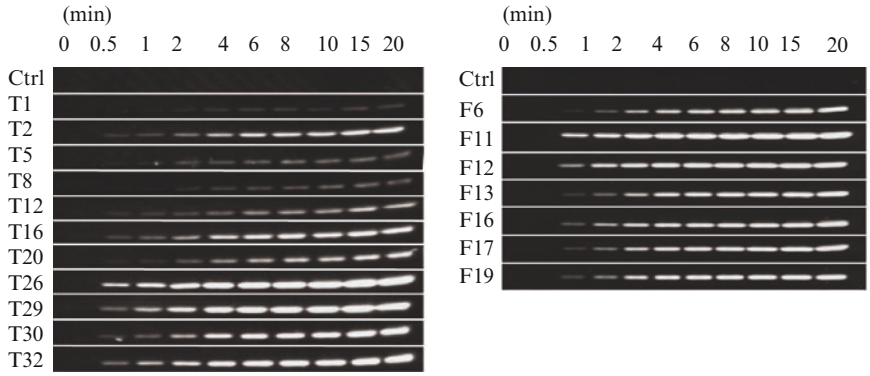

Fig. 3 Incorporation of labeled primary amine into peptide-GST fusion proteins. GST-fusion proteins with peptide corresponding to the identified substrate sequences (Fig. 2) were produced. Each recombinant protein was reacted with Dansly-Cd. At the time indicated, the reaction products were separated on 12.5% SDS-PAGE and illuminated by UV light. (*Upper*) TGase 2, (*lower*) Factor XIII

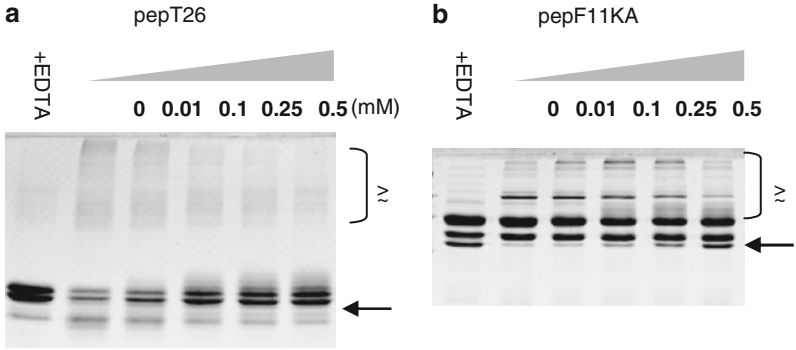

Fig. 4 Inhibition by the selected peptides on cross-linking reactions of TGase 2 and Factor XIIIa. Cross-linking reactions of casein (**a**) and (**b**) were performed in the presence of TGase 2 for 30 min and Factor XIIIa for 10 min, respectively. pepT26 and pepF11KA (0–0.5 mM) were added. A reaction performed in the absence of peptides and the presence of 5 mM EDTA was also loaded. The reaction products were analyzed by 12.5% (**a**) and 7.5% (**b**) SDS-PAGE followed by CBB staining. The asterisks and arrows indicate polymer and monomer molecules, respectively

3.3 The Peptide Sequence Exhibited the Specific Inhibition Activity for Cross-Linking Reaction

The peptides are supposed to competitively inhibit the cross-linking reaction by each TGase. Therefore, the synthesized peptide corresponding to the preferred substrate sequences were examined by co-existing with the TGases and its known substrates. In the presence of pepT26, the cross-linked casein products decreased and the uncrossed casein increased in a concentration-dependent manner (Fig. 4).

In the absence of any competing peptide, Factor XIIIa catalyzed the reduction of monomeric fibrin γ-chains, resulting in the production of α-polymers and γ-γ chains, which did not occur in the presence of EDTA. Knowledge of sequence specificity can also facilitate the design and optimization of potent and selective inhibitors. Although both pepT26 and pepF11KA are not highly homologous to the previously identified sequences, their sequences exhibited superior reactivities as glutamine-donor, suggesting that both peptides have more prominent inhibitory effects on the cross-linking reactions. Therefore, both peptides might feature as future research tools in investigation of cellular function and substrate recognition mechanisms of TGases.

Acknowledgements We thank Dr. K. Ikura (Kyoto Institute of Technology) for providing us guinea pig TGase 2. We also thank for Dr. T. Yoshimura (Nagoya University) for valuable suggestion in respect to the phage display library system.

References

1. Lorand, L. and Graham, R. M. Transglutaminases: crosslinking enzymes with pleiotropic functions, *Nat. Rev. Mol. Cell. Biol.* **4,** 140–156 (2003).
2. Fesus, L. and Piacentini, M. Transglutaminase 2: an enigmatic enzyme with diverse functions. *Trends Biochem. Sci.* **27,** 534–539 (2002).
3. Esposito, C. and Caputo, I. Mammalian transglutaminases. Identification of substrates as a key to physiological function and physiopathological relevance *FEBS J.* **272,** 615–631 (2005).
4. Sugimura, Y., Hosono, M., Yoshimura, T., Maki, M., and Hitomi, K. Screening for the preferred substrate sequences for transglutaminase 2 and Factor XIIIa. *J. Biol. Chem.* **281,** 17699–17706 (2006).
5. Sollid, L. M., Coeliac disease: dissecting a complex inflammatory disorder. *Nat. Rev. Immunol.* **2,** 647–655 (2002).
6. Fleckenstein, B., Molberg, Ø., Qiao, S., Schmid, D., Mulbe, F., Elgstoen, K., Jung, G., and Sollid, M. *J. Biol. Chem.* **277,** 34109–34116 (2002).
7. Hitomi, K. Transglutaminases in the skin epidermis *Eur. J. Dermatol.* **15,** 313–319 (2005).
8. Wada, F., Ogawa, A., Hanai, Y., Nakamura, A., Maki, M., and Hitomi, K. Analyses of expression and localization of two mammalian-type transglutaminases in Physarum Polycephalum, an acellular slime mold. *J. Biochem.* **136,** 665–672 (2004).

Some Characteristics of UNC-51 Phosphorylations of Both Actins and Tubulins

Huaize Tian and Sanetaka Shirahata

Abstract: Basic biochemical characterization of UNC-51, as a basic kinase for directly phosphorylating both tubulins and actins and involving their dynamics (being submitted to *Science Signaling*), is most significant and important in the general biology. Here, we show some characteristics (incubating time, temperature, pH and magnesium effects on UNC-51 phosphorylations of both actins and tubulins *in vitro*.

Keywords kinase • UNC-51 • tubulin • actin • cytoskeleton dynamics • axon formation.

1 Introduction

Microtubules and actin filaments are polymers of tubulin and actin, respectively, which are among the most highly conserved of all eukaryotic proteins. Furthermore, the microtubule and actin filament networks form the major cytoskeleton, a ubiquitous feature of cells that serves as the basic architecture of the cell, and the two networks have similar but distinct properties. Both networks are built from monomers that can reversibly polymerize and depolymerize; that is, the networks are dynamic. One or both networks is involved in such diverse processes and functions as axonogenesis [1], cell motility [2], muscle contraction [3], vesicle or organelle transport [4, 5], endocytosis [6], secretion [7], cell adhesion [8], signal transduction [9, 10], cell division [11, 12], microbial pathogenesis [13], apoptosis [14, 15], memory formation [16, 17], and aging [18].

H. Tian
Department of Biology, Faculty of Science, Kyushu University, Fukuoka, 812-8581, Japan

H. Tian and S. Shirahata
Laboratory of Cellular Regulation Technology, Graduate School of Systems Life Sciences, Kyushu University, Fukuoka, 812-8581, Japan

H. Tian
Neuronal Neo-Cytoskeletonology, International Health and Life Science Center Co., Ltd., Fukuoka, 813-0016, Japan

K. Ikura et al. (eds.), *Animal Cell Technology: Basic & Applied Aspects*,
Animal Cell Technology: Basic & Applied Aspects 15,
DOI 10.1007/978-1-4020-9646-4_50, © Springer Science+Business Media B.V. 2009

Coordination of the two networks is also very important to the overall structure and function of the cytoskeleton [19–21]. Microtubule- and actin-associated or -related proteins modify polymerization of microtubules and actin filaments [22, 23]. Although it has been proposed that the actin and microtubule networks have similar mechanisms for promotion of polymerization-depolymerization dynamics [24], the precise molecular mechanisms that regulate dynamics and coordinate the two network systems remain unclear.

Caenorhabditis elegans (*C. elegans*) is an excellent model for investigation of the general properties of morphogenesis and neuronal development in animals. In previous studies, the *unc-51* gene was identified and shown to be essential for multiple aspects of axonogenesis. UNC-51 protein is a novel putative serine/threonine kinase [25, 26]. Identification of the kinase substrates of UNC-51 may provide new insights into understanding the putative UNC-51 signaling pathway and more generally, understanding how neurons form. The presence of *unc-51* homologues in the mouse and human genomes [27, 28], as well as morphological and biochemical similarities between the nervous systems of *C. elegans* and mammals [29, 30], suggest that *unc-51*-related functions, including a role in axonogenesis, may be conserved. Heterologous expression of human *bcl-2* gene in *C. elegans* prevented programmed cell death of *C. elegans* [31], indicating that there are functional agreement and availability of heterologous expression system of a same conservative gene between mammalian cells and *C. elegans.*

Here, we show some characteristics of UNC-51 phosphorylations of both actins and tubulins.

2 Materials and Methods

2.1 Materials and Chemicals

The pCAGGS vector and HEK293 cells were kindly provided by Dr. K. Hayashi and Dr. T. Tahira (Division of Genome Analysis, Research Center for Genetic Information, Kyushu University) with the consent of Dr J. Miyazaki (Division of Stem Regulation Research, Osaka University Graduate School of Medicine) and K. Nakayama, respectively. pLBO containing C. elegans unc-51 cDNA was previously prepared [26]. Other major materials and chemicals are purchased from Sigma, Cytoskeleton, Molecular Probes, ICN Pharmaceuticals, etc. respectively.

2.2 Plasmid Constructs

The unc-51 cDNA was PCR amplified and a FLAG tag (5′ end) was ligated via EcoRI adapters. The products were introduced into EcoRI-site of pCAGGS vector as UNC-51WT construct. All PCR-generated fragments were confirmed by DNA-sequencing.

2.3 Cell-Transfection, Purification of FLAG-UNC-51

Transfections into HEK293 cells were performed using lipofectamine. Transfected cells were hydrolyzed in the CHAPS-containing lysis-buffer. The supernatant from lysates was passed over an anti-FLAG-gel column. Eluted FLAG-UNC-51 was passed by a Sephadex-G-25-gel column using 10 mM Hepes buffer (pH 7.4).

2.4 In Vitro Kinase Assay

Phosphorylations of tubulins and actins by FLAG-UNC-51 and its autophosphorylation were performed in a kinase reaction buffer containing 30 mM Hepes (pH 7.4), 5 mM $MgCl_2$, 5 mM $MnCl_2$, 10 mM NaF, 1 mM DTT, 50 μM [γ-^{32}P] ATP or [γ-^{32}P] GTP. Proteins were separated by 6.5% SDS-PAGE, detected with X-ray film.

3 Results

Basic biochemical characterization of UNC-51, as the first kinase for directly promoting depolymerization-dynamics of both microtubules and actin filaments (being submitted to *Science*), is significant and important.

3.1 Time Courses of UNC-51 Phosphorylations of α/β Tubulins and Actins

In Fig. 1, we showed time courses of phosphorylations of α/β tubulins and actins and its autophosphorylation by UNC-51. Phosphorylations of tubulin and actins and itself by UNC-51 increased in parallel and linearly with respect to the incubation time until 30 min, and phosphorylations reached a maximum after 60 min (Fig. 1a–c).

3.2 Temperature Effects on UNC-51 Phosphorylations of α/β Tubulins and Actins

Incubation of UNC-51 alone for 30 min in kinase reaction solution resulted in levels of phosphorylation with a parabolic relationship to incubation temperature in the range 10 to 50°C. Activity was highest at about 30°C (Fig. 1d). After storage of the affinity-purified UNC-51 at −80°C for 4 weeks, UNC-51 kinase activity was about 25% of control values. In addition, for samples stored for 1 week in a refrigerator (5°C), the activity level was less than 10% of control values (data not shown).

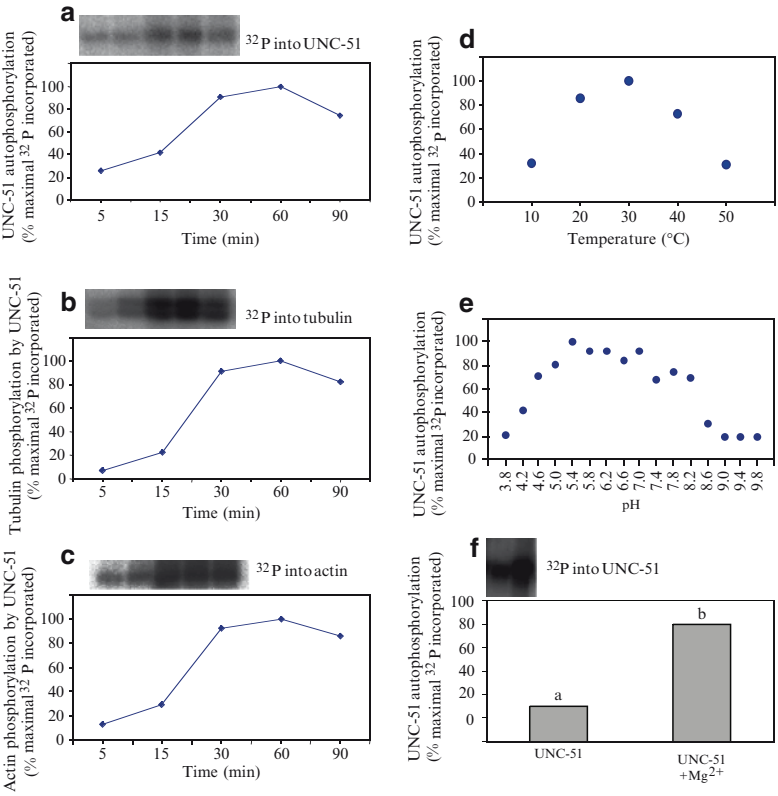

Fig. 1 Some characteristics of the affinity-purified UNC-51 phosphorylations of both actins and tubulins. (**a**), (**b**) and (**c**) Time courses of UNC-51 autophosphorylation and UNC-51 phosphorylations of tubulin (containing α and β isoforms) and actin. Results are presented as % of ^{32}P incorporated into UNC-51, tubulin and actin where 100% incorporation for 60 min was equal to 1.1×10^3 cpm/ng of UNC-51, 8.9×10^2 cpm/ng of tubulin and 1.2×10^2 cpm/ng of actin. (**d**) Temperature dependency of UNC-51 autophosphorylation. 100% ^{32}P incorporated into UNC-51 at 30°C for 30 min was equal to 1.1×10^3 cpm/ng of UNC-51. (**e**) pH dependency of UNC-51 autophosphorylation. 100% ^{32}P incorporated into UNC-51 at pH-5.4 was equal to 1.1×10^3 cpm/ng of UNC-51. (**f**) Magnesium ions promote autophosphorylation of UNC-51 by about fourfold of the corresponding free-Mg^{2+} reaction. The data shown in this and all subsequent figures are representative of replicate experiments with similar results

3.3 pH Effects on UNC-51 Phosphorylations of α/β Tubulins and Actins

As shown in Fig. 1e, UNC-51 can autophosphorylate in a broad range of pHs (pH 4.6–8.2) and can even autophosphorylate at pH 3.8 or pH 9.8 in vitro.

3.4 Mg^{2+} Promotes UNC-51 Kinase Activity

The addition of Mg^{2+} promoted autophosphorylation activity of UNC-51 by about fourfold higher than what was observed for an Mg^{2+}-free reaction and Ca^{2+} did not affect activity (Fig. 1f and data not shown).

4 Discussion

Cooperation and competition between the actin filament and microtubule networks are important for many types of morphogenesis [32], but the mechanisms that underlie them are poorly understood. Neurons, which have a single axon and multiple dendrites, provide a good model system for study of cellular polarity. We made use of this system to study the function of UNC-51, an evolutionarily conserved protein that is involved in axon formation in *C. elegans*. Many other proteins that exert a direct or indirect effect on microtubules or actin filaments have also been reported. For example, the microtubule-associated protein tau and the actin-associated protein cofilin can indirectly affect organization of microtubule and actin filaments, respectively, in living cells [22, 23]. Although there are the reports that phosphorylated tubulin and actin were unable to polymerize in vitro [33, 34], the data do not do much to help our understanding of how the microtubule and actin networks are controlled and/or coordinated. Here, we found that UNC-51 directly phosphorylates both tubulins and actins. Moreover, UNC-51 exerted an effect on the structures of both microtubules and actin filaments in living cells. It seems reasonable, then, to propose that the UNC-51 kinase is involved with coordination, competition and/or dynamics of the microtubule and actin filament networks. UNC-51 may also act on unknown other substrates, for example, it might phosphorylate microtubule-associated proteins or actin-associated proteins. Further study will be needed to determine the full spectrum of kinase substrates of UNC-51.

A parabolic relationship between the UNC-51 activity and the incubation temperature also suggests that there is a same relationship between UNC-51-dependent dynamics of microtubule or actin and the temperature from 10°C to 50°C (Fig. 1d), which may produce some hints to explain hyperthermia effects on the cytoskeleton and cell morphology [35] and how temperature greatly influenced the development and regeneration of the nervous system [36]. The pH range and Mg^{2+}-promotion for UNC-51 autophosphorylations are similarly consistent with what are know about the relationships between cytoskeletal dynamics and pH changes [37, 38] and intracellular Mg^{2+} [39], respectively.

Acknowledgments We are very thankful to Drs. Y. Oshima, K. Hayashi and T. Tahira, T. Tani, K. Nakayama, A. Yamanaka, K. Mizuno, K. Tawada, Y. Emoto, H. Arata, K. Katayama, Y. Fujiki, Y. Fukumaki, M. Kimura, S. Osaki, I. Ito and Y. Kato for kindly providing pCAGGS vector, HEK293T cells, pUcD2SRαMCS, Beckman Optima centrifuge, French press, the computer system, kind discussion, advice, help and encouragement. We express sincere gratitude to all members of both laboratories for their help and encouragement. This study was supported by The Japan Society for the Promotion of Science (Research for the Future grant number 97L00401), and by the Laboratory of Cellular Regulation Technology at Kyushu University, and by the International Health and Life Science Center of Japan.

References

1. Andersen, S.S.L. and Guo-qiang Bi. (2000). Axon formation: a molecular model for the generation of neuronal polarity. BioEssays *22*, 172–179.
2. Rodriguez, O.C., Schaefer, A.W., Mandato, C.A., Forscher, P., Bement, W.M. and Waterman-Storer, C.M. (2003). Conserved microtubule–actin interactions in cell movement and morphogenesis. Nat. Cell Biol. *5*, 599–609.
3. Chitaley, K. and Webb, R.C. (2001). Microtubule depolymerization facilitates contraction of vascular smooth muscle via increased activation of RhoA/Rho-kinase. Med. Hypotheses *56*, 381–385.
4. Bray, D. (1983). Particle transport. Nature 304, 683.
5. Morris, R.L. and Hollenbeck, P.J. (1995). Axonal transport of mitochondria along microtubules and F-actin in living vertebrate neurons. J. Cell Biol. *131*, 1315–1326.
6. Qualmann, B. and Kessels, M.M. (2002). Endocytosis and the cytoskeleton. Int. Rev. Cytol. *220*, 93–144.
7. Neco, P., Giner, D., Frances, M.M., Viniegra, S. and Gutierrez, L.M. (2003). Differential participation of actin- and tubulin-based vesicle transport systems during secretion in bovine chromaffin cells. Eur. J. Neurosci. *18*, 733–742.
8. Gumbiner, B.M. (1996). Cell adhesion: the molecular basis of tissue architecture and morphogenesis. Cell *84*, 345–357.
9. Gundersen, G.G. and Cook, T.A. (1999). Microtubule and signal transduction. Curr. Opin. Cell Biol. *11*, 81–94.
10. Pfitzer, G. (2001). Signal transduction in smooth muscle invited review: regulation of myosin phosphorylation in smooth muscle. J. Appl. Physiol. *91*, 497–503.
11. Cleary, A.L., Gunning, B.E.S., Wasteneys, G.O. and Hepler, P. (1992). Microtubule and F-actin dynamics at the division site in living *Tradescantia* stamen hair cells. J. Cell Sci. *103*, 977–988.
12. Baas, P.W. (1999). Microtubule and neuronal polarity: lessons from mitosis. Neuron *22*, 23–31.
13. Gruenheid, S. and Finlay, B.B. (2003). Insight cytoskeleton: microbial pathogenesis and cytoskeletal function. Nature *422*, 775–781.
14. Poruchynsky, M.S., Wang, E.E., Rudin, C.M., Blagosklonny, M.V. and Fojo, T. (1998). Bcl-xL is phosphorylated in malignant cells following microtubule disruption. Cancer Res. *58*, 3331–3338.
15. Sponne, I., Fifre, A., Drouet, B., Klein, C., Koziel, V., Pincon-Raymond, M., Olivier, J.L., Chambaz, J. and Pillot, T. (2003). Apoptotic neuronal cell death induced by the non-fibrillar amyloid-peptide proceeds through an early reactive oxygen species-dependent cytoskeleton perturbation. J. Biol. Chem. *278*, 3437–3445.
16. Rossum, D.V. and Hanisch, U.-K. (1999). Cytoskeletal dynamics in dendritic spines: direct modulation by glutamate receptors? Trends Neurosci. *22*, 290–295.
17. Zapara, T.A., Simonava, A.A. and Ratushnyak A.S. (2000). The effects of the dynamic state of the cytoskeleton on neuronal plasticity. Neurosci. Behav. Physiol. *30*, 347–355.
18. Gourlay, C.W., Carpp, L.N., Timpson, P., Winder, S.J. and Ayscough, K.R. (2004). A role for the actin cytoskeleton in cell death and aging in yeast. J. Cell Biol. *164*, 803–809.
19. Gavin, R.H. (1997). Microtubule-microfilament synergy in the cytoskeleton. Inter. Rev. Cytol. *173*, 207–242.
20. Fuchs, E. and Yang, Y. (1999). Crossroads on cytoskeletal highways. Cell *98*, 547–550.
21. Waterman-Storer, C.M. and Salmon, E.D. (1999). Positive feedback interactions between microtubule and actin dynamics during cell motility. Curr. Opin. Cell Biol. *11*, 61–67.
22. Drewes, G., Ebneth, A., Preuss., U., Mandelkov, E.M. and Mandelkov, E. (1997). MARK, a novel family of protein kinases that phosphorylate microtubule-associated proteins and trigger microtubule disruption. Cell *89*, 297–308.
23. Arber, S., Barbayannis, F.A., Hanser, H., Schneider, C., Stanyon, C.A., Bernard, O. and Caroni, P. (1998). Regulation of actin dynamics through phosphorylation of cofilin by LIM-kinase. Nature *393*, 805–809.

24. Mitchison, T.J. (1995). Evolution of a dynamic cytoskeleton. Phil. Trans. R. Soc. Lond. B *349*, 299–304.
25. Mclntire, S.L., Garriga, G., White, J., Jacobson, D. and Horvitz, H.R. (1992). Genes necessary for directed axonal elongation or fasciculation in C. elegans. Neuron *8*, 307–322.
26. Ogura, K., Wicky, C., Magnenat, L., Tobler, H., Mori, I., Muller, F. and Ohshima, Y. (1994). *Caenorhabditis elegans unc-51* gene required for axonal elongation encodes a novel serine/threonine kinase. Genes Dev. *8*, 2389–2400.
27. Yan, J., Kuroyanagi, H., Tomemori, T., Okazaki, N., Kuroiwa, A., Matsuda, Y., Suzuki, Y., Ohshima, Y., Mitani, S., Masuho, Y., Shirasawa, T. and Muramatsu M. (1999). Mouse ULK2, a novel member of the UNC-51-like protein kinases: unique features of functional domains. Oncogene *18*, 5850–5859.
28. Kuroyanagi, H., Yan, J., Seki, N., Yamanouchi,Y., Suzuki, Y., Takano, T., Muramatsu M. and Shirasawa, T. (1998). Human ULK1, a novel serine/threonine kinase related to UNC-51 kinase of *Caenorhabditis elegans:* cDNA cloning, expression, and chromosomal assignment. Genomics *51*, 76–85.
29. Rand, J.B., Duerr, J.S. and Frisby, D.L. (2000). Neurogenetics of vesicular transporters in C. elegans. FASEB J. *14*, 2414–2422.
30. Chisholm, A. and Tessier, L.M. (1999). Conservation and divergence of axon guidance mechanisms. Curr. Opin. Neurobiol. *9*, 603–615.
31. Vaux, D.L., Weissman, I.L. and Kim, S.K. (1992). Prevention of programmed cell death in Caenorhabditis elegans by human bcl-2. Science *258*, 1955–1957.
32. Vasiliev, J.M. (1987). Actin cortex and microtubular system in morphogenesis: cooperation and competition. J. Cell Sci. Suppl. *8*, 1–18.
33. Wandosell, F., Serrano, L., Hernandez, M.A. and Avila, J. (1986). Phosphorylation of tubulin by a calmodulin-dependent protein kinase. J. Biol. Chem. *261*, 10332–10339.
34. Sonobe, S., Takahashi, S., Hatano, S. and Kuroda, K. (1986). Phosphorylation of Amoeba G-actin and its effect on actin polymerization. J. Biol. Chem. *261*, 14837–14843.
35. Coakley, W.T. (1987). Hyperthermia effects on the cytoskeleton and cell morphology.Symp. Soc. Exp. Biol. *41*, 187–211.
36. Cancalon, P. (1985). Influence of temperature on various mechanisms associated withneuronal growth and nerve regeneration. Prog. Neurobiol. *25*, 27–92.
37. Begg, D.A. and Rebhun, L.I. (1979). PH regulates the polymerization of actin in the sea urchin egg cortex. J. Cell Biol. *83*, 241–248.
38. Schatten, G., Bestor, T., Balczon, R., Henson, J. and Schatten, H. (1985). Intracellular pH shift leads to microtubule assembly and microtubule-mediated motility during sea urchin fertilization: correlations between elevated intracellular pH and microtubule disassembly. Eur. J. Cell Biol. *36*, 116–127.
39. Prescott, A.R., Comerford, J.G., Magrath, R., Lamb, N.J.C. and Warn, R.M. (1988). Effects of elevated intracellular magnesium on cytoskeletal integrity. J. Cell Sci. *89*, 321–329.

Protein Phosphotase 1α Reverses UNC-51 Phosphorylations of Both Actins and Tubulins and a New Model of UNC-51-Inducing Axon Formation

Huaize Tian and Sanetaka Shirahata

Abstract Because UNC-51 can promote depolymerization-dynamics of microtubules (being submitted to *Science Signaling*), and Protein phosphotase 1α has microtubule-stabilizing functions (Liao, et al., 1998), we showed that protein phosphotase 1α efficiently dephosphorylated UNC-51 phosphorylations of actins and tubulins, and hypothesized a new model of UNC-51-inducing axon formation.

Keywords kinase • UNC-51 • tubulin • actin • depolymerization • PP1 • axon formation • model.

1 Introduction

Because UNC-51 can promote depolymerization-dynamics of both microtubules and actin filaments (being submitted to *Science*), and Protein phosphotase 1α has microtubule-stabilizing functions [1–4], we tested the ability of PP1 to reverse UNC-51-dependent phosphorylation. We propose that UNC-51 and PP1 may constitute a switch that reversely but coordinately regulates microtubules and actins dynamics during axon formation. A new model of UNC-51-inducing axon formation is hypothesized by us.

H. Tian
Department of Biology, Faculty of Science, Kyushu University, Fukuoka 812-8581, Japan

H. Tian and S. Shirahata
Laboratory of Cellular Regulation Technology, Graduate School of Systems Life Sciences, Kyushu University, Fukuoka 812-8581, Japan

H. Tian
Neuronal Neo-Cytoskeletonology, International Health and Life Science Center Co., Ltd. Fukuoka 813-0016, Japan

K. Ikura et al. (eds.), *Animal Cell Technology: Basic & Applied Aspects*,
Animal Cell Technology: Basic & Applied Aspects 15,
DOI 10.1007/978-1-4020-9646-4_51,

2 Materials and Methods

2.1 *In Vitro Dephosphorylation of UNC-51 Phosphorylations of Tubulins and Actins by PP1α*

Phosphorylation of tubulin and actin (Cytoskeleton Com.), and autophosphorylation of Flag-tagged UNC-51, were performed at 30°C for 30 min in the kinase reaction buffer for in vitro phosphorylation. Next, 1 μl PP1α or PP2B (with 0.1 mM $CaCl_2$) (Sigma Com.) were added to the reactions and the dephosphorylation reaction was incubated at 30°C for another 30 min.

3 Results and Discussion

3.1 *PP1α Can Dephosphorylate UNC-51 Phosphorylations of Actins and Tubulins*

As shown in Fig. 1, serine/threonine protein phosphotase 1α (recombinant PP1 catalytic subunit; PP1α) can efficiently dephosphorylate both phosphorylated rabbit muscle actins and bovine brain tubulins. However, PP2B (calcineurin) had little effect. Thus, we propose that UNC-51 and PP1 may constitute a switch that that reversely but coordinately regulates dynamics of microtubules and actins.

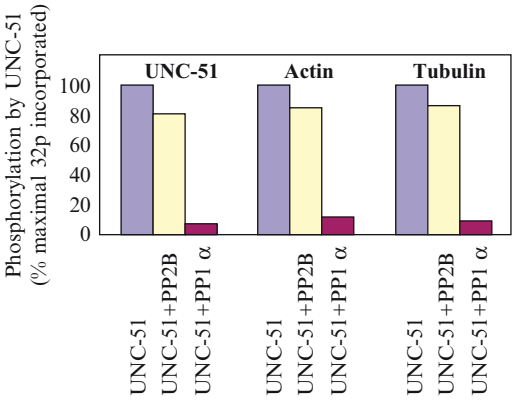

Fig. 1 PP1 reverses UNC-51 phosphorylations of actins and tubulins. Protein phosphotase 1 α efficiently dephosphorylated UNC-51 phosphorylations of actins and tubulins, and PP2B (calcineurin) could dephosphorylate the proteins to a lesser degree. The data shown in this figure is representative of replicate experiments with similar results

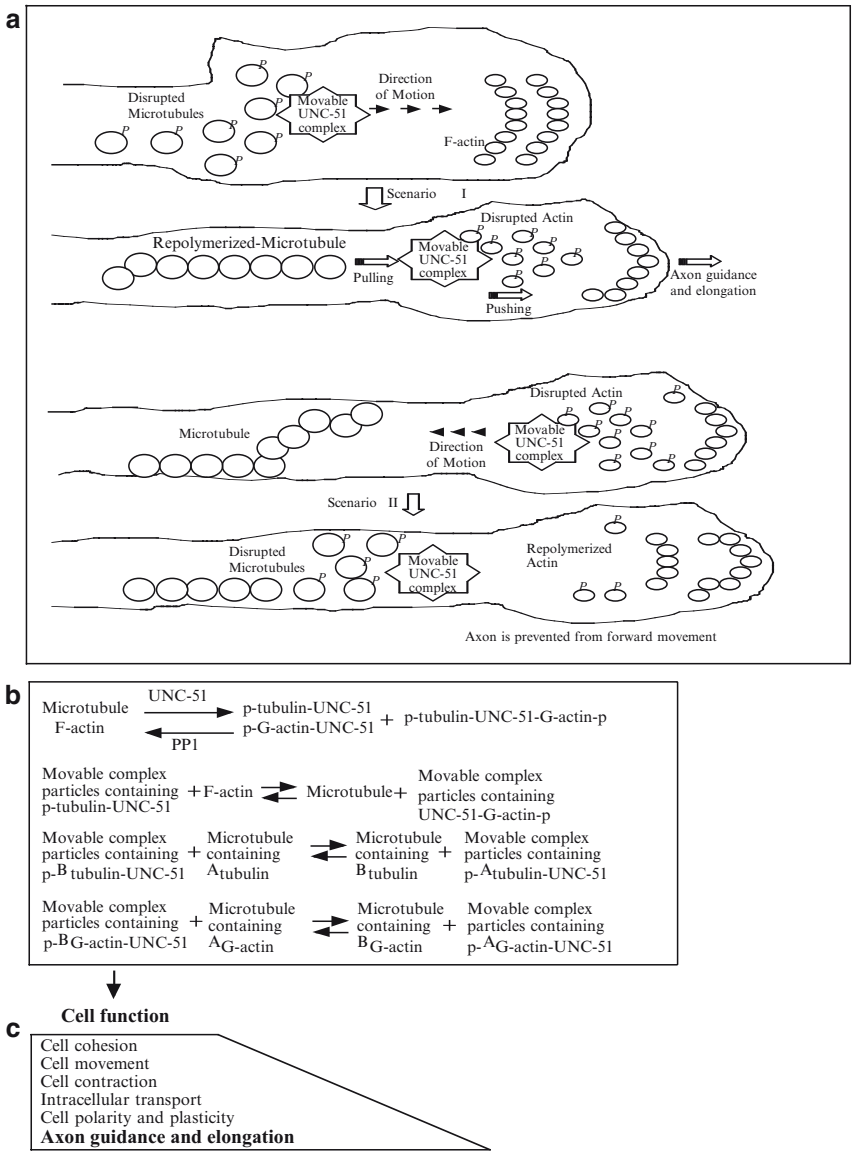

Fig. 2 A new model of UNC-51-mediated regulation of cytoskeletal dynamics and coordination of actin filaments and microtubules. (**a**) A new model for UNC-51 induction of neurite morphology. UNC-51 results in depolymerization of peripheral actin filaments and polymerization of rearward UNC-51-released tubulin, thus resulting in processes formation. By contrast, depolymerization of the rearward microtubules and tension from repolymerization of the forward actin prevent the cell from pushing through. We suggest that protrusion of lamellipodia or process and axon formation are coordinately induced by such a mechanism. (**b**) A chemical hypothesis for UNC-51 regulation of cytoskeletal dynamics and coordination of actin filaments and microtubules as shown pictorially in (**a**). (**c**) Possible cell functions affected by UNC-51 regulating dynamics and coordination of both actin filament and microtubules

3.2 A New Model of UNC-51 Mediated Cytoskeletal Dynamics

A new model of axon formation is presented as follows (Fig. 2). There would be a kind of competition and coordination between microtubule and F-actin for being bound, phosphorylated, depolymerized and transported by UNC-51 or movable UNC-51 complexes. This kind of competition and coordination can cause depolymerization of forward UNC-51-modified actin filaments and polymerization of rearward UNC-51-released tubulin or reversion in the peripheral region and some local region in a cell. Namely, when a forward UNC-51 depolymerizes the peripheral actin filaments in a cell, polymerization of rearward UNC-51-released tubulin, which is perhaps regulated by dephosphorylation by PP1, results in pushing out processes from the cell. Since rearward repolymerized microtubules come in contact with the UNC-51-depolymerized actin region, depolymerization of the rearward microtubules and tension from repolymerization of the forward actin prevent the cell from pushing through. It is suggested that the protrusion of the lamellipodia or process, subsequently axon formation are coordinately induced by such a mechanism. This model easily interprets the observation puzzle for a long time how local actin depolymerization leads to increased microtubule polymerization and neurite extension [5]. Our model provides support for and helps to explain previous reports that axon branching or formation occurs by destabilization and dynamic interactions of both microtubules and actin filaments [6–9].

In conclusion, we have shown that UNC-51 is an excellent candidate for a kinase that regulates cytoskeletal dynamics and coordinates of the microtubule and actin filament networks via phosphorylation, leading to disruption or depolymerization. Moreover, we propose a tubulin-UNC51-actin competition/coordination model to explain axon formation as a new intracellular signal-pathway. The data suggest that UNC-51 may be important for control of cell morphology and movement via regulation of the cytoskeleton. Roles for UNC-51 may extend to movement and/or function of mitochondria, as these organelles depend on both microtubule and actin filament systems. In the future, we hope to learn more about how polymerization of actin or tubulin relates to UNC-51-mediated phosphorylation.

Acknowledgments We are very thankful to Drs. K. Hayashi and T. Tahira, T. Tani, K. Nakayama, A. Yamanaka, K. Mizuno, K. Tawada, Y. Emoto, H. Arata, K. Katayama, Y. Fujiki, Y. Fukumaki, M. Kimura, S. Osaki, I. Ito and Y. Kato for kindly providing pCAGGS vector, COS cells, HeLa cells, HEK293T cells, pUcD2SRαMCS, Beckman Optima centrifuge, French press, the computer system, kind discussion, advice, help and encouragement. We express sincere gratitude to all members of both laboratories for their help and encouragement.

References

1. Liao, H., Li, Y., Brautigan, D.L. and Gundersen, G.G. (1998). Protein phosphatase 1 is targeted to microtubules by the microtubule-associated protein tau. J. Biol. Chem. *273*, 21901–21908.

2. Gurland, G. and Gundersen, G.G. (1993). Protein phosphatase inhibitors induce the selective breakdown of stable microtubules in fibroblasts and epithelial cells. Proc. Natl. Acad. Sci. USA *90*, 8827–8831.
3. Maier, G.D., Wright, M.A., Lozano, Y., Djordjevic, A., Matthews, J.P. and Young, M.R.I. (1995). Regulation of cytoskeletal organization in tumor cells by protein phosphatase- 1 and 2A. Int. J. Cancer *61*, 54–61.
4. Stephanie, L.B. et al. (2007). Spinophilin facilitates PP1-mediated dephosphorylation of pSer297 doublecortin in microtubule bundling at the axonal "wrist". Cell **129**, 579–591.
5. Andersen, S.S.L. and Guo-qiang Bi. (2000). Axon formation: a molecular model for the generation of neuronal polarity. BioEssays *22*, 172–179.
6. Dent, E.W. and Kalil, K. (2001). Axon branching requires interactions between dynamic microtubules and actin filaments. J. Neurosci. *21*, 9757–9769.
7. Edson, K., Weisshaar, B. and Matus, A. (1993). Actin depolymerisation induces process formation on MAP2-transfected non-neuronal cells. Development *117*, 689–700.
8. Bradke, F. and Dotti, C.G. (1999). The role of local actin instability in axon formation. Science *283*, 1931–1934.
9. Grenningloh, G., Soehrman, S., Bondallaz, P., Ruchti, E. and Cadas, H. (2004). Role of the microtubule destabilizing proteins SCG10 and stathmin in neuronal growth. J. Neurobiol. *58*, 60–69.

Overexpression of Conserved Kinase UNC-51 Inhibits the Transferrin's Endocytosis into the Mammalian Cells

Huaize Tian and Sanetaka Shirahata

Abstract UNC-51 overexpression can inhibit the transferrin endocytosis in the transfected COS-7 cells. We think that this inhibition of transferrin endocytosis should be caused by UNC-51-dependent microtubule-disruption (being submitted to *Science Signaling*).

Keywords kinase • UNC-51 • tubulin • actin • dynamics • endocytosis • transferrin.

1 Introduction

Endocytosis is crucial to many cellular functions, for example, axon formation and synaptic transmission, antigen presentation, cancer, pathogen entry [1–3]. But, the precise molecular mechanisms for endocytosis are unclear. Conserved UNC-51 is essential for the axon formation, thus, we expressed Myc-tagged UNC-51 in COS-7 cells to analyze how or whether UNC-51 affects the transferrin's endocytosis into the cells.

H. Tian
Department of Biology, Faculty of Science, Kyushu University Fukuoka 812- 8581, Japan

H. Tian and S. Shirahata
Laboratory of Cellular Regulation Technology, Graduate School of Systems Life Sciences, Kyushu University, Fukuoka 812-8581, Japan

H. Tian
Neuronal Neo-Cytoskeletonology, International International Health and Life Science Center Co., Ltd. Fukuoka 813-0016, Japan

K. Ikura et al. (eds.), *Animal Cell Technology: Basic & Applied Aspects*,
Animal Cell Technology: Basic & Applied Aspects 15,
DOI 10.1007/978-1-4020-9646-4_52,

2 Materials and Methods

2.1 Plasmid Constructs

The unc-51 cDNA was PCR amplified and a FLAG tag (5′ end) was ligated via EcoRI adapters. The products were introduced into EcoRI-site of pCAGGS vector as UNC-51WT construct. All PCR-generated fragments were confirmed by DNA-sequencing. Alexa 488-Transferrin (Molecular Probes).

2.2 Cell Transfection and Confocal Immunofluorescence Microscopy

To visualize the intracellular distributions of UNC-51 and transferrin simultaneously, Myc-tagged wild-type *unc-51* plasmids were transfected into COS-7 cells and cells were seeded on autoclaved glass cover slips in 90 mm dishes. After Alexa 488-Transferrin for 30 min at 37°C to endocytose, fixed in 3% (wt/vol) paraformaldehyde in 10 mM PBS (pH7.3) for 30 min, then permeabilized by treatment with 0.2% Triton X-100 in PBS for 5 min. After washing with PBS, each cover slip was then incubated with 40 μl of PBS-solution containing anti-Myc Secondary detection was carried out with an anti-mouse antibody conjugated to Texas Red. Nuclei were detected by DAPI staining of DNA (1:1,000 dilution in PBS, Molecular Probes). Samples were examined using the Zeiss LSM510 confocal microscopy system (100× oil objective) configured with an Argon/Krypton laser (488 and 568 nm excitation).

3 Results and Conclusion

In transfected cells expressing Myc-tagged UNC-51 (Fig. 1, red), transferrin had not been seen (green, white arrows). However, in untransfected cells, the transferrin endocytosis (green) can clearly be observed. The results suggest that UNC-51 overexpression can inhibit the transferrin endocytosis in the transfected COS-7 cells. We think that this inhibition of transferrin endocytosis should be caused by UNC-51-dependent microtubule-disruption (being submitted to Science), which is consistent with inhibition of transferring internalization by microtubule-disrupting drugs [4–7].

Conclusively, our data suggest that UNC-51 would function through inhibiting endocytosis by microtubule-disruption pathway.

Acknowledgments We are very thankful to Drs. K. Hayashi and T. Tahira, T. Tani, K. Nakayama, A. Yamanaka, K. Mizuno, K. Tawada, Y. Emoto, H. Arata, K. Katayama, Y. Fujiki, Y. Fukumaki,

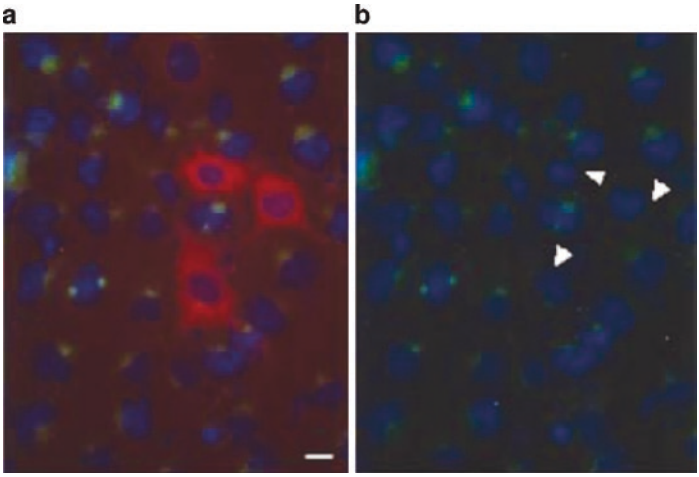

Fig. 1 Inhibition of transferrin endocytosis (*green, arrows*) with Myc-tagged UNC-51 overexpression (*red*) in the COS-7 cells. DAPI staining-DNA (*blue*). The images are representative for 3 different experiments performed in duplicate (scale bar 10 μm)

M. Kimura, S. Osaki, I. Ito and Y. Kato for kindly providing pCAGGS vector, COS cells, HeLa cells, HEK293T cells, pUcD2SRαMCS, Beckman Optima centrifuge, French press, the computer system, kind discussion, advice, help and encouragement. We express sincere gratitude to all members of both laboratories for their help and encouragement.

References

1. Riezman H, Woodman PG, Meer G, Marsh M (1997). Molecular mechanisms of endocytosis. Cell **91**, 731–738.
2. Marsh M and McMahon HT (1999). The structural era of endocytosis. Science **285**, 215–220.
3. Shintani T, Klionsky DJ (2004). Autophagy in health and disease: a double-edged sword. Science. **306**, 990–995.
4. Jin M and Snider MD (1993). Role of microtubules in transferring receptor transport from the cell surface to endosomes and the Golgi complex. J. Biol. Chem. **268**, 18390–18397.
5. Thatte HS, Bridges KR, Golan DE (1994). Microtubule inhibitors differentially affect translational movement, cell surface expression, and endocytosis of transferring receptors in K562 cells. J. Cell Physiol. **160**, 345–357.
6. Elkjaer ML, Birn H, Agre P, Christensen EI, Nielsen S (1995). Effects of microtubule disruption on endocytosis, membrane recycling and polarized distribution of Aquaporin-1 and gp330 in proximal tubule cells. Eur. J. Cell Biol. **67**, 57–72.
7. Subtil A, Dautry-Varsat A (1997). Microtubule depolymerization inhibits clathrin coated-pit internalization in non-adherent cell lines while interleukin 2 endocytosis is not affected. J. Cell Sci. **110**, 2441–2447.

Author Index

Subject Index